

**The selective conversion of biomass derived coumalic acid to functionalized aromatics and novel intermediates**

by

**Toni Pfennig**

A dissertation submitted to the graduate faculty

in partial fulfillment of the requirements for the degree of

**DOCTOR OF PHILOSOPHY**

Major: Chemical Engineering

Program of Study Committee:

R. Dennis Vigil, Major Professor

Brent H. Shanks

Jean-Philippe Tessonnier

D. Raj Raman

George A. Kraus

The student author, whose presentation of the scholarship herein was approved by the program of study committee, is solely responsible for the content of this dissertation. The Graduate College will ensure this dissertation is globally accessible and will not permit alterations after a degree is conferred.

Iowa State University

Ames, Iowa

2017

Copyright © Toni Pfennig, 2017. All rights reserved.

**TABLE OF CONTENTS**

ACKNOWLEDGMENTS.....	viii
ABSTRACT .....	ix
CHAPTER 1 INTRODUCTION .....	1
1.1 Introduction.....	1
1.2 Biomass Conversion Strategies to Fuels and Chemicals .....	3
1.3 Platform Chemicals from Biomass .....	5
1.3.1 C2 Platform.....	6
1.3.2 C3 Platform.....	7
1.3.3 C4 Platform.....	8
1.3.4 C5 and C6 Platform .....	8
1.4 Non-Selective Routes to Aromatics from Biomass .....	10
1.5 Selective Routes to Aromatics from Biomass .....	12
1.5.1 Selective Formation of Aromatics via Diels-Alder Chemistry.....	13
1.5.2 Selective Formation of Aromatics from Biomass Derived Furanics via Diels-Alder Chemistry.....	15
1.5.3 Selective Formation of Aromatics from Biomass Derived Chemicals via Diels-Alder Chemistry.....	18

1.5.4	Selective Formation of Aromatics from Biomass Derived 2-Pyrones via Diels-Alder Chemistry.....	21
1.6	Selective Routes to Novel Intermediates from Biomass.....	26
1.7	Conclusion .....	27
1.8	Thesis Outline .....	29
1.9	References.....	30
CHAPTER 2	THE FORMATION OF P-TOLUIC ACID FROM COUMALIC ACID: A REACTION NETWORK ANALYSIS.....	36
2.1	Abstract.....	36
2.2	Introduction.....	37
2.3	Experimental.....	40
2.3.1	Reagents and Materials .....	40
2.3.2	Apparatus and General Reaction Procedure .....	41
2.3.3	Sample Analysis.....	42
2.4	Results and Discussion .....	43
2.4.1	Elucidating the Reaction Network .....	43
2.4.1.1	The reaction network in the absence of catalyst .....	43
2.4.1.2	The reaction network in the presence of catalyst.....	48
2.5	Conclusions.....	57
2.6	Acknowledgements.....	58

2.7	References.....	58
2.8	Supplementary Information .....	60
CHAPTER 3	A NEW SELECTIVE ROUTE TOWARDS BENZOIC ACID AND DERIVATIVES FROM BIOMASS-DERIVED COUMALIC ACID.....	86
3.1	Abstract.....	86
3.2	Introduction.....	87
3.3	Experimental.....	90
3.3.1	Reagents and Materials.....	90
3.3.2	Apparatus and general Procedure .....	90
3.3.3	Sample Analysis.....	92
3.3.4	Computational.....	93
3.4	Results and Discussion .....	93
3.4.1	The Formation of Benzoic Acid from Coumalic Acid .....	93
3.4.2	Elucidating the Reaction Network.....	96
3.4.3	2-Pyrone Degradation Studies .....	97
3.4.4	Reaction Kinetics of Water Mediated Coumalic Acid Breakdown .....	99
3.4.5	Reaction Kinetics in the Absence of Catalyst.....	102
3.4.6	Diels-Alder Reaction Step .....	103
3.4.7	Decarboxylation Reaction Step.....	105
3.5	Conclusion .....	108



3.6	Acknowledgments.....	109
3.7	References.....	109
3.8	Supplementary Information .....	112
CHAPTER 4	MODULATING ACTIVITY AND SELECTIVITY OF 2-PYRONE- DERIVED BICYCLIC LACTONES THROUGH CHOICE OF CATALYST AND SOLVENT.....	129
4.1	Abstract.....	129
4.2	Introduction.....	130
4.3	Methods and Materials.....	134
4.3.1	Reagents and Material.....	134
4.3.2	Catalyst Preparation .....	134
4.3.3	Batch Reaction Experiments.....	134
4.3.4	In Situ NMR Experiments .....	136
4.3.5	Analytical Methods.....	137
4.3.6	Computational.....	139
4.3.6.1	Periodic density functional theory .....	139
4.3.6.2	Molecular density functional theory .....	140
4.4	Results and Discussion .....	141
4.4.1	Decarboxylation in the Presence of Catalyst .....	141
4.4.2	Reaction Kinetics of the $\gamma$ -Al <sub>2</sub> O <sub>3</sub> Catalyzed Decarboxylation.....	142

4.4.3	Computational Analysis of the $\gamma$ -Al <sub>2</sub> O <sub>3</sub> Catalyzed Decarboxylation .....	143
4.4.4	Adsorption of Water and (1) on Different $\gamma$ -Al <sub>2</sub> O <sub>3</sub> Surfaces .....	144
4.4.5	Decarboxylation of the Bicyclic Lactone (1) on $\gamma$ -Al <sub>2</sub> O <sub>3</sub> : Mechanism and Microkinetic Modeling .....	145
4.4.6	Characterization of Bicyclic Lactone (1) Immobilized on $\gamma$ -Al <sub>2</sub> O <sub>3</sub> by HR-MAS NMR .....	149
4.4.7	The Impact of Brønsted Acids on Conversion.....	153
4.4.8	Solvent Impact on Conversion of (1).....	157
4.4.9	Broader Implication .....	161
4.5	Conclusion .....	162
4.6	Acknowledgement .....	164
4.7	References.....	164
4.8	Supplementary Information .....	169
CHAPTER 5	IMPROVING SELECTIVITY OF TOLUIC ACID FROM BIOMASS- DERIVED COUMALIC ACID .....	189
5.1	Abstract.....	189
5.2	Experimental.....	190
5.2.1	Reagents and Material.....	190
5.2.2	Apparatus and General Procedure .....	191
5.2.3	Sample Analysis.....	192

5.2.4	Computational.....	193
5.3	Introduction.....	193
5.4	Results and Discussion .....	197
5.4.1	The Formation of Toluic Acid from Coumalic Acid.....	197
5.4.2	Reaction Kinetics in the Absence of Catalyst.....	201
5.4.3	Diels-Alder Reaction Step .....	202
5.4.4	Decarboxylation Reaction Step.....	207
5.5	Conclusion .....	210
5.6	Acknowledgement .....	211
5.7	References.....	211
5.8	Supplementary Information .....	215
CHAPTER 6	GENERAL CONCLUSIONS.....	221

## ACKNOWLEDGMENTS

I would like to take moment to thank my friends, colleagues, the department faculty and staff for making my time at Iowa State University a wonderful experience. I want to also offer my appreciation to those who were willing to support and help me, without whom, this thesis would not have been possible. Most importantly, I would like to thank my family that gave me guidance through difficult times and always supported me with their love and words of encouragement that have been invaluable to me.

*Ganz besonderer Dank ist vor allem meinen Großeltern Helmut Pfennig und Elsbeth Pfennig gewidmet. Ihre Unterstützung und aufmunternden Worte gaben mir Kraft und Willen diesen schweren Weg zu meistern.*

I am also very grateful to my major advisor Dr. Brent H. Shanks for his endurance and patience with me over the past four years. His support and guidance were an important part of my professional development. Most importantly, he gave me the personal freedom to develop the necessary problem-solving skills and to pursue my own ideas. His enthusiasm for high level and qualitative research has shaped my research expertise and set a high standard for my future goals.

Lastly, I would also like to thank my committee members, Dr. Jean-Philippe Tessonier, Dr. George A. Kraus, Dr. R. Dennis Vigil, and Dr. D. Raj Raman for their guidance and support throughout the course of this thesis.

**ABSTRACT**

The heavy reliance on petroleum as the raw feedstock for the production of chemicals imparts negative environmental effects and exerts economic pressure due to the diminishing availability of natural crude oil reserves. A change in the raw material supply can already be observed in the U.S., where petroleum is increasingly being replaced by inexpensive shale gas. The increased shale gas dependence, however, reduces the availability of >C<sub>4</sub> chemicals (e.g. aromatics). Since existing alternatives, such as selectively accessing aromatics from renewable carbon sources (e.g. biomass), are still facing significant limitations, there is a need to develop new technologies.

An innovative approach to selectively access bio-based aromatics in high yield is provided herein via a Diels-Alder/decarboxylation/palladium catalyzed dehydrogenation domino sequence starting from coumalic acid (or methyl coumalate) in conjunction with the inexpensive and easy to separate/recycle ethylene (or propylene). This approach is guided by an in-depth reaction network analysis, solvent and kinetic studies, and complemented by density functional theory (DFT) calculations with the goal of providing key insights into the formation of intermediates and by-products on the pathway to aromatics.

The solvent studies show that polar aprotic solvents including 1,4-dioxane,  $\gamma$ -valerolactone and acetone lead to excellent aromatic yield and selectivity (78 - 91 mol%) when starting with coumalic acid, whereas non-polar toluene provides only poor solubility of coumalic acid which is associated with by-product formation and, therefore, poor aromatic yield (< 55 mol%). Starting with methyl coumalate, however, improves yield and selectivity significantly (up to 99 mol%)

across all solvents tested, indicating that the starting substrate (ester vs acid) considerably impacts the formation of aromatics.

The kinetic analysis of relevant steps reveals that decarboxylation is the rate limiting step, which is in agreement with DFT calculations. This critical information enables the development of a tailored catalyst through which significant process optimizations are achieved, including the selective access to dihydrobenzenes from bicyclic lactones in high yield (> 98 mol%). Novel dihydrobenzene structures have interesting dual functionality and further expand the diverse coumalate platform with species that are challenging to access via conventional petroleum routes.

Further diversification of bicyclic lactones is achieved through the choice of solvent and catalyst (e.g. Brønsted and Lewis acids) by enabling highly selective pathway modifications. Lewis acids enhance decarboxylation, whereas Brønsted acids enable ring-opening of bicyclic lactones to produce novel chemical species. Ring-opening is also achieved when bicyclic lactone conversion is mediated in methanol, a polar protic solvent. Cleavage of the lactone bridge is, thereby, induced through methanolysis in the absence of a Brønsted acid, therefore providing another environmentally benign pathway.

Lastly, the combination of kinetic studies, DFT calculations and high resolution magic angle spinning NMR characterization reveals important insights into the Lewis acid ( $\gamma$ -Al<sub>2</sub>O<sub>3</sub>) catalyzed decarboxylation mechanism at the solvent-catalyst-interface and provides evidence of the catalytic active site responsible for decarboxylation. This knowledge can be broadly transferred for decarboxylation of a range of 2-pyrone derived bicyclic lactones and improve access to novel dihydrobenzenes and aromatics from biomass.

## CHAPTER 1

### INTRODUCTION

#### 1.1 Introduction

Throughout the 20<sup>th</sup> century, a significant shift in carbon-rich raw material was observed in the chemical industry. Early processes relied on coal to manufacture materials such as calcium carbide and aromatics, an important group of compounds used in the production of pharmaceuticals, dyes, explosives, and photographic chemicals. Throughout the 1930's, 60 % of organic materials were derived from coal compared to just 10 % from petroleum<sup>2</sup>. Following World War II, petroleum became an increasingly important raw material, accounting for 75 % of today's transportation fuel and commodity chemical production.<sup>1,2</sup>

In 2012, petroleum and other liquid fuel (NGPL, biofuels, CTL, and GTL) consumption accounted for 90<sup>3</sup> million barrels per day and is expected to increase to 121<sup>3</sup> million barrels per day by 2040. Similarly, natural gas consumption is projected to increase from 120<sup>3</sup> trillion cubic feet in 2012 to 203<sup>3</sup> trillion cubic feet by 2040 accounting for the largest growth of primary energy sources. This growth can be attributed to the high fuel efficiency and low cost of this feedstock.<sup>3</sup> As a result, natural gas plays an increasingly important role in energy security for the United States, exceeding 33 % of U.S energy supply in 2015<sup>4</sup> (Figure 1).

Advances in horizontal drilling and hydraulic fracturing technologies have made previously inaccessible reserves available, leading to a growth in domestic gas production in the U.S. from 1 % in 2000 to 20 % in 2010, with further growth projected to exceed 46 % by 2035.<sup>3</sup> Favorable geological conditions, fewer environmental restrictions, and continued technological innovations led to shale gas breakthrough, making the exploitation of this raw material economically feasible. However, atmospheric methane emissions, contamination of ground water,

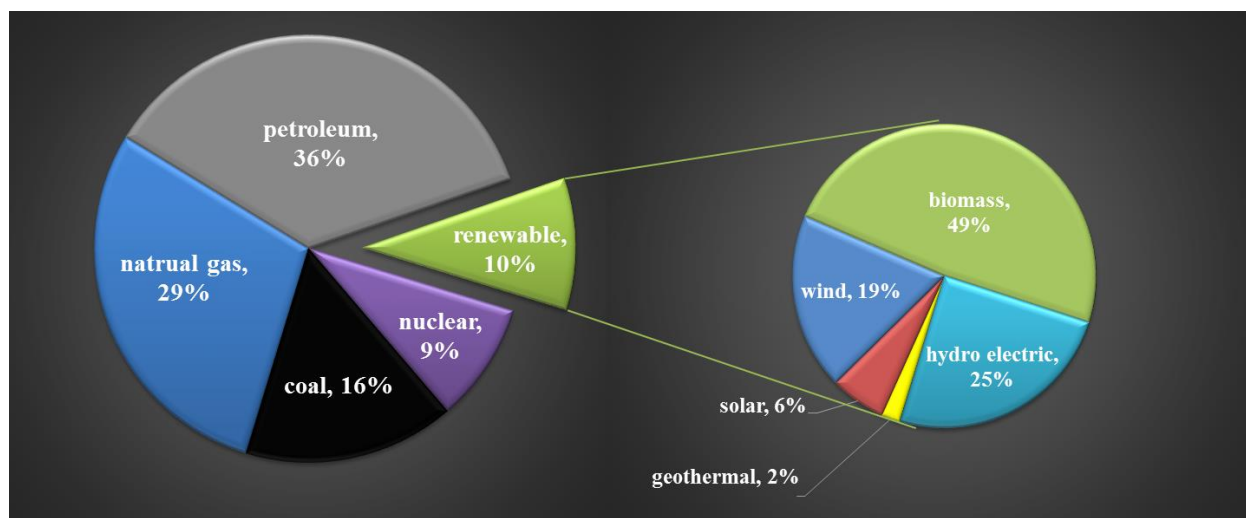


**Figure 1.** Energy consumption in the United States in 2015

deposition of heavy metals in the subsurface, and water shortages in certain areas are possible consequences of this technology.<sup>1</sup>

In addition to environmental concerns, increased utilization of shale gas in the United States has had a significant impact on the production of common chemicals. Specifically, the petrochemical feed has shifted from naphtha to cheap shale gas. Because the product stream is highly feedstock dependent, a significant decrease in propene (50 %), butadiene (30 %), and benzene (50 %) yields have been observed.<sup>1</sup> As important building blocks of the petrochemical industry, butadiene, propene, and benzene are used for many organic compounds and with no industrial relevant alternative to produce aromatics, there exists the a need to identify alternative sources for the production of these molecules.<sup>5,6</sup>

Biomass offers an abundant, carbon-rich raw material that could serve as a source for the synthesis of these compounds. Additionally, biomass is attractive due to increasing concerns about energy security, and environmental change from fossil fuel combustion.<sup>3,6</sup> Moreover, biomass has the inherent advantage of being a fast growing (relative to fossil fuel formation) renewable source



of carbon that can be transformed into fuels, chemicals, heat and power, which mitigates the release of carbon dioxide through cycles of regrowth and combustion.<sup>7</sup>

## 1.2 Biomass Conversion Strategies to Fuels and Chemicals

Biomass contains a number of different components that range from sugar (sucrose), starch, lignocellulosic biomass (cellulose, hemicellulose, lignin), to fats/oils, proteins, and minerals.<sup>8</sup> Starchy feedstocks, lignocellulosic feedstocks (Figure 2) and triglyceride feedstocks, are three general classes of biomass relevant for the production of renewable fuels and chemicals.<sup>7</sup> Triglycerides contain fatty acids and glycerol that find use in the production of biodiesel, personal care products, cosmetics, lubricants and surfactants.<sup>6,7</sup> The feedstock starch is composed of glucose units linked by  $\alpha$ -glycosidic bonds that can be easily hydrolyzed (enzymatically or chemically) into its monomeric subunits, which are then used in fermentation processes to produce bioethanol or bio-chemicals. In comparison to starch, cellulose is a rigid crystalline polymer that is comprised of glucose subunits that are linked via  $\beta$ -glycosidic bonds. While cellulose is a crystalline polymer comprised of C6 subunits, the hemicellulose fraction of biomass is an amorphous polymer that is built upon five different sugar monomers, D-xylose (most abundant), L-arabinose, D-galactose, D-glucose, and D-mannose. The most complex biomass polymer is lignin that is based on a complex phenolic structure, surrounding hemicellulose and cellulose. Lignocellulosic biomass is the most abundant part of the organic plant matter that contributes to the plants structural integrity and rigidity. Generally, lignocellulosic biomass entails about 25-30 % hemicellulose, 40-50 % cellulose, and 15-20 % lignin.<sup>7</sup> Due to its high abundance and moderate cost, it is considered as a very attractive feedstock in the production of biofuels and chemicals. Moreover, as the non-edible fraction of biomass, lignocellulosic biomass does not interfere with the production of food and feed.

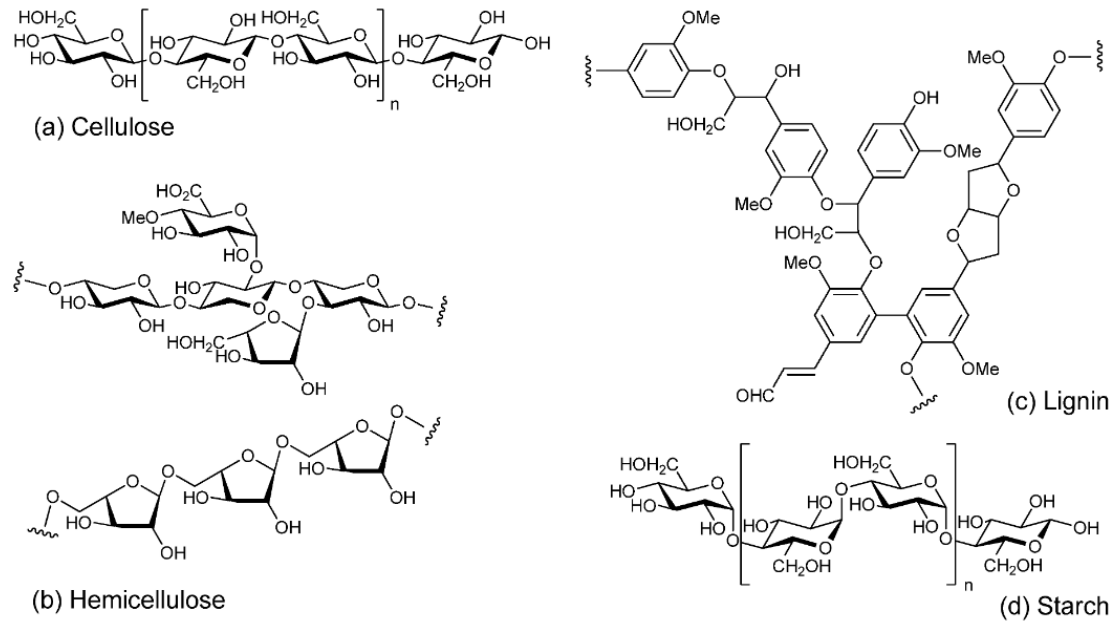


**Figure 2.** Chemical structures of (a) cellulose, (b) hemicellulose (top: glucuronoarabinoxylan and bottom: arabinan), (c) lignin, and (d) starch.<sup>9</sup>

There are two general routes for the production of fuels and chemicals from biomass that can be classified into thermochemical and biochemical conversion technologies. Thermochemical routes for the production of fuels and chemicals from biomass include gasification, pyrolysis and liquefaction (Figure 3).

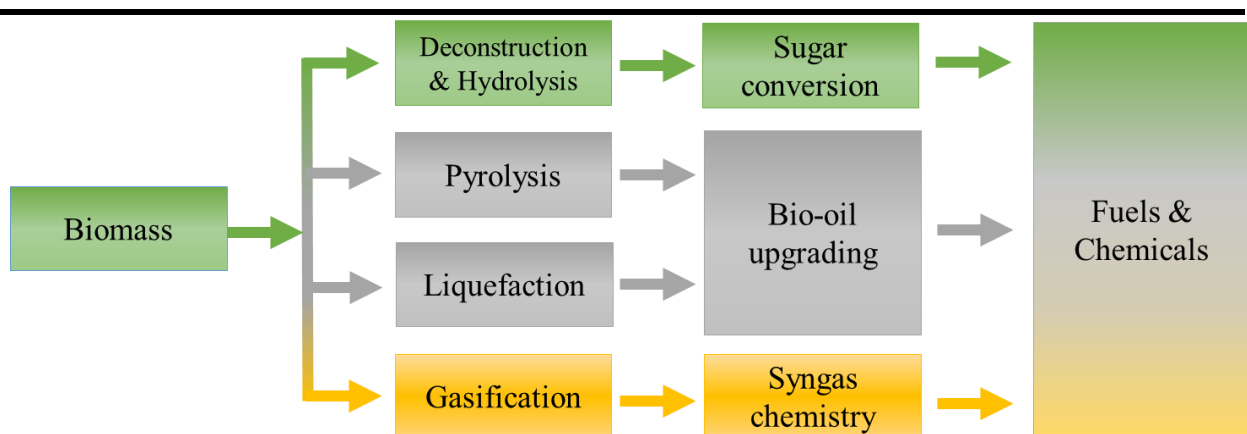


**Figure 3.** Biomass deconstruction and upgrading pathways.<sup>6</sup>

These processes convert lignocellulosic biomass at high temperatures and pressures to produce bio-oil and/or synthesis gas, which can be upgraded to higher value compounds.<sup>6-8</sup> In thermochemical conversion technologies, lignocellulosic biomass can be processed whole or first deconstructed into individual biomass fractions. Deconstruction is especially important when biochemical routes are envisioned, which are mainly based on C5 and C6 sugars isolated from biomass fractions such as starch, cellulose and hemicellulose. Both chemical (acid or base hydrolysis) and physical (milling, comminuting, and steam) pretreatment methods are used to permeate lignin and to extract hemicellulose and cellulose fractions. Further hydrolysis (enzymatically or chemically) of hemicellulose and cellulose gives access to the monomeric subunits xylose and glucose, respectively (Figure 3). These subunits are essential for the biochemical production of most renewable platform chemicals that can be further classified to bulk, fine, or specialty.

### **1.3 Platform Chemicals from Biomass**

In 2004 and updated in 2010, the Department of Energy (DOE) proposed a list of top value added chemicals derived from biomass.<sup>10,11</sup> (Figure 4). These “bio-based platform molecules” are synthesized through chemical or biochemical transformation of biomass and are essential to generate products that will afford a higher return on investment than transportation biofuels alone.<sup>12,13</sup> The C2, C3, C4, and C6 platform is of utmost importance to produce daily life consumer goods that are currently manufactured via petrochemical routes.

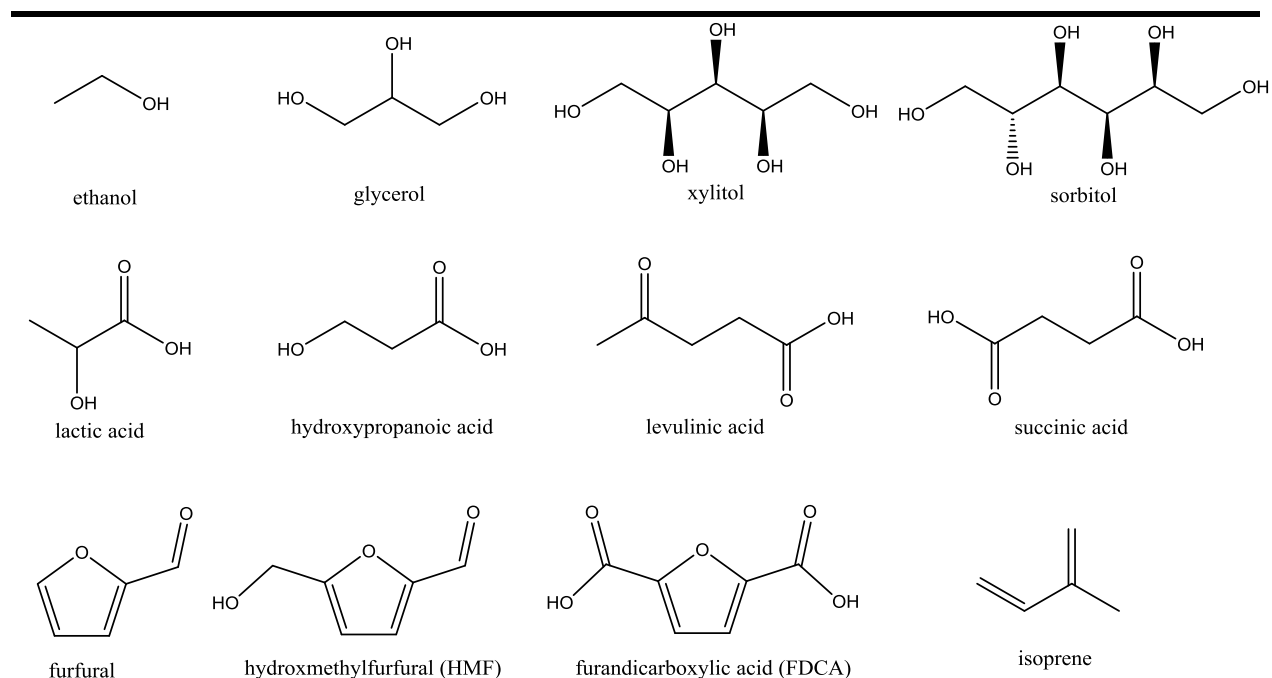


**Figure 4.** Proposed platform molecules

### 1.3.1 C2 Platform

In the petrochemical industry, ethylene is one of the most important building blocks obtained from petroleum fractions, natural gas, or shale gas.<sup>12</sup> It is used to manufacture commodity polymers such as polyethylene, poly ethylene terephthalate (PET), poly vinyl chloride (PVC), and polystyrene but also a wide variety of paints, adhesives and detergents.<sup>14</sup> Other important ethylene based bulk chemicals are acetic acid, dichlorethane, vinyl chloride, ethylene oxide, and many more.<sup>15</sup> In contrast, the biomass derived C2-platform is mainly built upon ethanol through fermentation of C5 and C6 sugars. Through catalytic conversion of bio-ethanol, ethylene becomes available providing a direct interface between the renewable biomass and the conversion infrastructure of the petrochemical industry. However, due to the current price of shale gas based ethane, the opportunity of bio-ethylene derivatives is limited.<sup>14</sup>

### 1.3.2 C3 Platform

Analogous to the petrochemical C3 platform which is built upon propylene, a renewable C3 platform can be accessed through chemical and biochemical pathways of biomass. Propylene is currently used to manufacture a broad range of chemicals such as acrylic acid, propylene oxide, propylene glycol and 1,4 butanediol.<sup>16</sup> An alternative to petrochemical derived propylene is the hydro-deoxygenation of glycerol to form propane, a coproduct of hydro treating vegetable oils and animal fats.<sup>17-19</sup> The subsequent dehydrogenation of propane produces renewable propylene. Alternatively, propylene can be obtained through dehydration of isopropanol and n-propanol that can be biochemically synthesized via fermentation.<sup>15</sup> Another renewable pathway to propylene is the gasification of biomass to syngas, followed by methanol synthesis, which can then be further upgraded to propylene via MTP (methanol to propylene) technology.<sup>20</sup> Finally, bio-ethanol dehydration to ethylene can be dimerized to give 1-butene. Through the isomerization-metathesis sequence of 1-butene and ethylene, propylene can be accessed.<sup>20</sup>

As a byproduct of biodiesel production, glycerol has become an economically relevant commodity<sup>11,12</sup> that generates a portfolio of value-added chemicals, particularly through reduction, dehydration, and fermentation.<sup>21-23</sup> Glycerol reduction through hydrogenolysis forms a family of derivatives including propylene glycol, ethylene glycol, acetol, and lactic acid.<sup>11</sup> Lactic acid is generally produced via fermentation of glucose. Its primary use is in the manufacture of polylactic acid (PLA) but also other industrially important products such as propylene glycol, acrylic acid and esters that can be obtained through catalytic conversion.<sup>11</sup>

Glycerol dehydration can also provide a variety of derivatives such as hydroxypropionaldehyde (3-HPA), and acrolein. Both are precursor of acrylic acid, a high volume chemical used for a wide array of end products. 3-HPA can also be converted to hydroxypropanoic

acid or 1,3-propanediol, an important polymer precursor for textiles and carpeting that can also be obtained through fermentation of glycerol<sup>24</sup> and glucose<sup>25</sup> with advanced genetically modified organisms.

### 1.3.3 C4 Platform

The biomass derived C4 platform can be accessed biochemically through anaerobic fermentation of sugars with *Clostridium acetobutylicum* and *Clostridium beijerinckii*, to obtain a mixture of acetone, butanol, and ethanol (ABE process).<sup>12,20</sup> Similarly, genetically engineered *E. coli* can produce alcohols, including isobutanol, 1-butanol, and 2-methyl-1-butanol are via the fermentation of glucose. Catalytic dehydration can be used to convert these butanol isomers to a variety of C4 olefins currently used in the chemical industry.<sup>12,26</sup> Another C4 platform is succinic acid, a very attractive bio-based molecule that can be biochemically synthesized via fermentation of bio-refinery sugars<sup>27</sup> using *Anaerobiospirillum succiniciproducens*<sup>28</sup>, genetically modified *Mannheimia succiniciproducens*<sup>29</sup>, or recombinant *E. coli*.<sup>30</sup> Succinic acid can be used in the synthesis of a wide array of chemicals such as succinate ester, 1,4-butanediol, tetrahydrofuran,  $\gamma$ -butyrolactone, and various pyrrolidinone derivatives as well as bio-based polymers such as nylons and polyesters.<sup>11</sup>

### 1.3.4 C5 and C6 Platform

The biomass derived C5 platform is mainly based on C5 sugars from the hemicellulose biomass fraction. The acid catalyzed dehydration of the C5 sugars xylose and arabinose produces furfural, a DOE identified platform molecule with an annual production of 200 kt.<sup>11</sup> Furfural is mainly used for the production of furfuryl alcohol<sup>15</sup>, which has applications in the manufacture of foundry resins with excellent chemical, thermal, and mechanical properties. It is also used to

produce synthetic fibers, rubber-resins, farm chemicals and chemical intermediates in the production of lysine, vitamin C, and dispersing agents.<sup>31-33</sup>

Isoprene, a C5 hydrocarbon mainly used for the production of polyisoprene rubber and butyl rubber is a high value hydrocarbon that is currently produced from petroleum.<sup>15</sup> Renewable alternative routes utilize bacteria from the *Bacillus* species to produce isoprene in high yields.<sup>34</sup>

Hydroxymethylfurfural (HMF) is synthesized via acid catalyzed dehydration of C6 sugars. Through chemical manipulation, HMF can be transformed into a portfolio of furan derivatives. Oxidation of HMF yields furan dicarboxylic acid (FDCA) which has been suggested as replacement for terephthalic acid (TPA) in the polymer industry.<sup>15</sup> HMF hydrogenolysis yields dimethyl furan (DMF), which can be used as a blender in transportation fuels<sup>7</sup> but finds also applications in the production of *p*-xylene<sup>35</sup>, an important aromatic building block in the manufacture of terephthalic acid and equally important dimethyl terephthalate.

Other renewable C5 and C6 technologies are based upon levulinic acid, xylitol, and sorbitol. Sorbitol is produced on a large scale from hydrogenation of glucose and finds application in the food industry. Other uses of sorbitol are in the manufacture of surfactants, polyurethanes, ascorbic acid, and isosorbide. Xylitol can be obtained from the hydrogenation of xylose, a C5 carbohydrate found in the biomass fraction hemicellulose. It is primarily used as a sustainable, naturally occurring sweetener.<sup>15</sup> Levulinic acid is obtained through acid treatment of C6 sugars and is of interest as a primary bio-refinery platform chemical. The formation of levulinic acid proceeds through dehydration of C6 sugars to HMF, which subsequently undergoes water mediated ring cleavage to form levulinic and formic acids.<sup>11,36</sup>

Despite these innovations, limited attention has been given to the renewable production of aromatics, one of the most important building blocks in the chemical industry. With a shortage of

aromatics induced through the shale gas revolution, a sole reliance on petroleum feedstocks can be problematic for the future manufacture of these chemicals. According to the U.S. Department of Energy, bio-based aromatic compounds have been identified with high priority for further investigation.<sup>10</sup> However, only a few renewable alternatives have been reported to access functionalized and non-functionalized aromatics from biomass. These can be broadly categorized into selective and non-selective biomass conversion technologies.

#### **1.4 Non-Selective Routes to Aromatics from Biomass**

Non-selective biomass technologies utilize all fractions of lignocellulosic biomass and are predominantly based on thermochemical conversion techniques such as gasification, pyrolysis, and liquefaction. Pyrolysis is the thermal depolymerization of lignocellulosic biomass in the absence of oxygen. High temperature in the range of 650 to 850 K generate more than 350 different compounds including acids, esters, ketones, and aromatics. During the pyrolysis process, vaporized biomass products react and are subsequently condensed into a liquid product called bio-oil. Liquefaction is a process where biomass is mixed with a solvent (generally water) and exposed to lower temperatures (525-725 K) but higher pressures (5-20 atm) to produce bio-oil.<sup>7</sup> Both pyrolysis and liquefaction produce bio-oils with high oxygen content. The introduction of a catalyst to the fast pyrolysis process, or catalytic fast pyrolysis, can increase selectivity and decrease oxygen content of the bio-oil. Depending on the lignocellulosic biomass fraction, HZSM-5 can produce a completely deoxygenated liquid product composed entirely of aromatics and other hydrocarbons. However, aromatic yields are low (20-30 % of biomass carbon) due to the formation of gases (mainly CO and CO<sub>2</sub>), coke and char.<sup>37-39</sup> Through structural modification of the zeolite such as bifunctional Ga/ZSM-5 catalyst, the aromatic yields can be increased.<sup>40</sup>



Based on catalytic fast pyrolysis, Anellotech developed a process to convert biomass such as wood waste, corn-stover and sugar cane bagasse into a mixture of BTX aromatics. Here, catalytic fast pyrolysis is performed in a fluidized bed reactor in which the biomass is rapidly heated in the absence of oxygen and transformed into a gas that is then catalytically upgraded into aromatic hydrocarbons.<sup>15</sup> Virent has developed a process that allows the manufacture of aromatics through aqueous phase reforming (APR) of a range of biomass feedstocks such as C5/C6 sugars, polysaccharides, organic acids, furfurals and other fractions of deconstructed biomass that are catalytically converted into a mixture of oxygenated hydrocarbons. Further upgrading of these intermediates over a modified ZSM-5 catalyst yields gasoline with high aromatic content.<sup>41</sup> From a technical perspective, aromatics from biomass can also be realized through a combination of technologies such as gasification followed by methanol synthesis, and a subsequent methanol-to-aromatics process.<sup>7,12,42,43</sup>

Utilizing biomass without fractionation into its subunits cellulose, hemicellulose and lignin gives thermochemical technologies a unique advantage compared to biochemical alternatives that require pretreatment of biomass to obtain C5 and C6 sugar monomers from hemicellulose and cellulose, respectively. On the contrary, thermochemical technologies have to face other challenges such as high water content in biomass that can influence the thermochemical processes.<sup>7,44</sup> Moreover, biomass contains impurities such as minerals that are detrimental to the catalyst and the removal of these impurities is required before catalytic upgrading is performed.<sup>6,7</sup> In addition, the high oxygen content of biomass produces oxygen-rich bio-oil that is unstable due to the presence of organic acids that can corrode steel vessels and piping. Hence, further upgrading through the use of catalysts is required in order to obtain a suitable petroleum or fuel replacement.<sup>7</sup> Similarly, gasification of biomass to syngas contains contaminants such as tar, particulate matter

and sulfur, chlorine and nitrogen compounds that must be removed before further catalytic transformation is envisioned.<sup>45</sup> Most importantly, no thermal processing technique selectively produces a single aromatic compound, limiting the feasibility of deriving chemicals from bio-oil or bio-syngas without significant improvements to upgrading and separation technologies.

## 1.5 Selective Routes to Aromatics from Biomass

The selective formation of bio-based aromatics is built upon upstream manipulation of C5 and C6 sugar based biomass fractions such as starch, cellulose, and hemicellulose. These fractions are obtained through pretreatment processes such as chemical or enzymatic hydrolysis that yield monomeric C5 and C6 subunits. This operation is more complex as compared to thermochemical conversion of raw feedstock and is thereby linked to higher cost.<sup>7</sup> Moreover, selective and high yielding formation of chemicals from sugars either biosynthetically or chemically is essential for the successful implementation of biomass as a raw material supply. From a biochemical perspective, this can be achieved through constant innovation of genetically engineered microorganisms to improve rate, titer, yield, product, and inhibitor tolerance of bioprocesses.<sup>46</sup> From a chemical perspective, this can be achieved through the development of new catalytic materials as biomass imposes new challenges including transport effects, catalytic activity, deactivation, and stability. Additionally, catalysts need to be selective in the presence of multiple functional groups and able to perform in the presence of unconventional solvents that are often required due to the unique properties of biomass derived molecules.<sup>6</sup> Finally, catalyst poisons such as biogenic impurities from fermentation processes need to be considered when new catalysts are designed.<sup>47</sup>

An elegant strategy to produce aromatics selectively was proposed by Arceo et al.<sup>48</sup> Here, bio-based benzoic acid (BA) synthesis is realized over formic acid mediated deoxygenation of

glucose derived quinic and shikimic acid. This process generates benzoic acid in very high yields (90 %) and is therefore an excellent renewable alternative to produce bio-based aromatics in a selective manner. Both quinic acid and shikimic acid can be obtained through fermentation of glucose using a recombinant *E. coli* biocatalyst.<sup>49</sup> Draths et al. engineered a shikimate-synthesizing *E. coli* that produced 27.2 g/L of shikimic acid, 12.6 g/L of quinic acid, and 4.4 g/L of 3-dehydroshikimic acid in 42 h. Further improvements through metabolic engineering yielded an *E. coli* strain that synthesized 60 g/L of quinic acid along with 2.6 g/L 3-dehydroquinic acid. Based on these observations, the yield of shikimic acid (14 %) and quinic acid (23 %) need further improvements to reach the maximum theoretical yield of 43 % from glucose based microbial synthesis<sup>49</sup>. In the last two decades, metabolic engineering innovations has led to overproducing shikimic acid *E. coli* strains with shikimic acid titers as high as 71 g/L associated to a 27 % shikimic acid yield.<sup>50</sup> High titers and yields are essential for the success of a biomass based synthesis strategy to manufacture useful chemicals from glucose.

Other biomass-derived aromatic synthesis routes have also been proposed. Microbial fermentation or direct chemical manipulation of C5 and C6 sugars followed by catalytic conversion have resulted in a portfolio biomass derived molecules such as DMF<sup>35,51-55</sup>, methyl furan<sup>56</sup>, furan<sup>35,57</sup>, HMF and oxidized HMF analogs<sup>58</sup>, butadiene<sup>59</sup>, isoprene<sup>60,61</sup>, acrylic acid<sup>57,60-62</sup>, muconic acid<sup>63,64</sup>, and sorbic acid<sup>65,66</sup>, etc., that can be utilized in the formation of functionalized and non-functionalized aromatics. The underlying principle of transforming these molecules into aromatics is founded on Diels-Alder chemistry.

### 1.5.1 Selective Formation of Aromatics via Diels-Alder Chemistry

The Diels-Alder reaction, first discovered in 1928 by Diels and Alder<sup>67</sup>, is one of the most powerful organic synthesis tools and is widely used to form complex six membered rings in a

regio- and stereo- controlled way. Its versatility makes the Diels-Alder cycloaddition a unique synthetic tool to construct simple and complex molecules. Since its discovery, extensive research yielded an array of Diels-Alder reactions such as, hetero-Diels-Alder, neutral-, normal-, and inverse electron-demand Diels-Alder reactions<sup>68</sup> that are based upon the same underlying principle, the formation of new carbon-carbon or carbon-heteroatom bonds. The reactivity of a Diels-Alder reaction is based upon the energy difference of the highest occupied molecular orbital (HOMO) and the lowest unoccupied molecular orbital (LUMO). A lower energy difference between the orbitals results in a lower transition state energy and thus the Diels-Alder reaction is favored. Electron donating or withdrawing substituents on the diene or dienophile can greatly enhance the rate of reaction. Withdrawing substituents lower the energy of both the HOMO and the LUMO, whereas donating substituents increase the HOMO and LUMO energy level. The withdrawing effect can be significantly enhanced when Lewis acid are deployed that coordinate with carbonyl oxygens and thereby increase the withdrawing effect.<sup>69</sup> Hence, the electronic mismatch of the orbitals can be altered to enhance the rate of reaction.

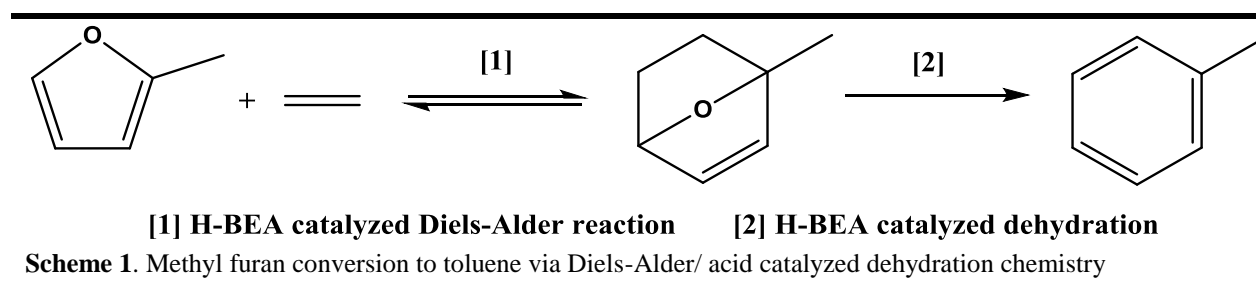
In a normal electron demand Diels-Alder (nEDDA) cycloaddition are usually limited to electron rich dienes and electron-poor dienophiles. The opposite is the case in an inverse electron demand Diels-Alder (iEDDA) reaction in which the diene is electron deficient and the dienophile electron-rich<sup>69,70</sup>. When the diene contains an electron-donating substituent and the dienophile an electron-withdrawing substituent, the nEDDA reaction is accelerated whereas an iEDDA reaction is accelerated when the diene contains an electron-withdrawing and the dienophile an electron-donating substituent.<sup>69,70</sup> This is governed by the electronics of the Diels-Alder reaction partner that allow for optimal orbital overlap.

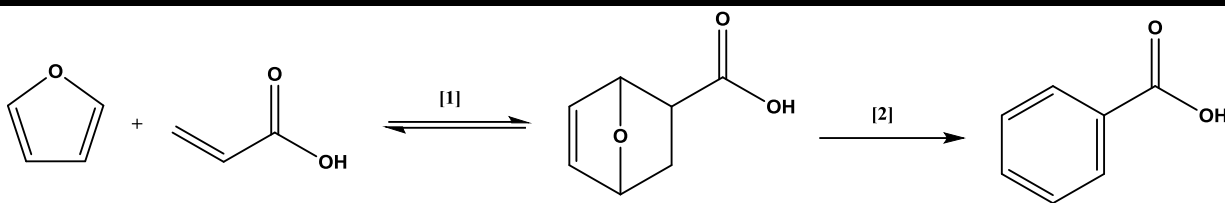
## 1.5.2 Selective Formation of Aromatics from Biomass Derived Furanics via Diels-Alder Chemistry

With an emerging bio-based economy, renewable platform chemicals such as furanic compounds (HMF, DMF, furan, and methyl furan) are of great interest in the production of aromatic chemicals such as BA, TPA, and BTX aromatics as these compounds are heavily used in the fuel industry, in consumer products and as precursors for polymers.<sup>35,53,57</sup> A sustainable source of aromatics is an excellent way to support the large demand of these petroleum based compounds. However, many biomass derived starting materials often suffer from low reactivity towards Diels-Alder cycloaddition.<sup>56-58,60,71,72</sup>

A perfect example is the reaction of biomass derived 2-methylfuran (obtained from furfural in high yield<sup>73</sup> (99.5 %)) with ethylene to form renewable toluene in a Diels-Alder/dehydration reaction cascade using H-BEA catalyst. This reaction, however, suffers from poor toluene selectivity that does not exceed 46 % as a result of simultaneous occurring side-reactions such as dimerization, trimer formation and ring-opening<sup>56</sup> (Scheme 1).

Another bio-based alternative to produce aromatics such as benzoic acid (BA), a product currently produced from petrochemical derived toluene, is the reaction of acrylic acid and furan. Here, acrylic acid is biochemically produced from glucose using *E. coli* in high yields (92 %)<sup>57</sup>. Bio-based furan on the other hand can be obtained through palladium catalyzed furfural





[1] Lewis acid zeolite catalyzed Diels-Alder reaction

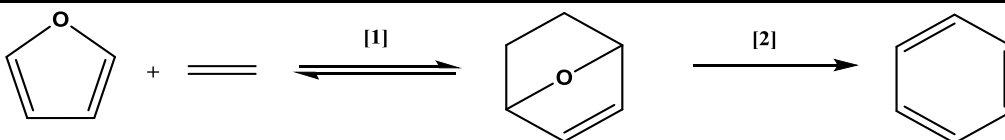
[2] Homogeneous acid catalyzed dehydration

**Scheme 2.** Furan conversion to BA via Diels-Alder/acid catalyzed dehydration chemistry

decarbonylation (>95 % selectivity)<sup>74</sup> using furfural that can be obtained from corn-stover (81 % furfural yield)<sup>75</sup>. A huge obstacle of the reaction between acrylic acid and furan, is that only moderate selectivities (43 %) of BA were achieved. Interestingly, using methyl acrylate instead of acrylic acid improved the overall selectivity (96 %) tremendously.<sup>57</sup>

Benzene is also accessible through similar chemistry starting with a Diels-Alder reaction of furan and ethylene followed by acid catalyzed dehydration that yields benzene with moderate selectivities of 35 % (Scheme 3). The substantial loss of carbon occurs through dimer and larger oligomer formation.<sup>35</sup>

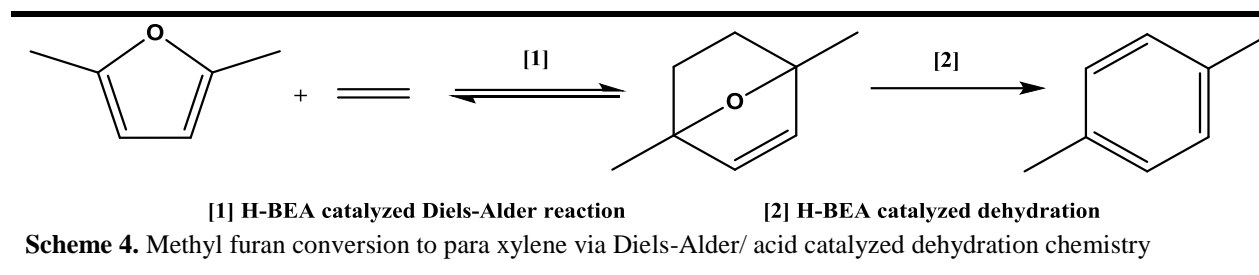
Using H-BEA zeolite, Chang et al. was able to synthesize renewable para xylene through a series of reactions in high yield (90 %) and selectivity (>90 %).<sup>35</sup> Here, ethylene and 2,5-dimethyl furan (DMF) were reacted via Diels-Alder cycloaddition followed by heterogeneous acid catalysed elimination of water (Scheme 4). A study performed by Román-Leshkov et al., showed that DMF can be produced in yields of up to 79 % through hydrogenolysis of HMF via a copper-ruthenium



[1] H-BEA catalyzed Diels-Alder reaction

[2] H-BEA catalyzed dehydration

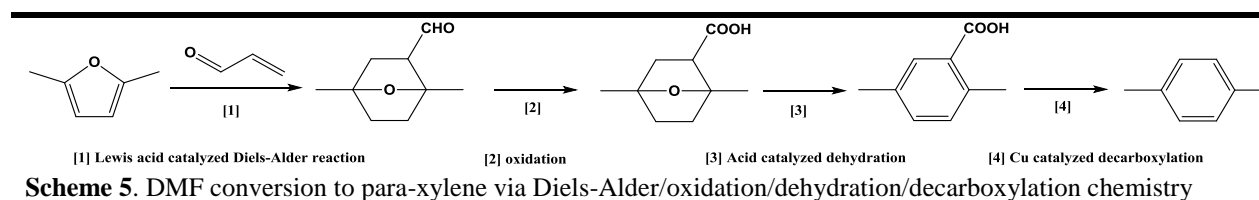
**Scheme 3.** Furan conversion to benzene via Diels-Alder/ acid catalyzed dehydration chemistry



catalyst.<sup>76</sup> Thus, the limiting step of the overall process is the hydrogenolysis of HMF to DMF.

Renewable *p*-xylene is of special interest as it can be utilized as drop-in replacement in the commercial production of TPA, which is a precursor of PET, a product exceeding annual global production of 50 million tonnes.<sup>13</sup> Thus, TPA is one of the most prevalent monomers in the chemical industry and has gained significant interest as a potential target for the bio-based chemical market.<sup>58,60-62,66,77,78</sup> Several research groups have devoted a great deal of attention towards bio-based TPA by investigating Diels-Alder transformations of numerous sugar based starting materials. For example, Shiramizu et al. developed a synthesis strategy to produce renewable *p*-xylene based on DMF and acrolein, both obtainable from biomass (Scheme 5).<sup>52</sup> This synthesis pathway consists of a sequential Diels-Alder reaction, oxidation, dehydration, and decarboxylation to obtain *p*-xylene with an overall yield of 34 %.

Pacheco et al. showed that oxidized variants of HMF undergo Diels-Alder reaction with ethylene followed by solid Lewis acid catalysed dehydration to produce TPA precursor.<sup>58</sup> This strategy, however, resulted in low to moderate selectivities of < 47 % and yields of < 24 %.

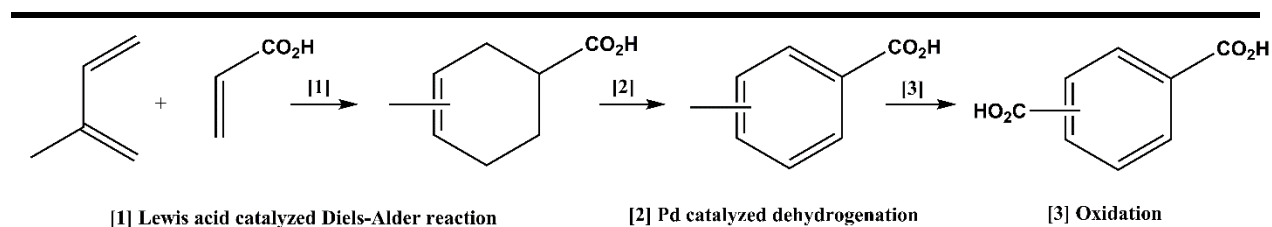


Instead of starting with a partially oxidized analog of HMF, requiring further oxidation of the reaction products to yield TPA, it was assumed that starting with FDCA would lead directly to TPA. However, this reaction afforded only negligible amounts of TPA at very slow rate of reaction.<sup>58</sup>

Additionally, HMF and furfural based technologies have the advantage that no fermentation step is required, which is often times challenging due to low titers, rates and yields. However, converting HMF to DMF, or oxidized variants of HMF requires additional steps that likely impact the overall selectivity of the process. The same applies for the concept of converting furfural to methyl furan or furan. More importantly, many of the furan based synthesis strategies still suffer from low overall selectivity and require further improvements to make these processes economically viable.

### 1.5.3 Selective Formation of Aromatics from Biomass Derived Chemicals via Diels-Alder Chemistry

Apart from the furan platform, Miller et al. selectively synthesized renewable aromatics based on isoprene and acrylic acid using homogeneous Lewis acids.<sup>60</sup> Both isoprene and acrylic acid can be obtained from biomass. In this work, it was shown that the un-catalyzed reaction between the diene isoprene and the dienophile acrylic acid underwent Diels-Alder cycloaddition



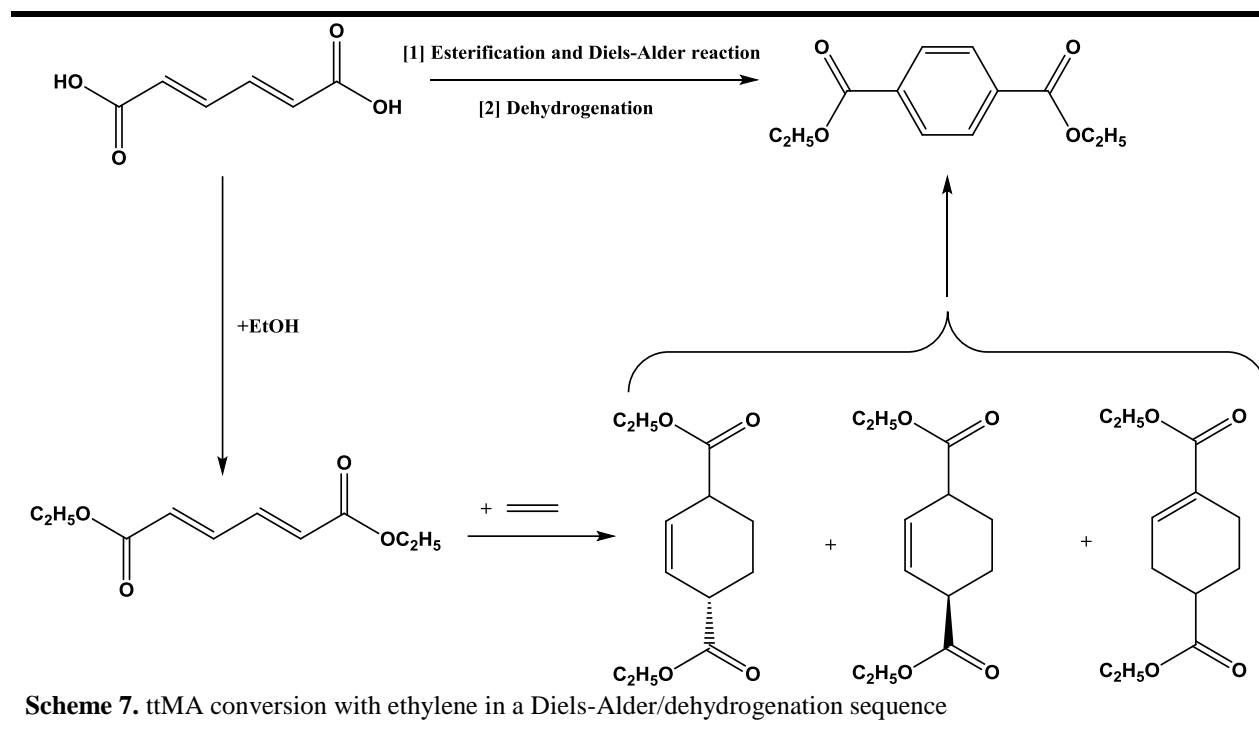
**Scheme 6.** Isoprene conversion to TPA using acrylic acid in a Diels-Alder/dehydrogenation/oxidation sequence



to methylcyclohex-3-ene-1-carboxylic acid isomers with a yield of 27 % and a para to meta-selectivity of 3:1. In contrast, the Lewis acid  $\text{TiCl}_4$ , significantly increased the reaction rate with better yields (94 %) and selectivity (23:1) in favor of the para isomer. Lowering the reaction temperature to 0 °C (48 h) further improved the selectivity to 37:1. Further dehydrogenation of the intermediates yield toluic acid isomers with a yield of *p*-toluic acid of 77 % that can be further oxidized to TPA (94 % yield) and isophthalic acid, two very important bulk chemicals in the petrochemical industry.

Wang et al. reported improved yield (80 %) and selectivity (100 %) towards the *p*-toluic acid intermediate starting from isoprene and acrylic acid utilizing the Lewis acid complex  $\text{BH}_3\text{-THF}$ . This reaction was followed by high yielding (91 %) dehydro-aromatization to *p*-toluic acid using concentrated sulfuric acid.<sup>61</sup>

Renewable TPA can also be obtained from trans-trans muconic acid via a Diels-Alder reaction with ethylene followed by dehydrogenation. Starting with cis-cis muconic acid synthesized through microbial fermentation<sup>79</sup>, trans-trans muconic acid is obtained in two isomerization steps. First, cis-cis muconic acid is isomerized to cis-trans muconic acid followed by a second isomerization step to trans-trans muconic acid (ttMA). This transformation is necessary to obtain the Diels-Alder active s-cis conformation of muconic acid. After isomerization was completed, ttMA was utilized and reacted with ethylene to yield TPA intermediates with a high selectivity (96 %). Subsequent palladium catalyzed dehydrogenation yields 55 % TPA and 45 % fully hydrogenated TPA.<sup>64</sup> A recent study was published reporting improved yields and selectivities in the formation of diethyl terephthalate. In this work, ttMA and ethylene were reacted in ethanol, which provided superior solubility of muconic acid resulting in 99 % selectivity towards



the cycloadduct (Scheme 7). The Diels-Alder reaction was followed by palladium catalyzed dehydrogenation to yield 80.6 % diethyl terephthalate.<sup>63</sup>

Although the isomerization of cis-cis muconic acid (ccMA) to ttMA resulted in isolated yields of up to 90 %, unfavorable reaction conditions are required making this process less appealing.<sup>80</sup> Concerning the muconic acid production, Frost and Draths reported titers as high as 36.8 g/L and yields of 22 % ( $\text{mol}_{\text{ccMA}}/\text{mol}_{\text{glucose}}$ ) in 1996.<sup>79</sup> Over a decade later, advances in metabolic engineering led to increased muconic acid titers and yields of 59.2 g/L and 30 % ( $\text{mol}_{\text{ccMA}}/\text{mol}_{\text{glucose}}$ ), respectively.<sup>81</sup> With maximum theoretical glucose carbon yield of 86 %, muconic acid biosynthesis through the shikimate pathway still needs further enhancement.<sup>80</sup>

Alternatively, the TPA intermediate *p*-toluic acid (pTA) can be obtained by reacting sorbic acid and ethylene via a Diels-Alder cycloaddition. High pressures (40 bar) and long reaction times (40 h) are required to achieve with high selectivity the Diels-Alder adduct, which can then be

dehydrogenated using palladium to get pTA. However, pTA selectivity through this process does not exceed 41 %.<sup>65</sup> Banella *et al.* reacted sorbic acid with acrylic acid to form a diacid intermediate following a 4 h reaction at 140 °C that resulted in high selectivity at complete conversion of the limiting reactant. Subsequent dehydro-aromatization utilizing concentrated sulfuric acid resulted in high pTA yield (86 %).<sup>66</sup> Although alternative routes to aromatics exist starting from isoprene, sorbic acid and muconic acid, many of these synthesis strategies have significant draw backs such as low overall selectivity and operate under unfavorable reaction conditions requiring further improvements to be economically appealing.

#### 1.5.4 Selective Formation of Aromatics from Biomass Derived 2-Pyrones via Diels-Alder Chemistry

Another class of molecules that can be successfully transformed into aromatics are 2-pyrones. 2-pyrones are ideal for Diels-Alder chemistry due to their predetermined s-cis configuration of the conjugated double bonds. The 2-pyrone coumalic acid (CMA) and its derivatives have received special interest and are the subject of extensive research due to the potential to serve as a bio-based platform molecule. CMA is obtained from acid catalyzed dimerization of malic acid in high yields (86 %).<sup>84</sup> Malic acid can be produced via fermentation

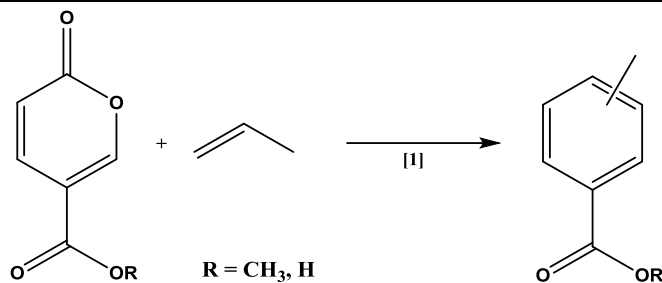
**Table 1.** The conversion of CMA and MeCMA to aromatics using alkenes via Diels-Alder/ decarboxylation/ dehydrogenation chemistry

Substrate	MeCMA conversion		Substrate	CMA conversion	
	Yield (%)	R group		Yield (%)	R group
1-Nonane	52	-(CH <sub>2</sub> ) <sub>6</sub> CH <sub>3</sub>	1-Heptene	85	-(CH <sub>2</sub> ) <sub>5</sub> CH <sub>3</sub>
1-Decane	70	-(CH <sub>2</sub> ) <sub>7</sub> CH <sub>3</sub>	1-Decane	72	-(CH <sub>2</sub> ) <sub>7</sub> CH <sub>3</sub>
1-Undecane	63	-(CH <sub>2</sub> ) <sub>8</sub> CH <sub>3</sub>	1-Undecane	69	-(CH <sub>2</sub> ) <sub>8</sub> CH <sub>3</sub>
1-Allyl benzene	83	-CH <sub>2</sub> Ph	1-Allyl benzene	79	-CH <sub>2</sub> Ph
Ally phenyl ether	61	-CH <sub>2</sub> OPh	Ally phenyl ether	65	-CH <sub>2</sub> OPh
Ally heptyl ether	51	-CH <sub>2</sub> O(CH <sub>2</sub> ) <sub>6</sub> CH <sub>3</sub>	Ally heptyl ether	66	-CH <sub>2</sub> O(CH <sub>2</sub> ) <sub>6</sub> CH <sub>3</sub>

using a metabolic engineered *S. cerevisiae* microorganism that is able to afford a theoretical yield of 2 mol malate per mol glucose.<sup>82</sup> This unique pathway proceeds via carboxylation of pyruvate, followed by reduction of oxaloacetate to malate yielding a redox- and ATP-neutral, CO<sub>2</sub> fixing pathway. Through further metabolic engineering, Novozymes developed a microorganism (*aspergillus oryzae*) that produces 1.38 mol malate per mol glucose (theoretical yield of 69 %) with astonishing high titers of 154 g/L.<sup>83</sup> High titer, yield, and rate are essential for the success of a biomass based platform. Moreover, the unique CO<sub>2</sub> fixating metabolic pathway to produce malate from glucose can mitigate the carbon loss obtained from the dimerization step to yield CMA, which is from carbon efficiency perspective desirable.

Since first reported in 1931<sup>84</sup>, CMA research has grown into a portfolio of bio-based aromatics.<sup>62,78,85-87</sup> Kraus et al. synthesized a series of aromatics from CMA and methyl coumalate (MeCMA) with a number of different alkenes<sup>87</sup> (Table 1). In this study it was shown that in the presence of a Pd/C catalyst exclusively the para isomer was formed with global yields between 51 and 85 %. In these reactions it is evident that steric effects of the dienophile guided the reaction towards the para product exclusively

Further exploration of the coumalate platform resulted in pTA, a TPA precursor. Reacting CMA with the olefin propylene (Scheme 8) in the presence of Pd/C can produce pTA in high yield (76 %).<sup>88</sup> Similar results were obtained when MeCMA was exposed to propylene with slightly higher yields of 79 %.<sup>88</sup> It is intriguing, that only the para substituted isomer was observed providing evidence that electronic effects are imposed upon the regioselective formation of Diels-Alder adducts. This is supported by the fact that the methyl group is one of the least sterically demanding functional groups giving less reason to believe this outcome is solely of steric nature.

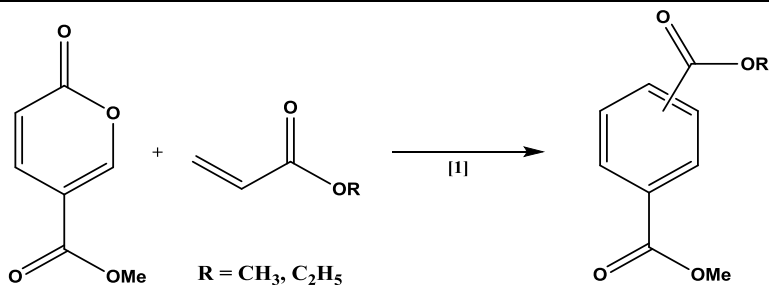


[1] Diels-Alder/decarboxylation,dehydrogenation sequence

**Scheme 8.** The conversion of MeCMA with propylene via a Diels-Alder/decarboxylation/dehydrogenation sequence

---

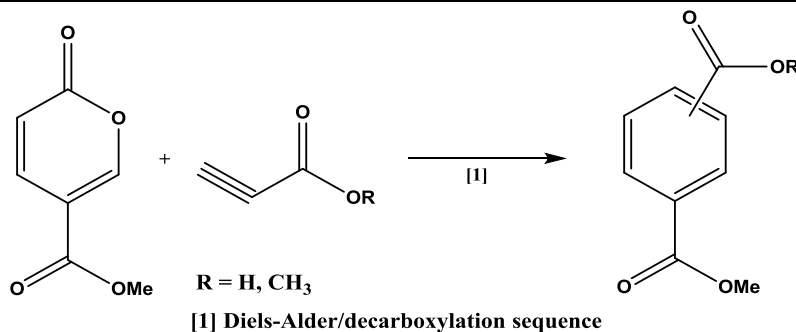
When the dienophiles were changed from alpha olefins to activated alkenes such as methyl or ethyl acrylate, a substantial shift in the product distribution was observed. Here, MeCMA reacted with methyl acrylate and ethyl acrylate to obtain 25 % and 35 % yields of 1,3- and 1,4- substituted aromatics, respectively (Scheme 9). Interestingly, with activated alkenes such as methyl- and ethyl acrylate a para to meta ratio of 3:1 was observed in both cases. Changing the system to activated alkynes such as propiolic acid and its methyl ester has the advantage that no dehydrogenation catalyst is needed (Scheme 10). Thus, Kraus et al. reacted propiolic acid and methyl propiolate with MeCMA yielding 64 % and 58 % of a mixture of 1,3- and 1,4- substituted aromatics, respectively, with a para to meta ratio of 1:1 in both cases.<sup>62</sup>



[1] Diels-Alder/decarboxylation/dehydrogenation sequence

**Scheme 9.** The conversion of MeCMA with methyl- and ethyl acrylate via a Diels-Alder/decarboxylation/dehydrogenation sequence

---

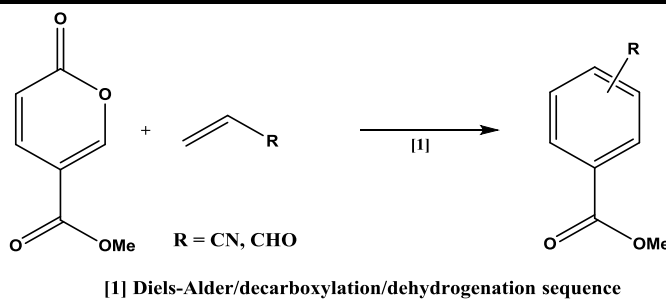


**Scheme 10.** The conversion of MeCMA with propionic acid and methyl propiolate via a Diels-Alder/decarboxylation/dehydrogenation sequence

---

Better regioselectivity was observed when the reaction was conducted with acrylonitrile with a global aromatic yield of 60 % and a para to meta ratio of 1.7:1. The selectivity towards the para substituted product was further enhanced by deploying the dienophile acrolein that afforded 47 % yield with a ratio of 4.3:1 (Scheme 11).

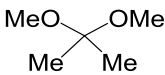
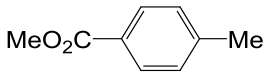
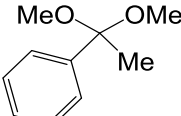
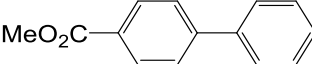
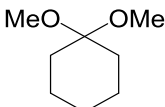
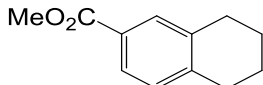
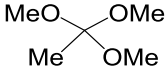
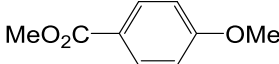
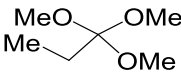
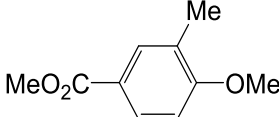
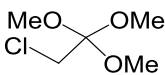
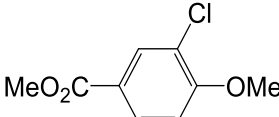
From these and previous findings it is evident, both steric and electronic effects play an influential role in the formation of aromatic regioisomers starting from the coumalate platform. Similarly, Lee *et al.* demonstrated a methodology which employs methyl coumalate with substituted cyclic vinyl ethers, ketals, and orthoesters to generate a broad spectrum of diverse aromatic systems.<sup>86</sup> This high yielding and regioselective approach delivers substituted aromatic molecules in a one-pot experimental procedure without the use of expensive Pd/C catalyst taking advantage of in-situ



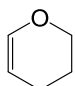
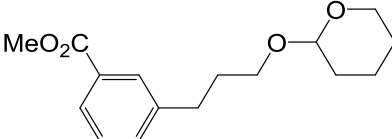
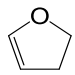
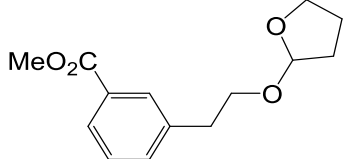
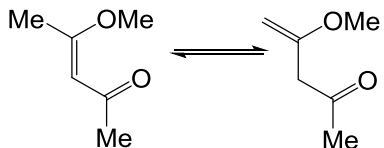
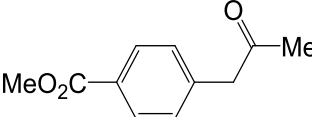
**Scheme 11.** The conversion of MeCMA with acrolein and acrylonitrile via a Diels-Alder/decarboxylation/dehydrogenation sequence

---

aromatization (Table 2 and 3).

Entry	Ketal or orthoester	Aromatic product	Yield (%)
1			89
2			85
3			81
4			73
5			94
6			72

**Table 2.** The conversion of MeCMA with ketals and orthoesters via a Diels-Alder/decarboxylation/dehydrogenation sequence<sup>86</sup>

Entry	Vinyl ether	Aromatic product	Yield (%)
1			77
2			61
3			79

**Table 3.** The conversion of MeCMA with vinyl ethers via a Diels-Alder/decarboxylation/dehydrogenation sequence<sup>86</sup>

## 1.6 Selective Routes to Novel Intermediates from Biomass

Despite the heavy focus on low cost high volume bulk chemicals from biological-derived intermediates, it is of great interest to broaden the bio-product scope with unique and novel chemicals that cannot be easily accessed from petrochemicals and have therefore gained little or no attention. As such, new and novel molecules can further expand the horizon of biomass-derived chemicals and are of potential interest in the development of next-generation nutraceuticals, pharmaceuticals consumer goods, specialty chemicals, *etc.* This can be achieved through chemical diversification of biological-derived intermediates providing access to a plethora of new and novel chemical species. Unlike “bio-based platform chemicals” that exclusively target drop-in replacements of existing petrochemicals, these novel molecules (also denoted as “bioprivileged molecules”)<sup>89</sup> cannot be effectively accessed via conventional petroleum based feedstocks and impart new or enhanced performance properties to current market products. Another attribute of bioprivileged molecules is the chemical diversity that grants access to other valuable species in an efficient way with a minimal number of transformation steps and high atom efficiency.<sup>89</sup> A notable example for a bioprivileged molecule is triacetic acid lactone (TAL), a compound natively produced by the plant *Gerbera hybrida*.<sup>90</sup> TAL can be biosynthetically synthesized through the metabolic pathway 2-pyrone synthase (2-PS) using genetically modified *Escherichia coli* and *Saccharomyces cerevisiae*.<sup>91-93</sup> The chemical diversity of TAL spans from commodity chemicals such as 2,4-pentanedion, sorbic acid and 1,3-pentadiene to specialty high value chemicals such as 3-alkyl pyrones, styrenylpyrones, 4-amino-2-pyrones, 4-hydroxy-2-pyridones, pogostone and other pogostone analogs with wide-ranging applications (e.g. food additives, antimicrobial activity, anti-obesity, anti-inflammatory, etc.).<sup>94-98</sup> As such, TAL provides all attributes of a bioprivileged candidate demonstrated through the versatile accessibility of new and interesting



molecules that would have scarcely received attention from the view of petroleum oriented retrosynthesis.

## 1.7 Conclusion

Petrochemicals are utilized in daily consumer goods across different market sectors and are prevalent especially in the form of aromatic compounds. With an increasing demand of fossil fuels, a raw material source whose availability will unambiguously expire in the not too far future, increasing prices are likely that can trigger unforeseeable events. A change in the feedstock supply away from petroleum can in part already be observed in the United States where naphtha is increasingly replaced by cheap shale gas, resulting in a decreased supply of BTX aromatics and other important petrochemical feedstocks. To ameliorate this problem, alternative resources are taken into consideration to supply the need of basic chemicals. These considerations are based upon thermochemical and biochemical routes to convert biomass into a range of products and energy. Thermochemical routes produce a broad array of chemicals, which further upgraded can be used as transportation fuels and are therefore not applicable for the selective formation of single aromatic compounds unless further fractionation is applied. Biochemical routes are shown to be more selective towards single molecules. Thus, the DOE proposed a list of platform molecules to generate a plethora of useful chemicals. However, less attention has been paid to synthesis strategies that aim the production of valuable aromatics and valuable intermediates. Today, only a few aromatic routes offer selective formation of aromatics. Other synthesis strategies are still facing significant limitations that arise from microbial synthesis of biomass derived sugars due to low titer, yield, and rate towards the desired chemicals. Also, catalytic conversion of sugars or fermentation products are often accompanied by low selectivity and yield.

To further expand the prospects of biomass derived aromatics and novel intermediates, new innovative processes are necessary to create sustainable and profitable chemicals from biomass. Predestined through its inherent functionality, CMA quickly entered the realm of biodiversity and created a broad array of functionalized aromatics and novel intermediates. Further supported through extraordinary results in microbial synthesis of malate, CMA can be excessed in large quantities, which is essential when larger production scales are envisioned. Even more appealing, is that metabolic engineering afforded a microorganism that is able to fixate CO<sub>2</sub>, which is from an atom economy perspective favorable. The Kraus group at Iowa State University guided the 2-pyrones coumalic acid and its methyl ester to its present success showing that coumalates are perfect candidates for diversification into a wide array of bio-based chemicals with high yielding synthesis strategies.

Despite the successful implementation of long chain alpha olefins that resulted high yields and only the 1,4-substituted aromatic isomer selectively, limitations were observed when coumalates were jointed with activated dienophiles that resulted in limited aromatic yield with undesired product distributions due to the regioselective nature of the Diels-Alder reaction. Accompanied by often high prices of some of the dienophiles (acrylic acid, acrolein, vinyl ethers), is from an economic point of view less attractive when cheap bulk aromatics such as TPA or BA are targeted. Moreover, performing the reaction with long chain alpha olefin puts another constrain on the overall process as the long alkyl chain has to be oxidized in order to obtain TPA, which is from an atom economy standpoint less desirable. Using propylene instead yielded pTA exclusively in high yield, which was unexpected given that the methyl group is one of the less sterically demanding functional groups and is therefore less likely to direct the regioselectivity to only the 1,4- substituted aromatic compounds. Hence, the fundamental understanding of the Diels-Alder/

decarboxylation/ dehydrogenation reaction network is essential to further steer the selectivity towards the product of interest. Based on the principle of an environmentally benign and carbon efficient overall process and given the scientific insights into numerous Diels-Alder synthesis strategies, the coumalate platform in combination with cheap and readily accessible alpha olefins might be a great alternative to manufacture cost competitive aromatics and other value-added intermediates.

## 1.8 Thesis Outline

In recent years, significant effort has been devoted to develop thermochemical and biochemical routes to produce biomass derived chemicals and fuels. With biochemical routes many biomass derived chemicals became accessible based on a few platform molecules such as ethanol, glycerol, HMF, sorbitol, lactic acid, succinic acid, and so forth. However, less attention has been given to the development of selective routes to produce value-added functionalized aromatic molecules and value-added intermediates. In an effort to develop selective synthesis strategies to produce functionalized aromatics and other unique bio-based molecules, this document presents four studies that are based on the biomass-derived 2-pyrone platform coumalic acid (or methyl coumalate). The first chapter provides background and a literature review of relevant topics. The second chapter explores the reaction network of the formation of *p*-toluic acid from coumalic acid and propylene. Chapter three provides detailed insights into the selective formation of benzoic acid and derivatives from the coumalic acid reaction with ethylene. The fourth chapter offers three new and alternative coumalic acid diversification pathways through solvent and catalytic pathway modifications of the Diels-Alder cycloadduct from coumalic acid and ethylene using various solvent and inexpensive and abundant catalytic materials such as zeolites, alumina, Amberlyst, and metals supported on gamma alumina. Chapter five provides a

combined in-depth kinetic and DFT analysis of the formation of methyl toluate acid from methyl coumalate and propylene which led to the development of an improved toluic acid (or methyl toluate) process. This development was in part guided through the knowledge obtained from previous chapters. Chapters two, three, four and five are stand-alone manuscripts and are formatted as such. Finally, chapter six provides a general conclusion and future directions.

## 1.9 References

1. Wagemann, K. *Chem. Bio. Eng. Rev.* 2015, **2**, 315-334.
2. American Chemical Society National Historic Chemical Landmarks. "Acetyl Chemicals from Coal Gasification." <http://www.acs.org/content/acs/en/education/whatischemistry/landmarks/chemicalsfromcoal.html> (accessed, December 10, 2016).
3. Energy Information Administration, "International Energy Outlook 2016." U.S. Department of Energy, August 2016
4. Energy Information Administration, "Energy Explained Your Guide To Understanding Energy." U.S. Department of Energy [http://www.eia.gov/energyexplained/index.cfm?page=us\\_energy\\_home](http://www.eia.gov/energyexplained/index.cfm?page=us_energy_home) (accessed, December 10, 2016 )
5. Brown, R. C.; Brown, T. R. *Biorenewable resources: engineering new products from agriculture*. John Wiley & Sons, 2013.
6. Behrens, M.; Datye, A. K.; *Catalysis for the Conversion of Biomass and Its Derivatives*. epubli, Berlin, Germany, 2013.
7. Alonso, D. M.; Bond, J. Q.; Dumesic, J. A. *Green Chem.* 2010, **12**, 1493-1513.
8. Bos, H. L.; Sanders, J. P. M. *Biofuel. Bioprod. Bior.* 2013, **7**, 246-259.
9. Kobayashi, H.; Ohta, H.; Fukuoka, A. *Catal. Sci. Technol.* 2012, **2**, 869-883.
10. Werpy, T.; Petersen, G.; Aden, A.; Bozell, J.; Holladay, J.; White, J.; Manheim, A.; Eliot, D.; Lasure, L.; Jones, S. *Top value added chemicals from biomass. Volume 1-Results of screening for potential candidates from sugars and synthesis gas*. No. DOE/GO-102004-1992. U.S. Department of Energy Washington DC, 2004.
11. Bozell, J. J.; Petersen, G. R. *Green Chem.* 2010, **12**, 539-554.

12. de Jong, E.; Jungmeier, G. "Biorefinery Concepts in Comparison to Petrochemical Refineries." *Industrial Biorefineries & White Biotechnology*. Elsevier, Amsterdam, 2015; pp 3-33.
13. Sheldon, R. A. *Green Chem.* 2014, **16**, 950-963.
14. Nexant, "Renewable Chemicals and Materials Opportunity Assessment." U.S. Department of Agriculture, January 2014.
15. de Jong, E.; Higson, A.; Walsh, P.; Wellisch, M. Bio-based chemicals value added products from biorefineries. *IEA Bioenergy, Task42 Biorefinery*. 2012.
16. Haveren, J. v.; Scott, E. L.; Sanders, J. *Biofuel. Bioprod. Bior.* 2008, **2**, 41-57.
17. Dinjus, E.; Arnold, U.; Dahmen, N.; Höfer, R.; Wach, W., Green Fuels – Sustainable Solutions for Transportation, in R. Höfer, ed., Sustainable Solutions for Modern Economies, RSC Publishing, Cambridge, 2009
18. Egeberg, R. G.; Michaelsen, N. H.; Skyum, L.; Topsoe, H. Presented at ERTC, 2009, Nov. 9-11.
19. Huber, G. W.; O'Connor, P.; Corma, A. *Appl. Catal., A*. 2007, **329**, 120-129.
20. Mathers, R. T. *J. Polym. Sci. A Polym. Chem.* 2012, **50**, 1-15.
21. Behr, A.; Eilting, J.; Irawadi, K.; Leschinski, J.; Lindner, F. *Green Chem.* 2008, **10**, 13-30.
22. Johnson, D. T.; Taconi, K. A. *Environ. Prog. Sustain.* 2007, **26**, 338-348.
23. Pagliaro, M.; Ciriminna, R.; Kimura, H.; Rossi, M.; Della Pina, C. *Angew. Chem. Int. Ed.* 2007, **46**, 4434-4440.
24. Cameron, D. C.; Altaras, N. E.; Hoffman, M. L.; Shaw, A. J. *Biotechnol. Prog.* 1998, **14**, 116-125.
25. Laffend, L. A.; Nagarajan, V.; Nakamura, C. E. "Bioconversion of a fermentable carbon source to 1,3-propanediol by a single microorganism." U.S. Patent No. 5,686,276. 11 Nov. 1997.
26. Taylor, J. D.; Jenni, M. M.; Peters, M. W. *Top. in Catal.* 2010, **53**, 1224-1230.
27. Bechthold, I.; Bretz, K.; Kabasci, S.; Kopitzky, R.; Springer, A. *Chem. Eng. Technol.* 2008, **31**, 647-654.
28. Meynial-Salles, I.; Dorotyn, S.; Soucaille, P. *Biotechnol. Bioeng.* 2008, **99**, 129-135.
29. Lee, S. J.; Song, H.; Lee, S. Y. *Appl. Environ. Microbiol.* 2006, **72**, 1939-1948.
30. Sanchez, A. M.; Bennett, G. N.; San, K. Y. *Biotechnol. Progr.* 2005, **21**, 358-365.

31. Jiménez-Gómez, C. P.; Cecilia, J. A.; Durán-Martín, D.; Moreno-Tost, R.; Santamaría-González, J.; Mérida-Robles, J.; Mariscal, R.; Maireles-Torres, P. *J. Catal.* 2016, **336**, 107-115.
32. Chen, X.; Li, H.; Luo, H.; Qiao, M. *Appl. Catal., A*. 2002, **233**, 13-20.
33. Nagaraja, B. M.; Padmasri, A. H.; David Raju, B.; Rama Rao, K. S. *J. Mol. Catal. A: Chem.* 2007, **265**, 90-97.
34. Kuzma, J.; Nemecek-Marshall, M.; Pollock, W. H.; Fall, R. *Curr. Microbiol.* 1995, **30**, 97-103.
35. Chang, C.-C.; Green, S. K.; Williams, C. L.; Dauenhauer, P. J.; Fan, W. *Green Chem.* 2014, **16**, 585-588.
36. Girisuta, B.; Janssen, L. P. B. M.; Heeres, H. J. *Chem. Eng. Res. Des.* 2006, **84**, 339-349.
37. Carlson, T. R.; Tompsett, G. A.; Conner, W. C.; Huber, G. W. *Top. Catal.* 2009, **52**, 241.
38. Karanjkar, P. U.; Coolman, R. J.; Huber, G. W.; Blatnik, M. T.; Almalkie, S.; Bruyn Kops, S. M.; Mountziaris, T. J.; Conner, W. C. *AIChE J.* 2014, **60**, 1320-1335.
39. Wang, K.; Kim, K. H.; Brown, R. C. *Green Chem.* 2014, **16**, 727-735.
40. Cheng, Y. T.; Jae, J.; Shi, J.; Fan, W.; Huber, G. W. *Ang. Chem.* 2012, **124**, 1416-1419.
41. 2017.
42. Behrens, M.; Studt, F.; Kasatkin, I.; Kühn, S.; Hävecker, M.; Abild, F.; Nørskov, K.; Schlögl, R. *Methanol Synthesis over Cu/ZnO/Al<sub>2</sub>O<sub>3</sub>: The Active Site in Industrial Catalysis*; SLAC National Accelerator Laboratory (SLAC): 2012.
43. Wang, T.; Tang, X.; Huang, X.; Qian, W.; Cui, Y.; Hui, X.; Yang, W.; Wei, F. *Catal. Today* 2014, **233**, 8-13.
44. Jahirul, M. I.; Rasul, M. G.; Chowdhury, A. A.; Ashwath, N. *Energies* 2012, **5**, 4952-5001.
45. Brown, R. C.; Brown, T. R. "Why are we producing biofuels" Brownia LLC, Ames 2012.
46. Miller, J. A.; Nagarajan, V. *Trends Biotechnol.* 2000, **18**, 190-191.
47. Schwartz, T. J.; Brentzel, Z. J.; Dumesic, J. A. *Catal. Lett.* 2015, **145**, 15-22.
48. Arceo, E.; Ellman, J. A.; Bergman, R. G. *ChemSusChem* 2010, **3**, 811-813.
49. Draths, K. M.; Knop, D. R.; Frost, J. W. *J. Am. Chem. Soc.* 1999, **121**, 1603-1604.
50. Ghosh, S.; Chisti, Y.; Banerjee, U. C. *Biotechnol. Adv.* 2012, **30**, 1425-1431.

51. Williams, C. L.; Chang, C.-C.; Do, P.; Nikbin, N.; Caratzoulas, S.; Vlachos, D. G.; Lobo, R. F.; Fan, W.; Dauenhauer, P. J. *ACS Catal.* 2012, **2**, 935-939.
52. Shiramizu, M.; Toste, F. D. *Chem. Eur. J.* 2011, **17**, 12452-12457.
53. Do, P. T. M.; McAtee, J. R.; Watson, D. A.; Lobo, R. F. *ACS Catal.* 2012, **3**, 41-46.
54. Patet, R. E.; Nikbin, N.; Williams, C. L.; Green, S. K.; Chang, C.-C.; Fan, W.; Caratzoulas, S.; Dauenhauer, P. J.; Vlachos, D. G. *ACS Catal.* 2015, **5**, 2367-2375.
55. Chang, C.-C.; Je Cho, H.; Yu, J.; Gorte, R. J.; Gulbinski, J.; Dauenhauer, P.; Fan, W. *Green Chem.* 2016, **18**, 1368-1376.
56. Green, S. K.; Patet, R. E.; Nikbin, N.; Williams, C. L.; Chang, C.-C.; Yu, J.; Gorte, R. J.; Caratzoulas, S.; Fan, W.; Vlachos, D. G.; Dauenhauer, P. J. *Appl. Catal., B* 2016, **180**, 487-496.
57. Mahmoud, E.; Yu, J.; Gorte, R. J.; Lobo, R. F. *ACS Catal.* 2015, **5**, 6946-6955.
58. Pacheco, J. J.; Davis, M. E. *Proc. Natl. Acad. Sci.* 2014, **111**, 8363-8367.
59. Diesen, R. W.; Burdett, K. A.; Dixit, R. S.; King, S. S. T. "Process for the cyclodimerization of 1,3-butadienes to 4-vinylcyclohexenes." U.S. Patent No. 5,329,057. 12 Jul. 1994.
60. Miller, K. K.; Zhang, P.; Nishizawa-Brennen, Y.; Frost, J. W. *ACS Sustain. Chem. Eng.* 2014, **2**, 2053-2056.
61. Wang, F.; Tong, Z. *RSC Adv.* 2014, **4**, 6314-6317.
62. Kraus, G. A.; Pollock Iii, G. R.; Beck, C. L.; Palmer, K.; Winter, A. H. *RSC Adv.* 2013, **3**, 12721-12725.
63. Lu, R.; Lu, F.; Chen, J.; Yu, W.; Huang, Q.; Zhang, J.; Xu, J. *Ang. Chem.* 2016, **128**, 257-261.
64. Frost, J. W.; Miermont, A.; Schweitzer, D.; Bui, V. "Preparation of trans, trans muconic acid and trans, trans muconates." U.S. Patent No. 8,426,639. 23 Apr. 2013.
65. Bérard, S.; Vallée, C.; Delcroix, D. *Ind. Eng. Chem. Res.* 2015, **54**, 7164-7168.
66. Banella, M. B.; Gioia, C.; Vannini, M.; Colonna, M.; Celli, A.; Gandini, A. *ChemSusChem* 2016, **9**, 942-945.
67. Diels, O.; Alder, K. *Justus Liebigs Ann. Chem.* 1928, **460**, 98-122.
68. Liao, W.; Yu, Z.-X. *The J. Org. Chem.* 2014, **79**, 11949-11960.

69. Fringuelli, F.; Taticchi, A. *The Diels-Alder Reaction: Selected Practical Methods*. Wiley&Sons, 2002.
70. Corma, A.; García, H. *Chem. Rev.* 2003, **103**, 4307-4366.
71. Narayana Murthy, Y. V. S.; Pillai, C. N. *Synth. Commun.* 1991, **21**, 783-791.
72. Ipaktschi, J. *Z. Naturforsch.*, 1986, **41**, 496.
73. Burnett, L. W.; Johns, I. B.; Holdren, R. F.; Hixon, R. M. *Ind. Eng. Chem.* 1948, **40**, 502-505.
74. Ozer, R. "Vapor phase decarbonylation process." U.S. Patent No. 9,067,904, 2015. 30 Jun. 2015.
75. Alonso, D. M.; Wettstein, S. G.; Mellmer, M. A.; Gurbuz, E. I.; Dumesic, J. A. *Energy Environ. Sci.* 2013, **6**, 76-80.
76. Román-Leshkov, Y.; Barrett, C. J.; Liu, Z. Y.; Dumesic, J. A. *Nature* 2007, **447**, 982-985.
77. J. Sheehan, R. "Terephthalic acid, dimethyl terephthalate, and isophthalic acid." *Ullmann's encyclopedia of industrial chemistry* 2000.
78. Lee, J. J.; Kraus, G. A. *Green Chem.* 2014, **16**, 2111-2116.
79. Frost, J. W.; Draths, K. M. "Synthesis of adipic acid from biomass-derived carbon sources." U.S. Patent No. 5,487,987, 1996.
80. Averesch, N. J. H.; Krömer, J. O. *Metab. Eng. Commun.* 2014, **1**, 19-28.
81. Bui, V.; Lau, M. K.; Macrae, D. "Methods for producing isomers of muconic acid and muconate salts." U.S. Patent No. 8,809,583. 2011.
82. Zelle, R. M.; de Hulster, E.; van Winden, W. A.; de Waard, P.; Dijkema, C.; Winkler, A. A.; Geertman, J. M.; van Dijken, J. P.; Pronk, J. T.; van Maris, A. J. *Appl. Environ. Microbiol.* 2008, **74**, 2766-77.
83. Brown, S.; Bashkirova, L.; Berka, R.; Chandler, T.; Doty, T.; McCall, K.; McCulloch, M.; McFarland, S.; Thompson, S.; Yaver, D.; Berry, A. *Appl. Microbiol. Biotechnol.* 2013, **97**, 8903-8912.
84. Diels, O.; Alder, K. *European J. Org. Chem.* 1931, **490**, 257-266.
85. Lee, J. J.; Pollock III, G. R.; Mitchell, D.; Kasuga, L.; Kraus, G. A. *RSC Adv.* 2014, **4**, 45657-45664.
86. Lee, J. J.; Kraus, G. A. *Tetrahedron Lett.* 2013, **54**, 2366-2368.
87. Kraus, G. A.; Riley, S.; Cordes, T. *Green Chem.* 2011, **13**, 2734-2736.



88. Riley, S. J. *Chemistry from Nature: From Natural Products to Biorenewables*. Iowa State University, Ames, IA, 2011.
89. Shanks, B. H.; Keeling, P. L. *Green Chem.* 2017, **19**, 3177-3185.
90. Eckermann, S.; Schroder, G.; Schmidt, J.; Strack, D.; Edrada, R. A.; Helariutta, Y.; Elomaa, P.; Kotilainen, M.; Kilpelainen, I.; Proksch, P.; Teeri, T. H.; Schroder, J. *Nature* 1998, **396**, 387-390.
91. Saunders, L. P.; Bowman, M. J.; Mertens, J. A.; Da Silva, N. A.; Hector, R. E. *J. Ind. Microbiol. Biotechnol.* 2015, **42**, 711-721.
92. Xie, D.; Shao, Z.; Achkar, J.; Zha, W.; Frost, J. W.; Zhao, H. *Biotechnol. Bioeng.* 2006, **93**, 727-736.
93. Cardenas, J.; Da Silva, N. A. *Metab. Eng.* 2014, **25**, 194-203.
94. Chia, M.; Schwartz, T. J.; Shanks, B. H.; Dumesic, J. A. *Green Chem.* 2012, **14**, 1850-1853.
95. Kraus, G. A.; Basemann, K.; Guney, T. *Tetrahedron Lett.* 2015, **56**, 3494-3496.
96. Kraus, G. A.; Wanninayake, U. K. *Tetrahedron Lett.* 2015, **56**, 7112-7114.
97. Kraus, G. A.; Wanninayake, U. K.; Bottoms, J. *Tetrahedron Lett.* 2016, **57**, 1293-1295.
98. Wanninayake, U. K. Ph.D., Iowa State University, 2016.

## CHAPTER 2

## THE FORMATION OF P-TOLUIC ACID FROM COUMALIC ACID: A REACTION NETWORK ANALYSIS

*A paper published in Green Chemistry 2017, 19, 3263-3271*

Toni Pfennig,<sup>a,b</sup> Robert L. Johnson,<sup>a,b</sup> and Brent H. Shanks<sup>a,b</sup>

<sup>a</sup> Department of Chemical and Biological Engineering, Iowa State University, Ames, IA 50011, USA.

<sup>b</sup> NSF Engineering Research Center for Biorenewable Chemicals (CBiRC), Ames, IA 50011, USA.

## 2.1 Abstract

Diels-Alder cycloaddition of biomass-derived 2-pyrone coumalic acid (CMA) with propylene provides an alternative pathway to produce toluic acid (TA), a precursor to terephthalic acid (TPA) which is a key component in the manufacture of polyethylene terephthalate (PET). To maximize yield and selectivity of the preferred isomer *p*-toluic acid (*p*-TA) we herein report a detailed reaction network that was established through investigating the influence of the dehydrogenation catalyst, solvent, temperature and reaction time on the formation of *p*-/*m*-TA. We further provide experimental results showing that the inverse electron demand Diels-Alder (IEDDA)/decarboxylation cascade of the reaction of CMA with propylene was not influenced by the catalyst, and, therefore, was solely dependent on temperature. Evident from changes in the *p*-/*m*-ratio of TA decreasing from 6.91 to 4.43 with increasing temperature and reaction time, *p*-TA was both the thermodynamic and kinetically favored product. TA formation from CMA and propylene afforded an overall yield of > 85 mol%, using  $\gamma$ -valerolactone (GVL) as the primary solvent. Throughout the reaction network analysis we observed that the TA intermediates 3-/4-

methylcyclohexa-1,5-diene carboxylic acid were reactive towards by-product formation whereas TA was quite stable under reaction conditions. Henceforth, rapid dehydrogenation of the diene intermediates is crucial to maximize selectivity of the desired aromatic product. Lastly, CMA thermally decomposes under reaction conditions which was rapidly accelerated by having as low as 5 vol% water in the solvent, demonstrating the importance of water-free solvent to limit CMA decomposition and maximize product yield.

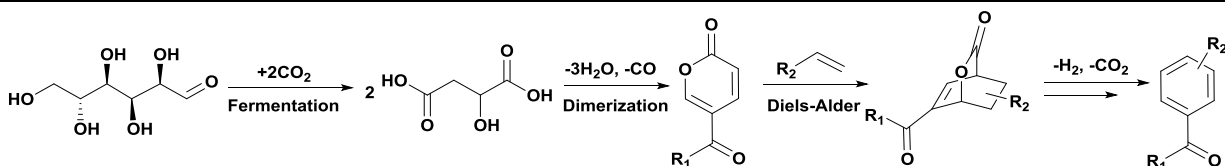
## 2.2 Introduction

As commodity chemicals are predominantly derived from fossil carbon new approaches using bio-based resources for the production of valuable chemicals has become of great interest in the field of green chemistry.<sup>1</sup> One consequence has been a noticeable shift in attention towards bio-based plastics in the last decade.<sup>2</sup> One of the most common thermoplastic polymers is polyethylene terephthalate (PET), which is used in beverage containers and fabrics.<sup>2-4</sup> PET is currently manufactured from terephthalic acid (TPA) and has reached an annual global production of over 50 million tons, corresponding to a \$58 billion/y market.<sup>1,4</sup> In addition to PET TPA is also used for several other applications such as dyes, synthetic perfumes, pharmaceuticals, pesticides and other chemicals.<sup>5</sup> TPA is commercially produced from the liquid phase oxidation of p-xylene using a catalyst combination of manganese, cobalt and bromine in glacial acetic acid.<sup>3,6,7</sup>

Recently, a strategy to partially produce PET from renewable biomass was developed in which sugar cane derived bioethanol was used to produce ethylene glycol.<sup>8</sup> The manufacturing of 100 % plant based PET, however, requires the replacement of petroleum derived p-xylene with its bio-based equivalent. Henceforth, several research groups have addressed this challenge by investigating Diels-Alder transformations of furanic compounds. For example, the reaction of ethylene and 2,5-dimethylfuran (DMF) followed by heterogeneous acid catalysed elimination of

water has been demonstrated to produce p-xylene.<sup>9-11</sup> Using an H-BEA zeolite, Chang et al. was able to achieve high yield (90 %) and selectivity (>90 %).<sup>10</sup> Alternatively, DMF can also be reacted with acrolein followed by oxidation, dehydration, and decarboxylation to produce p-xylene.<sup>12</sup> To further improve the prospects of a bio-based alternative for TPA, Pacheco et al. showed that oxidized variants of 5-hydroxymethylfurfural (HMF) undergo Diels-Alder reaction with ethylene followed by solid Lewis acid catalysed dehydration to produce intermediates to TPA and its important diester form, dimethyl terephthalate (DMT).<sup>13</sup> The oxidized HMF analogue FDCA (2,5-furandicarboxylic acid) for instance provides an attractive alternative to manufacture TPA directly via the aforementioned Diels-Alder/Lewis acid catalysed dehydration cascade. Unfortunately, the reaction of FDCA with ethylene followed by Lewis acid catalysed dehydration is not very promising resulting in effectively no conversion towards TPA.<sup>13</sup> However, use of FDCA as a bio-advantaged substitute for TPA is currently being pursued by commercial chemical manufacturers.

Another bio-based family of molecules, which can be transformed into a variety of aromatic molecules including precursors of TPA using Diels-Alder chemistry, are 2-pyrones such as coumalic acid (CMA) or methyl coumalate (MeCMA). These compounds undergo inverse-electron-demand Diels-Alder reactions with dienophiles to produce oxabicyclo-[2.2.2]-octene intermediates that readily decarboxylate into molecules that can be converted into TPA (Scheme 1).<sup>1, 3, 14, 15</sup> MeCMA can be obtained by esterification of CMA with methano<sup>13, 16</sup> and CMA can be



**Scheme 1.** Glucose to coumalic acid/methyl coumalate (R1=OCH3 or OH) followed by Diels-Alder reaction with dienophiles (R2=CH3, COOCH3, COCH3, COC2H5)

---

synthesized through dimerization of malic acid. Malic acid can be obtained through extraction or high yielding fermentation<sup>17, 18</sup> and has been cited as one of the 12 most promising bio-based platform molecules.<sup>1, 14, 15</sup>

Given the prospects of using bio-based 2-pyrones, such as CMA, and MeCMA to produce substituted aromatics including TPA, several studies have been conducted to explore how the reaction yields are influenced by the dienophiles used.<sup>1, 3, 14, 15</sup> Previous work has shown that the reaction of MeCMA with ethyl acrylate leads to high yields (> 90 %) of the desired aromatic esters with a p-/m- product distribution of 1:1.<sup>15</sup> Further studies showed that MeCMA and acrolein afforded a p-/m- ratio of 3:1. The higher p-/m- ratio, however, was tied to significantly lower product yields of 47 %.<sup>3</sup> To further improve the process and atom economy of the reaction, MeCMA can be replaced by CMA, which minimizes the number of processing steps (esterification of CMA to MeCMA followed by hydrolysis of the aromatic ester to the acid). Therefore, the investigation of the CMA Diels-Alder reactions is a promising alternative to improve the feasibility of TPA production from 2-pyrone feedstocks. Moreover, the possibility of producing bio-based propylene through dehydration of the fermentation product n-propanol<sup>19</sup> or methanol to propylene technology<sup>20</sup> from biomass gasification, provides an opportunity to manufacture a 100 % bio-based product.

The Diels-Alder reaction of CMA with propylene, leads directly to p-toluic acid (p-TA), a precursor to TPA. Experimental reaction studies with CMA showed that p-TA was formed predominantly at a high yield (76 %) with 5 % of the by-product p-toluic acid isopropyl ester.<sup>15</sup> The high regioselectivity towards p-TA was unexpected given the small steric demand of propylene.<sup>15</sup> One hypothesis was that the high regioselectivity was due to both steric and electronic effects directing the Diels-Alder reaction to preferentially form the para isomer.<sup>15</sup> Kraus et al.

attributed this observation to a different secondary orbital interaction between the LUMO of the dienophile and the pyrone oxygen contribution to the HOMO of the diene that favours the transition state leading to the para isomer.<sup>3</sup>

While using the Diels-Alder chemistry with 2-pyrones and various dienophiles has been shown in a number of experimental studies to be a powerful platform to synthesize bio-based aromatic compounds, little in depth study characterizing the reaction pathway for the addition of CMA and propylene has been conducted. Information from reaction studies is essential to more completely explore the effects of temperature, pressure, catalyst, solvent, and reaction time so as to increase product selectivity and overall yield.

The current study examined this range of reaction parameters to establish a more comprehensive understanding of the conversion of CMA to TA. The reaction information combined with NMR analysis was used to identify molecular structures and to construct a detailed molecular level description of the reaction network. Additionally, stability experiments for both CMA and TA were conducted to determine how the selectivity to the desired product p-TA could be affected. As substantial differences in product yields were found using solvents with significantly different physicochemical properties, experiments were conducted using toluene and  $\gamma$ -valerolactone (GVL) to test solvent effects on TA formation.

## **2.3 Experimental**

### **2.3.1 Reagents and Materials**

Coumalic acid (Sigma Aldrich, >97 %), p-toluic acid (Acros Organics, 98 %), m-toluic acid (Acros Organics, 99 %),  $\gamma$ -valerolactone (Sigma Aldrich, 98 %), toluene (Fisher, 99.9 %), d6-benzene (Cambridge Isotope Laboratories Inc., 99.5 %), sulfuric acid (Fisher, 96.6 %), propylene

(Matheson, >99.9 %), 2-propanol (Fischer Scientific, 99.9 %), 10 wt% Pd on activated carbon (Sigma Aldrich), methanol (Fischer, MS grade), water (Fischer, MS grade), acetic acid (MS grade), calcium chloride (Fisher, anhydrous), and sodium bicarbonate (Fisher, 100 %), were all used as purchased.

### 2.3.2 Apparatus and General Reaction Procedure

The Diels-Alder reactions of CMA and propylene were performed in a 50 ml batch micro reactor system (Parr 4590 Series). Reactions were run using  $\gamma$ -valerolactone (GVL) or toluene as the solvent. Catalytic reactions were conducted using a 10 wt% Pd/C catalyst, which was added to the CMA and solvent reaction solution before the reactor was sealed and purged with nitrogen to remove residual air. The reactor was then charged with 130 psig propylene until saturation of propylene in the solvent was reached. Subsequently, the temperature was increased to the desired reaction condition. After the reaction proceeded for the desired time, the reactor was cooled to room temperature and depressurized. The liquid phase reaction products were then collected, filtered through a cellulose filter and analysed by UPLC-PDA/QDa and GC-MS.

Non-catalytic reactions of CMA with propylene were also performed in 1,4-dioxane as the solvent to enable NMR analysis of the reaction intermediates. Since CMA and propylene conversion in 1,4-dioxane were identical compared to GVL and given that 1,4-dioxane has a substantial lower boiling point, simplified the solvent recovery without compromising temperature sensitive intermediates. The reactions performed in 1,4-dioxane followed the same procedure described above in which CMA was introduced to the solvent, purged with N<sub>2</sub> to remove residual air and charged with 130 psig propylene until saturation. After the reaction proceeded for the desired time, the reactor was cooled to room temperature and depressurized. The reaction products

were filtered, degassed with sonication. The solvent 1,4-dioxane was evaporated with a constant stream of dry air and the obtained crude material was dissolved in dms<sub>o</sub>-d<sub>6</sub> and analysed via NMR.

### 2.3.3 Sample Analysis

Reaction products were analysed with ultra-pressure liquid chromatography (UPLC) using a Waters Acquity H-Class System equipped with a Photodiode Array (PDA) and a QDa mass detector. UPLC separation was carried out on a Waters BEH Phenyl column (2.1x100 mm, 1.7  $\mu$ m particles), which was maintained at 45 °C. A gradient elution with a flow rate of 0.5 ml min<sup>-1</sup> was chosen to separate the compounds of interest. The mobile phases were methanol (MP-A) and water (MP-B) both containing 0.1 vol% acetic acid. The gradient used for elution was 25 vol% MP-A and 75 vol% MP-B for the initial 8 min, which was then increased in one step to 45 vol% MP-A and 55 vol% MP-B and held for 7 min. After a total runtime of 15 min, the mobile phase composition was returned to the initial conditions (25 vol% MP-A / 75 vol% MP-B) within 5 min and equilibrated for another 5 min. The injection volume was 2  $\mu$ L for each sample. The PDA detector monitored the effluent at a wavelength of 240 nm and 280 nm. The QDa detector operated in a range between 90-300 Da with a capillary voltage of  $\pm$  0.8 kV and a cone voltage of  $\pm$ 15 V.

Additionally, samples were analysed by GC using an Agilent 7890B gas chromatograph equipped with an Agilent DB-1701 column (60 m x 0.25 mm), a flame ionization detector (FID), a thermal conductivity detector (TCD) and an Agilent 5977A mass spectrometer (MS). The carrier gas was helium with a constant flow rate of 60 ml min<sup>-1</sup>. The separation was performed using an injector temperature of 270 °C and an initial oven temperature of 40 °C, which was maintained for the first 5 min of acquisition. The temperature was then changed to 240 °C using a heating rate of 5 °C min<sup>-1</sup>.



The NMR analysis was performed using a Bruker spectrometer equipped with a 14.1 Tesla superconducting magnet and acquired and processed using the TOPSPIN version. The samples were prepared by carrying out the Diels-Alder reaction using fully deuterated benzene as the solvent, to both reduce the solvent background and as a field calibration species.  $^1\text{H}$  spectra were acquired using a recycle delay of 1.5 sec. and  $30^\circ$   $^1\text{H}$  excitation pulse lengths.  $^1\text{H}$ - $^1\text{H}$  2D plots were acquired using a COSY pulse sequence, and  $^{13}\text{C}$ - $^1\text{H}$  2D plots were acquired using the HSQC pulse sequence.

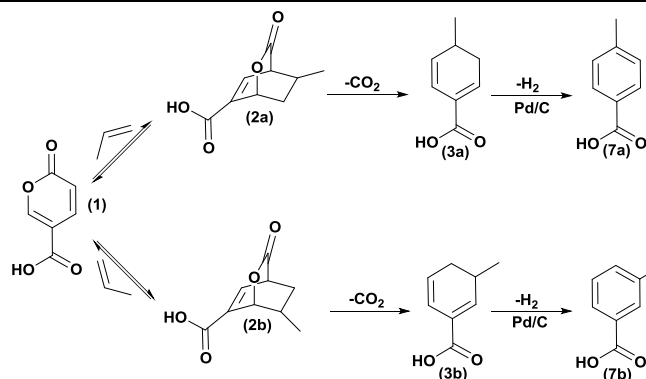
## **2.4 Results and Discussion**

### **2.4.1 Elucidating the Reaction Network**

The main reaction pathways involved in the formation of TA from CMA, were elucidated by comparing the products from a series of reactions carried out at different temperatures, duration and with or without catalyst. These experiments revealed key information regarding the formation of intermediates, products, and by-products, and determined if the Pd/C catalyst influenced the homogeneous Diels-Alder/decarboxylation reaction.

#### **2.4.1.1 The reaction network in the absence of catalyst**

To gain deeper insights into the reaction network for the formation of TA from CMA (1), experiments were first performed in which CMA and propylene were reacted in GVL at different reaction temperatures and times in the absence of catalyst thereby examining the Diels-Alder/decarboxylation sequence (1 to 2a/2b to 3a/3b) shown in Scheme 2. GVL was chosen as the solvent due to its bio-based origin, low toxicity and most importantly its excellent solubility of CMA. The goal of these experiments was to identify intermediates such as 2a/2b and 3a/3b by decoupling the Diels-Alder/decarboxylation sequence from the dehydrogenation reaction of 3a/3b



**Scheme 2.** Diels-Alder/decarboxylation/dehydration reaction sequence for the formation of TA from CMA. Diels-Alder (1→2a, 2b) /decarboxylation (2a, 2b→3a, 3b) sequence. Step 2.) Pd/C catalysed dehydrogenation (3a, 3b→7a, 7b).

to 7a/7b (Scheme 2). This approach could clarify whether the unidentified by-product formation reported earlier<sup>15</sup> resulted from intermediates on the pathway to the final TA product.

The results from the reactions in the absence of catalyst are summarized in Table 1. These data show that under all conditions tested only small amounts of TA were formed as would be expected due to no dehydrogenation catalyst being present and the absence of oxygen from the system. The UPLC-PDA/QDa chromatograms in Figure 1, show complete transformation of CMA (1) with increasing reaction time and temperature with concomitant increase in the reaction species shown in Scheme 2. After 2 h, the conversion of CMA reached 69.1 mol% at 140 °C with primarily CMA (1) and peak 2a/2b present. With increasing temperature and time, the peaks 1 and 2a/2b diminished while 3a/3b became more pronounced showing the progression of the CO<sub>2</sub> extrusion of 2a/2b to 3a/3b. To verify that peaks 2a/2b to 3a/3b were correctly identified as the bicyclic lactone intermediates, and methyl cyclohexa-1,5- diene carboxylic acids, 1D and 2D NMR analysis was performed.

Given the high boiling point of GVL these reactions were run in the polar aprotic solvent 1,4-dioxane as separating temperature sensitive bicyclic lactones 2a/2b from GVL would

**Table 1.** . Reaction times, temperatures, yields, p-/m- ratios and conversion of reactions of CMA and propylene in the absence of catalyst

Entry	T [°C]	t [h]	CMA Conv. [mol%]	TA Yield [mol%]
1	140	2	69.1 ± 1.4	< 1
2	140	4	89.1 ± 1.5	< 2
3	140	8	97.4 ± 1.3	< 4
4	160	2	93.1 ± 1.1	< 1
5	160	4	98.6 ± 0.4	< 2
6	160	8	99.3 ± 1.0	< 5
7	180	2	97.8 ± 0.0	< 4
8	180	4	99.7 ± 0.4	< 5
9	180	8	98.3 ± 0.3	< 10

Conditions: Solvent: GVL; CMA concentration in GVL: 20 mg/ml; catalyst: none; Stirring rate: 400 rpm; Propylene pressure at room temperature: 130 psig

compromise the molecular integrity of these compounds. Moreover, 1,4-dioxane was chosen as a good model system given that the CMA conversion and TA yield in 1,4-dioxane was identical to reactions performed in GVL (Table S1). This suggested that the reaction in 1,4-dioxane followed the same Diels-Alder/decarboxylation/dehydrogenation sequence. A summary of the quantitative

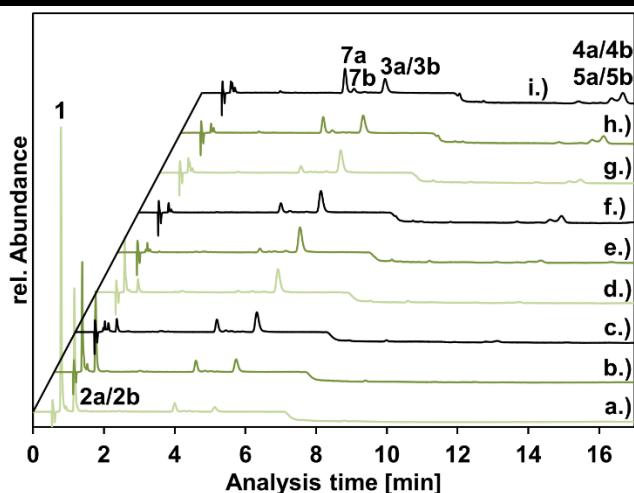
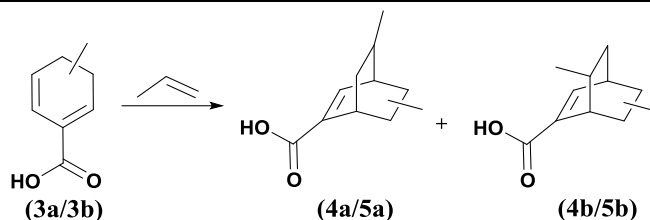


**Figure 1.** . UPLC-PDA/QDa analysis of the reaction of CMA and propylene at different reaction times 2 h (a, d, g); 4 h (b, e, h); 8 h (c, f, i) and temperatures 140 °C (a, b, c); 160 °C (d, e, f); 180 °C (g, h, i); Solvent: GVL; Catalyst: none; Peaks: 1 = CMA (m/z: 140), 2a/2b = bicyclic lactone intermediate (m/z: 182), 7a = p-TA (m/z: 136), 7b = m-TA (m/z: 136), 3a/3b = 3-/4-methyl cyclohexa-1,5-diene carboxylic acid (m/z: 138), 4a/4b, 5a/5b = bicyclic by-product (m/z: 180). PDA detector wavelength 240 nm.

results from the NMR analysis of reactions performed in 1,4-dioxane, are shown in Table 2. The annotated NMR spectra (Figure S1-S10) from 2 h at 140 °C, revealed that the majority of the products were coumalic acid (22.4 mol%), bicyclic intermediates 2a/2b (50.1 mol%) and diene intermediates 3a/3b (9.5 mol%) with only small amounts of TA (< 3 mol%) (Table 2). Moreover, NMR analysis of the reaction products further exhibited that the reaction network entailed significantly more detail about the nature of the Diels-Alder reaction of CMA and propylene as both 2a and 2b were present in endo/exo configuration (Figure S1-S6). This detailed and complex information was not discernible from the UPLC chromatograms (Figure 1) due to the challenge of isomer separation of compounds 2a/2b and 3a/3b which were convoluted with only two peaks visible. Figure 1 further shows, that at elevated temperatures and reaction times CMA (1), and the bicyclic lactones (2a/2b), were entirely consumed and formation of undesired by-products (4a/4b, 5a/5b) was observed. The by-product accumulation became even more pronounced at elevated temperatures (180 °C) and reaction times (8 h) as evident from the increasing peak area. Interestingly, through in-depth NMR analysis we confirmed the formation of four isomers of dimethylbicyclo[2.2.2]oct-2-ene-2-carboxylic acid (4a, 4b, 5a, 5b), shown in Figures S16-S22, formed through consecutive Diels-Alder reaction of 3a and 3b with propylene (Scheme 3). The formation of these Diels-Alder adduct species was further supported by compound specific GC-MS fragmentation pattern shown in Table S3. Through NMR analysis, 49.3 mol% was assigned to diene intermediates and 33.3 mol% to 4a/4b and 5a/5b and only a small amount to TA (3.2 mol%) present (Table 2). Hence, in the absence of catalyst there was significant by-products formation of 4a/4b and 5a/5b through consecutive Diels-Alder reaction of 3a and 3b with propylene providing evidence of the necessity of the catalyst to quickly dehydrogenate diene species 3a and 3b before Diels-Alder addition with propylene occurs.



**Scheme 3.** Diels-Alder reaction of **3a/3b** with propylene to **4a/5a** and **4b/5b**

To determine if the double Diels Alder product 4a/4b and 5a/5b underwent a retro Diels-Alder reaction to regenerate 3a and 3b, a two-step experiment was conducted. First, CMA was reacted with propylene for 8 h at 180 °C in the absence of catalyst to produce significant amounts of 4a/4b and 5a/5b. Next, the reactor was purged of propylene and heated to 180 °C for an additional 8 h to enhance the retro Diels-Alder reaction. The results of this experiment shown in Tables S4-S5 indicated that the by-product formation was irreversible as the concentrations of 4a/4b and 5a/5b did not change significantly.

**Table 2.** NMR quantification of the CMA and propylene reaction products in the absence of catalyst

Compound	140 °C 2 h rel. amount [mol%]	180 °C 8 h rel. amount [mol%]
1	22.4	-
2a	41.2	-
2b	8.9	-
3a	8.6	38.2
3b	0.9	7.6
1,3-diene isomer	-	3.5
7a	2.9	2.8
7b	-	0.5
4a, 4b, 5a, 5b	-	33.3
total	84.9	85.9
unknown	15.1	14.1

Conditions: solvent: 1,4-dioxane; CMA concentration in 1,4-dioxane: 20 mg/ml; catalyst: none; stirring rate: 400 rpm; pressure at room temperature: 130 psig propylene

### 2.4.1.2 The reaction network in the presence of catalyst

Reactions in the presence of catalyst were carried out with commercially available 10 wt% Pd/C, which was added to the reaction solution at two distinct time points to further emphasize the importance of the catalyst introduction and to determine the catalyst selectivity to form TA from 3a and 3b. This catalyst was chosen for the experiments due to its demonstrated ability to effectively dehydrogenate diene intermediates to form aromatics.<sup>1, 3, 14, 15</sup>

The first point of catalyst introduction was after the Diels-Alder/decarboxylation reaction to separate this sequence of reactions from catalytic dehydrogenation as visualized in Scheme 2. This was achieved by reacting CMA (1) and propylene for 8 h at 180 °C in the absence of catalyst, followed by a second step, in which the Pd/C catalyst was introduced to the reaction solution and then re-heated to 180 °C for another 8 h without propylene. The outcome of this two-step approach was a maximum combined yield of 43.1 mol% TA at 100 mol% conversion as shown in Table 3, Entry 1. UPLC analysis of the final reaction products showed there was still a significant amount of 4a/4b and 5a/5b present, Supplementary experiments in 1,4-dioxane and further emphasising that these species were quite stable and did not undergo retro Diels-Alder reactions. A comparison between the yield of TA from the two-step experiment in GVL (Table 3, Entry 1) and the aforementioned detailed NMR analysis of the analogous un-catalysed reaction in 1,4-dioxane, showed that after 8 h at 180 °C (Table 2), 49.3 mol% of the reaction products were assigned to diene intermediates 3a/3b (including a diene isomer with a 1,3-diene conformation), which was in agreement with the 43.1 mol% TA yield obtained from the two-step experiment (Table 3, Entry 1). This suggested that the Pd/C catalyst was highly selective towards converting the diene intermediates to TA. However, using this two-step approach led to a substantial amount (33.3 mol%) of 4a/ 4b and 5a/5b being formed. Importantly, when the yield of all diene intermediates

**Table 3.** Reaction times, temperatures, yields and degree of conversion of catalytic reactions of CMA and propylene using a one-pot and two-pot reaction procedure.

Entry	T [°C]	t [h]	CMA Conv. [mol%]	<i>p</i> -TA Yield [mol%]	<i>m</i> -TA Yield [mol%]
1 <sup>a</sup>	180	8	100	33.7	9.4
2	180	8	99.5	70.8	15.8

Conditions: Solvent: GVL; CMA concentration in GVL: 20 mg/ml; catalyst: 10 wt% Pd/C (100 mg); Stirring rate: 400 rpm; Pressure at room temperature: 130 psig propylene. a two-pot reaction: 180 °C 8 h reaction without catalyst followed by 180 °C 8 h reaction with catalyst

(3a, 3b, 1,3-isomer), products (7a, 7b) and by-products (4a, 4b, 5a, and 5b) were combined, 85.9 mol% of the starting material can be accounted for, leaving 14.1 mol% unassigned (Table 2). From these findings, it was essential to introduce the catalyst before intermediates 2a/2b decarboxylated to 3a/3b.

This hypothesis was tested through a one-step experiment in which the Pd/C catalyst was added to the CMA containing solution before the Diels-Alder/decarboxylation sequence took place. As with the two-step experiment, the Diels-Alder/ decarboxylation/dehydrogenation cascade was performed at 180 °C for 8 h. The results of this experiment are shown in Table 3, Entry 2.

As expected, the maximum combined yield of TA in the one-step experiment was 86.6 mol%, significantly higher than for the two-step experiment. This observation provided evidence that the catalyst introduction before decarboxylation of 2a/2b was critical to initiate the subsequent dehydrogenation of reactive diene intermediates 3a/3b to 7a/7b, which prevented the irreversible by-product formation of 4a/4b and 5a/5b. After completion of the one-step experiment, 13.4 mol% of the initial starting material CMA was permanently lost as a result of unidentified by-products formation. This observation was in agreement with the NMR results obtained from an 8 hr reaction of CMA and propylene at 180 °C in the absence of catalyst, where 85.9 mol% of the reaction

**Table 4.** Stability tests of CMA.

Entry	Solvent	Catalyst	T [°C]	t [h]	Conv. of CMA [mol%]
1	GVL	none	180	8	25
2	GVL + 5 Vol% Water	none	180	8	100

Conditions: solvent: GVL; CMA concentration in GVL: 20 mg/ml; stirring rate (400 rpm); pressure at room temperature (130 psig N<sub>2</sub>). Analysis via UPLC-PDA/QDa.

products were assigned to 3a, 3b, 7a, 7b, 4a, 4b, 5a, and 5b and 14.1 mol% was assigned to unknown by-products (Table 2).

As previous experiments strongly suggested that the origin of the unidentified by-products was attributed to concomitant breakdown of the CMA, experiments were conducted by reacting neat CMA in GVL without propylene at 180 °C for 8 h without catalyst (Table 4). Strikingly, in the absence of the catalyst 25 mol% of CMA was converted into unidentified by-products, which supported our hypothesis. Given the hygroscopic nature of GVL and the fact that 2-pyrones undergo ring-opening in water through nucleophilic addition<sup>21</sup>, a third test was conducted to test if water present in the solvent accelerated the breakdown of CMA under these conditions. This experiment showed that only 5 vol% water in GVL had a dramatic effect on the rate of CMA breakdown with no detectable CMA remaining after 8 h at 180 °C. These results indicated that the absence of water was critical to increase the final TA product yield.

Another possibility for the observed selectivity loss was TA instability and/or reactivity causing breakdown or additional reactions with excess propylene to form undesired by-products. Henceforth, a series of experiments were conducted in which neat TA was treated under reaction conditions (180 °C, 8 h) with propylene in the absence and presence of catalyst (Table 5). Either with or without the catalyst, the formation of TAIPr as previously suggested<sup>15</sup>, was not observed



**Table 5.** Stability test of p-/m-TA.

Entry	Solvent	Catalyst	T [°C]	t [h]	<i>p-/m-</i> TA ratio	By-products
1	GVL	Pd/C	180	8	1.00	not detected
2	GVL	none	180	8	1.00	not detected
3	Toluene	Pd/C	180	8	1.00	not detected
4	Toluene	none	180	8	1.01	not detected

Conditions: solvent (30 ml); p-TA (300 mg); m-TA (300 mg); catalyst: 10 wt.-% Pd/C (100 mg); stirring rate (400 rpm); pressure at room temperature (130 psig propylene) p-/m- ratio after reaction. Analysis via UPLC-PDA/QDa.

using GVL as the primary solvent. Given that toluene was used in those studies, stability tests of TA were also performed in toluene. As shown in Table 5, the nature of the solvent appeared to have no effect on the stability of TA as the formation of T*A*iPr was not observed. Analysis of the species present after the extended treatment at 180 °C further validated that no other by-products were formed, demonstrating that TA was stable under the tested reaction conditions. Moreover, the p-/m- product ratio of TA was not affected by either the catalyst or the solvent, which suggested that the regio-specificity for the TA product formation was solely determined by the Diels-Alder cycloaddition reaction. Hence, it was assumed that the previous observed selectivity loss of approximately 14 mol% in the CMA reaction with propylene was likely due to CMA break down.

Next, the influence of reaction temperature and time on the TA selectivity in the presence of the Pd/C catalyst was investigated through experiments in which CMA was reacted with propylene at different temperatures and times using GVL as the primary solvent. The results of these experiments are given in Table 6. Following 2 h at 140 °C, 68.4 mol% ± 1.1 mol% of the initial CMA was converted to 20.3 mol% ± 1.6 mol% p-TA and 2.9 mol% ± 0.2 mol% m-TA (Table 6, Entry 1) giving a p-/m-ratio of 6.91. With increasing reaction time, however, the p-/m-ratio decreased. As 68.4 mol% of the CMA was converted and only 23.2 mol% TA was formed it

**Table 4.** Reaction times, temperatures, yields, *p*-/*m*-ratios and degree of conversion of catalytic reactions of CMA and propylene.

Entry	T [°C]	t [h]	CMA Conv. [mol%]	<i>p</i> -TA Yield [mol%]	<i>m</i> -TA Yield [mol%]	<i>p</i> -/ <i>m</i> - TA ratio
1	140	2	68.4 ± 1.1	20.3 ± 1.6	2.9 ± 0.2	6.91 ± 0.24
2	140	4	87.1 ± 1.0	43.3 ± 6.3	6.9 ± 1.3	6.34 ± 0.36
3	140	8	96.6 ± 1.4	65.7 ± 2.4	12.2 ± 1.8	5.45 ± 0.58
4	160	2	94.0 ± 0.7	65.6 ± 1.5	13.3 ± 0.7	4.95 ± 0.35
5	160	4	96.9 ± 1.1	68.3 ± 4.1	14.6 ± 0.7	4.67 ± 0.12
6	160	8	99.2 ± 0.7	70.0 ± 2.8	14.8 ± 0.4	4.72 ± 0.15
7	180	2	97.1 ± 1.0	68.6 ± 2.7	15.5 ± 0.1	4.43 ± 0.13
8	180	4	99.0 ± 0.9	69.2 ± 1.3	15.4 ± 0.2	4.49 ± 0.04
9	180	8	99.5 ± 0.6	70.8 ± 3.4	15.8 ± 0.3	4.48 ± 0.15

Conditions: Solvent: GVL; CMA concentration in GVL: 20 mg/ml; catalyst: 10 wt% Pd/C (100 mg); Stirring rate: 400 rpm; Pressure at room temperature: 130 psig propylene.

appeared that the Diels-Alder reaction of CMA and propylene was significantly faster than the formation of the TA product. Furthermore, through the presence of intermediates 2a/2b and without observing an accumulation of the cyclohexadiene intermediates (3a, 3b), displayed in Figure 2, the decarboxylation step from 2a/2b to 3a/3b was apparently rate limiting. With increasing reaction times (8 h) the yield of the desired compound, *p*-TA, increased to 65.7 mol% ± 2.4 mol% accompanied with 12.2 mol% ± 1.8 mol% of *m*-TA, (Table 6, Entry 3). Therefore, as the reaction time was increased from 2 to 8 h at 140 °C, the *p*-/*m*-ratio declined from 6.91 ± 0.24 to 5.45 ± 0.58. The observed change of the product selectivity with increasing reaction time strongly suggested that a retro Diels-Alder reaction leading to a thermodynamic equilibrium between 2a and 2b was operative. After a 2 h reaction at 160 °C the conversion of CMA resulted in a 65.6 mol% ± 1.5 yield of *p*-TA with a *p*-/*m*-ratio of 4.95 ± 0.35 (Table 6, Entry 4). By further

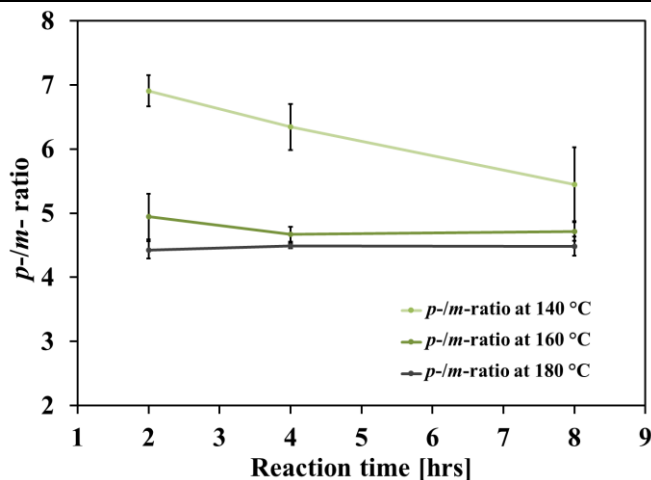


**Figure 3.** The change in the *p-/m-ratio* of TA with respect to reaction time and temperature.

increasing the reaction time to 8 h, the overall yield of the desired para isomer was maximized to 70.0 mol%  $\pm$  2.8 but was accompanied with a decrease of the *p-/m-* ratio to  $4.72 \pm 0.15$  (Table 6, Entry 6). Changing to 180 °C and 8 h had no significant impact on the yield of *p*-TA (70.8 mol%  $\pm$  3.4 mol%), (Table 6, Entry 9). At this temperature, the *p-/m-* ratio further declined to  $4.48 \pm 0.15$ . The change of the product selectivity at elevated temperatures suggested that the decarboxylation reaction of bicyclic lactone intermediates 2a/2b to diene intermediates 3a/3b proceeded significantly faster, not allowing the reaction to reach thermodynamic equilibrium, which ultimately constrained the para to meta selectivity. Although, the *p-/m-ratio* declined with increasing reaction temperature and time, *p*-TA was still the favoured isomer over *m*-TA, suggesting that *p*-TA was both the kinetically and thermodynamically favoured product (Figure 3).

For the 2 h reaction at 140 °C (Table 6, Entry 1), the large difference (45.2 mol%) in CMA reacted and TA formed suggested that significant amounts of the intermediates 2a/2b were present as 3a/3b were not observed. The chromatograms in Figure 2 corresponding to this point supported

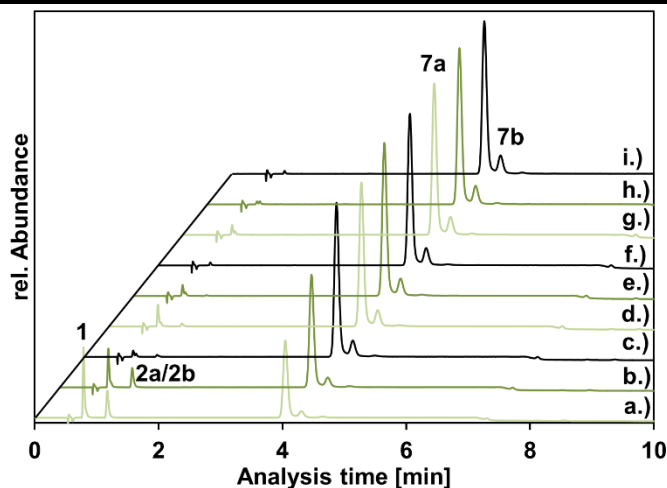
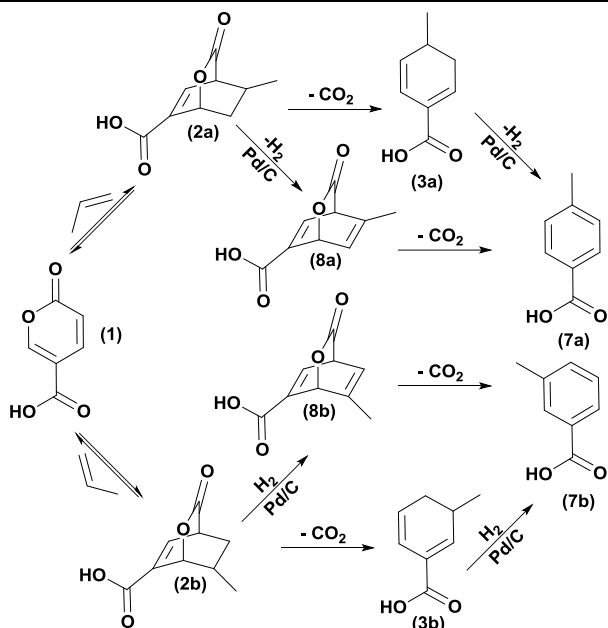


**Figure 2.** UPLC-PDA/QDa analysis of the CMA and propylene reaction at different reaction times 2 h (a, d, g); 4 h (b, e, h); 8 h (c, f, h) and temperatures 140 °C (a, b, c); 160 °C (d, e, f); 180 °C (g, h, i); Solvent: GVL; Catalyst: 100 mg, 10 wt.-% Pd/C; Peaks: 1 = CMA (m/z: 140), 2a/2b = bicyclic lactone intermediate (m/z: 182), 7a = p-TA (m/z: 136), 7b = m-TA (m/z: 136).

this observation. The chromatogram series, which tracked the reaction at 140 °C was particularly informative, as peak 2a/2b, was quite prominent after 2 h of reaction, but decreased with increasing reaction time whereas the intensity of the product peaks 7a and 7b grew. As such the formation of TA corresponded to the loss in peak intensity of the species 2a/2b. With increasing reaction temperature and time, the peak 2a/2b of the intermediate species and the peak of the starting material CMA became less prominent whereas the peaks for 7a and 7b further increased. Most importantly, no by-products 4a/4b and 5a/5b were observed with catalyst present, further emphasising that its formation (seen in non-catalytic experiments) originated from the reactive intermediates 3a/3b. This postulate was further emphasized as these intermediates 3a/3b were not observed in any of the catalytic experiments (Figure 2). A likely explanation for this observation was that the loss of CO<sub>2</sub> from intermediates 2a/2b was the rate limiting step followed by instantaneous dehydrogenation of intermediates 3a/3b to 7a/7b. Another possibility was the



**Scheme 4.** Two possible reaction pathways of the CMA to TA reaction cascade. First pathway: Diels-Alder (**1**→**2a**, **2b**)/decarboxylation (**2a**, **2b**→**3a**, **3b**)/dehydrogenation (**3a**, **3b**→**7a**, **7b**). Second pathway: Diels-Alder (**1**→**2a**, **2b**)/dehydrogenation (**2a**, **2b**→**8a**, **8b**)/decarboxylation (**8a**, **8b**→**7a**, **7b**).

catalytic dehydrogenation of species **3a/3b** into unstable intermediates **8a/8b** that underwent rapid decarboxylation to form the desired products **7a/7b** (Scheme 4). Comparison of non-catalytic (Figure 1) and catalytic (Figure 2) reactions at 140 °C and 2 h revealed that the peak areas of CMA (**1**) and the bicyclic lactone **2a/2b** were identical, suggesting that the consumption of the bicyclic lactone was solely caused by thermal decarboxylation since additional dehydrogenation would lead to an increased consumption of the bicyclic intermediates **2a/2b** associated with a smaller peak area of the bicyclic lactone peak. This in turn indicated that the consumption of **2a/2b** was not influenced by the catalyst at 140 °C.

Therefore, it appeared that decarboxylation of **2a/2b** to **3a/3b** was the predominant reaction pathway in the formation of **7a/7b** from CMA rather than the dehydrogenation of the bicyclic lactone **2a/2b** to **8a/8b** followed by extrusion of CO<sub>2</sub>. Additionally, the comparison of CMA

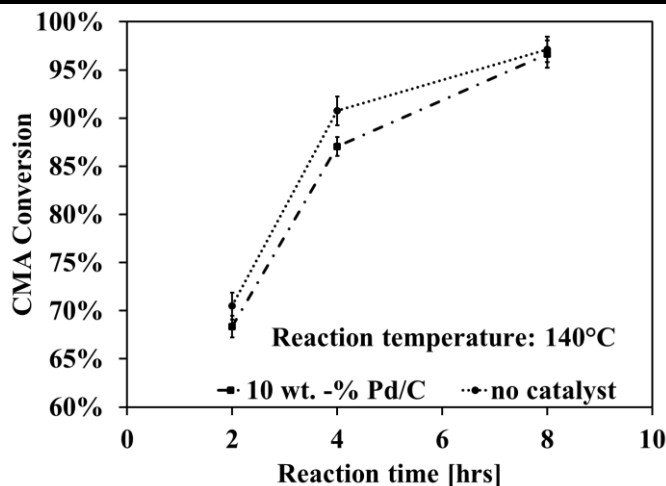
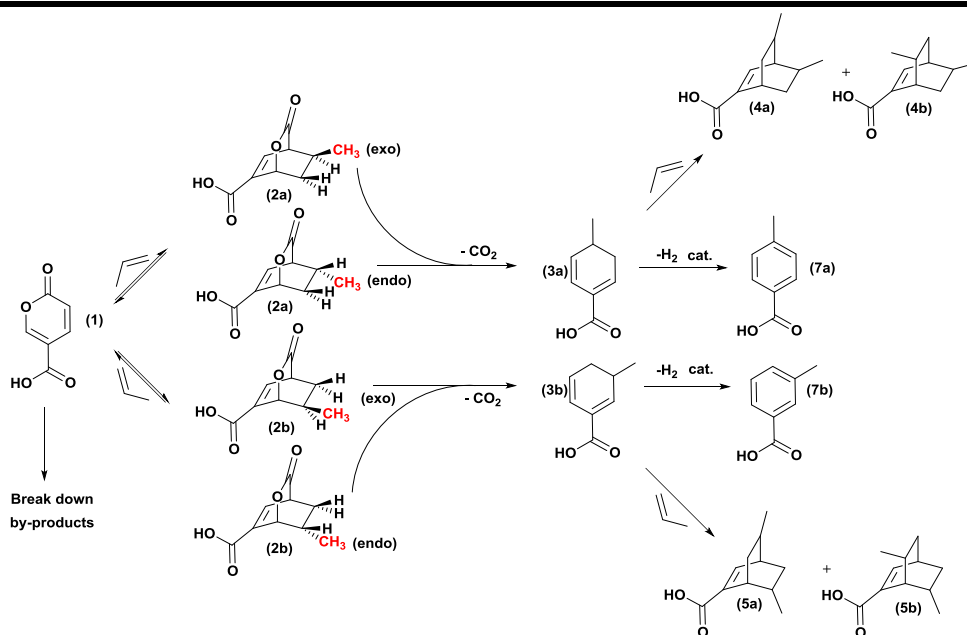


**Figure 4.** Comparison of the CMA conversion with and without the presence of Pd/C catalyst.

conversion in the presence and absence of catalyst at 140 °C, shown in (Figure 4), revealed a similar trend, leading to the conclusion that the Diels-Alder reaction was not affected by the dehydrogenation catalyst. With the aforementioned existence of CMA breakdown and the proven decarboxylation pathway of 2a/2b to 3a/3b, shown in Scheme 4, an overall reaction network was proposed (Scheme 5).



**Scheme 5.** Overall reaction network for the formation of TA from CMA and propylene.

## 2.5 Conclusions

In this work, a detailed reaction network of the product formation of TA from CMA was established including key insights into by-product formation. CMA was found to undergo two parallel reaction pathways; with propylene a reversible, inverse electron demand Diels-Alder reaction to form bicyclic lactone isomers 2a (endo/exo) and 2b (endo/exo) and as a break down to undesired by-products, which was accelerated in the presence of water in the solvent demonstrating minimal water content in the solvent was essential to achieve maximum product selectivity. The bicyclic lactone isomers 2a and 2b were found to be in equilibrium with CMA until CO<sub>2</sub> was irreversibly lost to form the diene intermediates 3a and 3b. It was shown that the presence of the catalyst was crucial to quickly dehydrogenate the diene species to form stable aromatics and to prevent consecutive Diels-Alder by-product formation with propylene. The p-/m-ratio of TA decreasing with time demonstrated a reversible retro Diels-Alder reaction leading to an equilibrium between 2a and 2b which in turn led to a change in the product distribution of 7a and 7b over time. The change in the p-/m- product selectivity became even more pronounced with increasing temperature which implied that at elevated temperatures the non-reversible CO<sub>2</sub> extrusion of the bicyclic lactone intermediate 2a/2b proceeded much faster, restricting the retro-Diels Alder reaction and preventing the system to reach its thermodynamic equilibrium. Although, the p-/m- ratio declined with increasing reaction temperature and time, the para product was still the favoured isomer, indicating that p-TA was both the kinetically and thermodynamically favoured product. Hence, the key to increase selectively to the para isomer of TA lies in shorter reaction times at lower reaction temperatures. With p-TA being the precursor of TPA, this route provides a bio-based alternative to PET and other useful chemicals based on TPA.

## 2.6 Acknowledgements

We gratefully acknowledge the NSF for funding (grant EEC-0813570), and the Iowa State University Chemical Instrument Facility staff members. Furthermore, we would like to acknowledge all co-workers at the Center for Biorenewable Chemicals (CBiRC) for their useful discussions.

## 2.7 References

1. J. J. Lee, G. R. Pollock III, D. Mitchell, L. Kasuga and G. A. Kraus, *RSC Adv.*, 2014, **4**, 45657-45664.
2. A. J. J. E. Eerhart, A. P. C. Faaij and M. K. Patel, *Energy Environ. Sci.*, 2012, **5**, 6407-6422.
3. G. A. Kraus, G. R. Pollock III, C. L. Beck, K. Palmer and A. H. Winter, *RSC Adv.*, 2013, **3**, 12721-12725.
4. R. A. Sheldon, *Green Chemistry*, 2014, **16**, 950-963.
5. V. Vaiano, G. Sarno, O. Sacco and D. Sannino, *Chem. Eng. J.*, 2017, **312**, 10-19.
6. C. E. H. Bawn and T. K. Wright, *Farad. Discuss.*, 1968, **46**, 164-172.
7. R. J. Sheehan, in *Ullmann's Encyclopedia of Industrial Chemistry*, Wiley-VCH Verlag GmbH & Co. KGaA, 2000.
8. Coca-Cola Company, Global Reporting Initiative Report, 2012, <http://www.coca-colacompany.com/sustainabilityreport/downloads/2012-sustainability-report.pdf> (accessed, 2016).
9. C. L. Williams, C.-C. Chang, P. Do, N. Nikbin, S. Caratzoulas, D. G. Vlachos, R. F. Lobo, W. Fan and P. J. Dauenhauer, *ACS Catal.*, 2012, **2**, 935-939.
10. C.-C. Chang, S. K. Green, C. L. Williams, P. J. Dauenhauer and W. Fan, *Green Chem.*, 2014, **16**, 585-588.
11. P. T. M. Do, J. R. McAtee, D. A. Watson and R. F. Lobo, *ACS Catal.*, 2012, **3**, 41-46.
12. M. Shiramizu and F. D. Toste, *Chem. Eur. J.*, 2011, **17**, 12452-12457.
13. J. J. Pacheco and M. E. Davis, *Proc. Natl. Acad. Sci.* 2014, **111**, 8363-8367.



14. G. A. Kraus, S. Riley and T. Cordes, *Green Chem.*, 2011, **13**, 2734-2736.
15. S. J. Riley, Ph.D., Iowa State University, 2011.
16. I. W. Ashworth, M. C. Bowden, B. Dembofsky, D. Levin, W. Moss, E. Robinson, N. Szczur and J. Virica, *Org. Process Res. Dev.*, 2002, **7**, 74-81.
17. X. Zhang, X. Wang, K. T. Shanmugam and L. O. Ingram, *Appl. Environ. Microbiol.*, 2011, **77**, 427-434.
18. S. H. Brown, L. Bashkirova, R. Berka, T. Chandler, T. Doty, K. McCall, M. McCulloch, S. McFarland, S. Thompson and D. Yaver, *Appl. Microbiol. Biotechnol.*, 2013, **97**, 8903-8912.
19. E. de Jong, A. Higson, P. Walsh and M. Wellisch, IEA Bioenergy, Task42 Biorefinery, 2012.
20. R. T. Mathers, *Journal of Polymer Science Part A: Polymer Chemistry*, 2012, **50**, 1-15.
21. M. Chia, M. A. Haider, G. Pollock, G. A. Kraus, M. Neurock and J. A. Dumesic, *J. Am. Chem. Soc.*, 2013, **135**, 5699-5708.

## 2.8 Supplementary Information

The formation of p-toluic acid from coumalic acid: A reaction network analysis

*A paper published in Green Chemistry 2017, 19, 3263-3271*

Toni Pfennig,<sup>a,b</sup> Robert L. Johnson,<sup>a,b</sup> and Brent H. Shanks<sup>a,b</sup>

<sup>a</sup> Department of Chemical and Biological Engineering, Iowa State University, Ames, IA 50011, USA.

<sup>b</sup> NSF Engineering Research Center for Biorenewable Chemicals (CBiRC), Ames, IA 50011, USA

### *Synthesis of reference materials for intermediates*

The intermediate 4-methylcyclohexa-1,5-diene carboxylic acid 3a was synthesized via non-catalytic reaction of CMA and propylene in toluene at 160 °C, 4 h and elevated pressure (~1200 psig). The purified product was isolated with the following procedure. First, the solvent was evaporated using a Rotavapor R205 (Büchi) equipped with a vacuum controller V-800 (Büchi), vacuum pump V-700 (Büchi), and a heating bath B-490 (Büchi) at 65 rpm, 100 mbar (absolute) and a temperature that was stepwise increased from 40 to 70 °C until an oily red-orange crude material was left behind. Second, the remaining material was recrystallized by adding 15 mL DI water which was heated in a water bath to 90 °C to fully dissolve all solid materials. Once the solid material was fully dissolved, the solution was slowly cooled to room temperature. Lastly, the liquid was placed in an ice bath and the solid fraction was separated via vacuum filtration through a cellulose filter and washed with cold water. The solid was analysed using <sup>1</sup>H-NMR and confirmed the expected 4-methylcyclohexa-1,5-diene carboxylic acid 3a with ~85 % purity and CMA remaining as the major by-product.

**4-methylcyclohexa-1,5-diene carboxylic acid** -  $^1\text{H-NMR}$  (600 MHz, benzene- $d_6$ ):  $\delta$  6.93 (t, 1H), 6.56 (d, 1H), 5.51 (dd, 1H), 2.06-1.96 (m, 1H) 1.96-1.88 (m, 1H), 1.67-1.58 (m, 1H), 0.71 (d, 3H); GC-MS  $m/z$ : 138.1

***NMR structural identification of intermediates, products and by-products***

Verification assignments of bicyclic lactone intermediates (2a (endo/exo), 2b (endo/exo)), methyl cyclohexa-1,5-dienecarboxylic acids (3a, 3b), toluic acid (7a, 7b), and bicyclic by-products (4a, 4b, 5a, 5b) were carried out via NMR, UPLC-PDA/QDa and GC-FID/MS analysis of reaction products of CMA and propylene in the absence of Pd/C catalyst in 1,4-dioxane. Given that the CMA conversion in 1,4-dioxane showed identical performance as compared to reactions performed in GVL (Table S1), it was safe to assume that the reaction in 1,4-dioxane followed the same Diels-Alder/decarboxylation/ dehydrogenation sequence. Thus, the synthesis of intermediates and by-products was performed in 1,4-dioxane to separate the solvent from the temperature sensitive intermediates and to analyze the products via NMR (Table S2).

**Table S1.** Comparison of CMA conversion to TA in different aprotic polar solvents

Entry	Solvent	T [°C]	t [h]	CMA Conversion [mol-%]	<i>p</i> -TA Yield [mol-%]	<i>m</i> -TA Yield [mol-%]
1	1,4-dioxane	180	8	99.5 ± 0.6	70.8 ± 3.4	15.8 ± 0.3
2	GVL	180	8	99.5 ± 5.4	71.9 ± 1.1	16.3 ± 0.8

Conditions: Solvent: 30 ml; CMA (600 mg); Stirring rate: (400 rpm); Propylene pressure at room temperature: (130 psig); Catalyst: 100 mg 10 wt.-% Pd/C

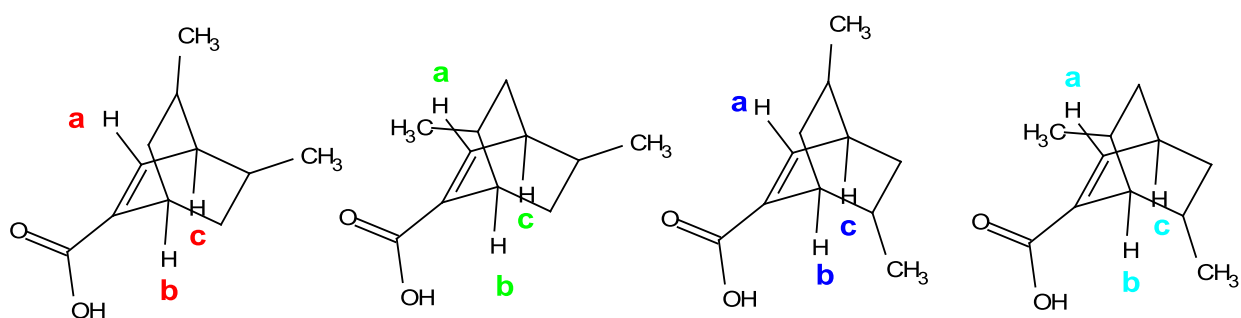
**Table S2.** Structural NMR experiments to identify intermediates and side-products

Entry	Solvent	Catalyst	T [°C]	t [h]	Analysis
1	1,4-dioxane	none	140	2	$^1\text{H-NMR}$ , HSQC, COSY
2	1,4-dioxane	none	180	8	$^1\text{H-NMR}$ , HSQC, COSY

Conditions: CMA concentration in 1,4-dioxane: 20 mg/ml; catalyst: none; Stirring rate: 400 rpm; Pressure at room temperature: 130 psig propylene; Reaction time: 8 h; Temperature: 180 °C

Bicyclic lactone intermediates 2a (endo/exo) and 2b (endo/exo) were synthesized at 140 °C for 2 h reaction time. A reaction performed at 180 °C and 8 h reaction time on the other hand gave access to cyclohexa-1,5-diene intermediates 3a and 3b and Diels-Alder by-products (4a, 4b, 5a, 5b) from the cycloaddition of 3a and 3b with propylene. NMR analysis of the reaction products, obtained from a 140 °C and 2 h reaction, confirmed that a significant amount of the starting material CMA was converted to the bicyclic lactone intermediates 2a (endo/exo) and 2b (endo/exo), diene intermediates 3a and 3b and toluic acid 7a and 7b (Table 2). The reaction products obtained after an 8 h reaction at 180 °C revealed the formation of cyclohexadiene intermediates (3a, 3b), and Diels-Alder by-products (4a, 4b, 5a, 5b) as the major compounds with small amounts of toluic acid (7a, 7b) (Table 2). The assignment of the by-products 4a, 4b, 5a, and 5b was further supported by UPLC-QDa and GC-MS analysis (Table S3 and S4). These by-products were shown to be stable under reaction conditions in the absence of propylene. After an 8 h reaction at 180 °C, the peak area of the by-products 4a, 4b, 5a, and 5b was not significantly changed (Table S5), indicating that no retro Diels-Alder reaction was operative.

The structural assignment of 4a, 4b, 5a, 5b of the complex NMR spectra shown in Figure S16 was not trivial as a result of overlapping peaks. Through UPLC-QDa, GC-MS analysis we identified four compounds with similar mass ( $m/z$ : 180.1). Additional NMR analysis revealed the formation of four isomers from Diels-Alder reaction of 3a and 3b with propylene (Scheme S1). Very indicative of the assignment of 4a, 4b, 5a, 5b were the four doublets of the allylic protons between 7.0 and 7.25 ppm without any correlation to other allylic protons in that region (Figure S17). Unlike the bicyclic lactone intermediates 2a/2b (Figure S3) that have allylic C-H protons that correlate to de-shielded C-H protons (5.5 ppm) as a result of neighboring oxygen atoms, the allylic C-H protons in Figure S18, correlate to more shielded C-H protons in the region of 2.2 to 3



**Scheme S1.** By-products from cycloaddition of cyclohexa-1,5-diene intermediates and propylene

**Table S3.** GC-MS major ion fragments of the Diels-Alder reaction by-products of **3a/3b** with propylene

By-product peak	Retention time [min]	Major ion fragments [m/z]
1	35.22	180.1, 138.1, 123.1, 105.1, 93.1, 91.1, 79.1, 77.1
2	35.32	
3	35.80	
4	35.88	

Conditions: CMA concentration in 1,4-dioxane: 20 mg/ml; catalyst: none; Stirring rate: 400 rpm; Pressure at room temperature: 130 psig propylene; Reaction time: 8 h; Temperature: 180 °C.

**Table S4.** Major ion fragments of the Diels-Alder by-products of **3a/3b** with propylene from UPLC-QDa analysis

Peak	Retention time [min]	Peak area [ $\mu\text{V}\cdot\text{sec}$ ]	Major ion fragment [m/z]
1	13.96	15999626	180.1
2	14.27		

Conditions: CMA concentration in 1,4-dioxane: 20 mg/ml; catalyst: none; Stirring rate: 400 rpm; Pressure at room temperature: 130 psig propylene; Reaction time: 8 h; Temperature: 180 °C

**Table S5.** Major ion fragments of the Diels-Alder by-products **4a**, **4b**, **5a**, and **5b** from UPLC-QDa analysis after retro Diels-Alder reaction in the absence of propylene

Peak	Retention time [min]	Peak area [ $\mu\text{V}\cdot\text{sec}$ ]	Major ion fragment [m/z]
1	13.96	15394927	180.1
2	14.27		

Conditions: CMA concentration in 1,4-dioxane: 20 mg/ml; catalyst: none; Stirring rate: 400 rpm; Pressure at room temperature: 130 psig N<sub>2</sub>; Reaction time: 8 h; Temperature: 180 °C

suggesting the formation of **4a**, **4b**, **5a**, and **5b** shown in Scheme S1. Moreover, the integration of all protons (a) or (b) in Scheme S1 are equal to one for each isomer in Figure S16. Figure S16 further shows that a total of four protons of (a) and four protons of (b) matched with a total of 24 CH<sub>3</sub> protons, further Supplementary the assignment of these by-products.

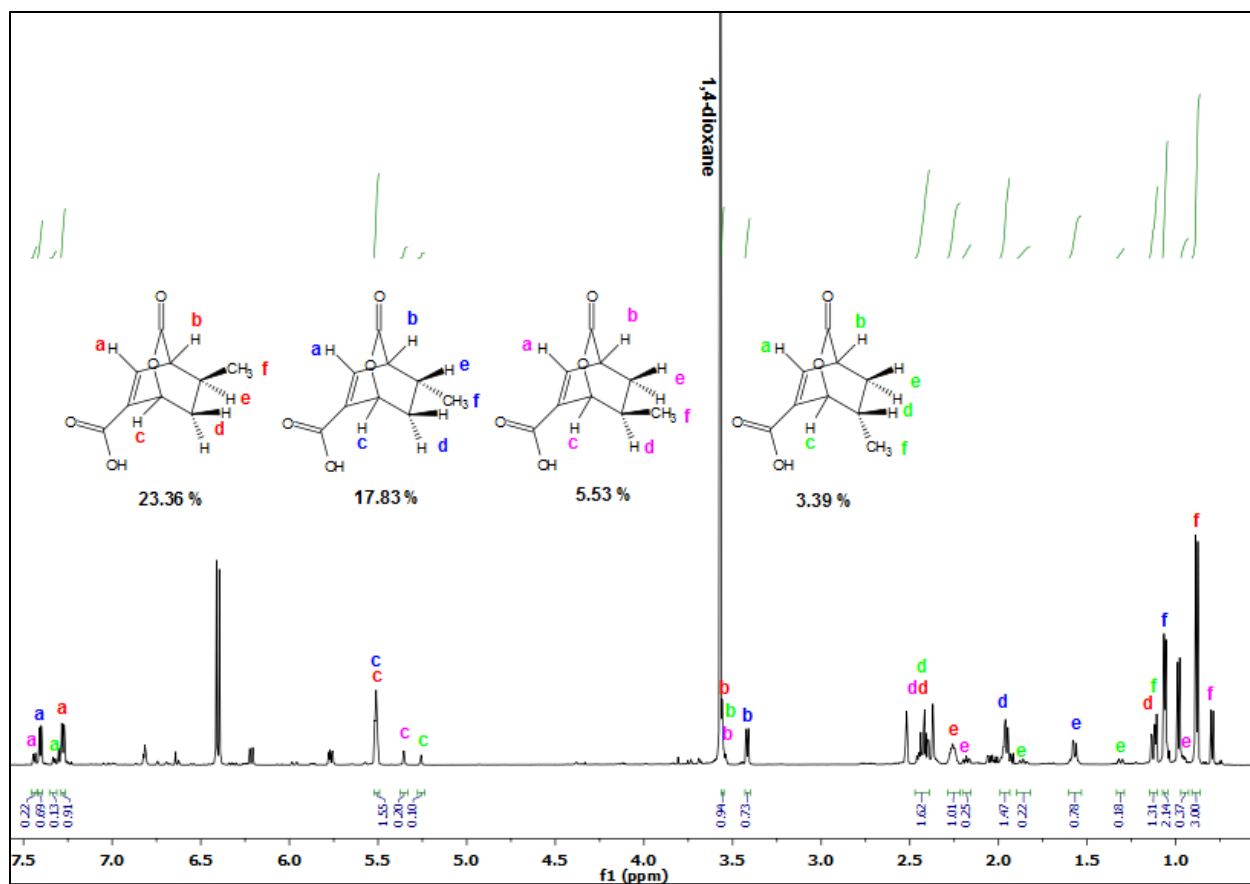


**Figure S1.** <sup>1</sup>H-NMR structural assignment of the bicyclic intermediates after a reaction of coumalic acid and propylene at 140 °C for 2 h in the absence of Pd/C catalyst

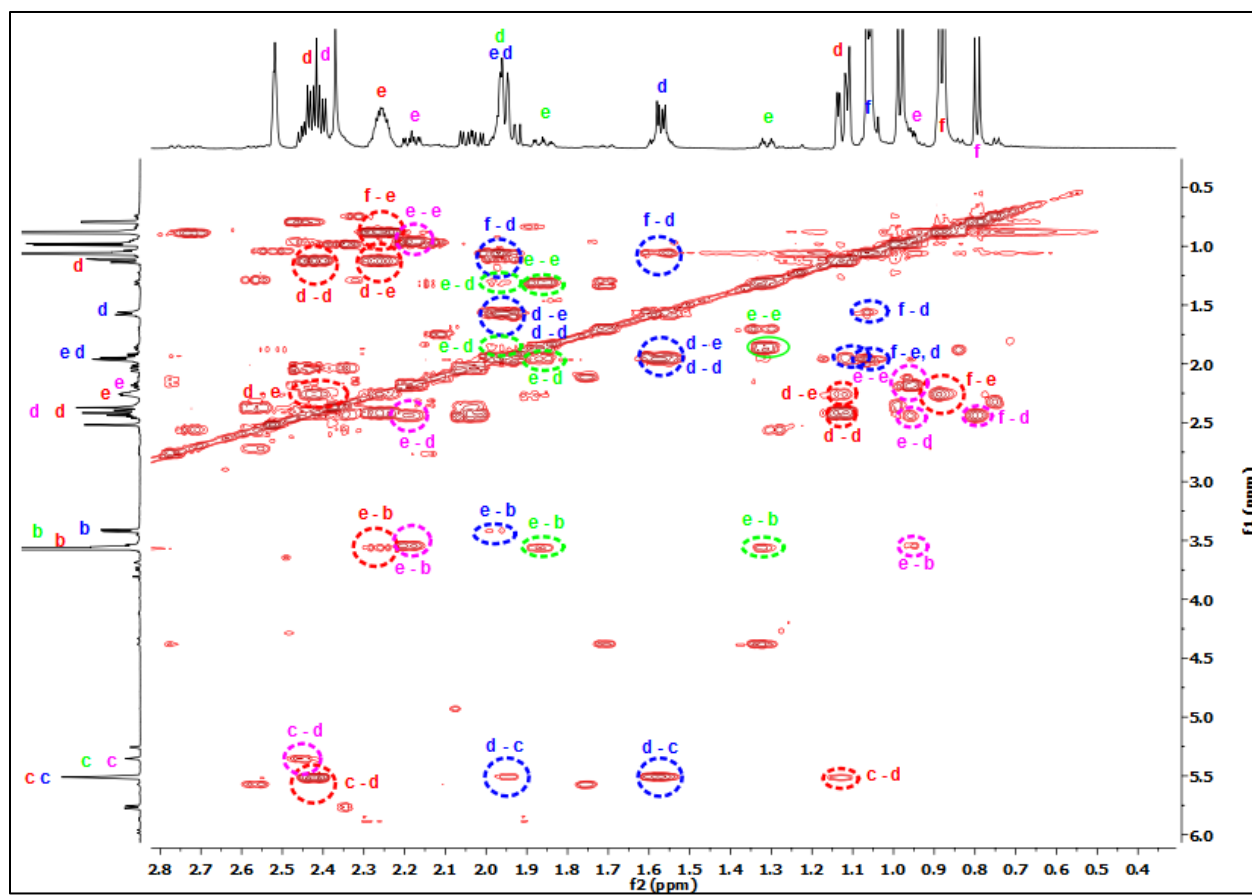


**Figure S2.**  $^1\text{H}$ - $^1\text{H}$  COSY structural assignment of the bicyclic intermediates after a reaction of coumalic acid and propylene at 140 °C for 2 h in the absence of Pd/C catalyst

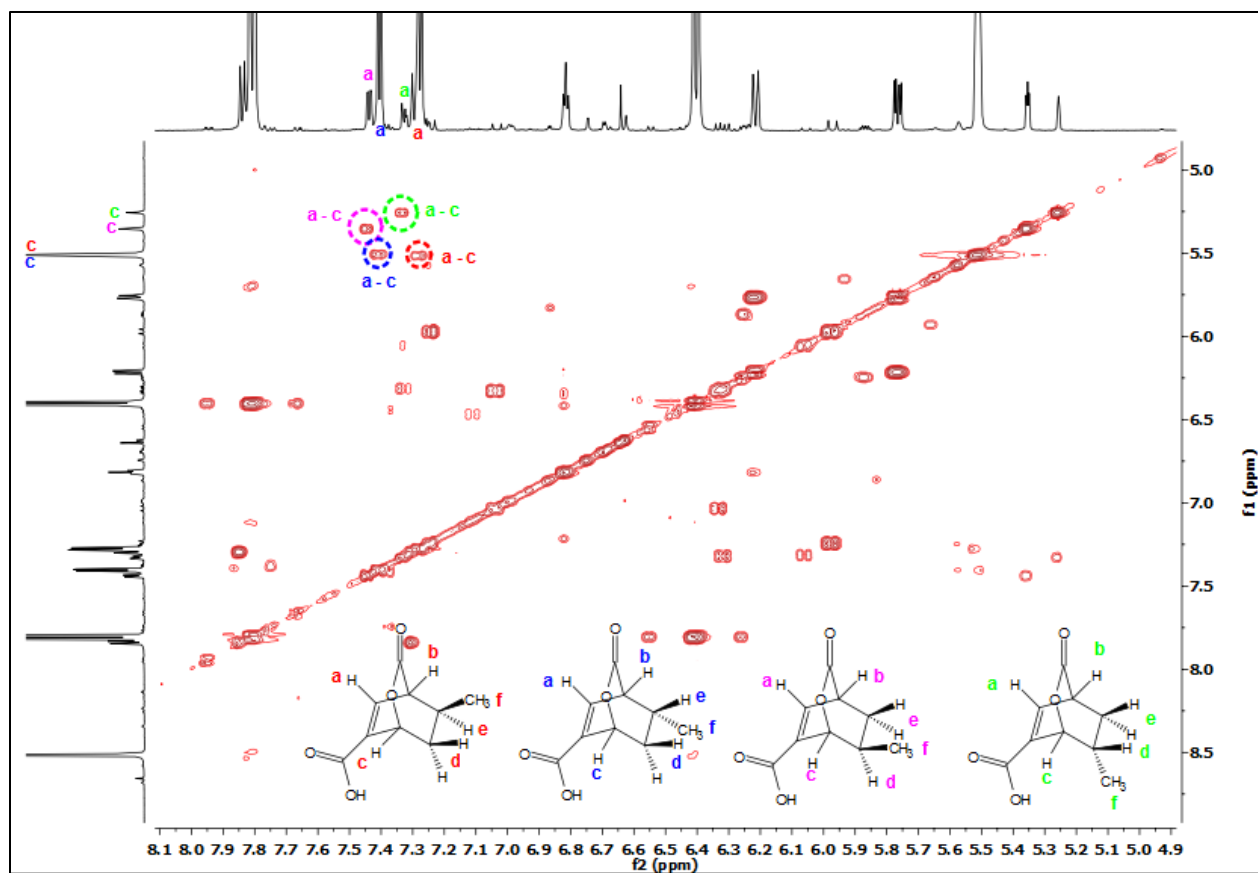


**Figure S3.**  $^1\text{H}$ - $^1\text{H}$  COSY structural assignment of the bicyclic intermediates after a reaction of coumalic acid and propylene at 140 °C for 2 h in the absence of Pd/C catalyst



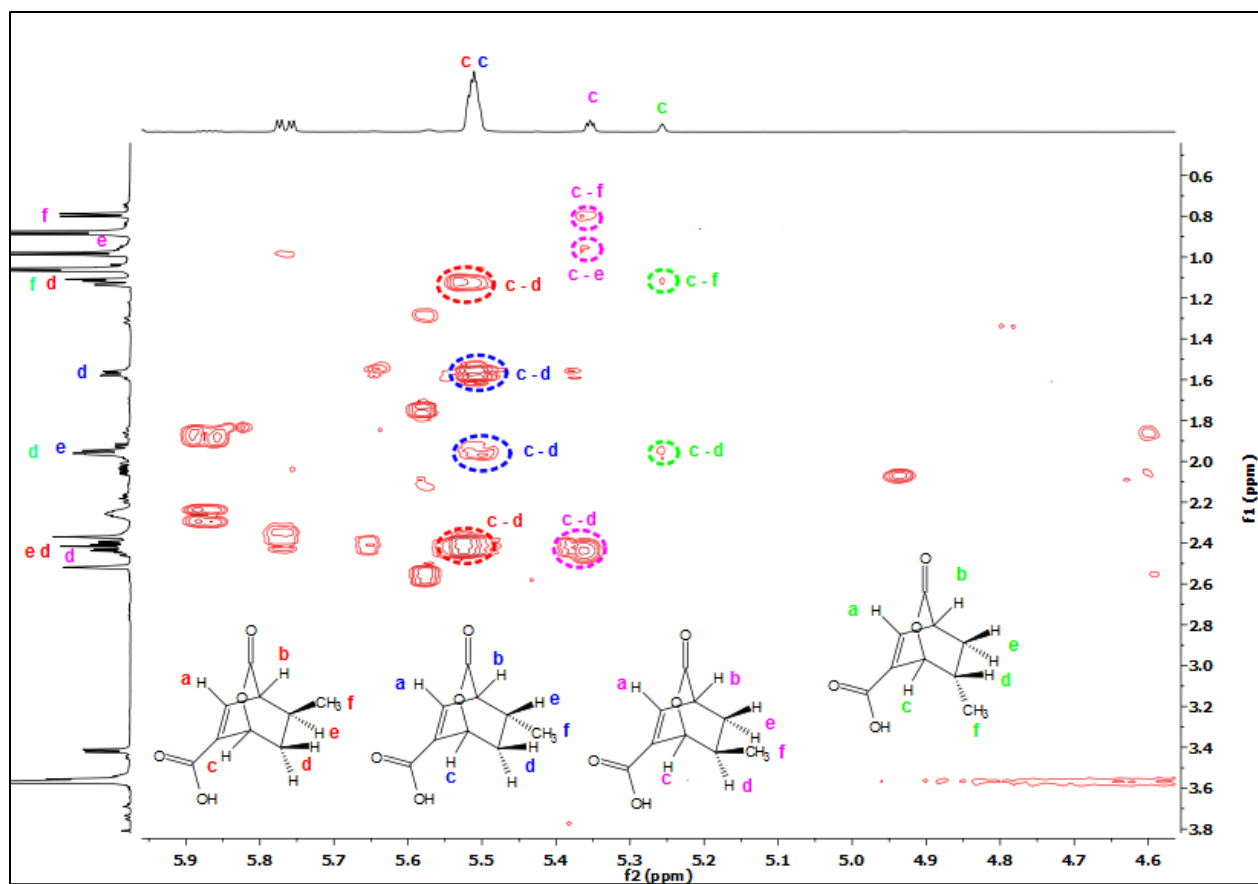


**Figure S4.**  $^1\text{H}$ - $^1\text{H}$  COSY structural assignment of the bicyclic intermediates after a reaction of coumalic acid and propylene at 140 °C for 2 h in the absence of Pd/C catalyst

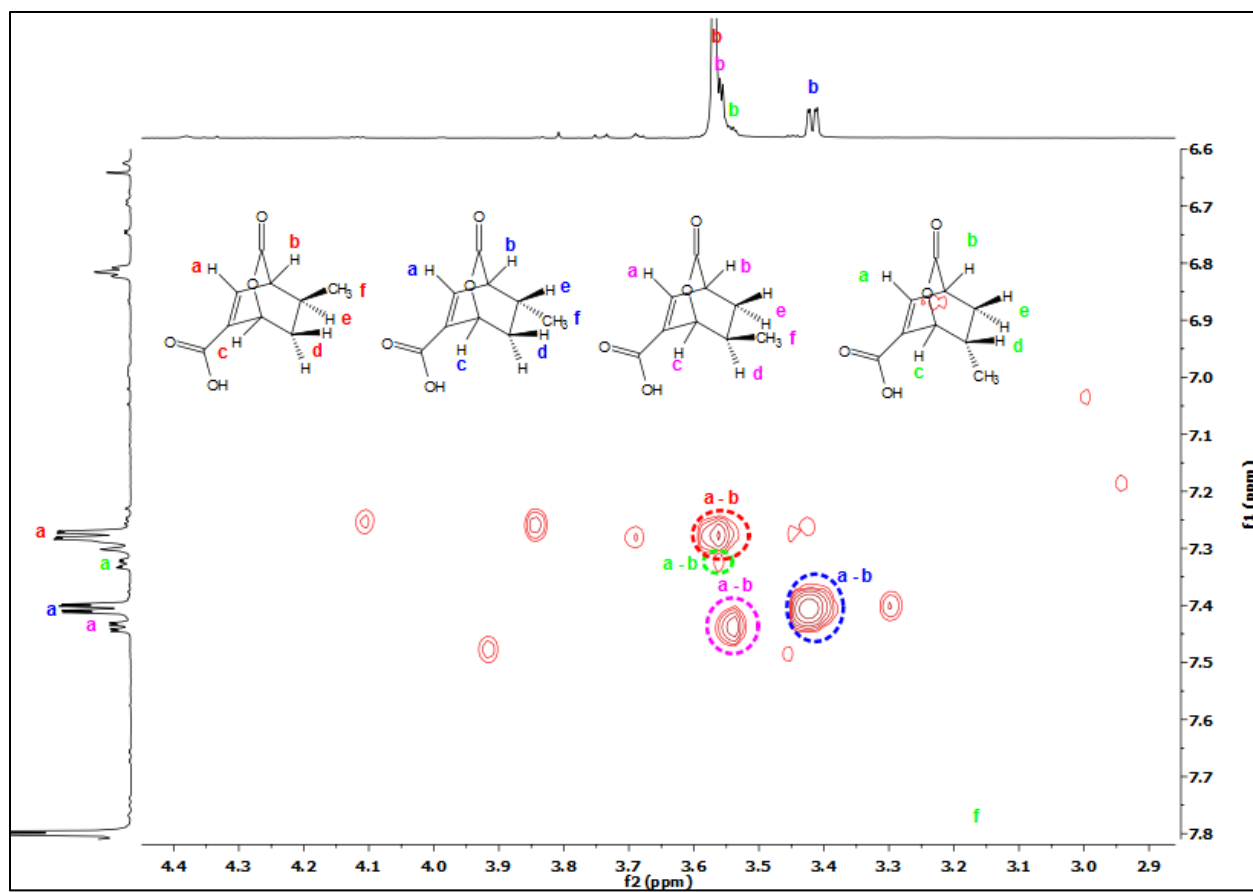


**Figure S5.**  $^1\text{H}$ - $^1\text{H}$  COSY structural assignment of the bicyclic intermediates after a reaction of coumalic acid and propylene at 140 °C for 2 h in the absence of Pd/C catalyst

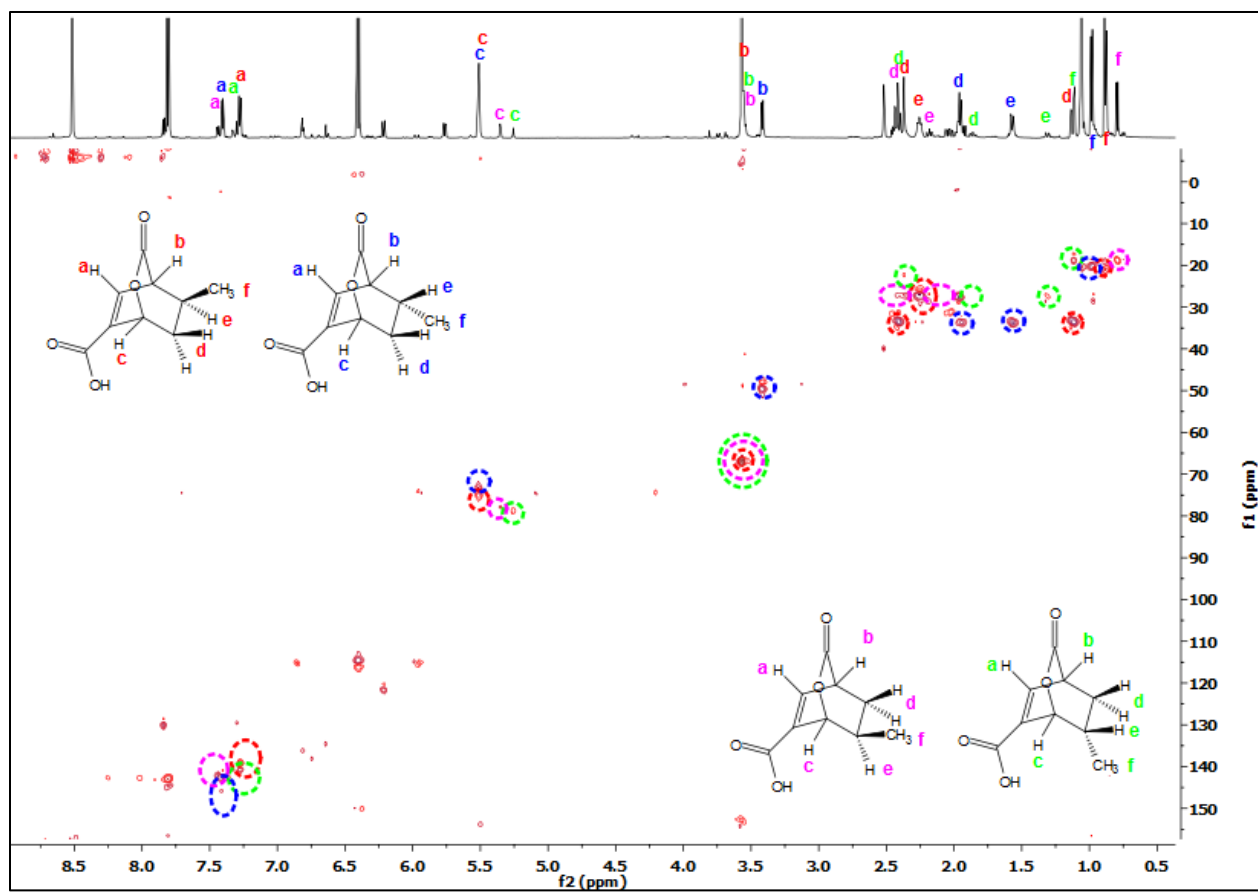


**Figure S6.**  $^{13}\text{C}$ - $^1\text{H}$ -HSQC structural assignment of coumalic acid, bicyclic lactone intermediates after a reaction of coumalic acid and propylene at 140 °C for 2 h in the absence of Pd/C catalyst

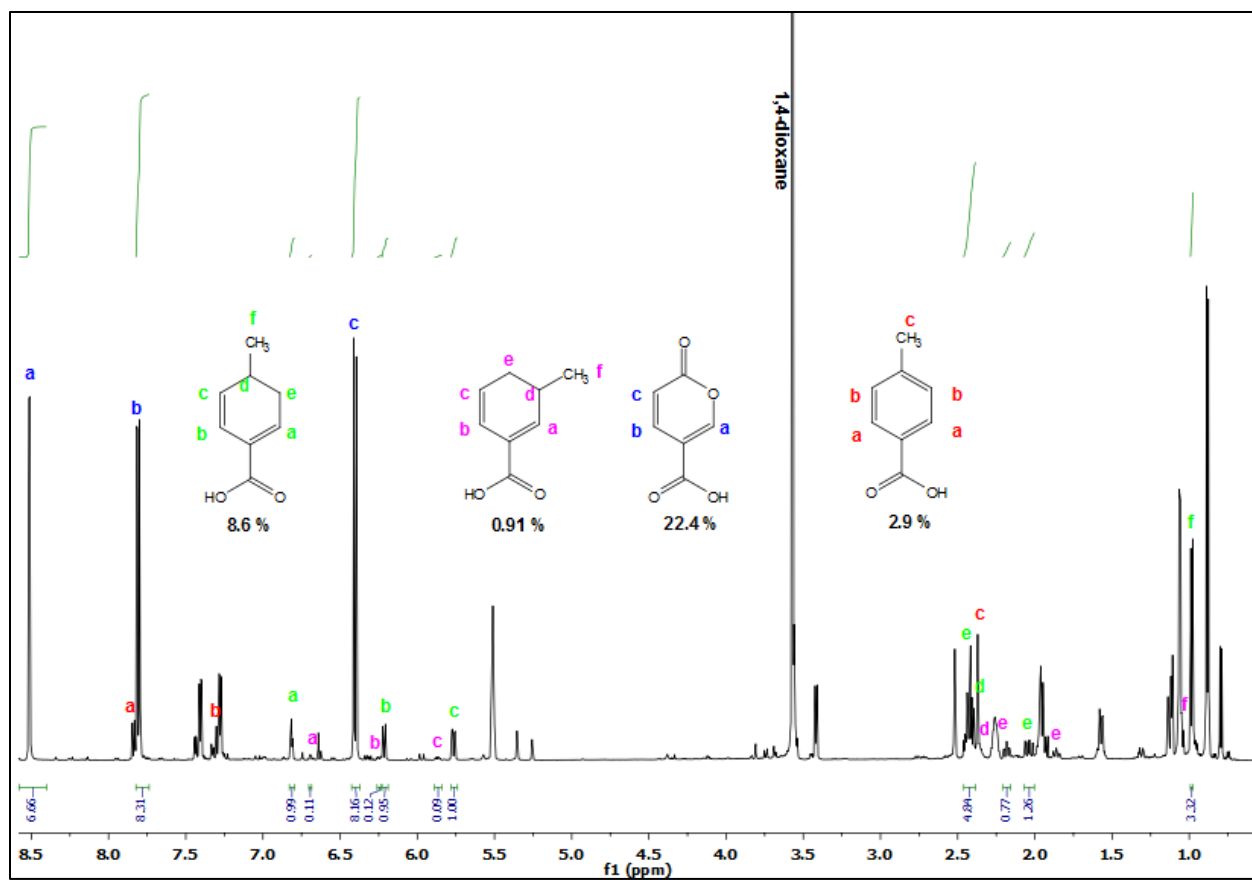


**Figure S7.**  $^1\text{H-NMR}$  structural assignment of coumalic acid, m-/p-diene intermediates and p-toluic acid after a reaction of coumalic acid and propylene at 140 °C for 2 h in the absence of Pd/C catalyst

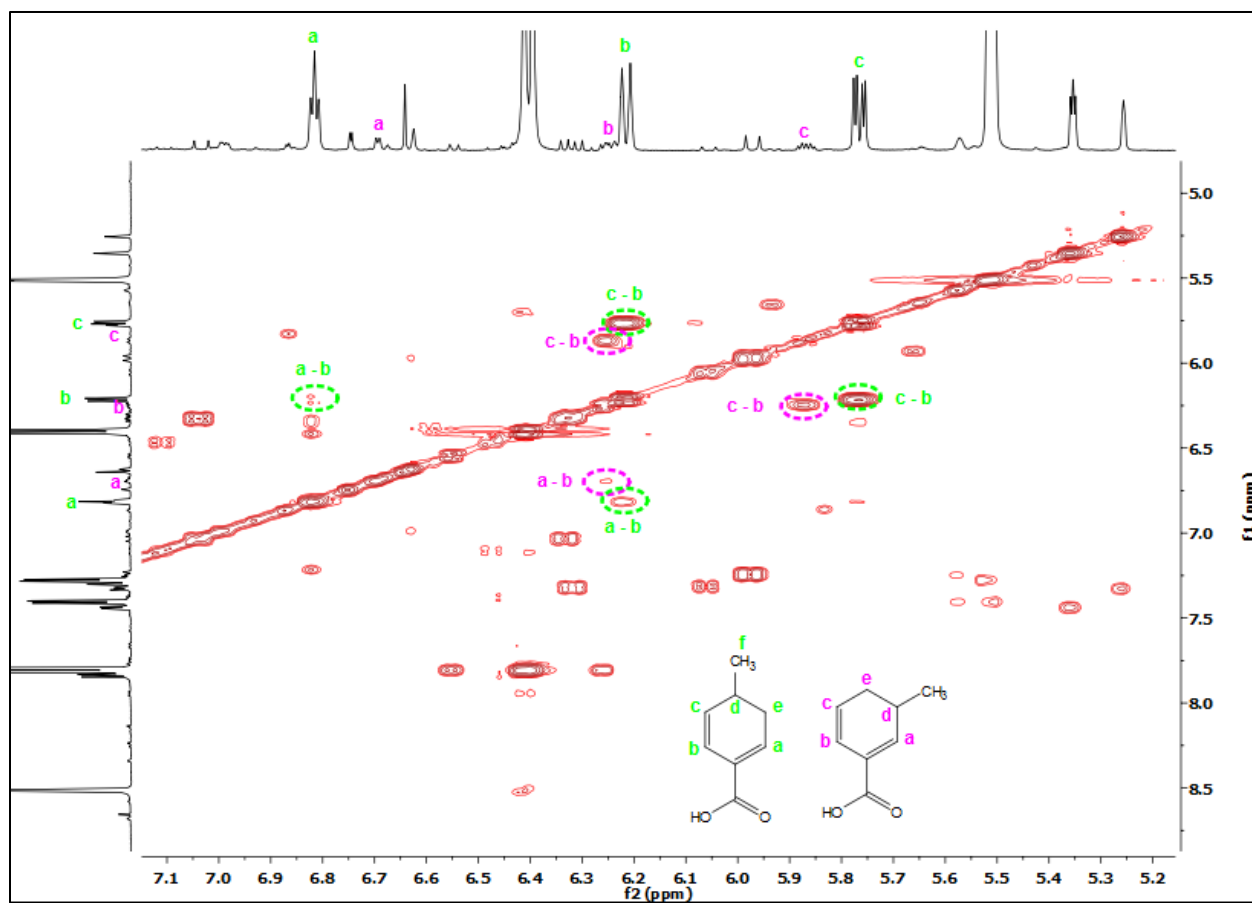


**Figure S8.**  $^1\text{H}$ - $^1\text{H}$  COSY structural assignment of coumalic acid, m-/p-diene intermediates and p-toluic acid after a reaction of coumalic acid and propylene at 140 °C for 2 h in the absence of Pd/C catalyst

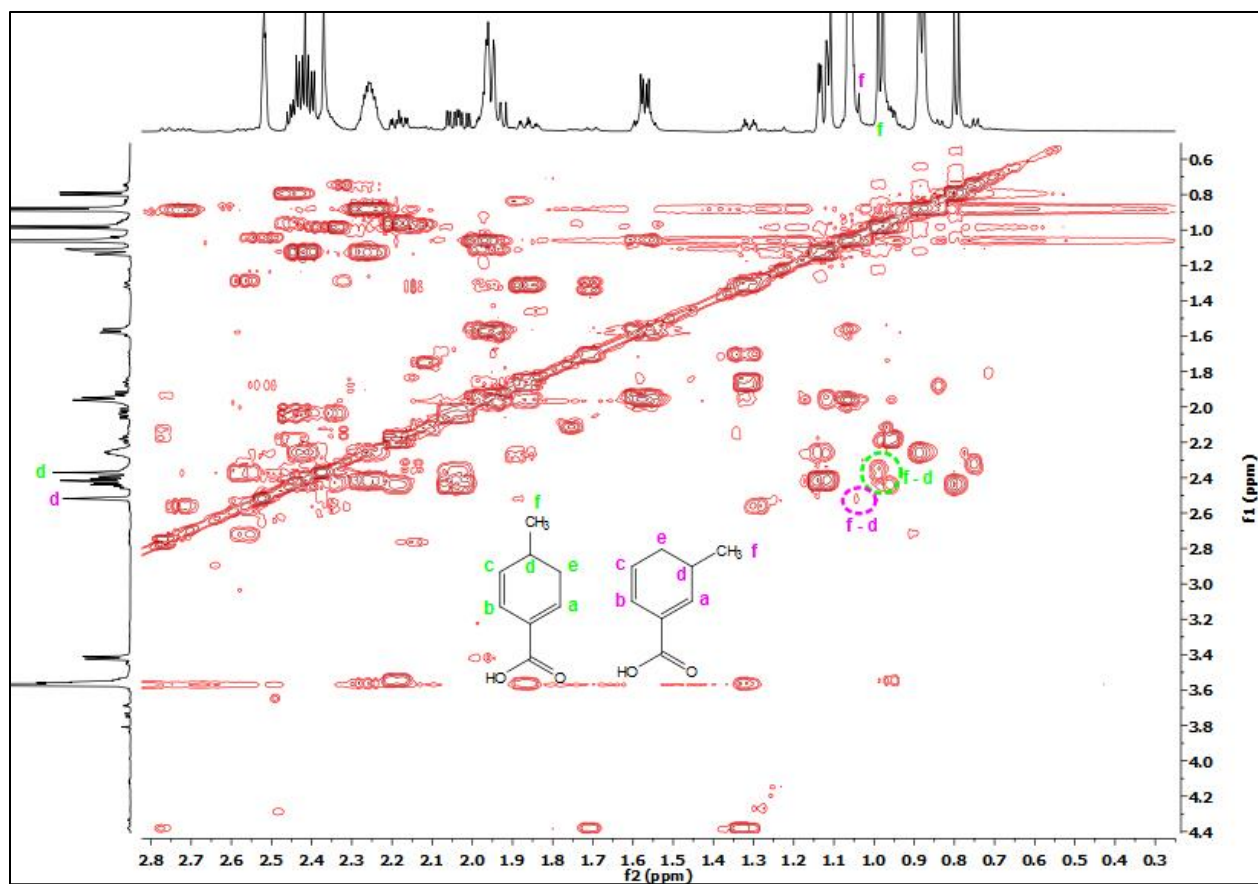


**Figure S9.**  $^1\text{H}$ - $^1\text{H}$  COSY structural assignment of coumalic acid, m-/p-diene intermediates and p-toluic acid after a reaction of coumalic acid and propylene at 140 °C for 2 h in the absence of Pd/C catalyst

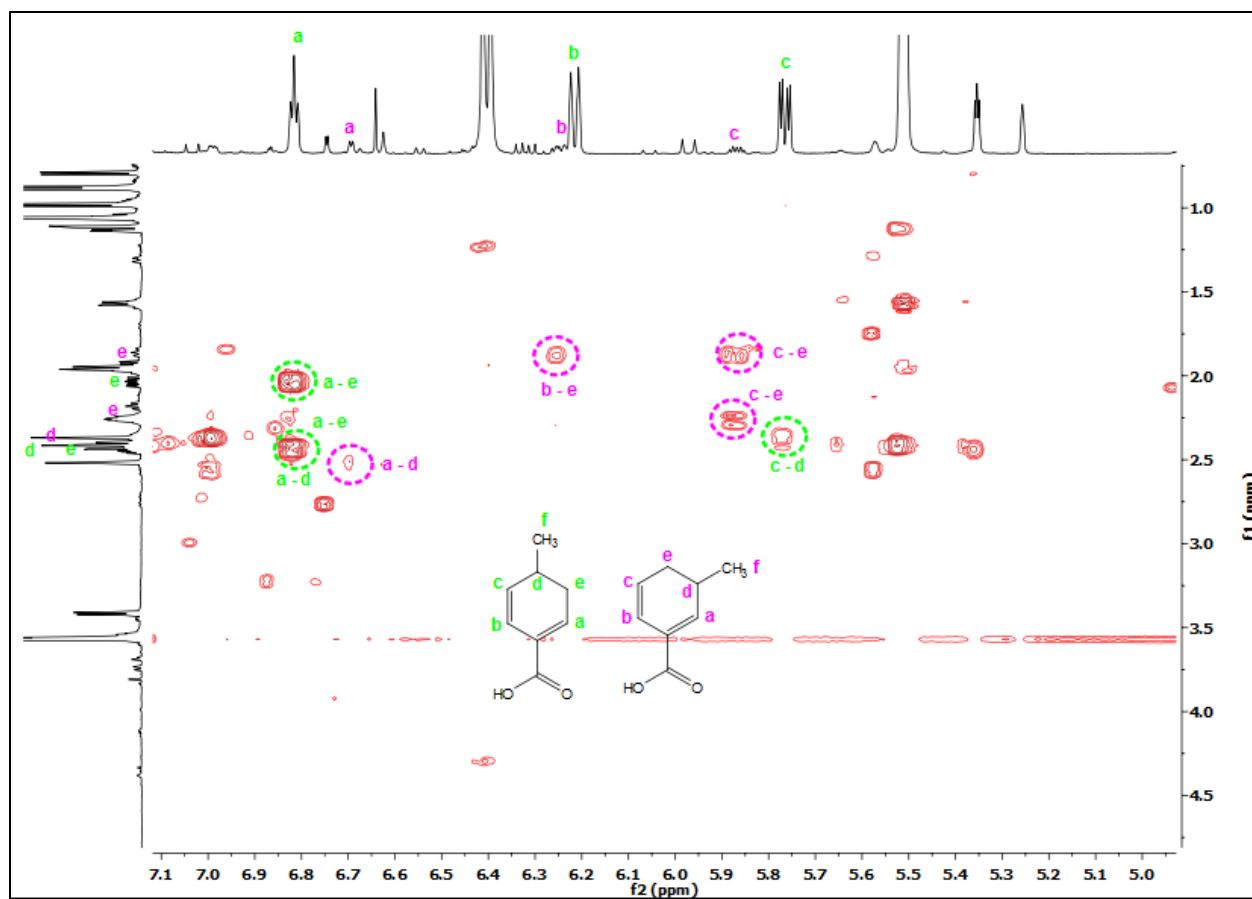


**Figure S10.**  $^1\text{H}$ - $^1\text{H}$  COSY structural assignment of coumalic acid, m-/p-diene intermediates and p-toluic acid after a reaction of coumalic acid and propylene at 140 °C for 2 h in the absence of Pd/C catalyst

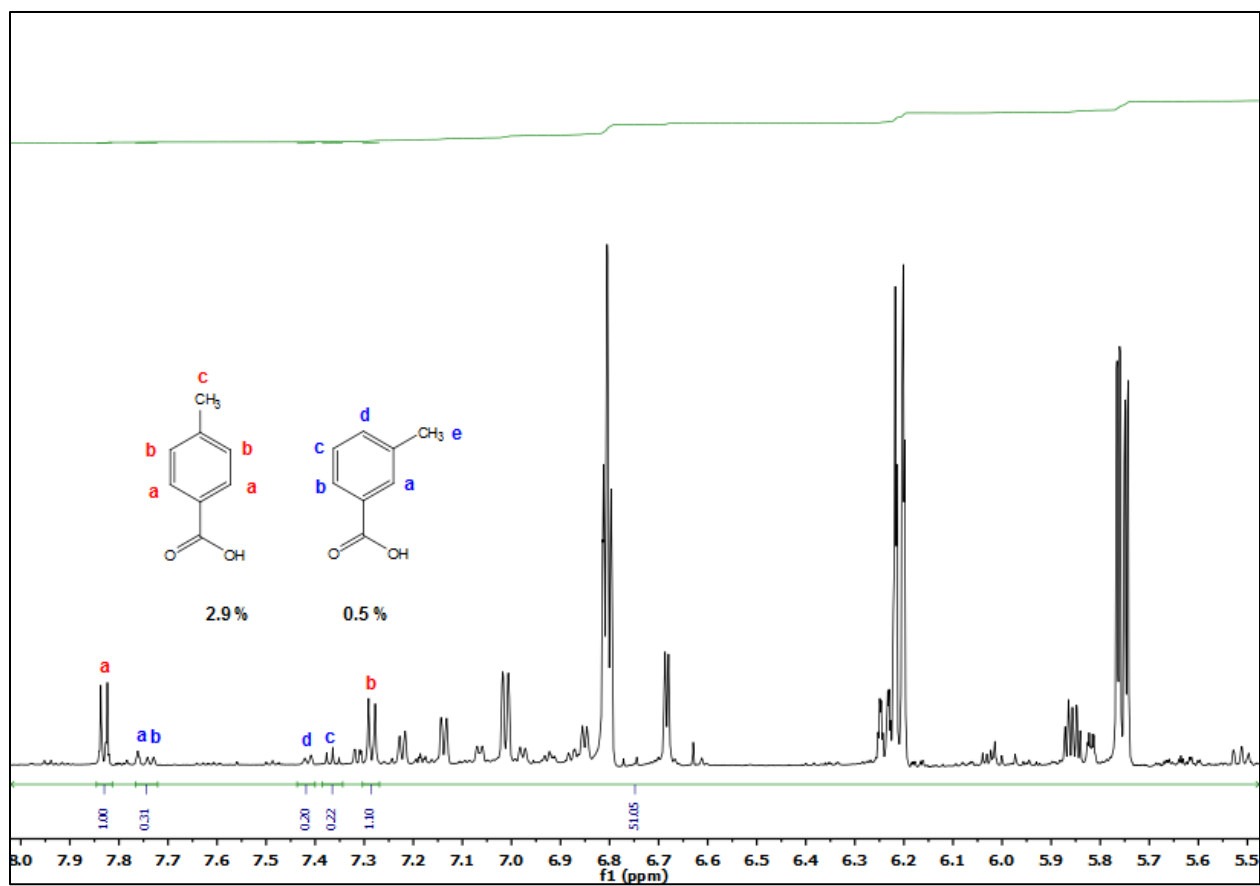


**Figure S11.** <sup>1</sup>H-NMR structural assignment of p/m--toluic acid after a reaction of coumalic acid and propylene at 180 °C for 8 h in the absence of Pd/C catalyst



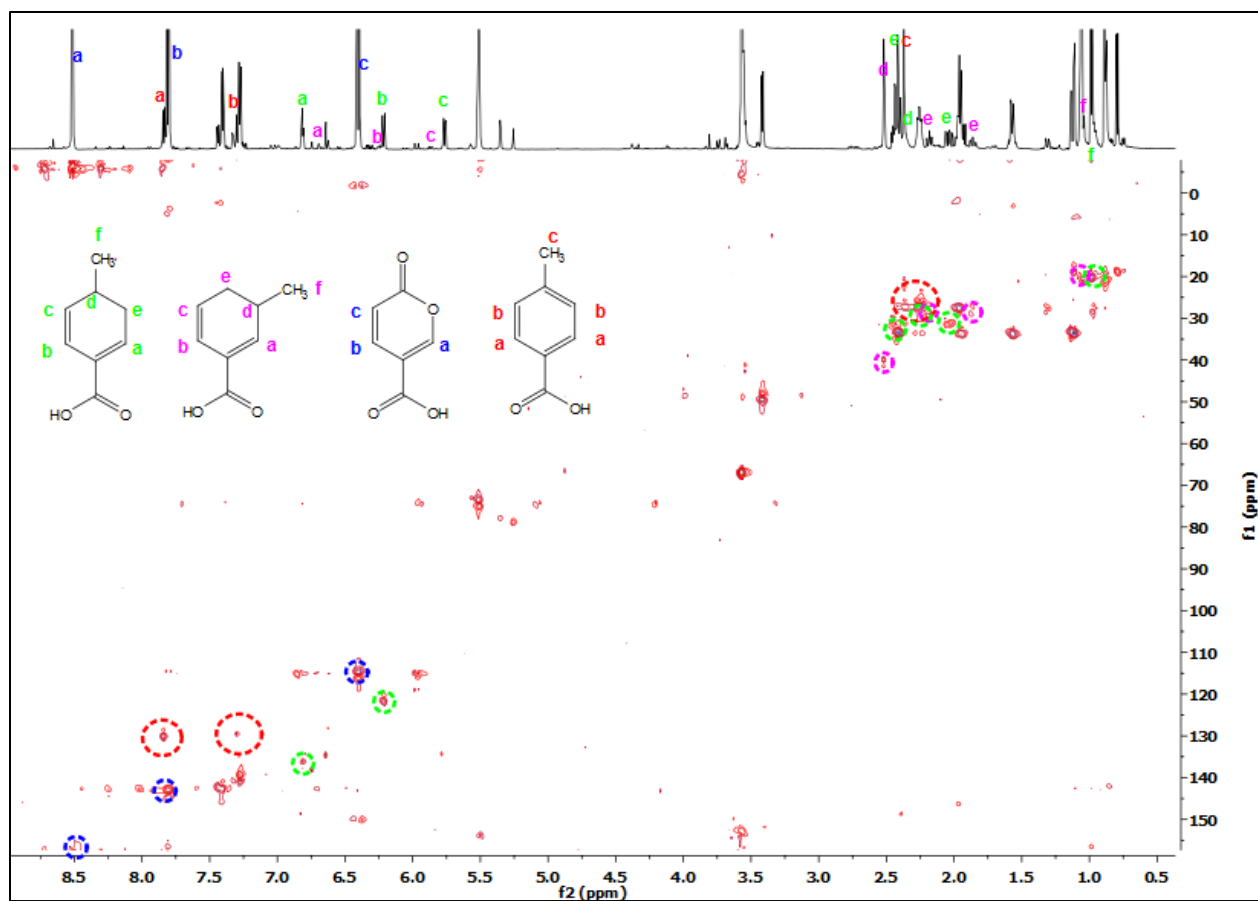


**Figure S12.**  $^{13}\text{C}$ - $^1\text{H}$ -HSQC structural assignment of coumalic acid, m-/p-diene intermediates and p-toluic acid after a reaction of coumalic acid and propylene at 140 °C for 2 h in the absence of Pd/C catalyst

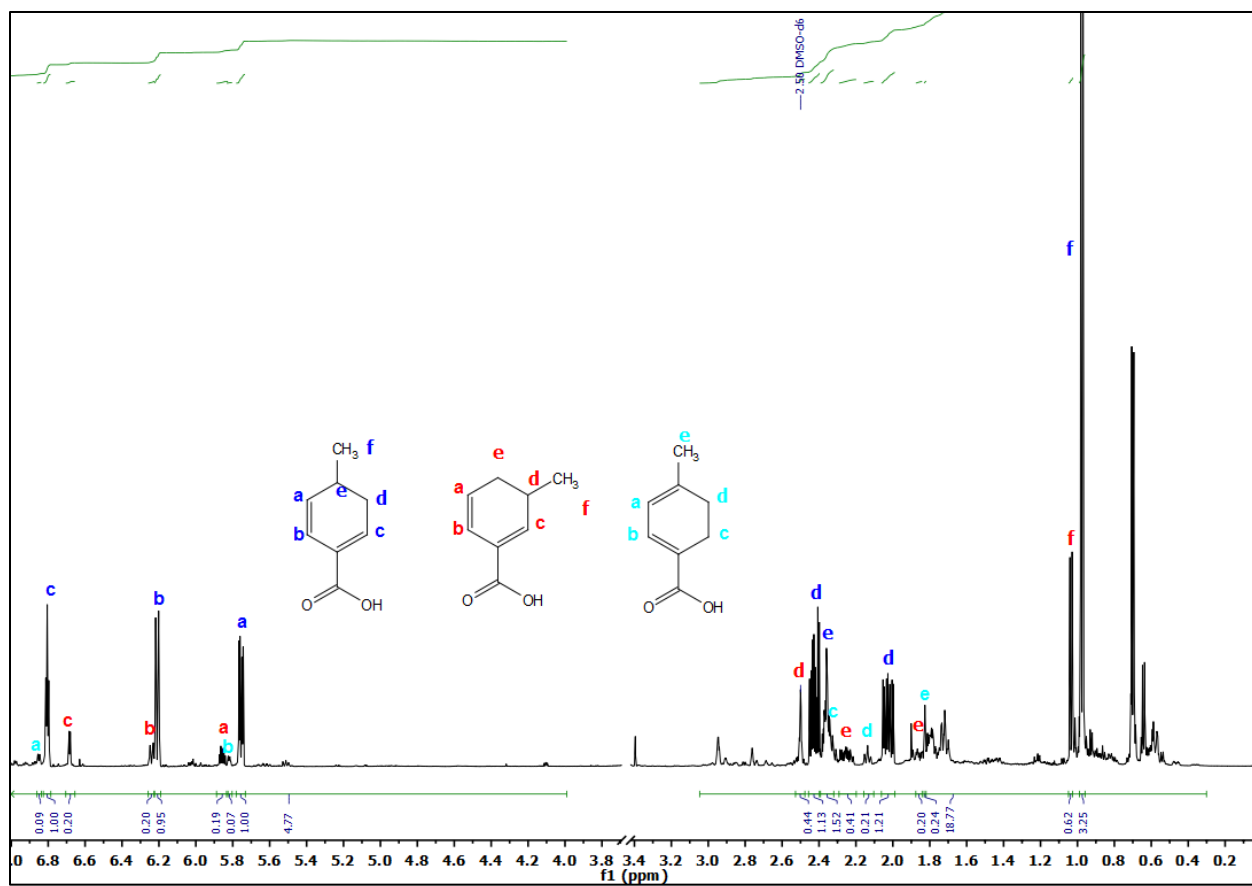


**Figure S13.** <sup>1</sup>H-NMR structural assignment of diene intermediates after a reaction of coumalic acid and propylene at 180 °C for 8 h in the absence of Pd/C catalyst

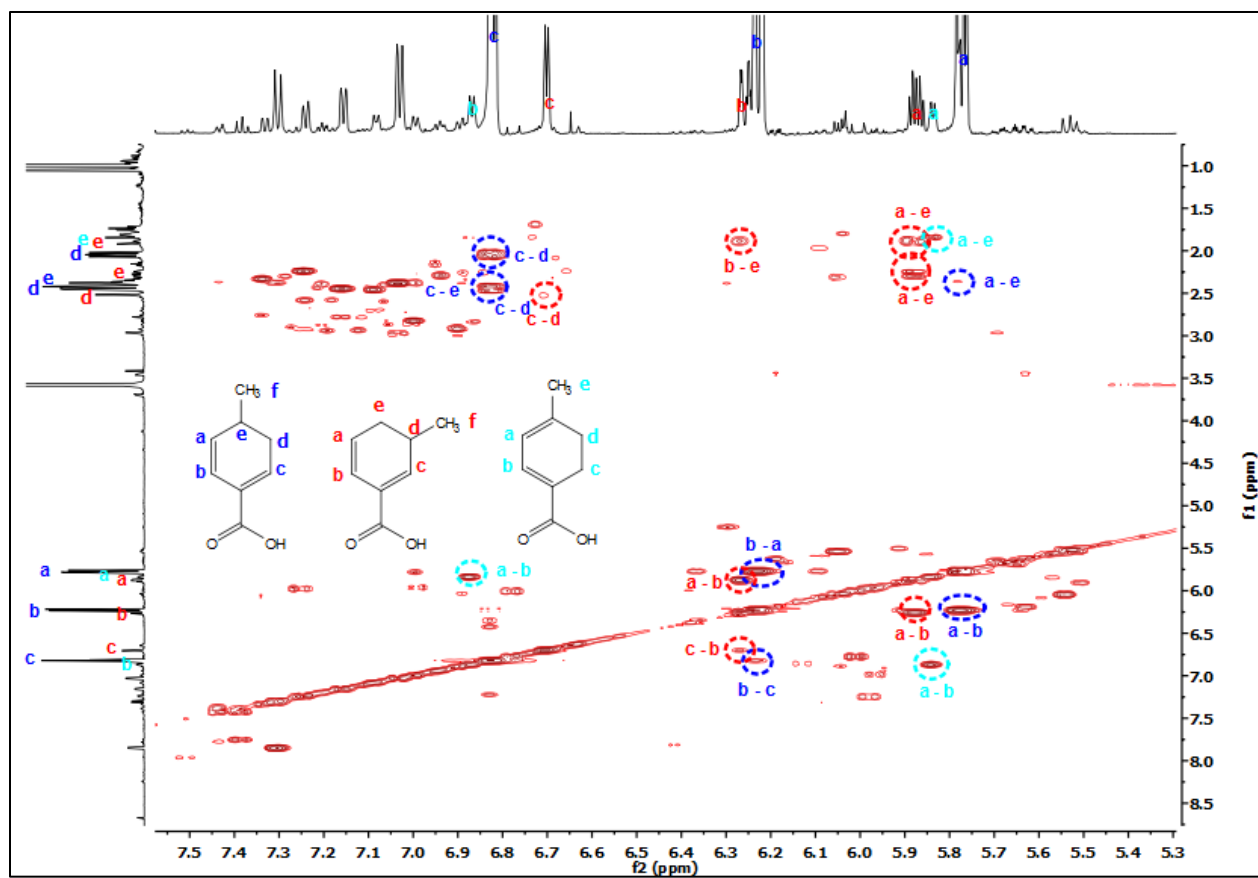


**Figure S14.**  $^1\text{H}$ - $^1\text{H}$  COSY structural assignment of diene intermediates after a reaction of coumalic acid and propylene at 180 °C for 8 h in the absence of Pd/C catalyst

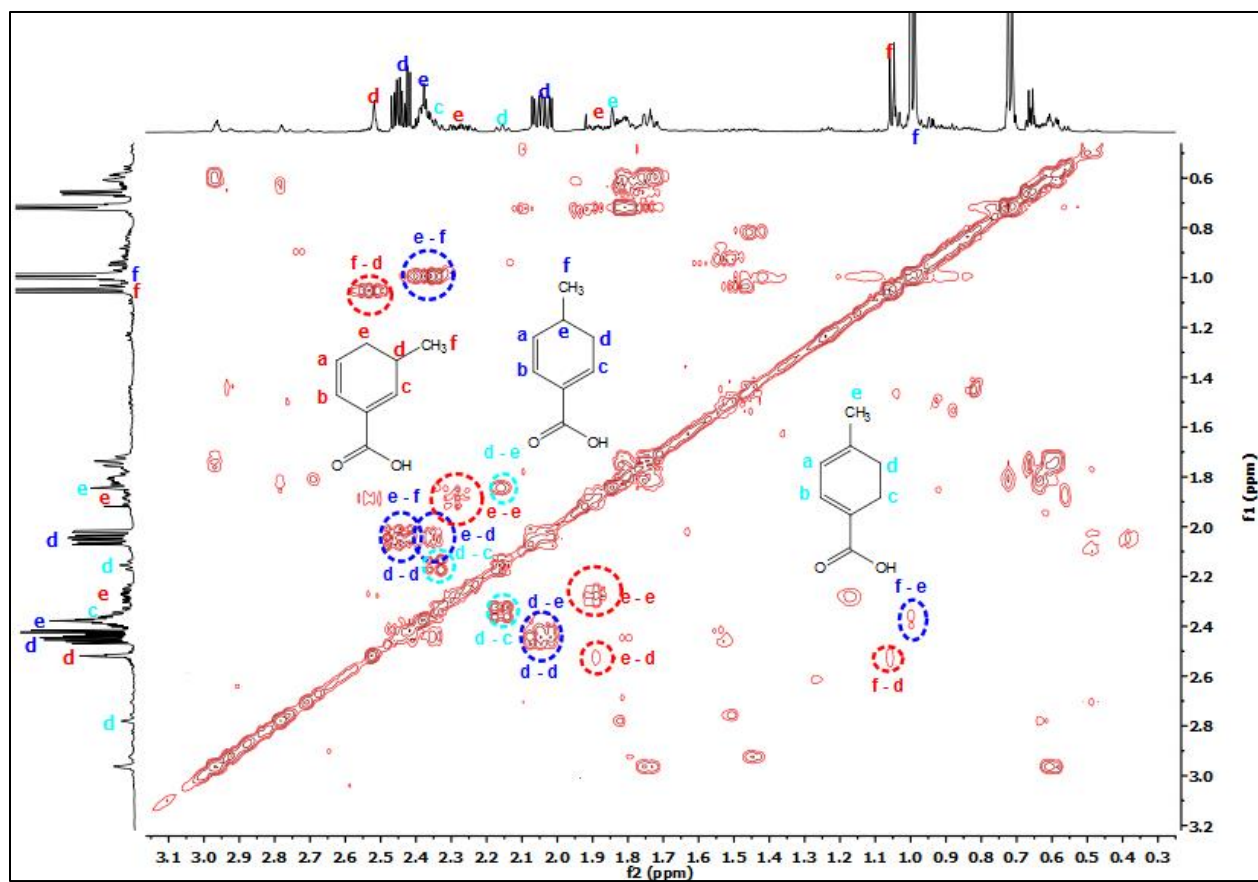


**Figure S15.** <sup>1</sup>H-<sup>1</sup>H COSY structural assignment of diene intermediates after a reaction of coumalic acid and propylene at 180 °C for 8 h in the absence of Pd/C catalyst

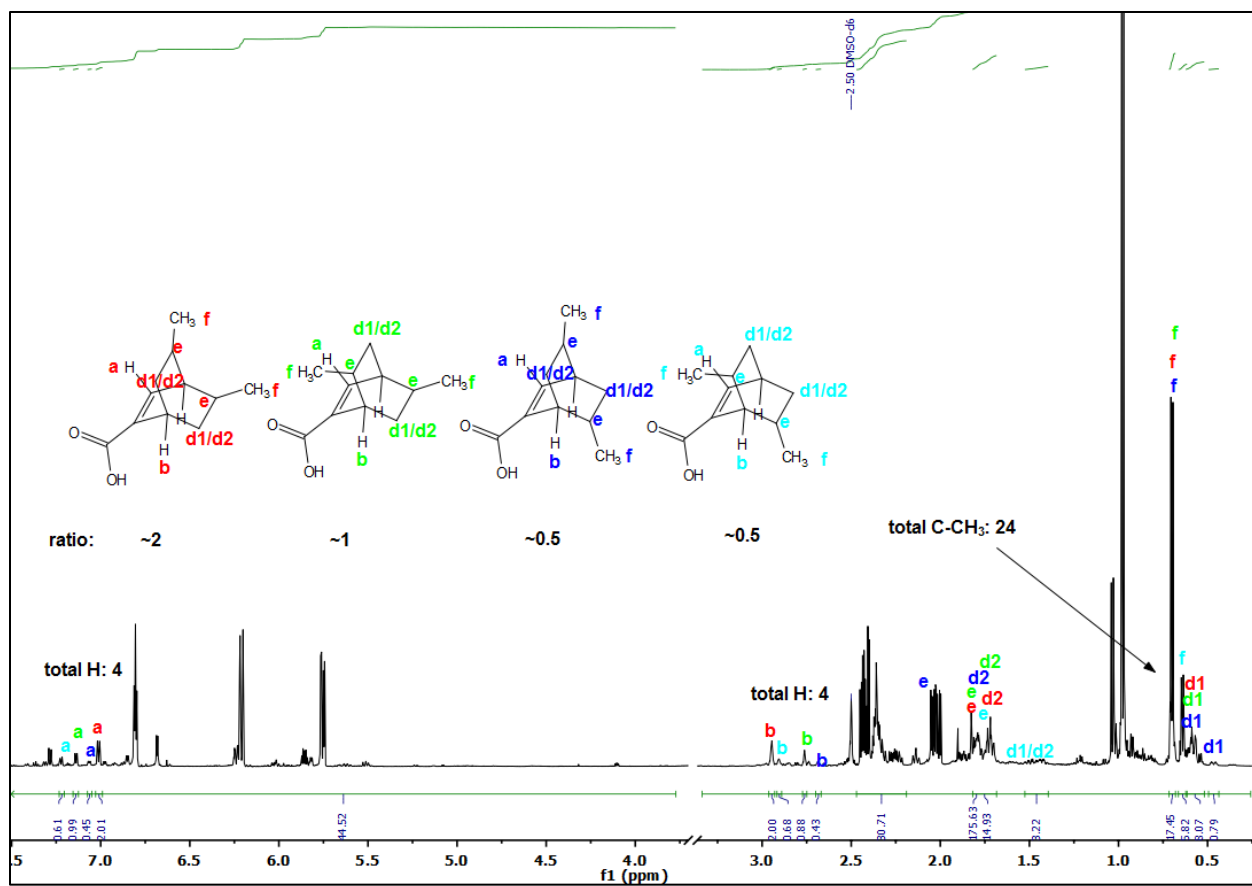


**Figure S16.**  $^1\text{H}$  NMR structural assignment of DDA by-products after a reaction of coumalic acid and propylene at 180 °C for 8 h in the absence of Pd/C catalyst

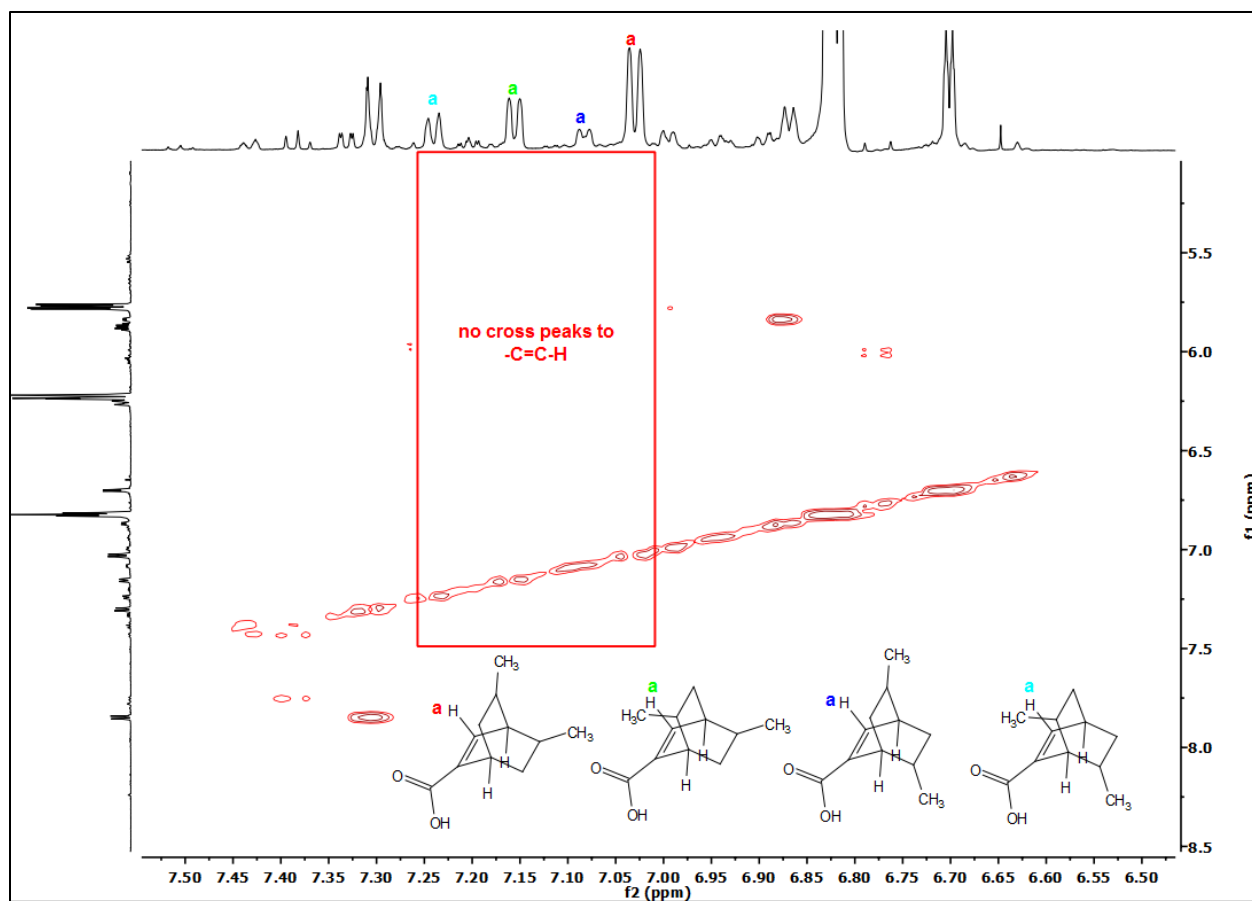


**Figure S17.**  $^1\text{H}$ - $^1\text{H}$  COSY structural assignment of DDA by-products after a reaction of coumalic acid and propylene at 180 °C for 8 h in the absence of Pd/C catalyst

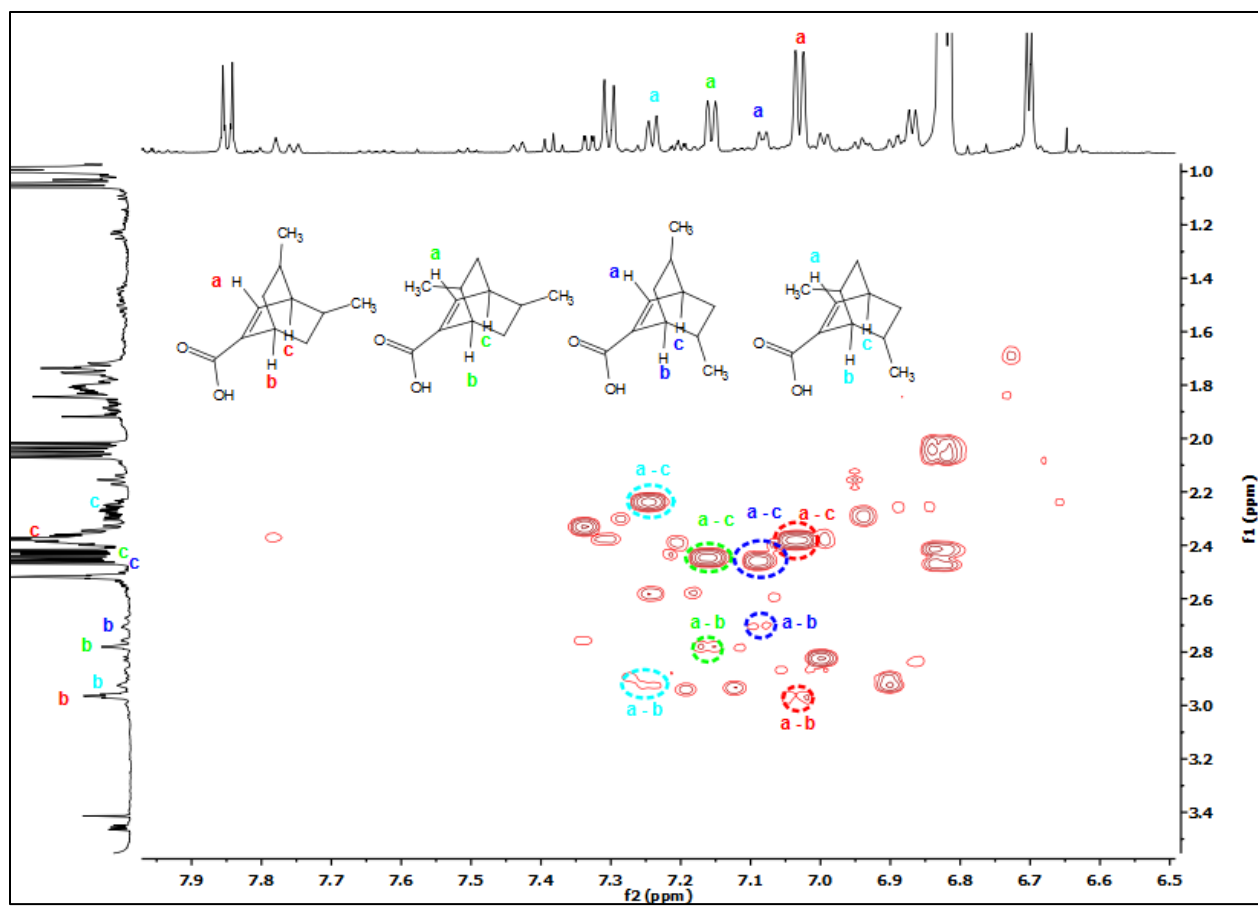


**Figure S18.**  $^1\text{H}$ - $^1\text{H}$  COSY structural assignment of DDA by-products after a reaction of coumalic acid and propylene at 180 °C for 8 h in the absence of Pd/C catalyst

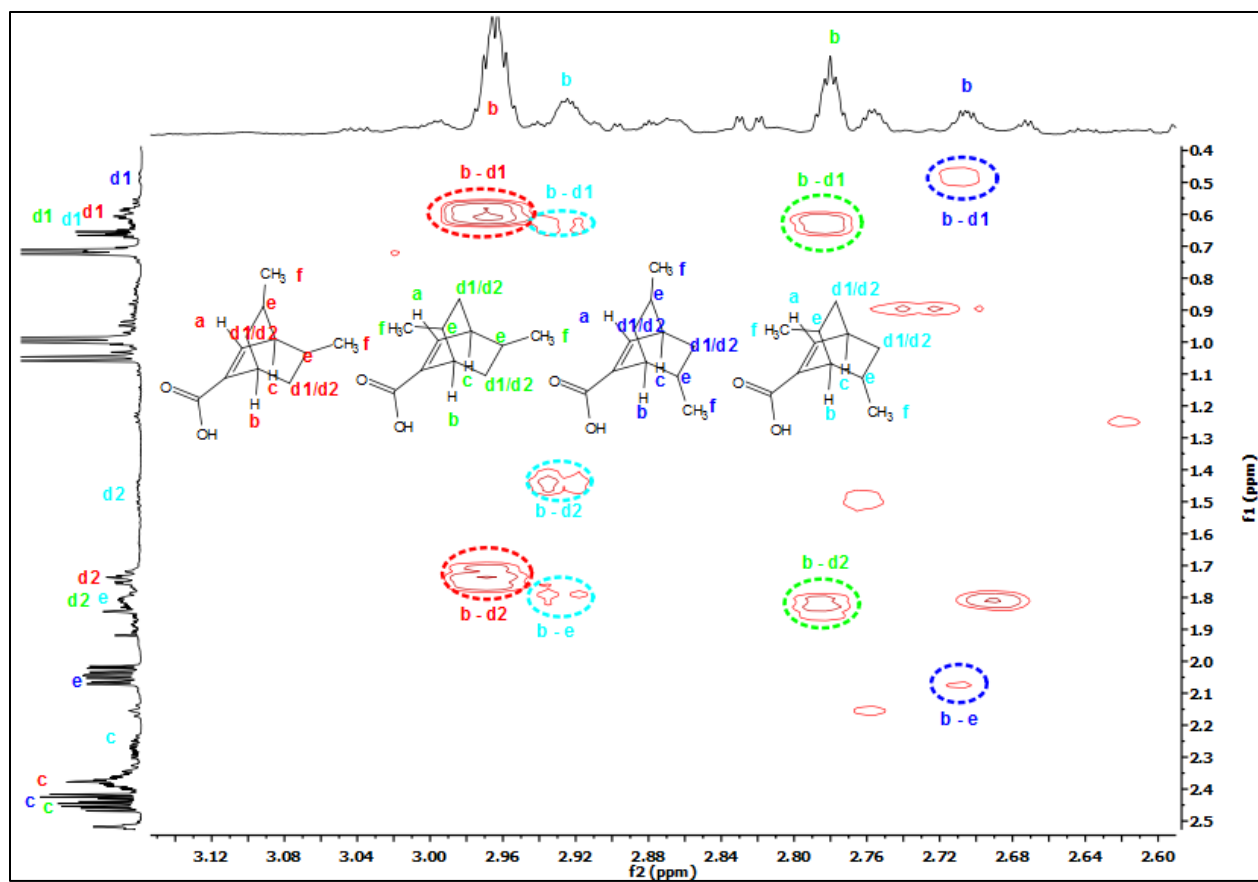


**Figure S19.** <sup>1</sup>H-<sup>1</sup>H COSY structural assignment of DDA by-products after a reaction of coumalic acid and propylene at 180 °C for 8 h in the absence of Pd/C catalyst



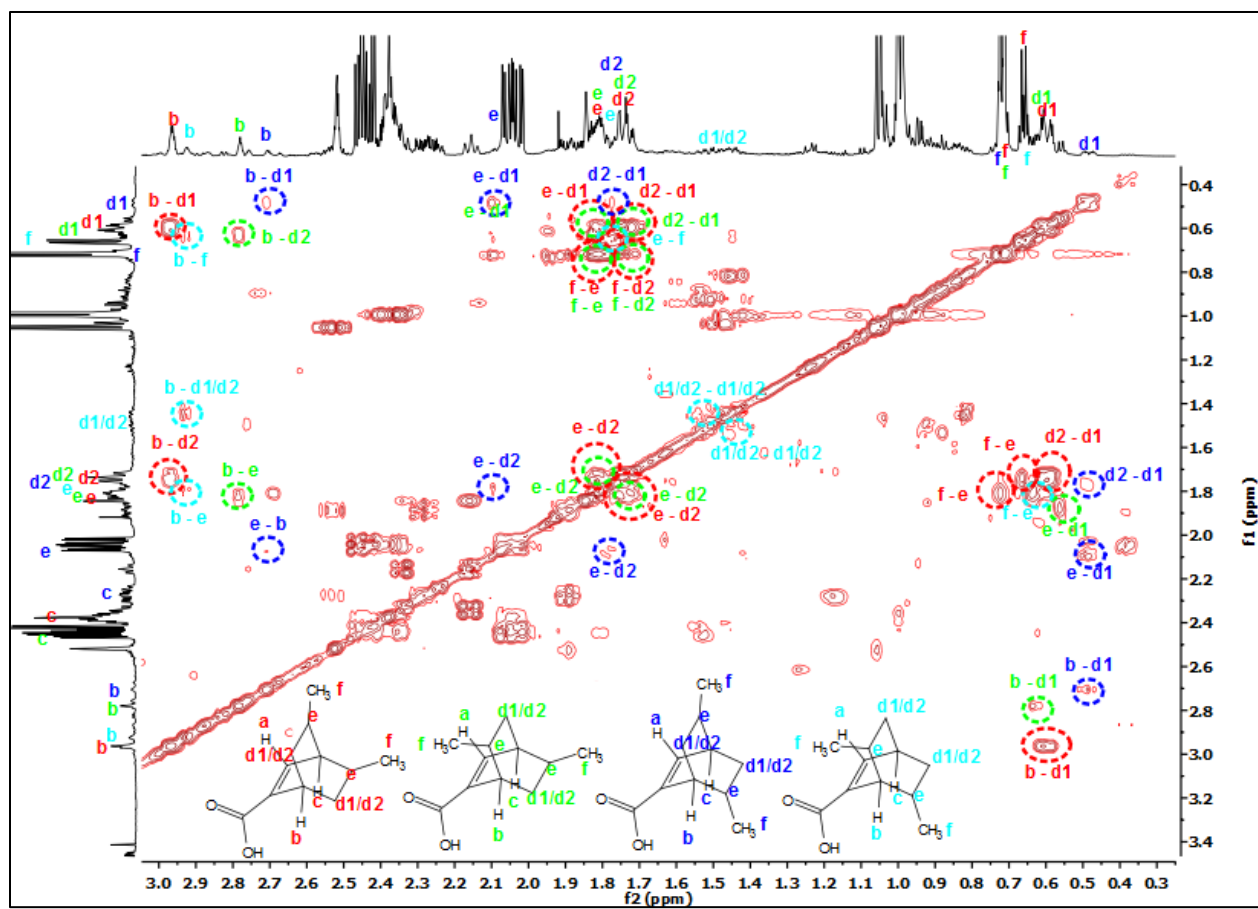


**Figure S20.**  $^1\text{H}$ - $^1\text{H}$  COSY structural assignment of DDA by-products after a reaction of coumalic acid and propylene at 180 °C for 8 h in the absence of Pd/C catalyst

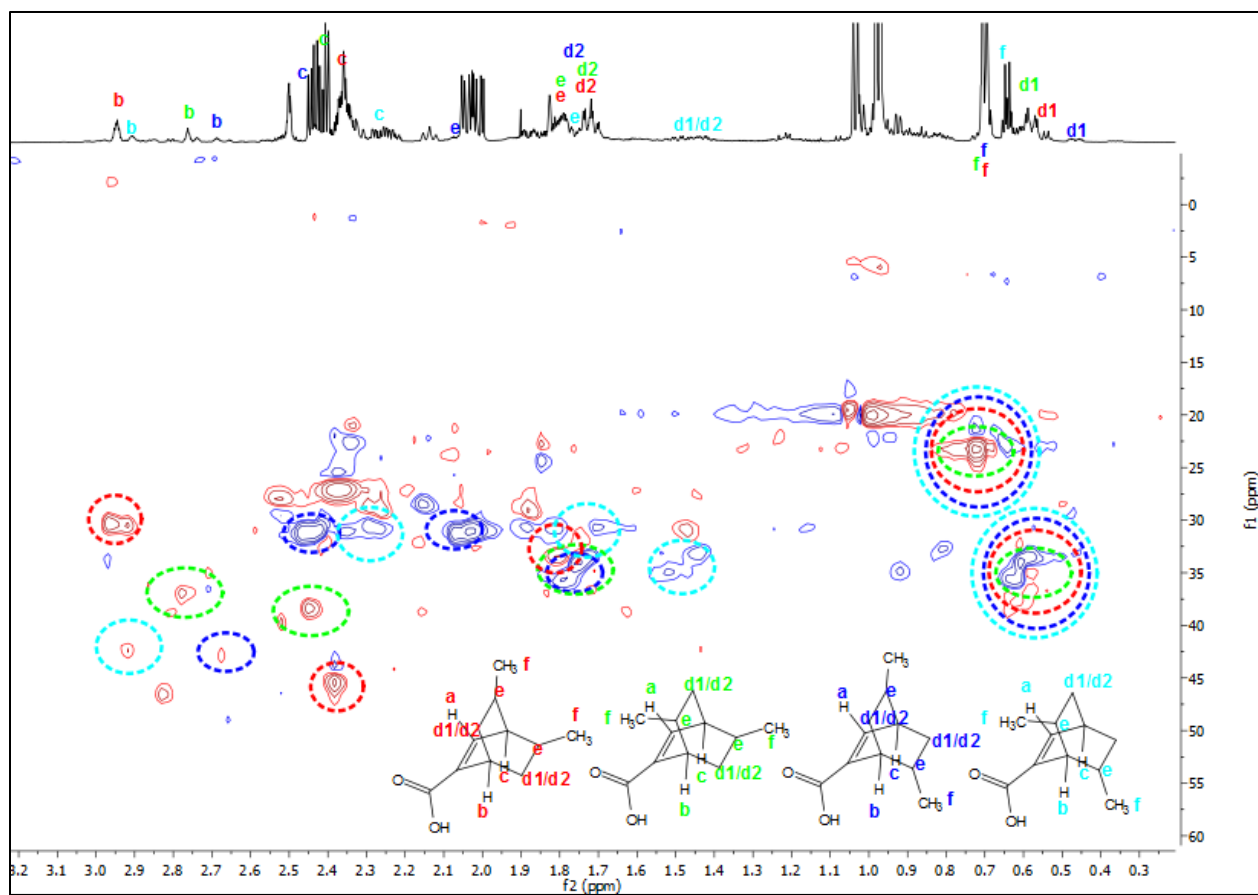


**Figure S21.**  $^{13}\text{C}$ - $^1\text{H}$  HSQC structural assignment of DDA by-products after a reaction of coumalic acid and propylene at 180 °C for 8 h in the absence of Pd/C catalyst

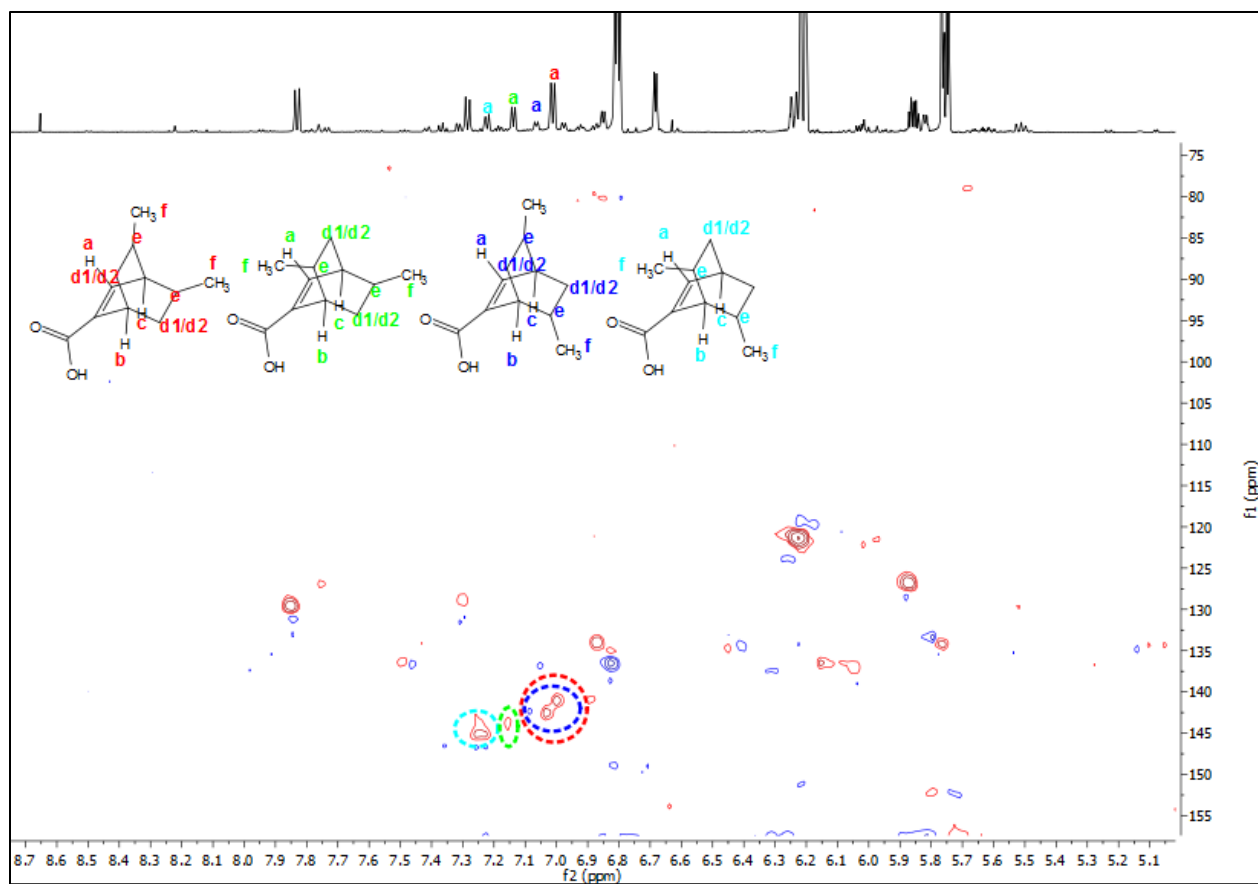


**Figure S22.**  $^{13}\text{C}$ - $^1\text{H}$  HSQC structural assignment of DDA by-products after a reaction of coumalic acid and propylene at 180 °C for 8 h in the absence of Pd/C catalyst

## CHAPTER 3

A NEW SELECTIVE ROUTE TOWARDS BENZOIC ACID AND DERIVATIVES  
FROM BIOMASS-DERIVED COUMALIC ACID

*A paper published in Green Chemistry 2017, 19, 4879-4888*

Toni Pfennig,<sup>a,b</sup> Jack M. Carraher,<sup>a,b</sup> Ashwin Chemburkar,<sup>c,b</sup> Robert L. Johnson,<sup>a,b</sup> Austin Anderson,<sup>a,b</sup> Jean-Phillipe Tessonier,<sup>a,b</sup> Matthew Neurock,<sup>c,b</sup> Brent H. Shanks<sup>a,b</sup>

<sup>a</sup> Department of Chemical and Biological Engineering, Iowa State University, Ames, IA 50011, USA.

<sup>b</sup> NSF Engineering Research Center for Biorenewable Chemicals (CBiRC), Ames, IA 50011, USA.

<sup>c</sup> Department of Chemical Engineering and Material Science, University of Minnesota, Minneapolis, MN, 55438, USA

### 3.1 Abstract

The selective production of aromatics from bio-based sources is an area of interest to expand the potential for greener alternatives to petroleum-derived chemicals. A scalable, efficient route to produce bio-based benzoates is demonstrated in up to 100 mol% yield by carrying out heterogeneous catalytic reactions in non-toxic bio-based solvents at moderate temperatures. This approach extends the 2-pyrone (coumalic acid/methyl coumalate) Diels-Alder platform by utilizing a bioavailable co-reactant ethylene. A detailed investigation using a combination of kinetic experiments, DFT calculations, and multi-dimensional NMR was carried out to determine the detailed reaction network, and corresponding activation energies for critical steps. Additionally, a series of experiments were conducted to maximize yields by comparing different solvents, for both coumalic acid and methyl coumalate. Our results show that the choice of solvent was a significant factor when coumalic acid was the reactant (yields 71-92 mol%), while methyl

coumalate was only minimally affected by the solvent (yields 95-100 mol%). Interestingly, the reaction network and kinetic analysis showed that the Diels-Alder reactions were not significantly different between coumalic acid and methyl coumalate, with the rate limiting step for both being decarboxylation with an activation barrier of 141 kJ/mol compared to 77 kJ/mol for the formation of the bicyclic adduct. Lastly, the reaction cascade was found to be highly susceptible to by-product formation when as little as 5 vol% water was present in the solvent, which demonstrates that the absence of water is essential for high yielding benzoate production.

### 3.2 Introduction

The search for alternatives to fossil-based feedstocks has led to rapid technological advances in the field of bio-renewable chemicals creating many potential opportunities for materials based on renewable carbon sources.<sup>1-6</sup> Technologies to produce aromatics from biomass-derived sources have become targets of interest due to the expansion of shale gas extraction, which has led to a relatively reduced availability of >C4 building blocks, including aromatics.<sup>2, 6, 7</sup> Aromatics are among the most important building blocks used by the chemical industry for the production of a wide array of products, so there is an incentive for the development of selective processes to produce aromatics from bio-based feedstocks.<sup>2, 6, 7</sup>

Benzoic acid (BA) is a large scale commodity chemical with an annual production of 638 kt<sup>8</sup> currently produced by the partial oxidation of toluene using a cobalt-manganese catalyst. BA is used in a wide variety of applications including plasticizers, preservatives, dyes/perfumes and as a feed to produce other chemicals including phenol, caprolactam, and benzaldehyde. Hence, a renewable pathway to produce BA would have broad ranging impacts throughout the chemical value chain.

One route to make bio-based BA is through a formic acid mediated dehydration of quinic or shikimic acid produced via fermentation. This process has several desirable features including high yields for the chemical transformation of quinic and shikimic acids into benzoic acid (up to 90%)<sup>2</sup> and high titers up to 60 g/L for quinic acid and 71 g/L shikimic acid starting from the substrate glucose and using metabolically engineered *E. coli*.<sup>9,10</sup> Although, the primary drawback of this approach is the intrinsically low maximum theoretical yield of the shikimic/quinic acid fermentation of 43 %, and to date the highest yields reported correspond to an overall mol/mol yield of 23, and 27 %.<sup>10</sup> This fermentation bottleneck creates a significant problem for efficient utilization of the glucose feedstock. As a major fraction of the total cost of the fermentation step is the glucose feedstock, its inefficient utilization would have a significant negative impact on the cost required to produce BA.

An alternative pathway to bio-based BA and its methyl ester (MeBA) is through a furanic based platform utilizing a Diels-Alder reaction sequence of furan with methyl acrylate (or acrylic acid) showing moderate yields up to 51 mol%.<sup>7</sup> Additionally Diels-Alder reactions of methyl furan with ethylene provides a viable pathway to produce bio-based toluene, which could be utilized as a drop-in replacement for production of BA. Toluene selectivities, however, never exceeded 46 mol% due to by-product formation.<sup>11</sup> Improvement to this selectivity would require approaches to improve the stability of the bio-based starting materials thereby minimizing by-product formation.

Another approach utilizing biological and chemical catalysis to produce partially biomass-derived methyl benzoate (MeBA) is based on the bio-based cyclic lactone methyl coumalate (MeCMA). The formation of bio-based MeBA is accomplished using a one-pot Diels-Alder/decarboxylation/dehydrogenation reaction sequence between MeCMA and butyl vinyl ether with excellent yields up to 89 mol%.<sup>12</sup>

Bio-based 2-pyrones can be produced by the fermentation of glucose to form malic acid<sup>13,14</sup> followed by acid catalyzed dimerization of malic acid to coumalic acid (Scheme 1).<sup>12</sup> The synthesis of 2-pyrone coumalic acid (CMA) via this route has several attractive features. First, the atom efficiency of the malic acid fermentation is highly favorable, with the capability to even utilize a CO<sub>2</sub> fixating pathway allowing for a theoretical yield of 2 moles of malate per mole of glucose (Scheme 1).<sup>14</sup> Second, efficient fermentation technology is already developed for this route. For example, Novozymes currently uses a metabolically engineered *Aspergillus oryzae* capable of producing 1.38 mol malate per mol glucose at a theoretical yield of 69 % and with high titers of 154 g/L, which could be implemented on an industrial scale.<sup>13</sup>

An approach to improve the viability of the 2-pyrone CMA/MeCMA platform is to utilize a less expensive dienophile as the co-reactant. In theory ethylene should work in an analogous fashion as butyl vinyl ether, but at a substantially lower cost with nearly perfect atom efficiency. Additionally, as the production of ethylene from bio-ethanol is commercially demonstrated, a potential exists for 100 % bio-based process.<sup>3</sup>

As part of the development of new biomass-derived and renewable processes, we report herein report on the synthesis of BA or MeBA from CMA or MeCMA, respectively, and ethylene with very high yields of >91 mol-% utilizing a one-pot sequential Diels-Alder/decarboxylation/dehydrogenation reaction path. Considering the industrial importance of renewable BA, and the lack of available comprehensive information about this alternative route in the literature, the focus of this work is to provide detailed information of the reaction network, and intrinsic kinetics of individual reaction steps, which can be used to improve the overall process.

### 3.3 Experimental

#### 3.3.1 Reagents and Materials

Coumalic acid (>97 %),  $\gamma$ -valerolactone (98 %), and 10 wt% Pd on activated carbon were obtained from Sigma Aldrich. Toluene (99.9 %), methanol (MS grade), water (MS grade), acetic acid (MS grade) were obtained from Fischer Scientific. Methyl coumalate (98 %) and ethylene (99.5 %) were obtained from Acros Organics and Matheson, respectively. The deuterated solvents benzene- $d_6$  (99.5 %), dioxane- $d_8$  (99.5 %) were obtained from Cambridge Isotope Laboratories Inc. All chemicals were used without further purification.

#### 3.3.2 Apparatus and general Procedure

Reaction kinetic measurements for the overall reaction of CMA (or MeCMA) and ethylene were performed using a 50 ml micro reactor system from Parr (4590 Series). Catalytic reactions were carried out using a 10 wt% Pd/C catalyst, which was added to the CMA (or MeCMA) containing solution before the reactor was sealed and purged five times with nitrogen to remove residual air. The reactor was then charged with ethylene for approximately 30 min until saturation of ethylene in the solvent was achieved. Subsequently, the system temperature was increased to the desired reaction condition with a heating rate of 10 K min<sup>-1</sup>. Samples were periodically withdrawn from the reactor through a high pressure sampling tip tube to follow the reaction progress over time. Samples were withdrawn once the reactor reached the desired reaction temperature as the starting point reference. After the liquid phase reaction products were collected, the samples were filtered through a 0.2 micron syringe filter and analyzed via NMR, UPLC-PDA/QDa and GC-FID/MS.



The Diels-Alder reaction evaluation of CMA or MeCMA with ethylene were performed at a temperature range between 90-120 °C without the presence of catalyst following the reaction procedure described above. The solvent 1,4-dioxane was used due to its superior solubility of both CMA and MeCMA.

The decarboxylation reaction studies of the Diels-Alder product (DAP) decarboxylation were performed at a temperature range between 140-160 °C, using high pressure NMR tubes from Wilmad-Labglass. The reactant (2) for this study was synthesized via Diels-Alder reaction of CMA (or MeCMA) and ethylene in 1,4-dioxane at 110 °C for 16 h giving high yield (>98 %). Through evaporation (using a stream of dry air) of the solvent, the reaction product (2) was obtained and subsequently dissolved in dioxane-*d*<sub>8</sub>. The solution was then transferred into the high-pressure NMR tubes. Before the tube was sealed, 2.5 μL of an internal standard (dimethylformamid, DMF) was added to perform quantitative analysis. Subsequently, the tubes were placed into a heated oil bath to initiate the decarboxylation reaction. The tubes were periodically taken out of the oil bath cooled to room temperature and the reaction products were analyzed via <sup>1</sup>H-NMR. Running the reaction in a deuterated solvent allowed for direct NMR sample analysis of the reaction products without further sample workup.

Reaction kinetics measurements of water mediated CMA breakdown was performed using different amounts of D<sub>2</sub>O added to the solution comprising the deuterated solvent dioxane-d<sub>8</sub> and the reactant CMA. This reaction was conducted using high pressure NMR tubes from Wilmad-LabGlass that were loaded with the reaction solution, sealed and heated without exposing the reaction solution to the gaseous reactant ethylene to exclusively investigate the stability of CMA under reaction conditions. Here, a 0.15 M stock solution of coumalic acid and 0.025 M solution of DMSO<sub>2</sub> (internal standard) was prepared in deuterated dioxane-*d*<sub>8</sub>. A total volume of 300 μL of

stock solution were added to the high pressure NMR tubes (Wilmad-Labglass) and H<sub>2</sub>O or D<sub>2</sub>O were added to yield 0-5 vol%. NMR tubes were sealed and heated to 171 °C. Samples were removed and allowed to cool to room temperature prior to collection of <sup>1</sup>H NMR spectra.

To elucidate the reaction network of the MeCMA reaction with ethylene, 2D-NMR structural assignments were carried out using different NMR techniques such as <sup>1</sup>H-NMR, <sup>1</sup>H-<sup>1</sup>H COSY, <sup>13</sup>C-<sup>1</sup>H HSQC. The products analyzed via 2D-NMR were obtained from the reaction of MeCMA and ethylene following a 48 h reaction at 90 °C in the absence of the Pd/C catalyst.

### 3.3.3 Sample Analysis

NMR sample analysis of the reaction mixtures obtained from the batch reactions were carried out using a Bruker spectrometer equipped with a 14.1 Tesla superconducting magnet. The data were acquired and processed using TOPSPIN (version 3.0) and MestReNova (version 10.0.1-14719), respectfully. These samples were prepared using fully deuterated benzene-d<sub>6</sub> or dioxane-d<sub>8</sub>, to both reduce the solvent background and as a species to use for field calibration. <sup>1</sup>H spectra were acquired using a recycle delay of 1.0 sec. and 30° <sup>1</sup>H excitation pulse lengths. <sup>1</sup>H-<sup>1</sup>H 2D plots were acquired using a COSY pulse sequence, and <sup>13</sup>C-<sup>1</sup>H 2D plots were acquired using a HSQC pulse sequence.

Reaction products were also analyzed with ultra-pressure liquid chromatography (UPLC) using a Waters Acquity H-Class System equipped with a Photodiode Array (PDA) and a QDa mass detector. UPLC separation was carried out on a Waters BEH Phenyl column (2.1x100 mm, 1.7 μm particles). Additionally, samples were analyzed by GC using an Agilent 7890B gas chromatograph equipped with an Agilent DB-1701 column (60 m x 0.25 mm), a flame ionization

detector (FID), and an Agilent 5977A mass spectrometer (MS). The methyl ester version of (1), (3), (4), (5), and (6) were verified with NIST MS spectral library.

### 3.3.4 Computational

All of the calculations reported herein were performed using density functional theory with the M062X<sup>37,38</sup> hybrid functional as implemented in Gaussian 09<sup>39</sup>. Optimizations were performed with a 6-311G+(d,p)<sup>40</sup> basis set on an ultrafine grid and tight convergence criterion for force. Solvation was modeled implicitly using the SMD model.<sup>41</sup> Thermal corrections and partition functions were calculated within Gaussian at 298.15 K and subsequently used to calculate enthalpy and Gibbs free energies of all species. A factor of  $RT \ln(24.46)$  was added to the free energies of all species to account for change of reference state from 1 atm to 1 M in solution. For degradation in water, additional corrections were applied corresponding to 55.56 M concentration of the bulk solvent.

## 3.4 Results and Discussion

### 3.4.1 The Formation of Benzoic Acid from Coumalic Acid

Experiments were conducted to examine the BA and MeBA yields obtained in several solvents using either CMA or MeCMA, respectfully. The reaction between CMA and ethylene in a nonpolar solvent, toluene, resulted in 71 mol% yield of BA at 100 mol% CMA conversion (Table 1, Entry 1). This outcome was similar to reported yields (76 %) for the Diels-Alder reaction of CMA with propylene in toluene,<sup>15, 16</sup> which was thought to be due to CMA being sparingly soluble in toluene leading to a substantial amount of CMA being converted to unidentified by-products. Therefore, a solvent was used to increase the solubility of CMA in order to improve the overall reaction yield. We have previously shown that  $\gamma$ -valerolactone (GVL) is a good polar aprotic

**Table 1.** Conversion of CMA/MeCMA with ethylene to BA/MeBA

Entry	Reactant	Solvent	Conv. (1) [mol%]	Selectivity			
				(5) [mol%]	(3) [mol%]	(4) [mol%]	(6) [mol%]
1	CMA	Toluene	100	71	[a]	[a]	[a]
2	CMA	GVL	100	76	[a]	[a]	[a]
3	CMA	1,4-Dioxane	100	91±1.5	[a]	5.8 [d]	[a]
4	MeCMA	Toluene	100	100±2	[b]	[b]	7±2[c]
5	MeCMA	GVL	100	99±1	[b]	[b]	2±10[c]
6	MeCMA	1,4-Dioxane	100	95±1	2±7[c]	2±3[c]	5±8[c]
7	CMA	Acetone	100	91	[a]	[a]	[a]

Reaction conditions: Temperature: 180 °C; reaction time: 4 h; starting concentration: 10 mg ml<sup>-1</sup> MeCMA/CMA (1) in 1,4-dioxane; pressure: 500 psig ethylene; agitation: 400 rpm, Pd/C catalyst: 100 mg; [a] unable to quantify by-products with UPLC-PDA/QDa; [b] by-products not detected with GC-FID/MS; [c] cyclohexadiene (3) and cyclohexene (6) intermediates were quantified based on methyl benzoate (5) as reference due to the similar FID response factor. Double Diels-Alder by-product (4) was approximated using methyl benzoate (5) as reference material; [d] quantified via <sup>1</sup>H-NMR

solvent for this reaction system due to structural similarities.<sup>16</sup> The use of GVL resulted in only a slightly higher BA yield of 76 mol% (Table 1, Entry 2 and Figure S1). Still, a considerable amount (~24 mol%) of the initial CMA was lost to by-product formation. Results from previous studies suggested that CMA stability was limited in GVL under reaction conditions due to the presence of residual water in GVL.<sup>16</sup> This hypothesis was tested by using the polar aprotic solvents, 1,4-dioxane or acetone, resulting in a significant improvement in the BA yield (Table 1, Entry 3 and 7). The reaction profile of the CMA consumption over time is displayed in Figure S2. At 100 mol% CMA conversion the BA selectivity was 91 mol% after a 4 h reaction at 180 °C for both solvents. From UPLC-PDA/QDa analysis, it was evident that small amounts of (4) and (6) (see Scheme 2) were present. Additionally, the formation of (4) was verified with NMR analysis showing that roughly 6 mol% of (4) was formed (Table 1, Entry 3). At this reaction temperature, the dehydrogenation reaction was extremely rapid as evident from the lack of an observable amount of the diene intermediate (3). This result was consistent with previous studies<sup>16</sup> in which we have

shown that the dehydrogenation of the diene species proceeded significantly faster than the decarboxylation of the bicyclic intermediate, thereby suggesting that the decarboxylation of the cycloadduct was the limiting step in the reaction network.<sup>16</sup> Kinetic studies and DFT calculations corroborate that decarboxylation is the rate limiting step, which will be discussed in the subsequent sections.

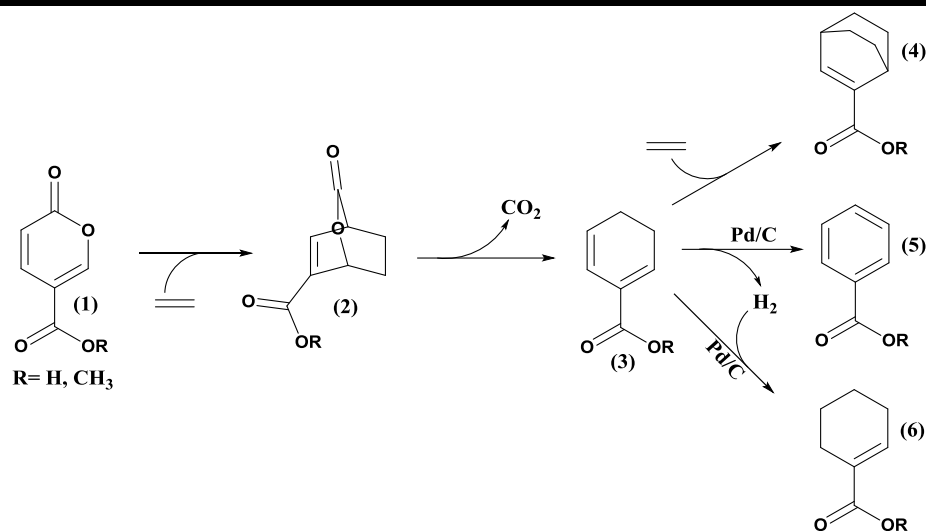
Literature reports suggest that changing the functional group on the starting substrate could significantly influence the stability and reactivity towards Diels-Alder reactions.<sup>15, 17, 18</sup> This effect was demonstrated by Pacheco et al. using furanic dienes showing different product selectivities when various oxidized versions of HMF were reacted with ethylene, which was purported to be the outcome of different functionalities of the oxygenated furans.<sup>17</sup> Furthermore, Bérard et al. observed that the reaction of sorbic acid with ethylene resulted in only low conversion (3 %), while using the ethyl ester of sorbic acid instead, afforded a ~5 fold increase in conversion (14 %).<sup>18</sup> A similar phenomena was also observed with 2-pyrones showing improved yields when reacting MeCMA instead of CMA with propylene.<sup>15</sup>

Therefore, reactions were also run using MeCMA as the reactant to determine if starting with the methyl ester of CMA (MeCMA) would alter the reaction. Interestingly, the reaction in toluene showed tremendous improvement in yield with 100 mol% selectivity after complete conversion (Table 1, Entry 4 and Figure S3). The higher selectivity with MeCMA was also consistent with the hypothesis of the importance of the solubility of the starting substrate in the 2-pyrone conversion. Similarly, when the polar aprotic solvent GVL was used to mediate the MeCMA and ethylene reaction, a conversion of 100 mol% with nearly 100 mol% MeBA selectivity (Table 1, Entry 5 and Figure S4) was achieved. As the CMA conversion in GVL only resulted in a selectivity of 76 mol% (Table 1, Entry 2 and Figure S1), the esterification of the

carboxylate moiety likely played a significant role in improving the selectivity. Since CMA conversion to BA achieved the highest selectivity in 1,4-dioxane, we also performed the MeCMA conversion in 1,4-dioxane. As shown in Table 1, Entry 6 reported only a slightly better product selectivity (95 mol%) compared to CMA (91 mol%). GC-MS analysis suggested that the remaining five percent was attributed to the unreacted methyl cyclohexa-1,5-diene carboxylate intermediate (3), the formation of methyl cyclohex-1-ene carboxylate (6), and the double Diels-Alder (DDA) by-product (4), which was believed to be the outcome of a consecutive Diels-Alder reaction of (3) with ethylene (Scheme 2). The concentration profile of (1), (2), (3), (4), (5) and (6) over time is displayed in Figure S17. The formation of (2), (3), and (6) were validated via 2D-NMR COSY and HSQC experiments (see Figure S1-S11) and will be explained in detail in the following section.

### 3.4.2 Elucidating the Reaction Network

To elucidate where by-product formation was occurring, experiments were performed to determine the reaction network. Given the extensive work on Diels-Alder reactions of 2-pyrones<sup>12, 19-29</sup> a reaction network was postulated, which is depicted in (Scheme 2). The reaction of CMA/MeCMA with ethylene follows a series of reactions that include Diels-Alder adduct formation (2), decarboxylation of the adduct to yield (3) and a Pd/C catalyzed dehydrogenation reaction to form the desired aromatics (5). In the presence of the Pd/C catalyst additional minor products (4) and (6) were observed (Table 1, Entry 6). The formation of (6) is likely the result of a Pd catalyzed hydrogenation of (3). The hydrogen needed for this step was likely formed through dehydrogenation of (3) to (5). Data shown in Figure S5 support the proposed reaction network which is evident via the clear trend showing how the conversion of (1) resulted in the formation of intermediates (2) and (3) and small amounts (< 8 mol%) of (4) and (6) while (5) was formed.



**Scheme 2.** Network for the reaction of CMA/MeCMA with ethylene

Structural identification of the intermediates (2), (3) and by-products (4) were determined by performing 1D and 2D NMR experiments of the reaction products from the MeCMA reaction with ethylene in the absence of catalyst to examine the Diels-Alder/decarboxylation sequence (see Figure S6-S16 and Table S1-S3). These analyses confirmed the formation of (2), (3) and (4). Without the catalyst, the by-product (6) was not observed. Therefore, it appeared that the formation of (6) was only realized when there was formation of hydrogen from dehydrogenation of (4) to (5). Similar observations were made when CMA was used as the starting substrate.

### 3.4.3 2-Pyrone Degradation Studies

Loss in selectivity due to MeCMA and CMA degradation was examined. These reactions were performed in the absence of ethylene or catalyst and the results are given in Table 2 and Figures S17-S18. The results are consistent with a previous study<sup>16</sup> showing that CMA stability is compromised in GVL as 25 mol% of the starting material is degraded after 8 h at 180 °C (Table 2, Entry 1). Identical tests in 1,4-dioxane showed that both CMA and MeCMA were significantly more stable with only 3 mol% of MeCMA and 10 mol% of CMA being converted (Table 2, Entry

**Table 2.** Stability tests of CMA and MeCMA in 1,4-dioxane at 180 °C and 8 h in the absence of water and Pd/C<sup>a</sup>

Entry	Reactant	Solvent	CMA Conv. (mol%)
1	CMA	GVL	25 <sup>15</sup>
2	CMA	GVL + 5 Vol% H <sub>2</sub> O	100 <sup>15</sup>
3	CMA	1,4-dioxane	10
4	MeCMA	1,4-dioxane	3
5	CMA	1,4-dioxane + 5 Vol% H <sub>2</sub> O	100
6	MeCMA	1,4-dioxane + 5 Vol% H <sub>2</sub> O	100

Reaction conditions: Temperature: 180 °C, reaction time: 8 h, starting concentration: 10 mg ml<sup>-1</sup> MeCMA/CMA (1) in 1,4-dioxane, pressure: 500 psig N<sub>2</sub>, agitation: 400 rpm

3 and 4). This observation demonstrated that not only the solvent, but also the state of the starting substrate (acid vs ester) impacts the stability of the 2-pyrone. Given the observed selectivity loss (Table 1, Entry 2, 3 and 6) it appears that CMA breakdown occurs concomitantly while forming (2), thus, impacting the global yield of the desired aromatic product.

In a previous study, it was shown that the presence of small amounts of water accelerated CMA degradation.<sup>16</sup> A similar water mediated breakdown was observed by Chia et al. when the 2-pyrone, triacetic acid lactone (TAL), was exposed to water and heat.<sup>30</sup> They report that TAL undergoes ring-opening in the presence of water but is stable in aprotic polar solvents.

To determine if the esterified 2-pyrone was more resistant to breakdown due to water, MeCMA stability experiments were also performed in 1,4-dioxane with 5 vol% of water. (Table 2, Entry 6). These results show that esterification did little to prevent breakdown in the presence of water, since both CMA and MeCMA were entirely consumed. Based on these observations, it is evident that the presence of water in the solvent has to be minimized to maximize yields of the Diels-Alder reaction products.

Overall, GVL is an environmentally friendly renewable solvent with many positive characteristics such as low toxicity and biodegradability<sup>31-33</sup> and, as such, is a desirable solvent for

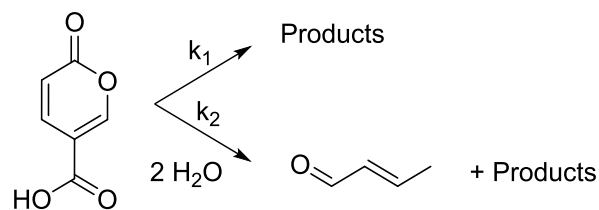


the conversion of MeCMA to MeBA. However, when BA formation was targeted, the effect of GVL on CMA stability was not as high since 25 mol% of the starting material was lost most likely through a concomitant degradation pathway (Table 1, Entry 2). Moreover, the high boiling point of GVL would make the product separation difficult. As such, a low boiling bio-based acetone solvent could be utilized for increased BA selectivity of 91 mol% and would be an environmentally-advantaged substitute.

### 3.4.4 Reaction Kinetics of Water Mediated Coumalic Acid Breakdown

The reaction kinetics and products from the water-mediated breakdown of CMA were determined using NMR analysis with deuterated dioxane-*d*<sub>8</sub>. Dioxane, an aprotic polar solvent, was chosen as the ideal model system due to minimal by-product formation and CMA/MeCMA degradation. Moreover, fully deuterated dioxane-*d*<sub>8</sub> was commercially available allowing the kinetic studies to be performed in a closed system (high pressure NMR tube from Wildmad-Labglass), which simplified the product identification and quantification without further sample workup.

Different D<sub>2</sub>O concentration (1-5 vol%) were added to the reaction mixture to identify the CMA breakdown dependence with respect to the water concentration. The main product identified via <sup>1</sup>H NMR after a 6.4 h reaction at 171 °C with 3 vol% D<sub>2</sub>O was 2-butenal yielding 14.5 mol% at 25.3 mol% conversion (Figure S19). Minimal 2-butenal was observed with 1 vol% D<sub>2</sub>O and virtually none with 0 vol% D<sub>2</sub>O. The rate constant for the CMA breakdown reaction, was obtained from initial conversion data (no more than 20 mol% conversion). For each D<sub>2</sub>O concentration experiment, a pseudo-first order reaction in CMA was fit to the data. The changes with respect to water in this regime were considered negligible as the reactions were carried out in excess D<sub>2</sub>O (e.g. [D<sub>2</sub>O] was about 4 times [CMA]<sub>0</sub> at 1 vol% D<sub>2</sub>O). Fits of ln([CMA]<sub>t</sub>/[CMA]<sub>0</sub>) vs time were

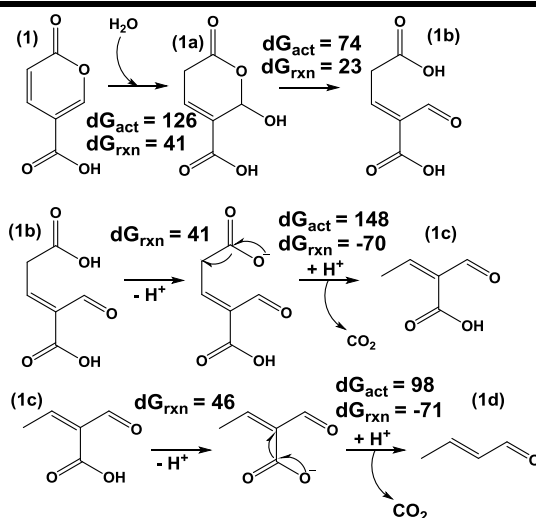


**Scheme 3.** General degradation of coumalic acid in the absence and presence of water

linear and the observed rate constant ( $k_{obs}$ ) was obtained from the slope. Interestingly, the plot of the pseudo-first order rate constants  $k_{obs}$  as a function of  $[D_2O]$  revealed a second order dependence on  $[D_2O]$  with an independent degradation pathway when no  $D_2O$  was added (Figure 1). Therefore, an overall rate law for CMA degradation was expressed as:

$$r_{CMA} = -k_{obs}[CMA] = -(k_1 + k_2 [D_2O]^2)[CMA] \quad (1)$$

The degradation of coumalic acid with and without the presence of water can be captured by the paths shown in Scheme 3. Further insights into the steps and mechanisms responsible for the degradation of CMA to 2-butenal were established by carrying out density functional theory calculations (Scheme 4). The results suggest that water initiated degradation of CMA proceeds via



**Scheme 4.** CMA breakdown mechanism to 2-butenal in the presence of water. Units (kJ/mol)

a nucleophilic attack of water on the double bonds in CMA. The intermediate formed (1a) subsequently undergoes ring-opening via keto-enol tautomerization to form a keto intermediate (1b). The presence of water molecules facilitates this ring-opening by providing a hydrogen bonding network to enable rapid proton shuttling and a low energy paths for keto-enol tautomerization and ring-opening. The intermediate (1b) has two carboxylic groups, which can then undergo decarboxylation yielding 2-butenal. This is very similar to a previously reported mechanism for water catalyzed ring-opening and decarboxylation of triacetic acid lactone.<sup>29</sup>

To further validate whether CMA breakdown is solely responsible for the observed selectivity loss (Table 1, Entry 2, 3 and 6) or is a result of by-product formation on the pathway to BA, the rate constants of CMA breakdown and CMA Diels-Alder addition with ethylene were compared. Based on the rate constants provided in Figure 1 and calculated from the Diels-Alder reaction step (Table S4), it is evident that the CMA degradation proceeds significantly slower (>100 times) than the Diels-Alder addition step. Therefore, the observed loss in product selectivity less likely originates from 2-pyrone breakdown as opposed to by-product formation from

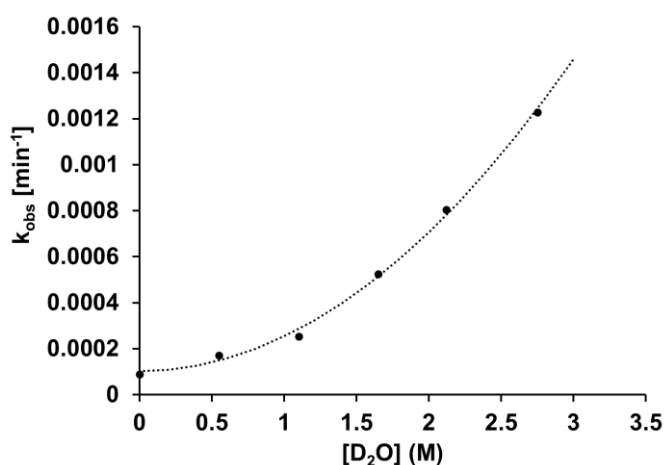


**Figure 1.** Plot of  $k_{\text{obs}}$  as a function of  $[\text{D}_2\text{O}]$ . Experimentally determined  $k_{\text{obs}}$  are represented as points and the line is a simulated fit to  $k_{\text{obs}} = k_1 + k_2 \times [\text{D}_2\text{O}]^2$  where  $k_1 = 1.03 \times 10^{-4} \text{ min}^{-1}$  and  $k_2 = 1.51 \times 10^{-4} \text{ M}^{-2} \text{ min}^{-1}$ .

---

intermediates on the pathway to BA. This was further supported by DFT calculations which predicted that the Gibbs free energy of activation barrier for water addition (126 kJ/mol) was ~15 kJ/mol higher than ethylene addition (111 kJ/mol). The increase in the barrier is likely due to hydrogen bonding stabilization of the reactant by water. Moreover, the Gibbs free energy of reaction for ethylene addition (-79 kJ/mol) was calculated to be much more exothermic than that for water addition (41 kJ/mol) suggesting that the Diels-Alder adduct is thermodynamically favored over CMA decomposition. Therefore, it appears that the selectivity loss of 24 mol% originates from intermediates (2) or (3) on the pathway to BA when reacting CMA with ethylene in GVL (Table 1, Entry 2).

Given that reactions performed in dry polar aprotic solvents resulted in selectivities >90 mol% (with <10 mol% known by-products (4) and (6)), it appears that residual water in GVL is responsible for the selectivity loss likely from intermediate (2) or (3). To test this hypothesis, reactions of (2) were performed in situ (NMR tubes) in dioxane-*d*<sub>8</sub> at 180 °C for 4 h in the presence of 5 vol% D<sub>2</sub>O and without a catalyst. The results from these experiments suggest that species in the <sup>1</sup>H-NMR spectra are primarily attributed to unidentified by-products that originate from either (2) or (3) on pathway to (5) when water is present. From this observation, it is clearly critical to avoid water in the system to maximize product yield by minimizing by-product formation from the reactive intermediates.

### 3.4.5 Reaction Kinetics in the Absence of Catalyst

Kinetic measurements were performed in 1,4-dioxane which is an excellent model solvent for detailed kinetic analyses as it has a low boiling point, results in minimal by-product formation during reaction and is readily available commercially in the fully deuterated dioxane-d<sub>8</sub> form to perform complementary in situ NMR analysis. Choosing a solvent with a low boiling point

(compared to GVL) was critical for isolation, identification and quantification (via NMR) of the temperature sensitive reactant CMA (1) and intermediates (2) and (3) for both the Diels-Alder and decarboxylation reactions. Fully resolved spectra of the formation of (2) and (3) are depicted in Figure 2 showing that the peak assignments and the method of quantification via NMR was unambiguous with carbon balances of >96 mol%.

### 3.4.6 Diels-Alder Reaction Step

The activation barrier associated with the formation of the Diels-Alder (DA) adduct (2) was investigated by comparing the rate of consumption of CMA at temperatures ranging from 90-120 °C. Under these conditions, the cycloadduct was formed in high yields without breakdown of CMA simplifying the examination of the kinetics of this single step. The net rate of cycloadduct formation can be written as the forward rate of cycloaddition formation via Diels Alder reaction between CMA and ethylene minus the rate of the back reaction involving the retro Diels-Alder (rDA) of the cycloadduct. Assuming both of these reactions are elementary, the net rate can be written as that in equation 2. This equation can be simplified (Equation 3) based on the experimental conditions since ethylene was in ~10x excess, which was validated by plots of  $\ln([CMA]_t/[CMA]_0)$  versus time all giving linear relationships (Figure S20 and S21( MeCMA)). The experimental results and spectra (Figure 2) suggested that the rDA reaction had only a minimal contribution as (2) can be obtained with yields of 98 mol%, which further showed that  $k_{1,DA} \gg k_{1,rDA}$  and justified the simplification of equation (3) into (4). DFT calculations also fully support this since ethylene addition is predicted to be highly exothermic (-127 kJ/mol).

$$-r_{CMA} = k_{1,DA}[CMA][Ethylene] - k_{1,rDA}[DAP] \quad (2)$$

$$-r_{CMA} = k'_{1,DA}[CMA] - k_{1,rDA}[DAP] \quad (3)$$

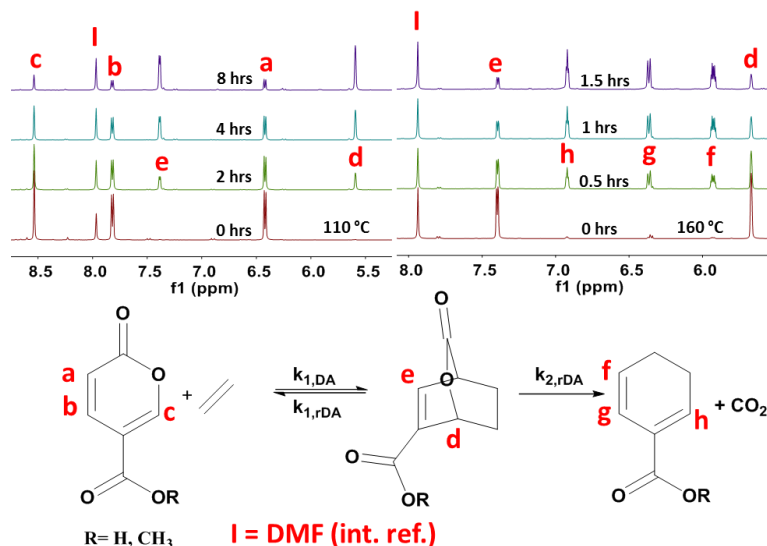


**Figure 2.** NMR trace of the Diels-Alder and decarboxylation reaction

$$-r_{CMA} = k'_{1,DA}[CMA] \quad (4)$$

The observed rate constants at temperatures in the range of 90-120 °C are given in Table S4. The activation energy (EA) for the Diels-Alder reaction of CMA (or MeCMA) (depicted in Figure 3A) was calculated based on the slope of the Arrhenius plot shown in Figure 3B and Figure S21. The reaction of CMA and MeCMA with ethylene, resulted in a similar activation barrier of 77 kJ/mol. The experimental values were compared to the DFT-calculated barriers, which showed excellent agreement as the calculated enthalpic activation barriers were 67 and 68 kJ/mol, respectively. Therefore, the functionality (acid or ester) had negligible influence on the 2-pyrone reactivity (Table S4). Literature reports for the cycloaddition of CMA derivatives and dienophiles with donating or withdrawing substituents report activation barriers that range from 28<sup>34</sup> to 118<sup>21</sup> kJ/mol when using butyl vinyl ether or methyl acrylate, respectively. Given the nature of an inverse electron demand Diels-Alder cycloaddition, dienophiles with higher electron density from

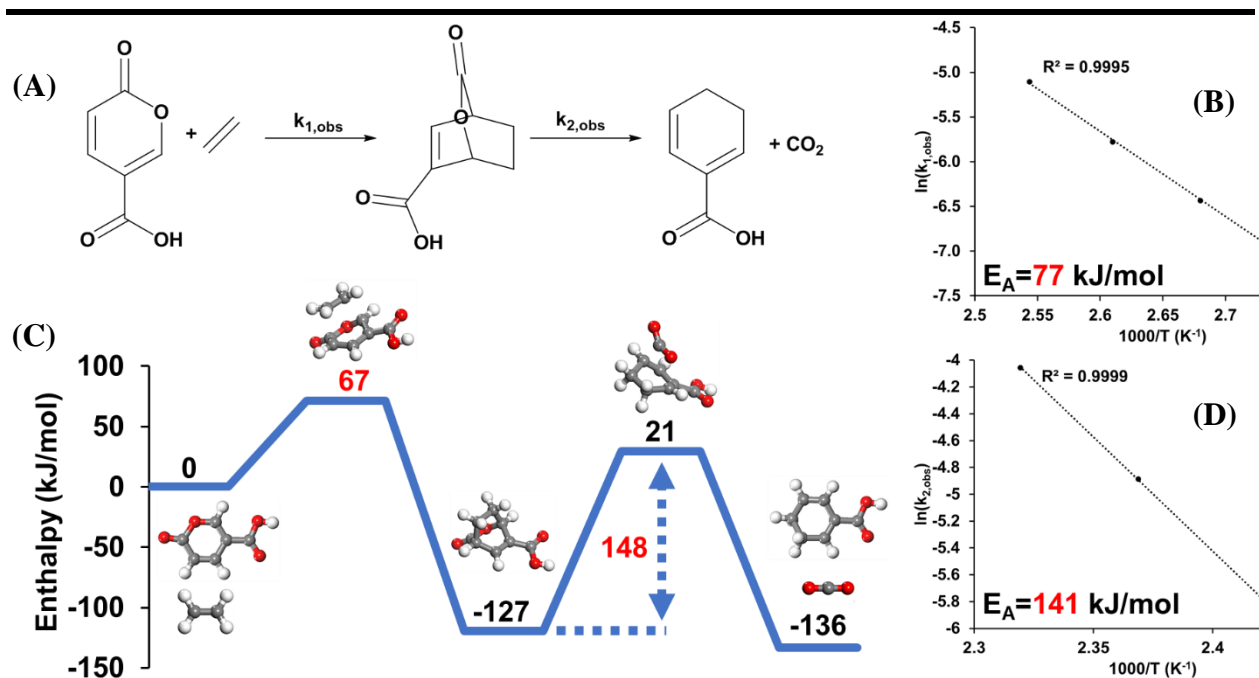


**Figure 3.** Network kinetic analysis of coumalic acid reaction with ethylene. (A) Diels-Alder reaction followed by thermal CO<sub>2</sub> extrusion. (B) Measured activation energy of the Diels-Alder reaction of CMA and ethylene in 1,4-dioxane at temperatures between 90-120 °C. (C) DFT-calculated reaction energy profile diagram for the CMA reaction with ethylene to the Diels-Alder adduct followed by decarboxylation to cyclohexa-1,5-diene carboxylic acid intermediate and CO<sub>2</sub>. (D) Measured activation energy of the thermal decarboxylation reaction of CMA-DAP in 1,4-dioxane at temperatures between 140-150 °C

donating substituents should react more readily than dienophiles with electron withdrawing substituents.<sup>34, 35</sup> With an activation barrier of 77 kJ/mol, the reaction of CMA (MeCMA) and ethylene showed that the unactivated dienophile resulted in intermediate Diels-Alder reactivity.

### 3.4.7 Decarboxylation Reaction Step

Examination of the bicyclic lactone (DAP) intermediate decarboxylation was carried out at temperatures ranging from 140-160 °C. The reactant, intermediate (2), was prepared using a 16 h reaction at 110 °C in 1,4-dioxane, which yielded almost pure DAP (2) with only trace amounts of intermediate (3) and unreacted (1). Decarboxylation reactions were performed using high pressure Wilmad-Labglass NMR tubes. The synthesized DAP (2) was dissolved in dioxane-*d*<sub>8</sub>

within the tubes and the decarboxylation reactions as a function of time was measured via NMR (Figure 2).

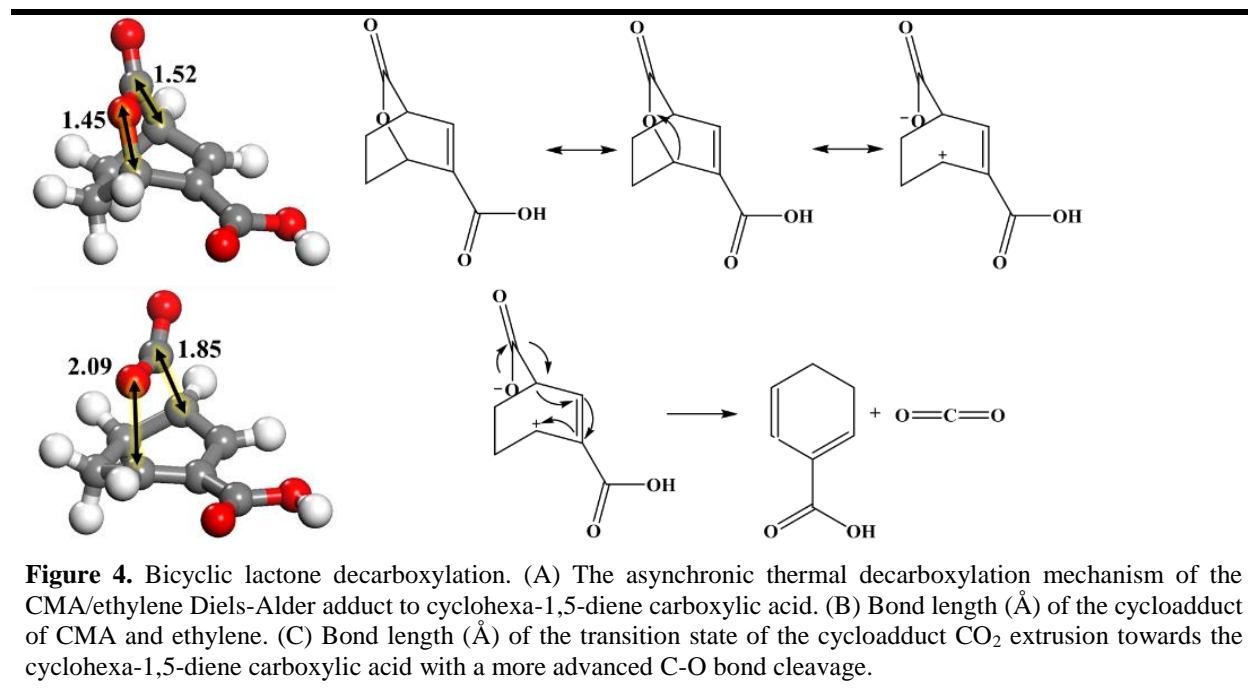
The rate law for the decarboxylation step was assumed to follow unimolecular first order kinetics (Equation 5).

$$-r_{DAP} = k_{2,rDA}[DAP] \quad (5)$$

During the decarboxylation reactions, no accumulation of CMA (or MeCMA) was observed at any of the temperatures tested, which provided additional support that  $k_{1,DA} \gg k_{1,DA}$  and helped to validate the assumption that the equilibrium between CMA (or MeCMA) and DAP (2) was strongly shifted towards DAP formation. Plots of  $\ln([DAP]_t/[DAP]_0)$  vs time resulted in linear trends for all temperatures tested (Figure S22-23).

The activation barriers for the decarboxylation of CMA/MeCMA-derived (2) (142/133 kJ/mol) were calculated based on the slope of the Arrhenius plots (Figure 3D and Figure S22) using the observed rate constants (Table S5). DFT calculations predicted an enthalpic activation barrier of 148 kJ/mol for both bicyclic lactones (CMA-DAP and MeCMA-DAP) as shown in Figure 3C. The DFT barriers agree well with those from experiment. Abdullahi et al. reported that the decarboxylation of the bicyclic lactone formed from ethyl coumalate and butyl vinyl ether also result in a high activation barrier of 111 kJ/mol which is also in close agreement with the DFT results that give a CO<sub>2</sub> extrusion barrier of 120 kJ/mol.<sup>36</sup> By comparing these results with our experimental activation energy, it is evident that the decarboxylation step is significantly influenced by the degree of functionalization of the bicyclic lactone intermediate. DFT energy mapping calculations (Figure 4) further suggested a mechanism where the CO<sub>2</sub>-bridge leaves in an asynchronous fashion with a significantly elongated C-O bond in the transition state. As such,





the C-O bond cleavage occurs prior to C-C bond cleavage, which is in agreement with observations from the literature.<sup>36</sup>

From this analysis we conclude that the rate-limiting step in this reaction network is the decarboxylation reaction of (2). We observed that all reactions run with catalyst led to only minimal accumulation of (3), suggesting that the rate of (3) dehydrogenation is much more rapid than the rate of (3) formation. These results provide critical insight for what should be targeted to further enhance the overall process. Clearly, finding a catalyst to reduce the activation barrier of the rate-limiting decarboxylation would allow for this reaction to be carried out under milder reaction conditions, which would improve overall yields by reducing the extent to which by-products were formed.

### 3.5 Conclusion

In this work, we have shown that the Diels-Alder chemistry between CMA (or MeCMA) and ethylene can yield high conversion and selectivity towards BA (or MeBA), which provides a renewable alternative to current benzoate production. We were able to effectively elucidate the reaction network and revealed kinetic information such as activation energies for the Diels-Alder and the decarboxylation step. Although CMA stability studies revealed two independent breakdown pathways as a function of water concentration resulting in 2-butenal as the main by-product, the CMA decomposition rate was significantly slower than the Diels-Alder cycloaddition indicating that CMA stability is not a contributing factor. Instead, we have shown that the selectivity loss is a result of the formation of (4) and (6) and that in the presence of water intermediates on the pathway to BA led to by-product generation. Thus, the avoidance of water is critical to improve overall selectivity. Utilizing MeCMA gave diminished by-product formation, consequently improving benzoate selectivity.

Kinetic studies revealed that the activation barrier of the decarboxylation reaction was considerably higher than for the Diels-Alder reaction, giving evidence that the extrusion of CO<sub>2</sub> is the rate limiting step, which is in agreement with DFT results. The high activation barrier of the CO<sub>2</sub> extrusion afforded the successful isolation of (2), granting access to bicyclic molecules in high yield and selectivity that could be utilized as synthetic starting substrates to synthesize a broad array of new compounds. For instance, we have shown that diene intermediates (3) can be obtained from bicyclic lactones (2) through controlled thermal extrusion of CO<sub>2</sub>, providing access to novel molecules with dual-functionality. These insights can be leveraged to produce a plethora of products based on the coumalate conversion platform.

### 3.6 Acknowledgments

We gratefully acknowledge funding from the National Science Foundation under Award EEC-0813570, the Iowa State University Chemical Instrument Facility staff members, and the Minnesota Supercomputing Institute (MSI) at the University of Minnesota. Furthermore, we would like to acknowledge all co-workers at CBiRC for their support.

### 3.7 References

1. R. L. D'Ecclesia, E. Magrini, P. Montalbano and U. Triulzi, *Energ. Econ.*, 2014, **46**, S11-S17.
2. E. Arceo, J. A. Ellman and R. G. Bergman, *ChemSusChem*, 2010, **3**, 811-813.
3. C. H. Christensen, J. Rass-Hansen, C. C. Marsden, E. Taarning and K. Egeblad, *ChemSusChem*, 2008, **1**, 283-289.
4. G. Fiorentino, M. Ripa and S. Ulgiati, *Biofuels, Bioprod. Biorefin.*, 2017, **11**, 195-214
5. J. v. Haveren, E. L. Scott and J. Sanders, *Biofuel, Bioprod. Biorefin.*, 2008, **2**, 41-57.
6. K. Wagemann, *ChemBioEng Rev.*, 2015, **2**, 315-334.
7. E. Mahmoud, J. Yu, R. J. Gorte and R. F. Lobo, *ACS Catal.*, 2015, **5**, 6946-6955.
8. World Health Organisation, Benzoic acid and Sodium benzoate. Concise international chemical assessment document, 2000, vol. 26.
9. S. Ghosh, Y. Chisti and U. C. Banerjee, *Biotechnol. Adv.*, 2012, **30**, 1425-1431.
10. K. M. Draths, D. R. Knop and J. W. Frost, *J. Am. Chem. Soc.*, 1999, **121**, 1603-1604.
11. S. K. Green, R. E. Patet, N. Nikbin, C. L. Williams, C.-C. Chang, J. Yu, R. J. Gorte, S. Caratzoulas, W. Fan, D. G. Vlachos and P. J. Dauenhauer, *Appl. Catal., B*, 2016, **180**, 487-496.
12. J. J. Lee, G. R. Pollock Iii, D. Mitchell, L. Kasuga and G. A. Kraus, *RSC Adv.*, 2014, **4**, 45657-45664.
13. S. H. Brown, L. Bashkirova, R. Berka, T. Chandler, T. Doty, K. McCall, M. McCulloch, S. McFarland, S. Thompson and D. Yaver, *Appl. Microbiol. Biotechnol.*, 2013, **97**, 8903-8912.

14. R. M. Zelle, E. de Hulster, W. A. van Winden, P. de Waard, C. Dijkema, A. A. Winkler, J. M. Geertman, J. P. van Dijken, J. T. Pronk and A. J. van Maris, *Appl. Environ. Microbiol.*, 2008, **74**, 2766-2777.
15. S. J. Riley, Ph.D., Iowa State University, 2011.
16. T. Pfennig, R. L. Johnson and B. H. Shanks, *Green Chem.*, 2017, **19**, 3263-3271.
17. J. J. Pacheco and M. E. Davis, *Proceedings of the Natl. Acad. Sci. U. S. A*, 2014, **111**, 8363-8367.
18. S. Bérard, C. Vallée and D. Delcroix, *Ind. Eng. Chem. Res.*, 2015, **54**, 7164-7168.
19. J. J. Lee and G. A. Kraus, *Green Chem.*, 2014, **16**, 2111-2116.
20. J. J. Lee and G. A. Kraus, *Tetrahedron Lett.*, 2013, **54**, 2366-2368.
21. G. A. Kraus, G. R. Pollock III, C. L. Beck, K. Palmer and A. H. Winter, *RSC Adv.*, 2013, **3**, 12721-12725.
22. G. A. Kraus, S. Riley and T. Cordes, *Green Chem.*, 2011, **13**, 2734-2736.
23. I. E. Markó, G. R. Evans, P. Seres, I. Chellé and Z. Janousek, *Pure Appl. Chem.*, 1996, **68**, 113-122.
24. G. H. Posner and Y. Ishihara, *Tetrahedron Letters*, 1994, **35**, 7545-7548.
25. N. P. Shusharina, *Russ. Chem. Rev.*, 1974, **43**, 851.
26. I. E. Markó and G. R. Evans, *Tetrahedron Lett.*, 1994, **35**, 2767-2770.
27. I. E. Markó and G. R. Evans, *Tetrahedron Lett.*, 1994, **35**, 2771-2774.
28. I. E. Markó, G. R. Evans and J.-P. Declercq, *Tetrahedron*, 1994, **50**, 4557-4574.
29. K. Afarinkia, V. Vinader, T. D. Nelson and G. H. Posner, *Tetrahedron*, 1992, **48**, 9111-9171.
30. M. Chia, M. A. Haider, G. Pollock, G. A. Kraus, M. Neurock and J. A. Dumesic, *J. Am. Chem. Soc.*, 2013, **135**, 5699-5708.
31. D. M. Alonso, S. G. Wettstein and J. A. Dumesic, *Green Chem.*, 2013, **15**, 584-595.
32. G. Strappaveccia, L. Luciani, E. Bartollini, A. Marrocchi, F. Pizzo and L. Vaccaro, *Green Chem.*, 2015, **17**, 1071-1076.
33. D. Fegyverneki, L. Orha, G. Láng and I. T. Horváth, *Tetrahedron*, 2010, **66**, 1078-1081.
34. A. Corma and H. García, *Chem. Rev.*, 2003, **103**, 4307-4366.

35. F. Fringuelli and A. Taticchi, *The Diels-Alder Reaction: Selected Practical Methods*, Wiley, 2002.
36. M. H. Abdullahi, L. M. Thompson, M. J. Bearpark, V. Vinader and K. Afarinkia, *Tetrahedron*, 2016, **72**, 6021-6024.
37. Y. Zhao and D. G. Truhlar, *J. Chem. Phys.*, 2006, **125**, 194101.
38. Y. Zhao and D. G. Truhlar, *Acc. Chem. Res.*, 2008, **41**, 157-167.
39. M. J. Frisch, G. W. Trucks, H. B. Schlegel, G. E. Scuseria, M. A. Robb, J. R. Cheeseman, G. Scalmani, V. Barone, B. Mennucci, G. A. Petersson, H. Nakatsuji, M. Caricato, X. Li, H. P. Hratchian, A. F. Izmaylov, J. Bloino, G. Zheng, J. L. Sonnenberg, M. Hada, M. Ehara, K. Toyota, R. Fukuda, J. Hasegawa, M. Ishida, T. Nakajima, Y. Honda, O. Kitao, H. Nakai, T. Vreven, J. A. Montgomery, Jr., J. E. Peralta, F. Ogliaro, M. Bearpark, J. J. Heyd, E. Brothers, K. N. Kudin, V. N. Staroverov, R. Kobayashi, J. Normand, K. Raghavachari, A. Rendell, J. C. Burant, S. S. Iyengar, J. Tomasi, M. Cossi, N. Rega, J. M. Millam, M. Klene, J. E. Knox, J. B. Cross, V. Bakken, C. Adamo, J. Jaramillo, R. Gomperts, R. E. Stratmann, O. Yazyev, A. J. Austin, R. Cammi, C. Pomelli, J. W. Ochterski, R. L. Martin, K. Morokuma, V. G. Zakrzewski, G. A. Voth, P. Salvador, J. J. Dannenberg, S. Dapprich, A. D. Daniels, O. Farkas, J. B. Foresman, J. V. Ortiz, J. Cioslowski, and D. J. Fox, *Gaussian 09*, Revision A.02, Gaussian, Inc., Wallingford CT, 2016.
40. M. J. Frisch, J. A. Pople and J. S. Binkley, *J. Chem. Phys.*, 1984, **80**, 3265-3269.
41. A. V. Marenich, C. J. Cramer and D. G. Truhlar, *J. Phys. Chem. B*, 2009, **113**, 6378-6396

### 3.8 Supplementary Information

A new selective route towards benzoic acid and derivatives from biomass-derived coumalic acid

*A paper published in Green Chemistry 2017, 19, 4879-4888*

Toni Pfennig,<sup>a,b</sup> Jack M. Carraher,<sup>a,b</sup> Ashwin Chemburkar,<sup>c,b</sup> Robert L. Johnson,<sup>a,b</sup> Austin Anderson,<sup>a,b</sup> Jean-Philippe Tessonnier,<sup>a,b</sup> Matthew Neurock,<sup>c,b</sup> Brent H. Shanks\*<sup>a,b</sup>

<sup>a</sup> Department of Chemical and Biological Engineering, Iowa State University, Ames, IA 50011, USA.

<sup>b</sup> NSF Engineering Research Center for Biorenewable Chemicals (CBiRC), Ames, IA 50011, USA.

<sup>c</sup> Department of Chemical Engineering and Material Science, University of Minnesota, Minneapolis, MN, 55438, USA

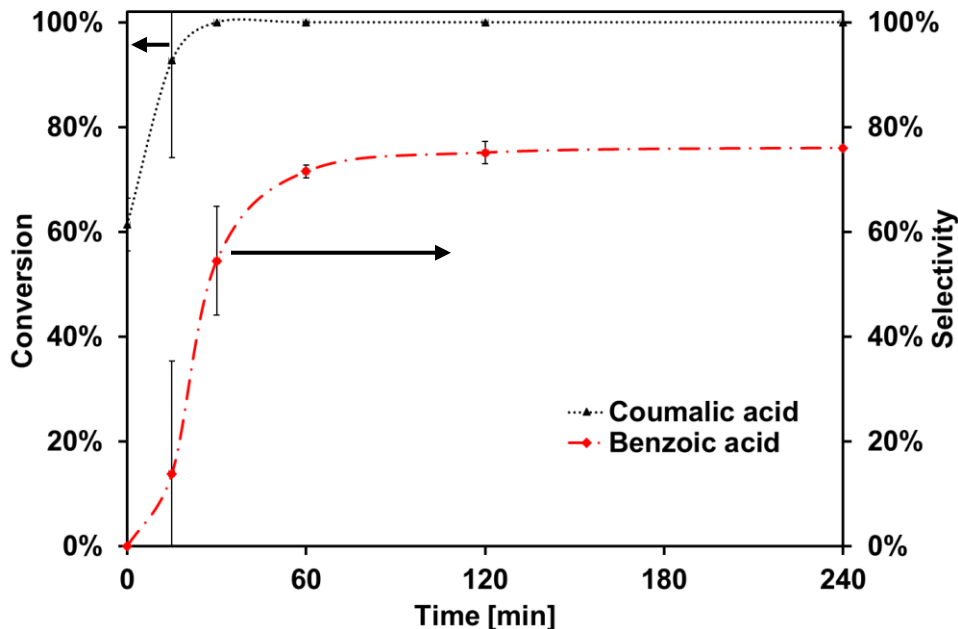


**Figure S1.** The conversion of coumalic acid to benzoic acid at 180 °C using 10 wt.-% Pd/C and the solvent GVL

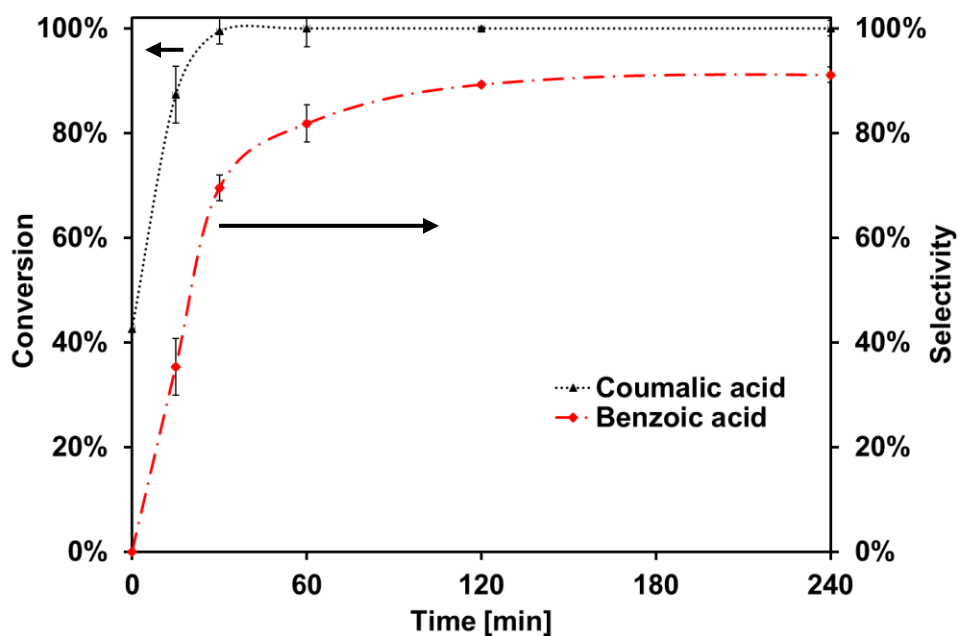


**Figure S2.** The conversion of coumalic acid to benzoic acid at 180 °C using 10 wt.-% Pd/C and the solvent 1,4-dioxane

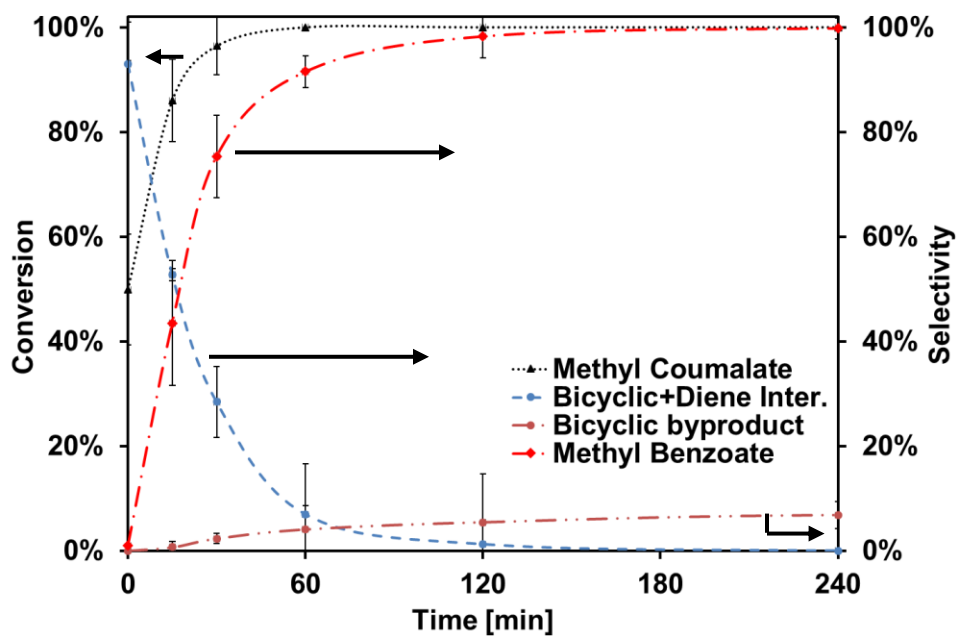


**Figure S3.** The conversion of methyl coumalate to methyl benzoate at 180 °C using 10 wt.-% Pd/C and the solvent toluene

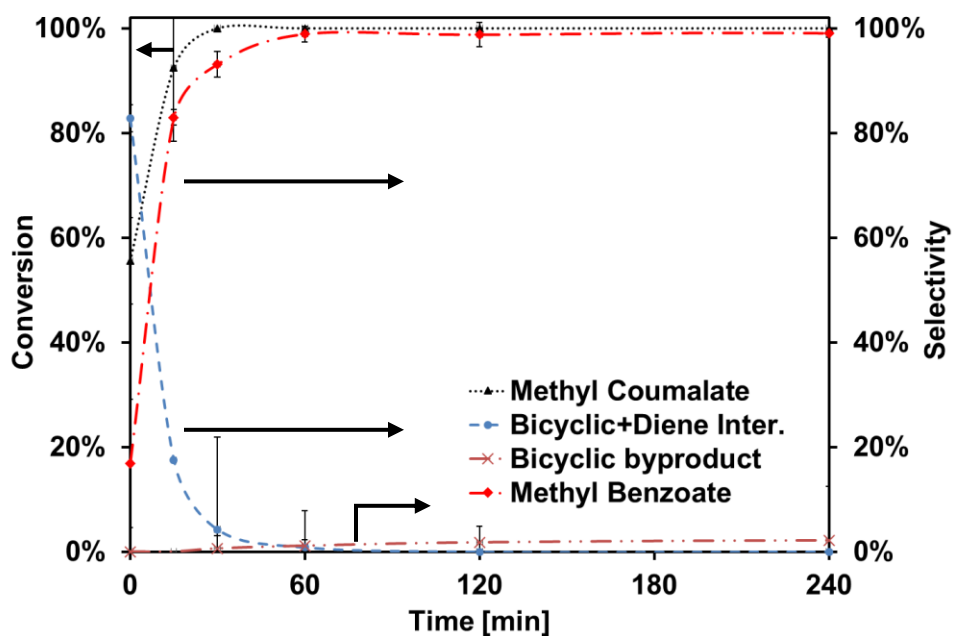


**Figure S4.** The conversion of methyl coumalate to methyl benzoate at 180 °C using 10 wt.-% Pd/C and the solvent GVL

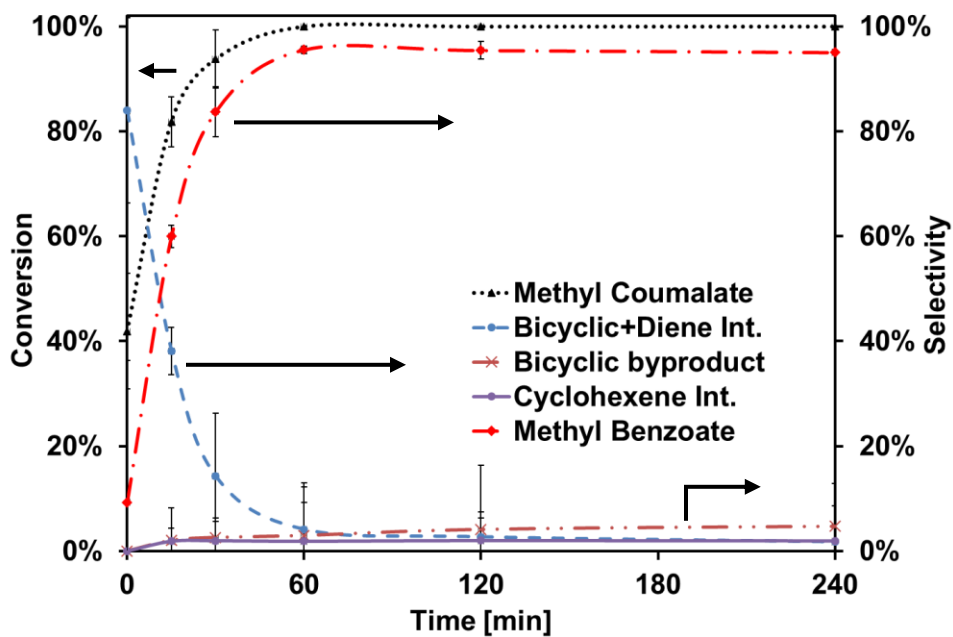
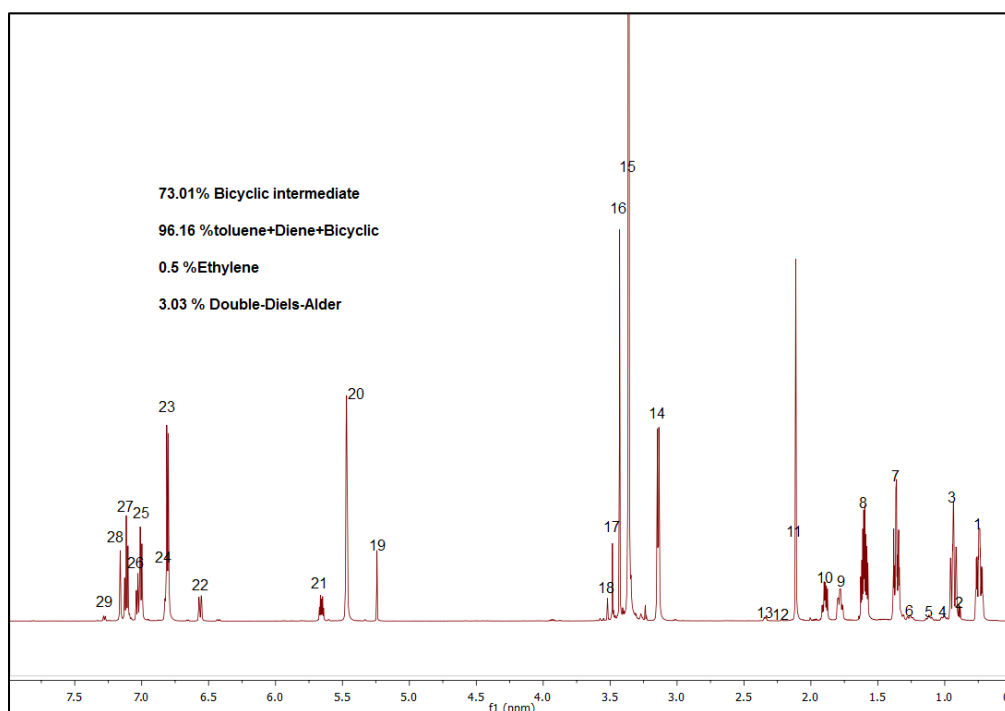


**Figure S5.** The conversion of methyl coumalate to methyl benzoate at 180 °C using 10 wt.-% Pd/C and the solvent 1,4-dioxane

*Structural assignment of intermediates and by-products*



The structural assignment of intermediates, products and by-products were identified via 2D-NMR experiments of the reaction products obtained from a 48 h reaction of MeCMA and ethylene in benzene- $d_6$  (Figure S1). Fully deuterated benzene- $d_6$  was used due to its cheapness (compared to dioxane- $d_8$ ) and as a result of identical findings when compared to dioxane- $d_8$ . We identified the bicyclic lactone intermediate and cyclohexa-1,5-diene intermediate as well as the double Diels-Alder by-product from cycloaddition of the diene intermediate and ethylene (Figure S1-11). Additionally, GC-MS and UPLC-QDa analysis provided the mass of the identified compounds. The toluene peak in Figure S1-S11 was the result of residual toluene (solvent used to mediate reactions) in the reactor head space and can thus, be neglected.

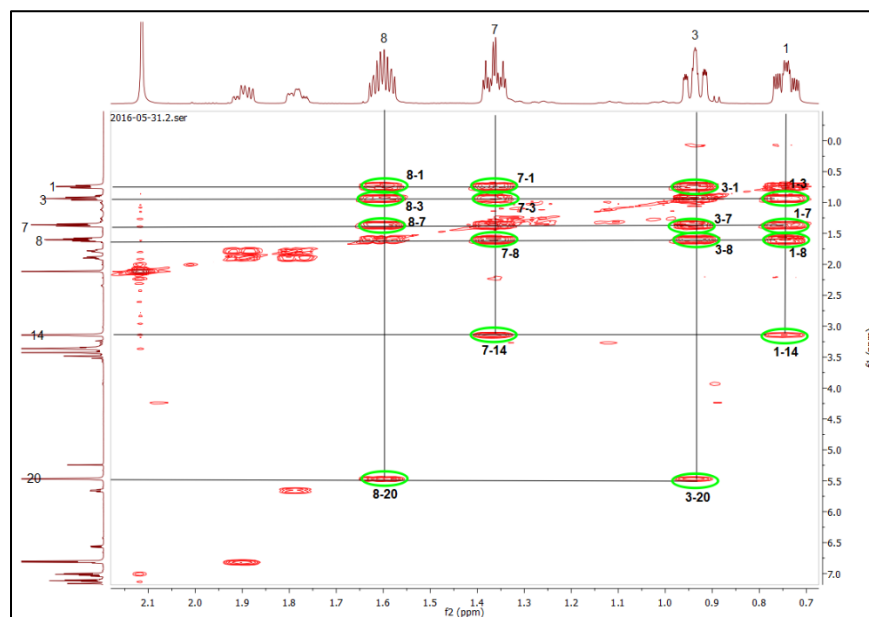


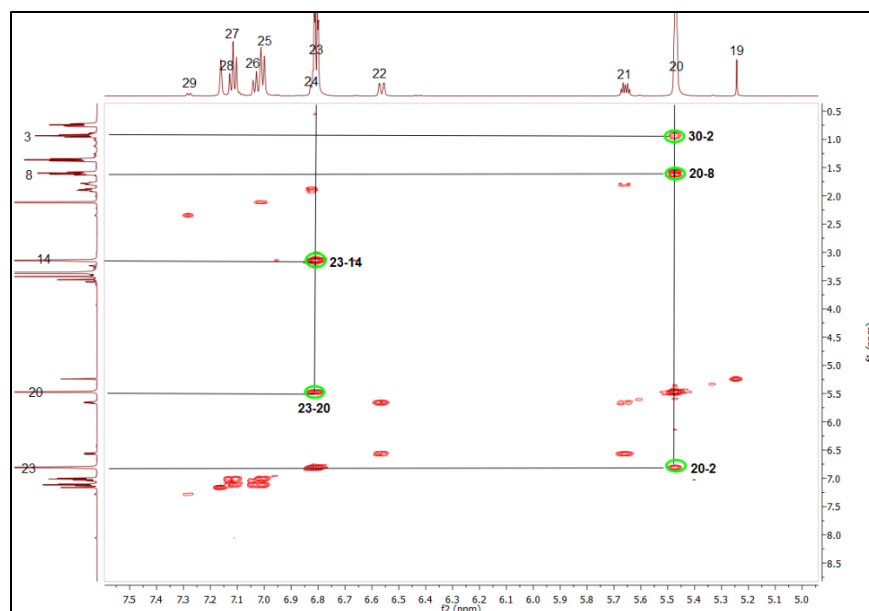
**Figure S6.**  $^1\text{H}$ -NMR of the reaction of MeCMA and ethylene at 90 °C for 48 h (600 MHz, benzene- $d_6$ ).

**Methyl -3-oxo-2-oxabicyclo[2.2.2]oct-5-ene-6-carboxylate intermediate (DAP):**  $^1\text{H}$  NMR (600 MHz, Benzene- $d_6$ )  $\delta$  6.81 (dd,  $J = 6.5, 2.3$  Hz, 1H), 5.47 (dt,  $J = 4.0, 1.9$  Hz, 1H), 3.36 (s, 3H), 1.66 – 1.55 (m, 1H), 1.40 – 1.31 (m, 1H), 0.98 – 0.87 (m, 1H), 0.80 – 0.69 (m, 1H),  $m/z$ : 180.1.

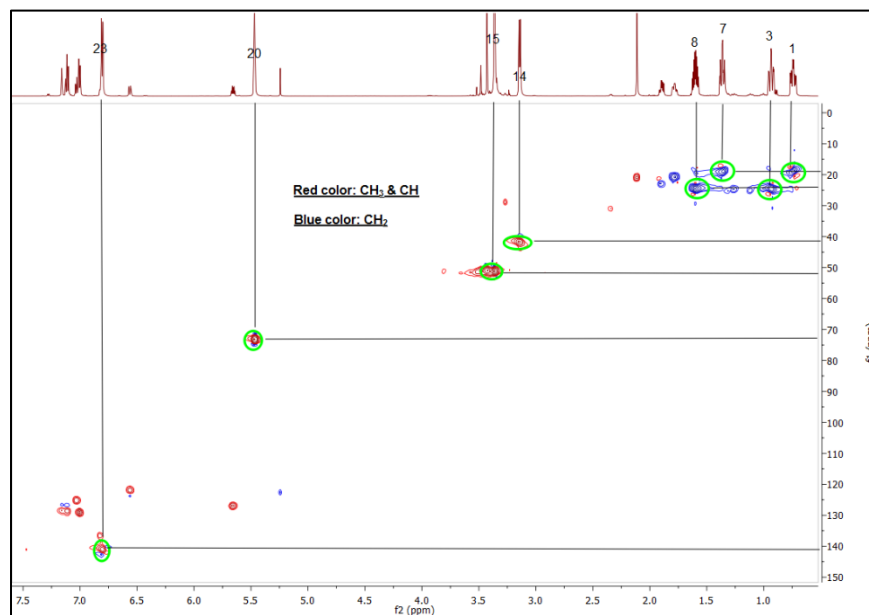
**Table S1.** Tabulated NMR assignment of methyl -3-oxo-2-oxabicyclo[2.2.2]oct-5-ene-6-carboxylate intermediate (DAP).

<sup>1</sup> H-label	$\delta$ <sup>1</sup> H, ppm, (mult)	$\delta$ <sup>13</sup> C	<sup>1</sup> H Int.	<sup>1</sup> H- <sup>1</sup> H-COSY	rel. mol-%
1	0.74 (m)	19.24	1.00	1-3, 1-7, 1-8, 1-14	73.01
3	0.94 (m)	24.82	1.04	3-1, 3-7, 3-8, 3-20	
7	1.36 (m)	19.08	1.06	7-1, 7-3, 7-8, 7-14	
8	1.60 (m)	24.33	1.03	8-1, 8-3, 8-7, 8-20	
15	3.36 (m)	51.49	2.99	-	
20	5.47 (s)	73.08	0.94	20-2, 20-8, 20-2	
23	6.81 (dd)	140.86	1.08	23-14, 23-20	

**Figure S7.** <sup>1</sup>H-<sup>1</sup>H- COSY of the methyl -3-oxo-2-oxabicyclo[2.2.2]oct-5-ene-6-carboxylate intermediate from the reaction of MeCMA with ethylene (600 MHz, benzene-*d*<sub>6</sub>)



**Figure S8.**  $^1\text{H}$ - $^1\text{H}$ - COSY of the methyl -3-oxo-2-oxabicyclo[2.2.2]oct-5-ene-6-carboxylate intermediate from the reaction of MeCMA with ethylene (600 MHz, benzene- $d_6$ )

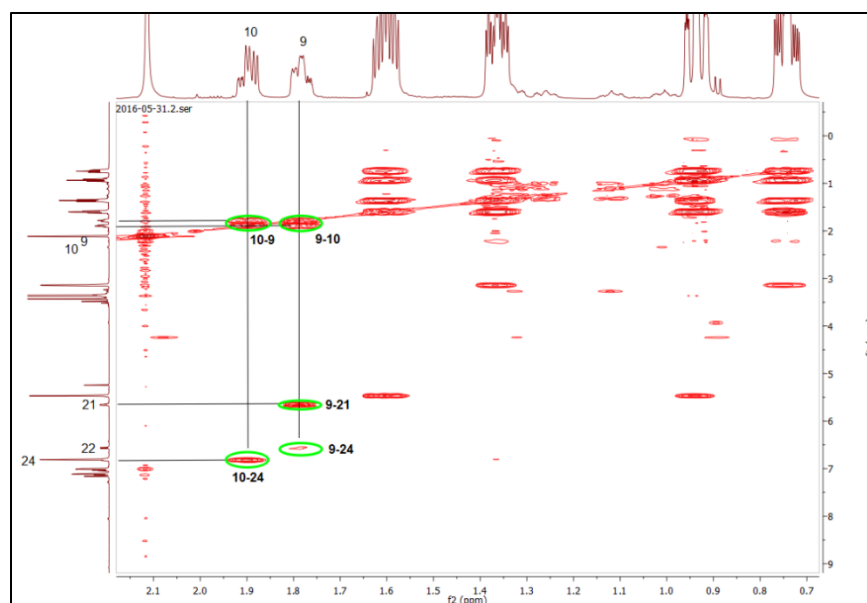


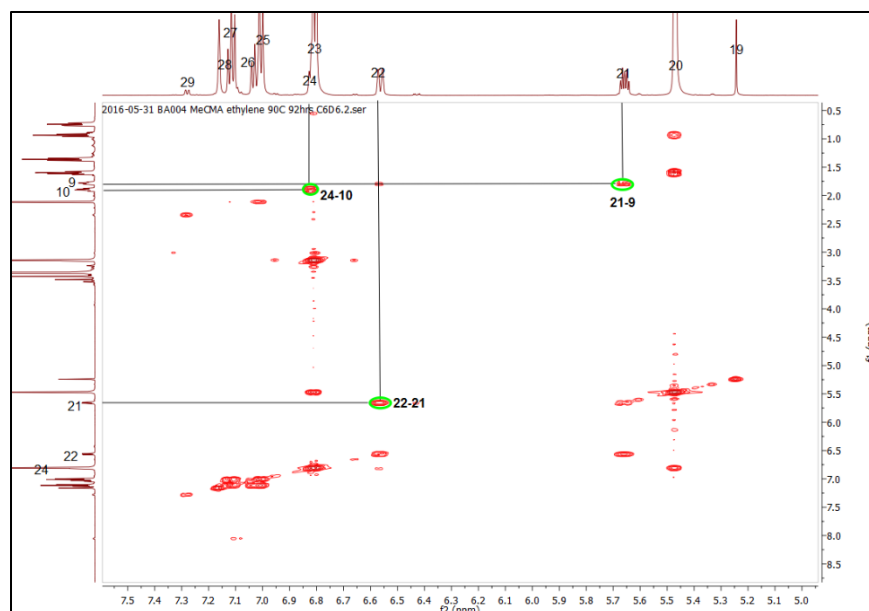
**Figure S9.**  $^{13}\text{C}$ - $^1\text{H}$ - HSQC of the methyl -3-oxo-2-oxabicyclo[2.2.2]oct-5-ene-6-carboxylate intermediate from the reaction of MeCMA with ethylene (600 MHz, benzene- $d_6$ )

**Methyl cyclohexa-1,5-diene carboxylate (Diene):**  $^1\text{H}$  NMR (600 MHz, Benzene- $d_6$ )  $\delta$  6.56 (dq,  $J = 9.9, 1.9$  Hz, 1H), 5.68 – 5.64 (m, 1H), 8.45 – 0.52 (m, 102H), 3.43 (s, 3H), 1.93 – 1.86 (m, 2H), 1.81 – 1.75 (m, 2H),  $m/z$ : 138.1.

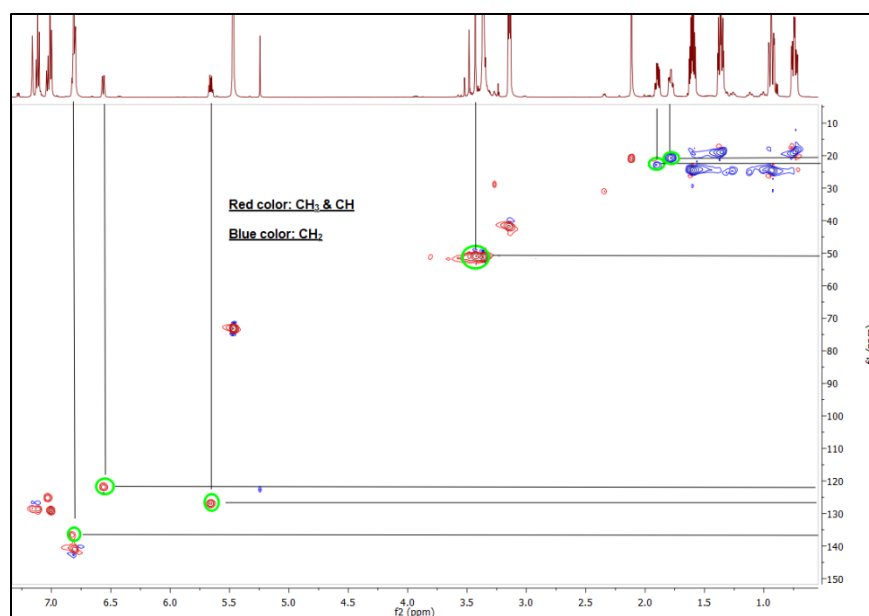
**Table S2.** Tabulated NMR assignment of the methyl cyclohexa-1,5-diene carboxylate intermediate

<sup>1</sup> H-label	$\delta$ <sup>1</sup> H, ppm, (mult)	$\delta$ <sup>13</sup> C	<sup>1</sup> H Int.	<sup>1</sup> H- <sup>1</sup> H-COSY	rel. mol-%
9	1.79	20.60	2.40	9-10, 9-21, 9-24	11.10
10	1.90	22.71	2.40	10-9, 10-24	
16	3.43	50.64	3.16	-	
21	5.66	126.98	1.13	21-9, 21-22	
22	6.56	121.66	1.04	22-10, 22-21	
24	6.82*	136.45	1.04	24-10	

**Figure S10.** <sup>1</sup>H-<sup>1</sup>H- COSY of the methyl cyclohexa-1,5-diene carboxylate intermediate from the reaction of MeCMA with ethylene (600 MHz, benzene-*d*<sub>6</sub>)



**Figure S11.**  $^1\text{H}$ - $^1\text{H}$ -COSY of the methyl cyclohexa-1,5-diene carboxylate intermediate from the reaction of MeCMA with ethylene (600 MHz, benzene- $d_6$ )

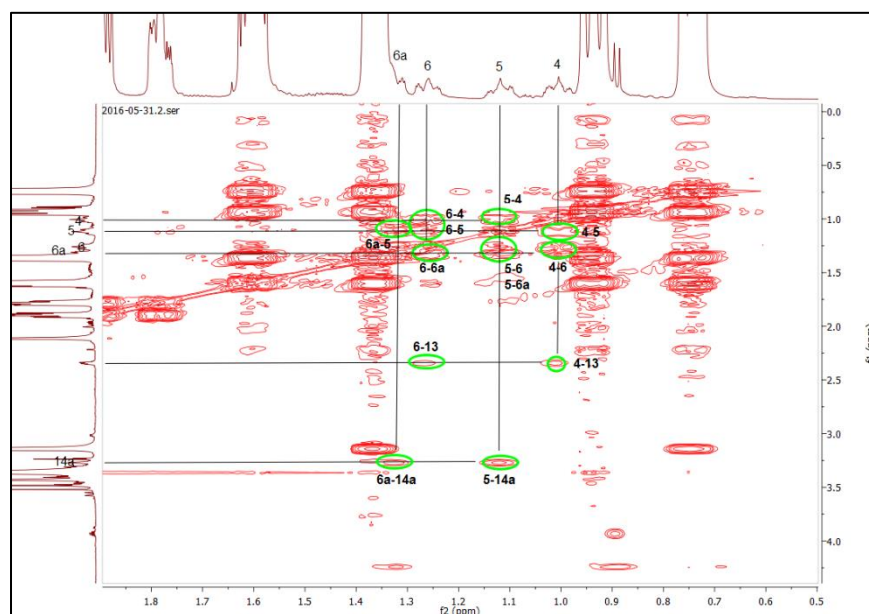


**Figure S12.**  $^{13}\text{C}$ - $^1\text{H}$ -HSQC of the methyl cyclohexa-1,5-diene carboxylate intermediate from the reaction of MeCMA with ethylene (600 MHz, benzene- $d_6$ )

**Methyl bicyclo[2.2.2]oct-2-ene-2-carboxylate:**  $^1\text{H}$  NMR (600 MHz, Benzene- $d_6$ )  $\delta$  7.28 (dd,  $J$  = 6.9, 1.7 Hz, 1H), 3.48 (s, 3H), 3.28 – 3.25 (m, 1H), 2.36 – 2.32 (m, 1H), 1.33 – 1.29 (m, 2H), 1.29 – 1.23 (m, 2H), 1.16 – 1.08 (m, 2H), 1.05 – 0.97 (m, 2H),  $m/z$ : 166.1.

**Table S3.** Tabulated NMR assignment of methyl bicyclo[2.2.2]oct-2-ene-2-carboxylate

<sup>1</sup> H-label	$\delta$ <sup>1</sup> H, ppm, (mult)	$\delta$ <sup>13</sup> C	<sup>1</sup> H Int.	<sup>1</sup> H- <sup>1</sup> H-COSY	rel. mol-%
4	1.01 (m)	24.36	1.62	4-5, 4-6, 4-6a, 4-13	3.03
5	1.12 (m)	24.88	1.92	5-4, 5-6, 5-6a, 5-14a	
6	1.26 (m)	24.57	2.11	6-4,6-5, 6-6a, 6-13	
6a	1.31 (m)	25.08	1.78	6a-4, 6a-5, 6a-6, 6a-14a	
13	2.34 (m)	31.01	0.84	13-4, 13-6, 13-29	
14a	3.27 (m)	28.74	1.21	14a-5, 14a-6a, 14a-29	
17	3.48 (s)	51.63	2.92	-	
29	7.28 (dd)	144.33	0.88	29-13, 29-14a	

**Figure S13.** <sup>1</sup>H-<sup>1</sup>H- COSY of the methyl bicyclo[2.2.2]oct-2-ene-2-carboxylate from the reaction of MeCMA with ethylene (600 MHz, benzene-*d*<sub>6</sub>)

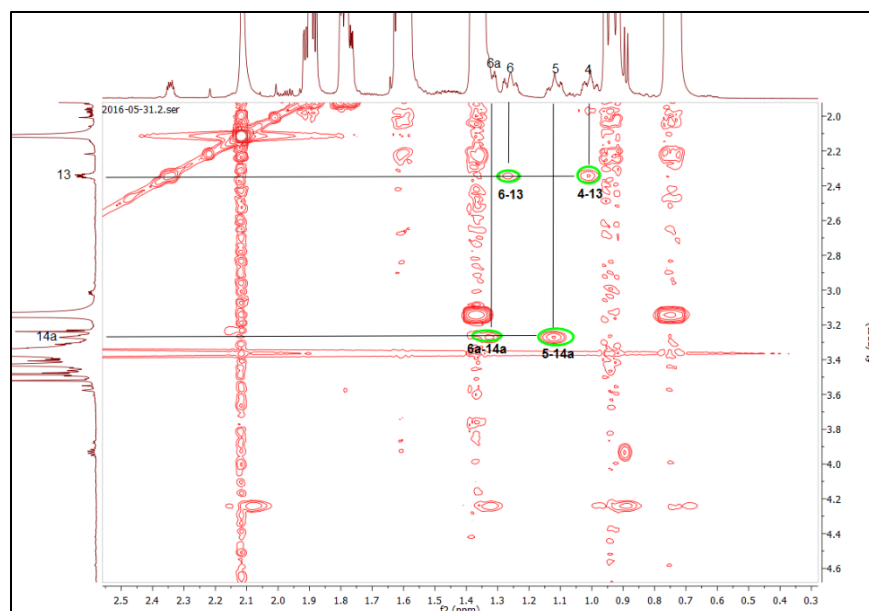


**Figure S14.**  $^1\text{H}$ - $^1\text{H}$ - COSY of the methyl bicyclo[2.2.2]oct-2-ene-2-carboxylate from the reaction of MeCMA with ethylene (600 MHz, benzene- $d_6$ )

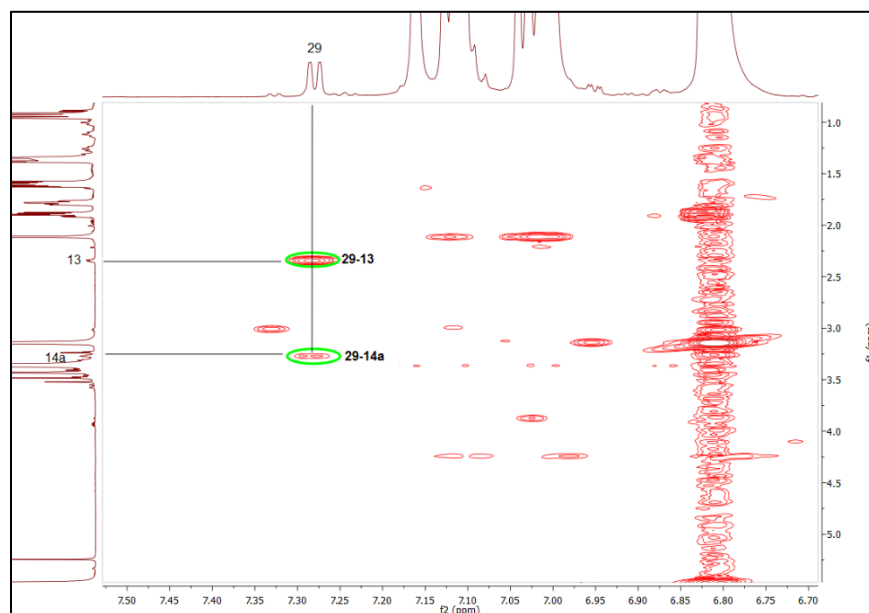


**Figure S15.**  $^1\text{H}$ - $^1\text{H}$ - COSY of the methyl bicyclo[2.2.2]oct-2-ene-2-carboxylate from the reaction of MeCMA with ethylene (600 MHz, benzene- $d_6$ )

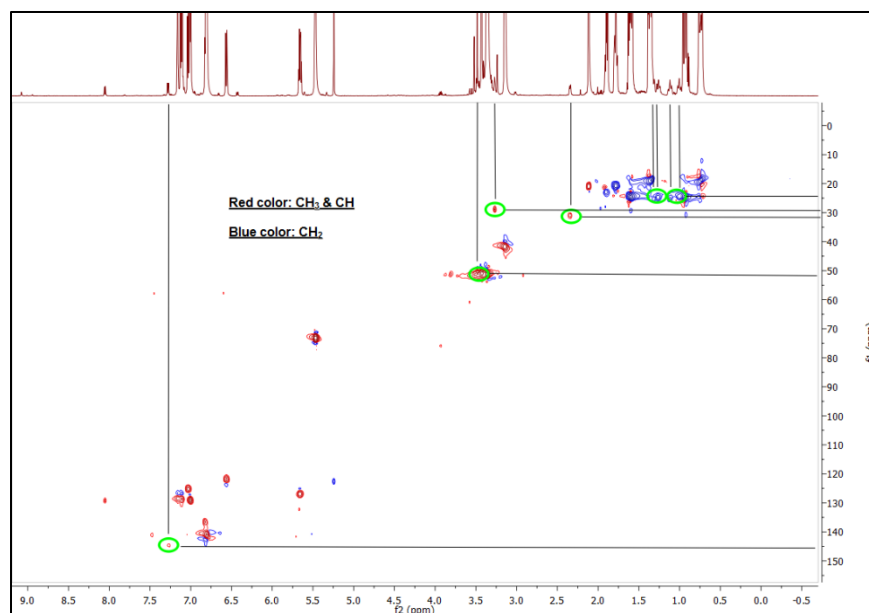


**Figure S16.**  $^{13}\text{C}$ - $^1\text{H}$ -HSQC of the methyl bicyclo[2.2.2]oct-2-ene-2-carboxylate from the reaction of MeCMA with ethylene (600 MHz, benzene- $d_6$ )

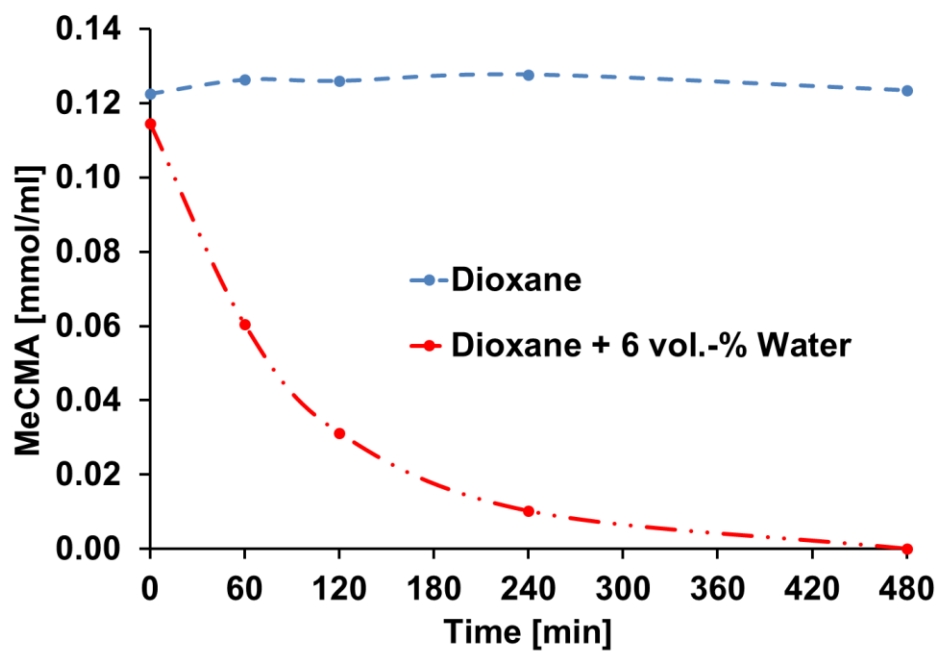


**Figure S17.** Stability test of coumalic acid in 1,4-dioxane in the presence and absence of water at 180 °C



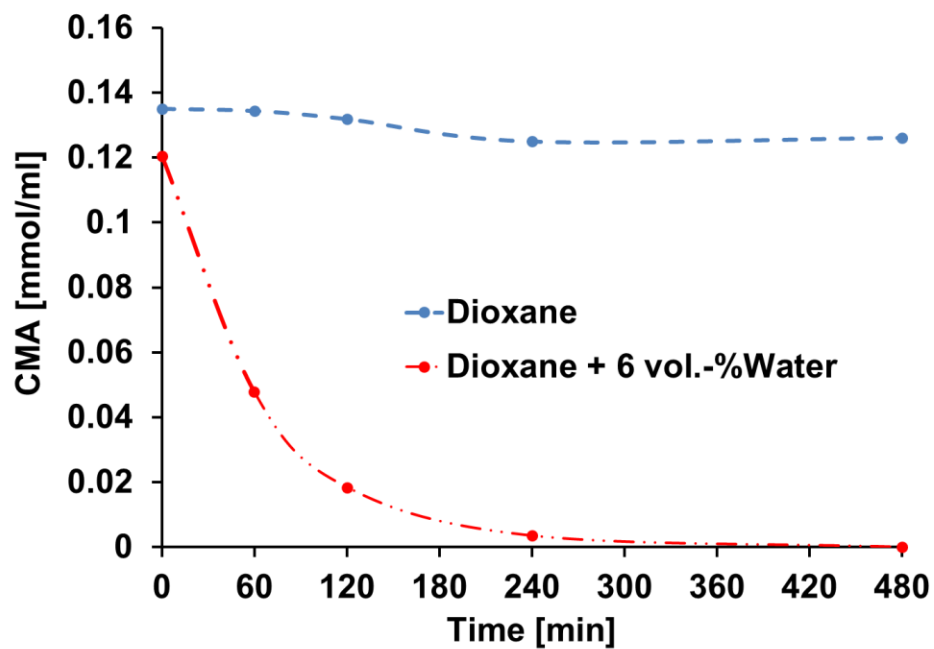


**Figure S18.** Stability test of methyl coumalate in 1,4-dioxane in the presence and absence of water at 180 °C

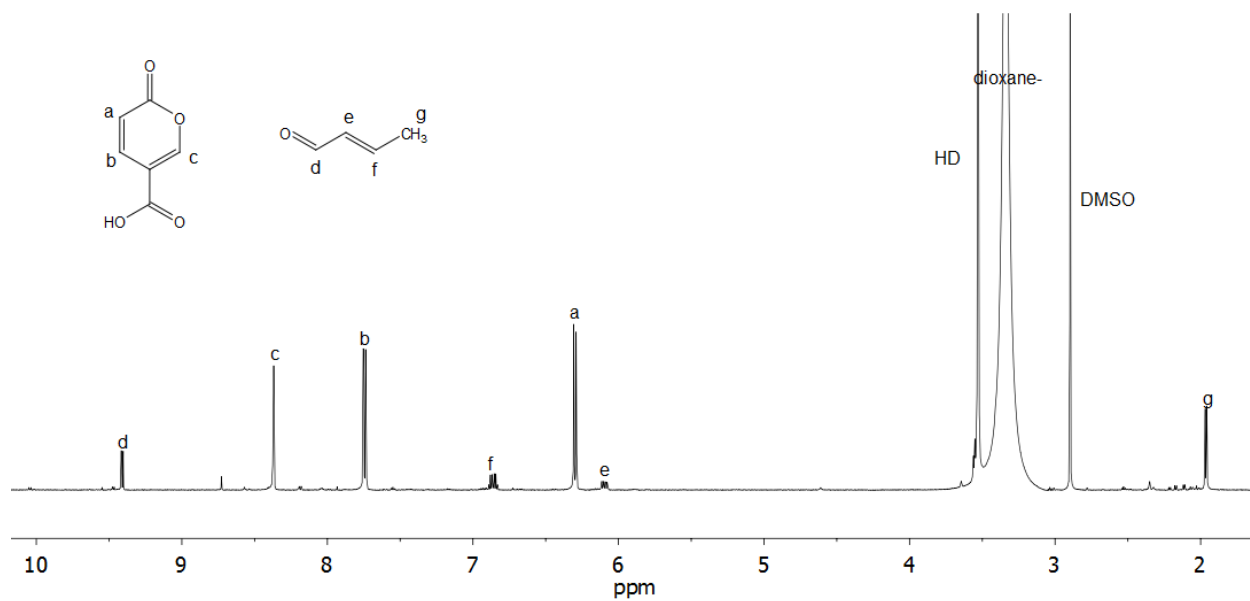


**Figure S19.** <sup>1</sup>H NMR (600 MHz, dioxane-*d*<sub>8</sub>) of 0.15M coumalic acid and 3 vol.-% H<sub>2</sub>O after 386 min at 171 °C.

**Table S4.** Rate constants and activation energy of the Diels-Alder reaction of coumalates with ethylene

Entry	Substrate	Temp. [°C]	$10^3 1/T [K^{-1}]$	$10^{-3} k_{obs} [min^{-1}]$	lnk	$E_A [kJ/mol]$
1	MeCMA	90	2.75	0.99	-6.92	76.74
2	MeCMA	100	2.68	2.03	-6.20	
3	MeCMA	110	2.61	4.15	-5.49	
4	MeCMA	120	2.54	6.72	-5.00	
5	CMA	90	2.75	0.82	-7.11	77.06
6	CMA	100	2.68	1.61	-6.43	
7	CMA	110	2.61	3.10	-5.77	
8	CMA	120	2.54	6.07	-5.10	

**Table S5.** Rate constants and activation energy of the decarboxylation reaction of the bicyclic intermediate DAP from coumalate reaction with ethylene

Entry	Substrate	Temp. [°C]	$10^3 1/T [K^{-1}]$	$10^{-3} k_{obs} [min^{-1}]$	lnk	$E_A [kJ/mol]$
1	MeCMA-DAP	140	2.42	2.56	-5.97	132.79
2	MeCMA-DAP	149	2.36	5.65	-5.18	
3	MeCMA-DAP	160	2.31	15.24	-4.18	
4	CMA-DAP	139	2.42	2.81	-5.88	141.56
5	CMA-DAP	149	2.36	7.56	-4.88	
6	CMA-DAP	158	2.32	17.31	-4.06	

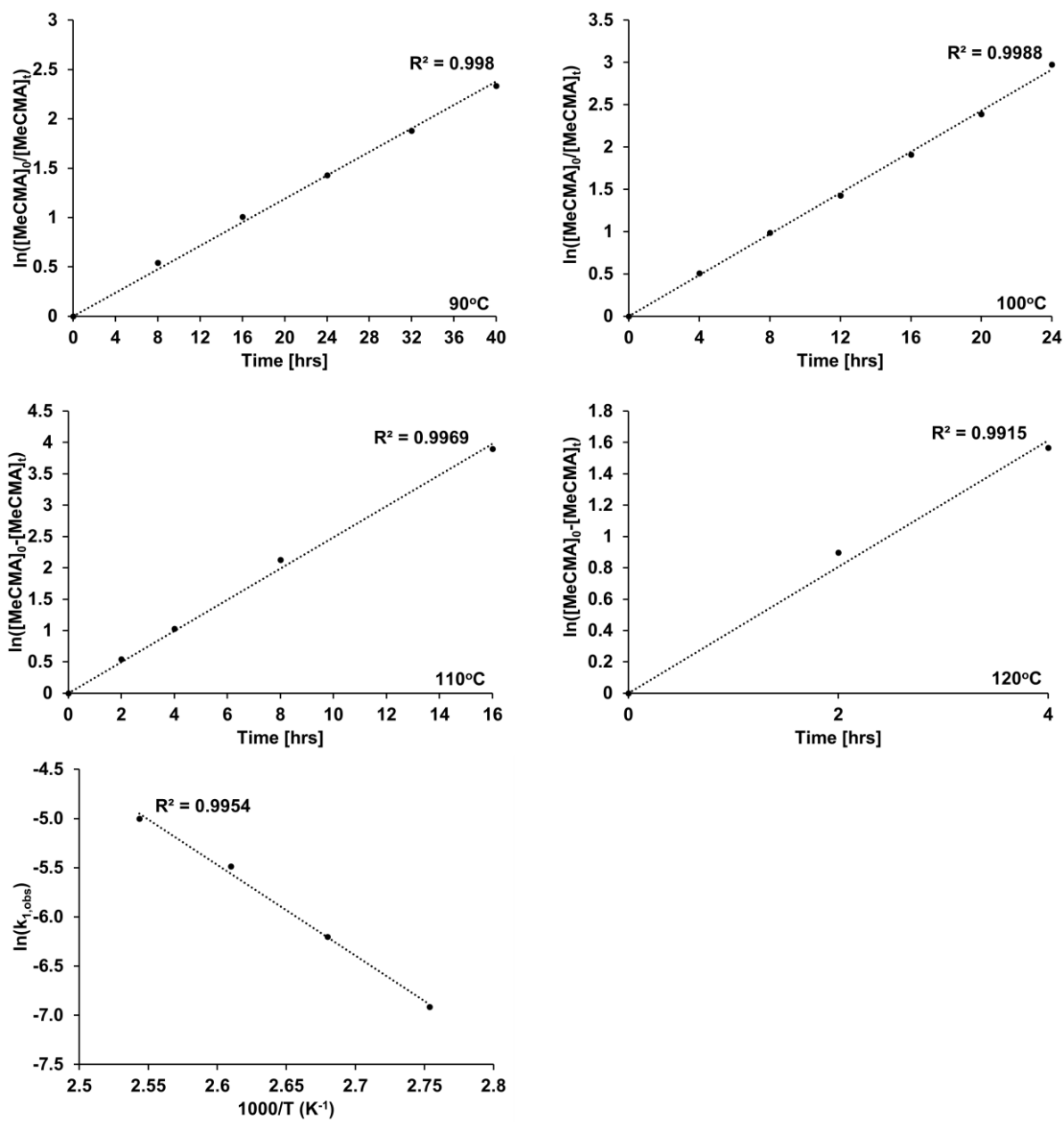


Figure S20. Diels-Alder reaction kinetics of methyl coumalate and ethylene at different temperatures

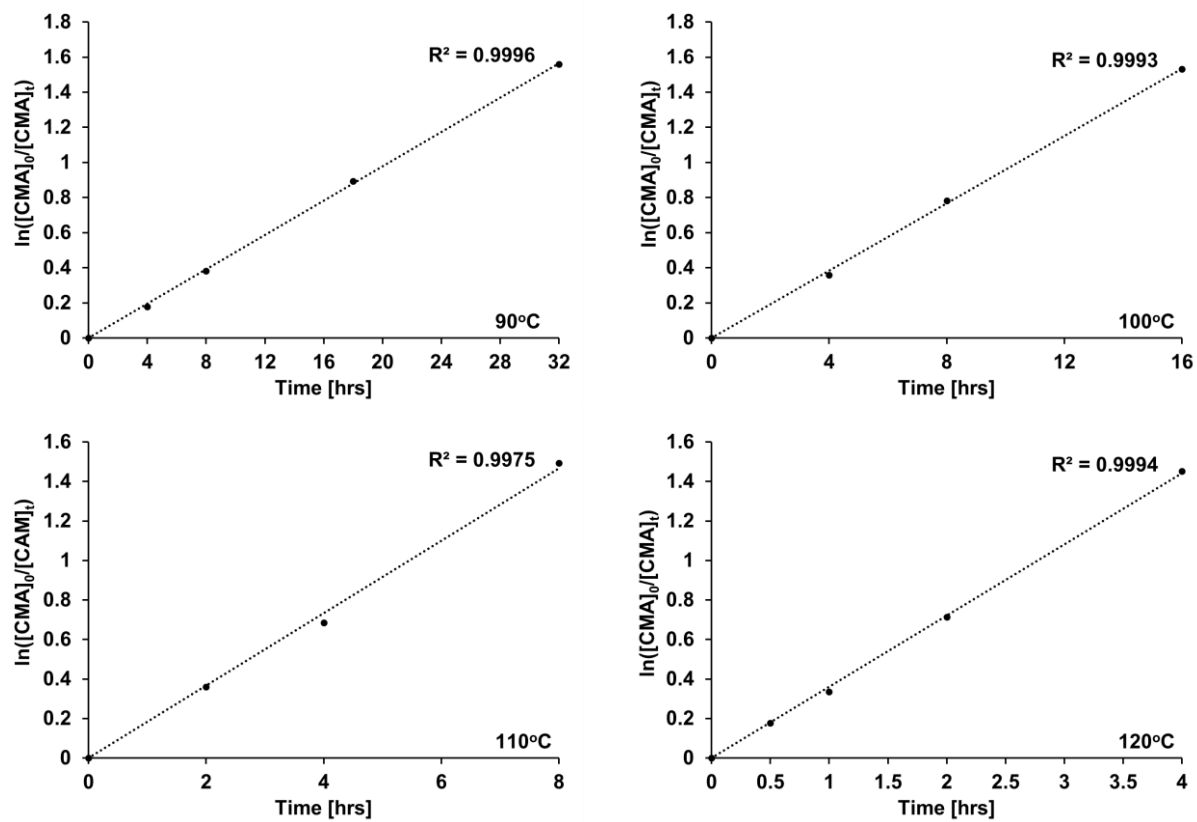
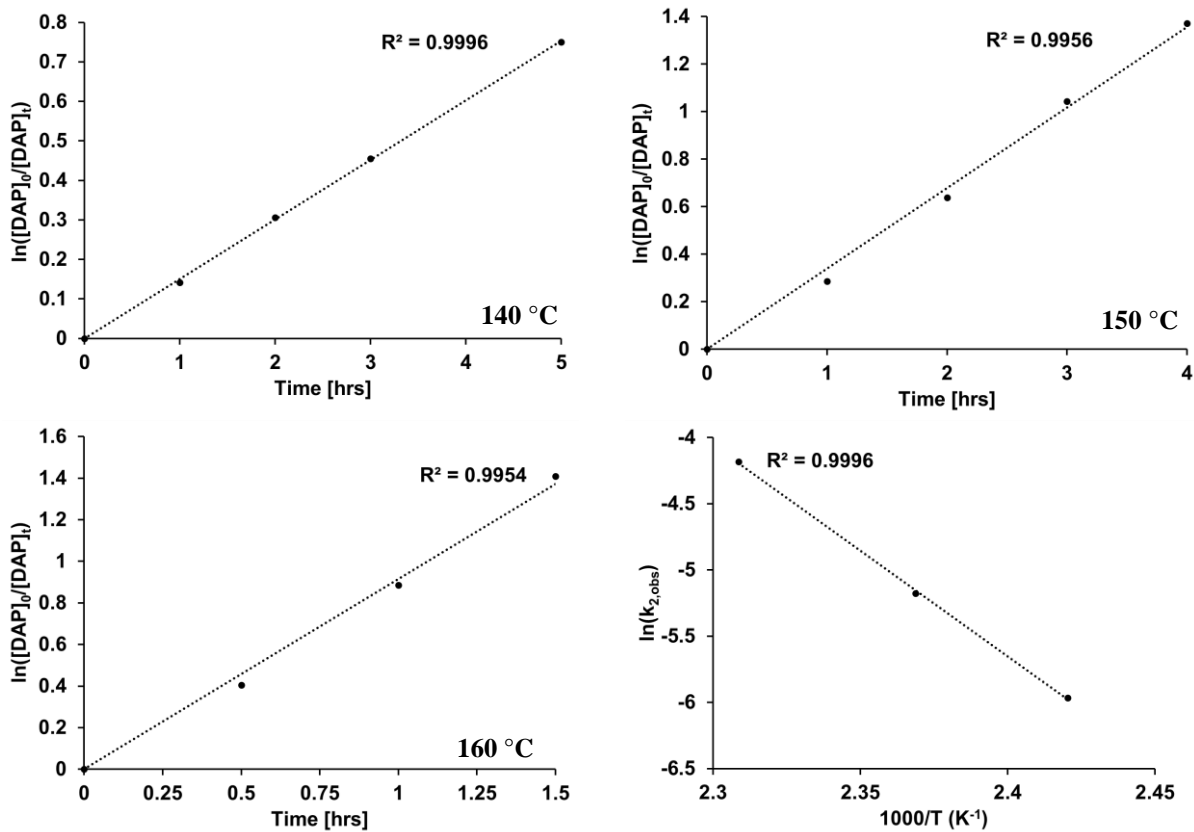
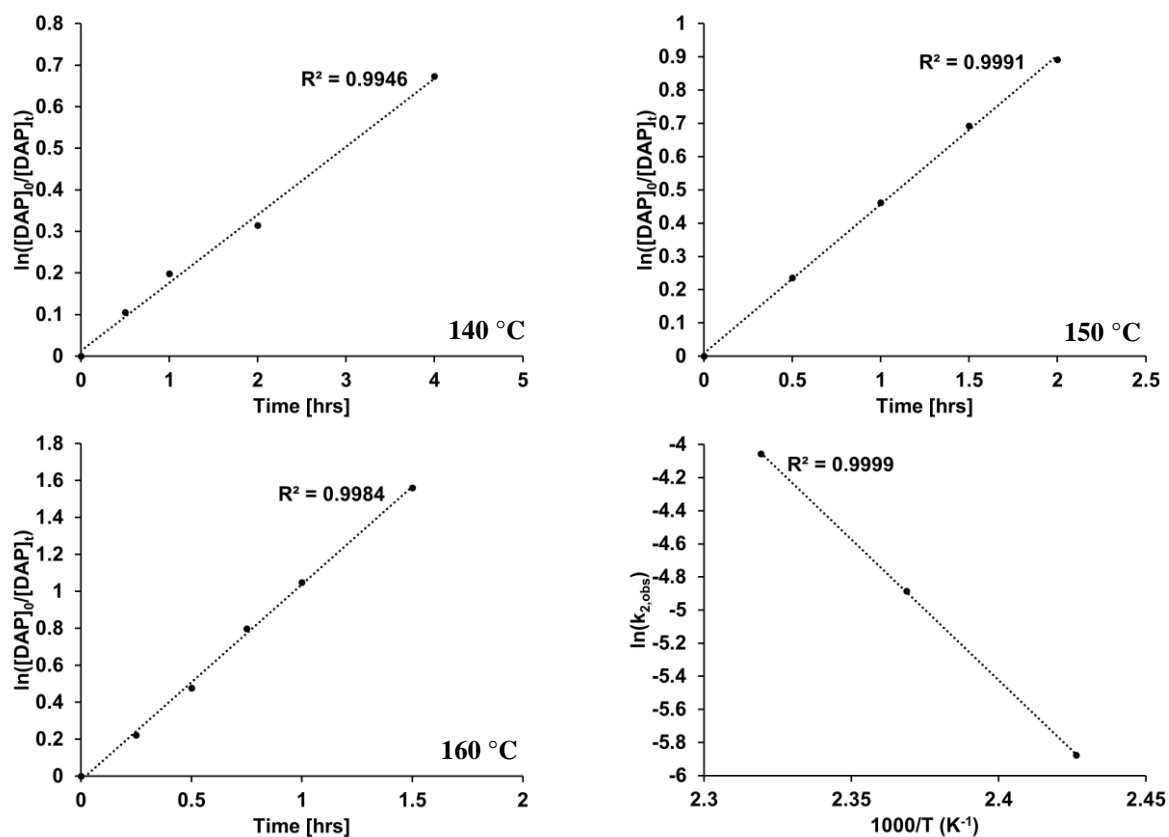


Figure S21. Diels-Alder reactions kinetics of coumalic acid and ethylene at different temperatures



**Figure S22.** Decarboxylation reaction kinetics of the Diels-Alder product of methyl coumalate and ethylene at different temperatures and the corresponding Arrhenius plot.



**Figure S23.** Decarboxylation reaction kinetics of the Diels-Alder product of coumalic acid and ethylene at different temperatures and the corresponding Arrhenius plot

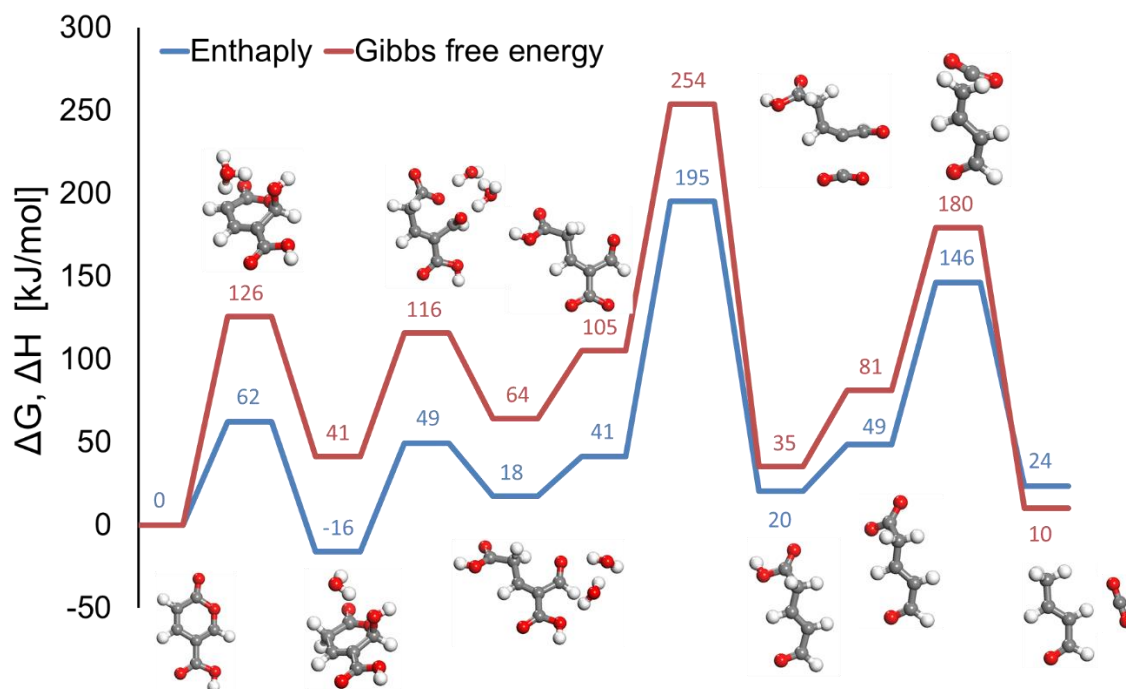


**Figure S24.** Reaction profile diagram of the coumalic acid breakdown in water

## CHAPTER 4

**MODULATING ACTIVITY AND SELECTIVITY OF 2-PYRONE-DERIVED BICYCLIC LACTONES THROUGH CHOICE OF CATALYST AND SOLVENT**

*A paper submitted to the Journal of the American Chemical Society*

Toni Pfennig,<sup>a,d</sup> Ashwin Chemburkar,<sup>c,d</sup> Robert L. Johnson,<sup>a,d</sup> Mathew J. Ryan,<sup>b</sup> Matthew Neurock,<sup>c,d</sup> Aaron J. Rossini,<sup>b</sup> Brent H. Shanks<sup>\*a,d</sup>

<sup>a</sup> Department of Chemical and Biological Engineering, Iowa State University, Ames, IA, 50011, USA

<sup>b</sup> Department of Chemistry, Iowa State University, Ames, IA, 50011, USA

<sup>c</sup> Department of Chemical Engineering and Material Sciences, University of Minnesota, Minneapolis, MN 55455, USA

<sup>d</sup> NSF Engineering Research Center for Biorenewable Chemicals (CBiRC), Ames, IA 50011, USA

#### 4.1 Abstract

2-Pyrones, such as coumalic acid, are promising bio-based molecules that through Diels-Alder reactions can provide access to a wide range of bio-based chemicals, including molecules with functionality that are not easily accessible via conventional petrochemical routes. A complete reaction network and kinetic parameters for three individual diversification routes that start from a single bicyclic lactone produced via the Diels-Alder cycloaddition of coumalic acid and ethylene were examined experimentally and probed through complementary first-principle density functional theory (DFT) calculations, in situ nuclear magnetic resonance (NMR) spectroscopy and thin film solid-state NMR spectroscopy. These experiments provide insights into the routes for several molecular structures from bicyclic lactones by leveraging Lewis or Brønsted acid catalysts to selectively alter the reaction pathway. The bicyclic lactone bridge can be decarboxylated to

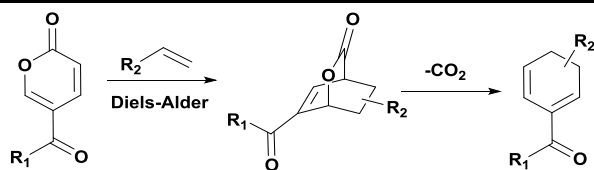
access dihydrobenzenes at a substantially reduced activation barrier using  $\gamma$ -Al<sub>2</sub>O<sub>3</sub> as the catalyst or selectively ring-opened via Brønsted acids to yield 1,3-diacid six membered rings. DFT computations and microkinetic modeling in combination with experimental results provide molecular insights into the catalytically active sites on  $\gamma$ -Al<sub>2</sub>O<sub>3</sub> and provide a general mechanism for the catalyzed bicyclic lactone decarboxylation in polar aprotic solvents, which involves CO<sub>2</sub> extrusion as the kinetically relevant step. Solid-state NMR spectroscopy provides direct evidence of strong binding of the bicyclic lactone to the  $\gamma$ -Al<sub>2</sub>O<sub>3</sub> surface, fully consistent with DFT simulation results and experimental reaction kinetics. In addition, the role of the solvent was examined and found to be an additional means to improve reaction rates and selectively produce new structures from the bicyclic intermediate. The rate of the decarboxylation reaction was increased dramatically by using water as the solvent whereas methanol acted as a dienophile and selectively induced ring-opening, showing that both pathways are operative in the absence of catalyst. Taken together, the results demonstrate a novel approach for selective diversification of the coumalate platform to a range of molecules.

## 4.2 Introduction

New technologies to extract non-renewable carbon feedstocks, such as shale gas, exert significant economic pressure on the potential to manufacture bio-based commodity chemicals. This challenge creates the need to develop flexible chemical conversion platforms that can be used to pivot from biomass-derived bulk chemicals to higher value chemicals. Leveraging novel transformation pathways from biomass feedstocks via bioprivileged molecules provides an attractive means to access higher value chemicals such as next-generation nutraceuticals, antimicrobials, pharmaceuticals, consumer goods, specialty chemicals, etc., in a manner that is cost competitive compared to traditional petrochemical routes.<sup>1</sup>



As a potential bioprivileged molecule platform, Diels-Alder conversion of 2-pyrone coumalic acid (CMA) provides a highly versatile pathway to the synthesis of a wide range of bio-based chemicals through the utilization of a variety of dienophiles.<sup>2-6</sup> Particularly important are those dienophiles that are less expensive and lead to more efficient downstream separations. Renewable CMA can be synthesized from malic acid via acid catalyzed dimerization,<sup>6</sup> with malic acid being readily produced from biomass via fermentation with genetically modified microorganisms.<sup>7-9</sup> Given that malic acid has been cited as one of the 12 most promising bio-based platform chemicals,<sup>10</sup> considerable effort has already been invested into the biochemical conversion of glucose to malate. A particularly interesting feature of 2-pyrone Diels-Alder reactions is the formation of stable bicyclic lactones that are highly functionalized, stereochemically rich building blocks which can be used as versatile synthetic intermediates.<sup>11-22</sup> Decarboxylation of these structures leads to synthetically valuable dihydrobenzenes<sup>20,23-25</sup> (DIH) with potential applications in the manufacture of medically useful products (Scheme 1). DIH can then be utilized for chemical diversification, granting access to polycyclic systems<sup>11,18,19,21,24,26,27</sup> and aromatics<sup>2-6,11,18,22,25,26</sup> with wide-ranging applications. Although bicyclic compounds can be accessed from 2-pyrones in high yield, their selective transformation via thermal decarboxylation can be challenging due to degradation<sup>23</sup> or in situ aromatization<sup>4-6,11,18,25</sup>, which limit the selective access of interesting and potentially value-added diene structures in high purity.

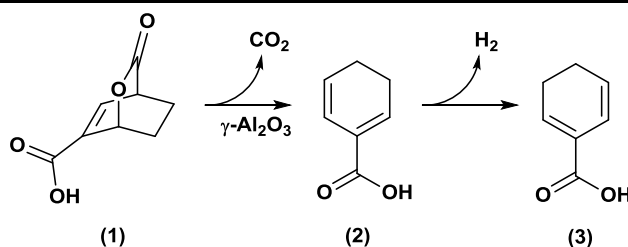


**Scheme 1.** 2-pyrone diversification)

---

In-situ aromatization of these conjugated diene species is especially favored when the desired diene contains a leaving group (e.g. alkoxy), demonstrated by reactions of methyl coumalate in combination with ketals, acetals, captodative dienophiles or vinyl ethers, which lead to high aromatic yields without the requirement of a dehydrogenation catalyst.<sup>4-6</sup> We recently demonstrated that the catalytic production of benzoic acid from CMA and ethylene proceeds via a sequence of reactions including Diels-Alder, decarboxylation, and palladium catalyzed dehydrogenation. The rate for this reaction is limited by the decarboxylation of the bicyclic lactone intermediate to the respective DIH resulting in an activation energy of 142 kJ/mol.<sup>28</sup> Given the high activation barrier of de-carboxylation of the bicyclic lactone molecules, an effective catalyst that activates the decarboxylation step is of great interest to allow for CO<sub>2</sub> extrusion under milder reaction conditions. This could preserve the diene functionality and prevent in situ aromatization and formation of other decomposition products.

Herein, we report a highly selective technology platform to synthesize DIHs through the use of Lewis and Brønsted acid catalysts that alter the reaction path of the bicyclic intermediate that forms. This approach can be applied to other bicyclic lactone systems, opening the door to the production of many different specialty chemicals without the requirement of numerous dienophiles. We demonstrate this approach using a bicyclic lactone (1) derived from CMA in



**Scheme 2.**  $\gamma\text{-Al}_2\text{O}_3$  catalyzed decarboxylation.

---

conjunction with inexpensive and easily separable ethylene (Scheme 2). Detailed kinetic experiments, density functional theory calculations, and thin layer solid-state high resolution magic angle spinning (HR-MAS) NMR spectroscopy which were carried out show that bicyclic intermediate (1) derived from the Diels-Alder addition of 2-pyrone and ethylene undergoes a direct decarboxylation on the surface of  $\gamma$ -Al<sub>2</sub>O<sub>3</sub> to form cyclohexa-1,5-diene-1-carboxylic acid (2) and show that the coordinatively saturated Al-species selectively drives the decarboxylation reaction to completion. Through in situ <sup>1</sup>H-NMR spectroscopy experiments, we further demonstrate that the presence of Brønsted acids result in the ring-opening of the bicyclic intermediate followed by an acid catalyzed dehydration leading to cyclohexa-1,3-diene-1,3-dicarboxylic acid in high selectivity.

The impact of solvents in steering the reaction was also explored. Using solvents that can serve as weak nucleophiles (e.g. methanol) provides an alternative path for transforming (1) to (5)-(methoxycarbonyl)cyclohexa-1,5-diene-1-carboxylic acid with high selectivity (>99 mol%). Conversely, polar protic water leads to enhanced decarboxylation of (1) to (2) as compared to the polar aprotic 1,4-dioxane. These routes offer catalyst-free pathways with the potential to be broadly applied to bicyclic lactone molecules. Lastly, we applied these findings to synthesize benzoic acid (3) by using a bifunctional 1 wt% Pd/ $\gamma$ -Al<sub>2</sub>O<sub>3</sub> catalyst to activate the rate limiting decarboxylation step, reduce the reaction temperature, and show the full conversion of (2) to (3) with a selectivity > 99 mol%.

## 4.3 Methods and Materials

### 4.3.1 Reagents and Material

Pd(II)-, Cu(II)-, Ce(III)-, Zn(II)-acetate (>99.9 %), coumalic acid (>97 %), 10 wt% Pd/C, sulfuric acid- $d_2$  (96-98 wt%, 99.5 atom % D), D<sub>2</sub>O (99.9 atom % D) and Davisil (Silica Gel, 150 Å, >99 %) were obtained from Sigma Aldrich. DMSO- $d_6$  (99.9 %), dioxane- $d_8$  (99 %), methanol- $d_4$  (99.8 %) were obtained from Cambridge Isotope Laboratories Inc. Dimethylformamid (99.9 %), 1,4-dioxane (99.9 %) and sodium bicarbonate (> 99.7 %) were obtained from Fisher Scientific. Methyl coumalate (Acros Organics, 98 %). Ethylene (99.5 %, Matheson). Zeolites ZSM-5 (CBV5524G), Y-Zeolite (CBV 720), and ZSM-5 (CBV2314), were obtained from Zeolyst International in very high purity (100 wt%),  $\gamma$ -Al<sub>2</sub>O<sub>3</sub> (Strem Chemicals, Inc., >99.8 %), Amberlyst 45 (Dow >98%). All chemicals were used without further purification.

### 4.3.2 Catalyst Preparation

The 5 wt% metal catalysts were prepared via incipient wetness impregnation using  $\gamma$ -Al<sub>2</sub>O<sub>3</sub>, and the respective metal acetate salts of Cu, Fe, Zn, and Ce, dried at 65 °C (24 h) and calcined at 450 °C (6 h) in a steady flow (200 mL/min) of air.

### 4.3.3 Batch Reaction Experiments

The Diels-Alder product (1) was obtained from batch reactions at 110 °C for 16 h using a 50 mL 4590 Parr reactor setup. Mechanical agitation was maintained at 400 rpm using a magnet-driven stirrer. 300 mg of CMA was placed into the reactor vessel and 30 mL of 1,4-dioxane was added to mediate the reaction, resulting in a starting concentration of 71.38  $\mu$ mol/mL. After the reactor was sealed, the reactor was purged five times to replace residual air with nitrogen. Next, the reactor was charged for 30 min with 500 psig ethylene to ensure saturation of ethylene in the

solvent. Under these conditions the re-actions were performed in large excess of ethylene. After charging the vessel with ethylene, the reactor was heated to the desired reaction temperature using a controlled heating ramp of 10 K/min. After completion of the reaction, the reactor vessel was purged to replace unreacted ethylene with nitrogen. A sample was withdrawn and the solvent was carefully evaporated with dry air before 600  $\mu\text{L}$  fully deuterated solvent ( $\text{DMSO-}d_6$ ) and 2.5  $\mu\text{L}$  internal standard (DMF) were added. Finally, the samples were analyzed via  $^1\text{H-NMR}$ .

Batch reactions for the catalyst screening experiments were performed in 10 mL thick-walled glass vial reactors (Alltech) equipped with magnetic stir bars. Agitation and heat were provided using a temperature controlled oil-bath that was regulated with an Isotemp Digital Plate Stirrer from Fisher Scientific. The glass vial reactor was loaded with 4 mL of a 71.38  $\mu\text{mol/mL}$  solution of (1) in 1,4-dioxane. 25 mg of catalyst was added before the vial was sealed and placed into the hot oil bath to initiate the reaction. After the reaction was completed, the product was filtered through a 0.2 micron syringe filter to remove the catalyst from the products. A sample was then taken and the solvent was removed via careful evaporation. Fully deuterated  $\text{DMSO-}d_6$  (600  $\mu\text{L}$ ) and 2.5  $\mu\text{L}$  of internal standard DMF (Dimethylformamid) were added to the crude material for quantification via  $^1\text{H-NMR}$ .

The  $\gamma\text{-Al}_2\text{O}_3$  catalyzed decarboxylation reactions were carried out in a 50 ml 4590 Parr reactor. The vessel was charged with 30 mL of a 71.36  $\mu\text{mol/mL}$  solution containing (1). 200 mg of the  $\gamma\text{-Al}_2\text{O}_3$  catalyst ( $\sim 53 \mu\text{m}$  particle size) was added before the reactor was sealed and purged 5 times with nitrogen to remove residual air while agitation was applied (400 rpm). Next, the respective reaction temperature was obtained using a controlled heat ramp of 10 K/min. After the reactor reached the desired temperature a sample was withdrawn as a reference using a high pressure sampling dip tube. Further samples were withdrawn periodically to obtain a concentration

profile over time. After the reaction was completed, all samples were filtered via a 0.2 micron syringe filter and the solvent was carefully evaporated with dry air before 600  $\mu\text{L}$  deuterated solvent ( $\text{DMSO-}d_6$ ) and 2.5  $\mu\text{L}$  internal standard DMF were administered. The samples were then analyzed via  $^1\text{H-NMR}$ .

#### 4.3.4 In Situ NMR Experiments

The general procedure for the in situ kinetic measurements was performed using high-pressure NMR tubes from Wilmad-Labglass. The solvents used for the decarboxylation and ring-opening experiments were  $\text{D}_2\text{O}$ , dioxane- $d_8$ , and methanol- $d_4$ , respectively. As aforementioned, reactant (1) for this study was synthesized via Diels-Alder reaction of CMA and ethylene in 1,4-dioxane at 110  $^\circ\text{C}$  and 16 h, with a high yield (>98 %). Through careful evaporation of the solvent using dry air, the reaction product (1) was obtained and subsequently dissolved in the respective deuterated solvent. The solution was then transferred into the high-pressure NMR tubes. The tubes were placed into the Bruker Avance III 600 MHz spectrometer and heated to the respective temperature to initiate the reaction. The progress of the reaction was subsequently monitored over time.

The water-mediated decarboxylation of the sodium salt of the bicyclic lactone (1) was performed in  $\text{D}_2\text{O}$  at temperatures in the range of 50-90  $^\circ\text{C}$ . 50 mg of the reactant (1) was dissolved in 1 mL of  $\text{D}_2\text{O}$  (263.16  $\mu\text{mol/mL}$ ). The sodium salt of (1) was synthesized via neutralization using sodium bicarbonate.

The methanol- $d_4$ -mediated reactions were performed in a temperature range of 90-110  $^\circ\text{C}$  using 71.38  $\mu\text{mol}$  of (1) that was dissolved in 300  $\mu\text{L}$  (237.93  $\mu\text{mol/mL}$ ) of methanol- $d_4$ .

The ring-opening reactions in 1,4-dioxane using D<sub>2</sub>SO<sub>4</sub> as a catalyst were performed in a temperature range of 70-110 °C. 71.38 μmol of (1) was dissolved in 300 μL (237.93 μmol/mL) dioxane-*d*<sub>8</sub> and 5 μL of D<sub>2</sub>SO<sub>4</sub> were added to catalyze the reaction.

To elucidate the reaction network, all compounds were verified via NMR structural assignments performed using different techniques including <sup>1</sup>H-NMR, <sup>1</sup>H-<sup>1</sup>H COSY, <sup>13</sup>C-<sup>1</sup>H HSQC and validated using UPLC-QDa(ESI) mass analysis.

#### 4.3.5 Analytical Methods

The batch reaction solution products were analyzed via NMR using a Bruker spectrometer equipped with a 14.1 Tesla superconducting magnet. The data were acquired and processed using TOPSPIN (version 3.0) and Mestre Nova (version 10.0.1-14719), respectively. NMR samples were prepared using fully deuterated solvents, to both reduce the solvent background and to perform field calibration. Additionally, a 2.5 uL DMF internal standard was added for quantification. All <sup>1</sup>H spectra were acquired using a recycle delay of 3.0 sec. and 30° <sup>1</sup>H excitation pulse lengths. <sup>1</sup>H-<sup>1</sup>H 2D NMR spectra were acquired using a COSY pulse sequence, and <sup>13</sup>C-<sup>1</sup>H 2D NMR spectra were acquired using a HSQC pulse sequence.

Ultra-pressure liquid chromatography (UPLC) was also applied to analyze known species in the reaction products and to obtain the amount of each compound. A Waters Acquity H-Class System equipped with a Photodiode Array (PDA) and a QDa mass detector was used to perform the analysis. UPLC separation was carried out on a Waters BEH Phenyl column (2.1x100 mm, 1.7 μm particles).

The samples for HR-MAS/solid-state NMR experiments were prepared by first drying γ-Al<sub>2</sub>O<sub>3</sub> overnight at 120 °C in a convection oven to remove residual adsorbed water. Next, 30 mg

$\gamma$ -Al<sub>2</sub>O<sub>3</sub> was weighed into a 2 mL polypropylene screwcap vial and then transferred into the glovebox. The vials were allowed to sit with the cap re-moved in the glovebox for 48 h prior to impregnation. Samples were impregnated with a liquid loading of 1  $\mu$ L/mg and allowed to equilibrate overnight with the cap on. Following impregnation the samples were then packed into 2.5 mm rotors inside the glove box to pre-vent excess moisture from being introduced.

All solid-state NMR experiments were performed on a 9.4 T (400 MHz) Bruker Avance III HD NMR spectrometer with a 2.5 mm HXY triple resonance probe. A 25 kHz MAS frequency was used for all experiments. <sup>1</sup>H solid-state NMR spectra were obtained with a rotor synchro-nized spin echo pulse sequence. Proton detected 2D <sup>27</sup>Al $\rightarrow$ <sup>1</sup>H D-RINEPT HETCOR spectra were obtained using the previously described D-RINEPT pulse sequence.<sup>40,41</sup> The symmetry based recoupling sequence supercycled (S) was used for dipolar recoupling.<sup>52</sup> Proton detected 2D <sup>1</sup>H{<sup>13</sup>C} CP-HETCOR spectra were obtained with the previously described pulse sequence.<sup>38,39</sup> The contact time for the <sup>1</sup>H $\rightarrow$ <sup>13</sup>C forwards CP transfer was 2000  $\mu$ s and different 2D spectra were obtained with contact times of 200  $\mu$ s, 500  $\mu$ s and 2000  $\mu$ s for the <sup>13</sup>C $\rightarrow$ <sup>1</sup>H backwards CP transfer. CP was performed with a <sup>13</sup>C spin lock pulse with an RF field of ca. 91 kHz and a <sup>1</sup>H spin lock pulse with a nominal RF field of ca. 68 kHz. The amplitude of the <sup>1</sup>H spin lock pulses was linearly ramped from 85% to 100% RF field to broaden the CP match conditions.<sup>53</sup> In both the <sup>13</sup>C and <sup>27</sup>Al NMR experiments SPINAL-64 <sup>1</sup>H heteronuclear decou-pling<sup>54</sup> was performed during the indirect dimension evolution period with a 100 kHz RF field. Details on acquisition parameters for the 2D spectra (number of scans, indirect dimension points, etc.) are described in the Figure captions.



## 4.3.6 Computational

### 4.3.6.1 Periodic density functional theory

All of the calculations carried out on model  $\gamma$ -Al<sub>2</sub>O<sub>3</sub> surfaces were carried out using periodic plane-wave density functional theory methods as implemented in the Vienna ab initio simulation package (VASP).<sup>55-58</sup> The PBE functional<sup>59</sup> was used to calculate exchange and correlation energies. The D3 method<sup>60</sup> was used to estimate the dispersive interactions. A plane wave energy cutoff of 396 eV was used for all periodic calculations reported herein. Optimizations were performed in two steps. First, wave-functions were converged to within 10<sup>-4</sup> eV, until the maximum force upon each atom was less than 0.1 eV/Å. In step two, wave-functions were converged to within 10<sup>-6</sup> eV, with maximum allowable force upon each atom less than 0.05 eV/Å. Step two calculations were carried out spin-polarized and monopole/dipole moments were calculated to correct for energies. Transition states were obtained using the nudged elastic band method<sup>61,62</sup> and the dimer method.<sup>60</sup>

Calculations were performed on 1x1 unit cells of 110 and 2x1 unit cells of 100 surfaces of  $\gamma$ -Al<sub>2</sub>O<sub>3</sub>. The bulk structure of  $\gamma$ -Al<sub>2</sub>O<sub>3</sub> reported elsewhere was used.<sup>63</sup> For hydroxylated surfaces, structures found by Sautet and co-workers were used.<sup>33,64</sup> For 110 surfaces, the periodic slab models consisted of 8 layers (Al:O = 3:2) separated by vacuum with bottom two layers frozen to bulk position. While for the 100 surfaces, 4 layers (Al:O = 3:2) were modeled with the bottom two layers frozen to bulk positions. Optimizations on the 1x1 unit cells of 110 surfaces were performed on a 3x3x1 k65 point mesh while a k point mesh of 2x2x1 was used for the 2x1 unit cells of 100 surfaces.

The entropies of adsorbed molecules were estimated by equations 1 and 2, where  $S_{ad}^{\circ}(T)$  is the entropy of adsorbed molecule and  $S_{gas}^{\circ}(T)$  is the ideal gas entropy of that molecule. These values roughly correspond to the loss of 1/3rd entropy of the molecules in the gas phase.<sup>66</sup>

$$S_{ad}^{\circ}(T) = 0.70 \times S_{gas}^{\circ}(T) - 3.3R, \text{ for } S_{gas}^{\circ}(T) < 60 R \quad (1)$$

$$S_{ad}^{\circ}(T) = 0.99 \times S_{gas}^{\circ}(T) - 20.7R, \text{ for } S_{gas}^{\circ}(T) > 60 R \quad (2)$$

As an approximation, the entropy of a weakly physisorbed molecule was estimated by subtracting just the 1/3rd transitional component. Since, the transition state for decarboxylation was in close resemblance to the reactant state, the entropy of activation was assumed to be negligible.

#### 4.3.6.2 Molecular density functional theory

Molecular density functional theory calculations were performed using the M062X67 hybrid functional as implemented in Gaussian 09.68 6-311G+(d,p) basis set<sup>69</sup> on an ultrafine grid and tight convergence criterion for force was used for all stationary and saddle point calculations. The SMD solvation model<sup>69</sup> was used to implicitly model the effect of solvation. In cases where the solvent directly participated in reaction, explicit solvent molecules were used in conjunction with implicit solvation. Enthalpies and Gibbs free energies were calculated at standard state and 298.15 K within Gaussian 09. A correction factor of  $RT \ln(24.46)$  was added to the free energies of species having standard concentration of 1 M. While for bulk solvents, (water and methanol), corrections corresponding to 55.5 M for water and 24.9 M for methanol were applied.

## 4.4 Results and Discussion

### 4.4.1 Decarboxylation in the Presence of Catalyst

To overcome the high activation barrier required to de-carboxylate (1) to form the DIH (2), a catalyst that can selectively activate the decarboxylation step is required. Given that Brønsted acids and Lewis acids facilitate Diels-Alder reactions<sup>13,18,20,21,27,29-31</sup>, we hypothesized that these acid catalysts could also enable retro-Diels-Alder extrusion of CO<sub>2</sub> from bicyclic lactones to generate DIH.

Starting with  $\gamma$ -Al<sub>2</sub>O<sub>3</sub> as a Lewis acid catalyst,<sup>32</sup> we found that (1) can be effectively decarboxylated to (2) at 120 °C (Table 1, Entry 2). The 47 mol% conversion of (1) resulted in a yield of 43 mol% of (2) and small amounts of (3) (Scheme 3). This is a significant improvement over the control experiment which gave only 9 mol% conversion of (1) at identical reaction conditions but in the absence of a catalyst (Table 1, Entry 1). It is evident from these experiments that  $\gamma$ -Al<sub>2</sub>O<sub>3</sub> can be effectively used as a highly active decarboxylation catalyst for bicyclic lactones. Additional experiments were performed with Lewis acid metals supported on  $\gamma$ -Al<sub>2</sub>O<sub>3</sub> including 5 wt.-% Zn/ $\gamma$ -Al<sub>2</sub>O<sub>3</sub>, Cu/ $\gamma$ -Al<sub>2</sub>O<sub>3</sub>, Fe/ $\gamma$ -Al<sub>2</sub>O<sub>3</sub> and Ce/ $\gamma$ -Al<sub>2</sub>O<sub>3</sub>. The Cu/ $\gamma$ -Al<sub>2</sub>O<sub>3</sub> showed

**Table 1.** Bicyclic lactone (2) conversion in the presence of Lewis acid and Brønsted acid catalysts

Entry	Catalyst	(1) Conv. [mol%]	(2) Yield [mol%]	(3) Yield [mol%]	(4) Yield [mol%]	(5) Yield [mol%]	(6) Yield [mol%]	By- products [mol%]
Control	-	8.88	3.26	1.14	-	-	-	4.44
1	Davisil (150 Å)	16.03	15.13	1.82	-	-	-	-
2	ZSM-5 (CBV5524G)	12.31	8.11	2.56	-	-	-	1.46
3	Y-Zeolite (CBV720)	100	53.06	1.54	-	35.20	13.27	-
4	$\gamma$ -Al <sub>2</sub> O <sub>3</sub>	53.06	43.29	4.2	-	-	-	5.57
5	Amberlyst 45	50.51	13.27	1.78	11.74	13.27	-	10.45
6	Amberlyst 45 <sup>a</sup>	90.05	13.68	1.86	31.7	38.53	3.11	1.17

Conditions: Reaction time 2 h, reaction temperature 120 °C, stirring rate 500 rpm, starting concentration (volume) 71.38  $\mu$ mol/ml (4 ml), solvent 1,4-dioxane, 25 mg catalyst. <sup>a</sup> 50 mg catalyst+40  $\mu$ L D<sub>2</sub>O.

a slight improvement in the decarboxylation activity with a 58 mol% yield at 59 mol% conversion (Table 1, Entry 2). Zn, Fe, and Ce on  $\gamma$ -Al<sub>2</sub>O<sub>3</sub> showed either similar or lower decarboxylation activity (Table 1, Entry 3-5). Cu, Zn, and Ce were chosen due to their known Lewis acid activities.<sup>29-31</sup> A more comprehensive correlation between Lewis acidity of the synthesized catalysts and the decarboxylation activity will be subject of future experimental investigation.

Through this approach, we showed that  $\gamma$ -Al<sub>2</sub>O<sub>3</sub> is an excellent decarboxylation catalyst for bicyclic lactones to access novel diene species (e.g. (2)) in high selectivity at significantly reduced temperatures. Given that some bi-cyclic lactones and diene species are susceptible to degradation and in situ aromatization at elevated temperatures,  $\gamma$ -Al<sub>2</sub>O<sub>3</sub> can be generally applied to overcome this challenge.

#### 4.4.2 Reaction Kinetics of the $\gamma$ -Al<sub>2</sub>O<sub>3</sub> Catalyzed Decarboxylation

To gain a more detailed understanding of the role of the  $\gamma$ -Al<sub>2</sub>O<sub>3</sub> in catalyzing decarboxylation, an in-depth kinetic investigation of the conversion of (1) to (2) over  $\gamma$ -Al<sub>2</sub>O<sub>3</sub> was performed using temperatures between 130-160 °C in 1,4-dioxane. The Weisz-Prater number was calculated to be < 1 for the reaction conditions used which verified the absence of mass transfer limitations (see Supporting Information).

Assuming a first-order reaction with respect to (1), we obtained linear trends of  $\ln([1]_0/[1]_t)$  with respect to time (Figure S1) from which the rate constants (Table S1) were calculated to generate the Arrhenius plot shown in Figure S1. The resulting activation barrier was found to be 108 kJ/mol, which is significantly lower than non-catalyzed decarboxylation (142 kJ/mol<sup>28</sup>) and provides evidence that  $\gamma$ -Al<sub>2</sub>O<sub>3</sub> strongly impacts the decarboxylation step.

### 4.4.3 Computational Analysis of the $\gamma$ -Al<sub>2</sub>O<sub>3</sub> Catalyzed Decarboxylation

DFT calculations and microkinetic analyses were carried out to gain further insights into the nature of the active sites on  $\gamma$ -Al<sub>2</sub>O<sub>3</sub> and the surface-catalyzed decarboxylation mechanism. As discussed below, HR-MAS NMR spectroscopy provides experimental evidence of a strongly adsorbed bicyclic lactone species (1) on the  $\gamma$ -Al<sub>2</sub>O<sub>3</sub> surface as well as high surface hydroxylation. This information was used to guide DFT computations.

Different surfaces such as 110, 100 and 111 faces can exist on  $\gamma$ -Al<sub>2</sub>O<sub>3</sub> particles under reaction conditions. The 111 surface typically exposes only oxygen atoms and is extremely difficult to dehydrate under realistic conditions, while the other surfaces tend to exist with an appropriate OH coverage and exposed Al sites that can be catalytically active.<sup>33</sup> Therefore, in the present work, we explored different Al sites on the 110 and 100 surfaces with different levels of hydroxylation

The fully dehydrated 110 surface exposes Al<sub>III</sub> and Al<sub>IV</sub> sites while the dehydrated 100 surface exposes different types of Al<sub>V</sub> sites.<sup>34</sup> However, all of these sites are typically covered by OH groups, leading to stabilization of these terminations. OH groups preferentially occupy the sites with high Lewis acidity (Al<sub>III</sub> > Al<sub>IV</sub> > Al<sub>V</sub>). On the 110 surface, the Al<sub>III</sub> sites are converted to tetragonal Al<sub>IV</sub> sites and are potentially blocked by OH groups. Alternatively, the Al<sub>IV</sub> sites are converted to Al<sub>V</sub> sites that are still catalytically active. However, Al<sub>V</sub> sites can further be hydroxylated to Al<sub>VI</sub> sites, rendering them fully saturated and possibly catalytically inactive. This is predicted to occur at the Al<sub>V</sub> sites on the 100 surface, generating saturated Al<sub>VI</sub> sites. Results by Digne *et al.* suggest that under reacting temperatures (120 °C – 150 °C), the OH coverage can be as high as 15 OH/nm<sup>2</sup> and 13 OH/nm<sup>2</sup> on the 110 and 100 surfaces respectively, which can expose both catalytically active Al<sub>V</sub> sites and catalytically inactive tetrahedral Al<sub>IV</sub> and octahedral Al<sub>VI</sub>

sites.<sup>34</sup> At OH cover-age of 15 OH/nm<sup>2</sup>, all Al sites on the 110 surface are covered by hydroxyls and water molecules. We find that the coverage of H<sub>2</sub>O\* is 40% and that of OH\* is 60%. On the other hand, on the 100 surface, the OH coverage of 13 OH/nm<sup>2</sup> results in an OH\* coverage of 25%, H<sub>2</sub>O\* coverage of 50% and empty Al site (\*) coverage of 25%. Given that the  $\gamma$ -Al<sub>2</sub>O<sub>3</sub> catalyst was not heat treated (dehydroxylated) prior to the decarboxylation experiments and that the solvent used in our experiments contained residual water (0.028 mol%), the Al<sub>2</sub>O<sub>3</sub> surface was likely highly hydroxylated. Therefore, in order to determine appropriate hydroxyl surface coverage and to assess its impact on the adsorption behavior of species (1), we first calculated the Gibbs free energy of adsorption of water and (1) on the various sites on surfaces with different levels of OH coverage. An ab-initio thermodynamic analysis was then performed to predict the OH coverage of the most abundant surface under these conditions. Further, detailed energetics were calculated to deduce activation barriers of the surface catalyzed decarboxylation which were then compared to results obtained from microkinetic modeling.

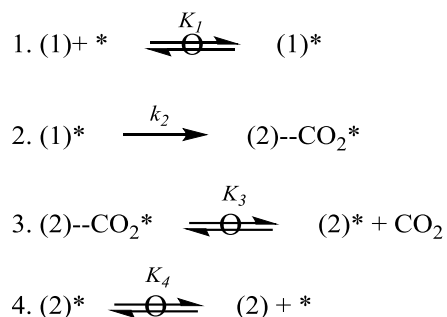
#### 4.4.4 Adsorption of Water and (1) on Different $\gamma$ -Al<sub>2</sub>O<sub>3</sub> Surfaces

The standard gas phase Gibbs free energy of adsorption for the bicyclic lactone (1) and water were carried out at 140 °C for the 110 and 100 Al<sub>2</sub>O<sub>3</sub> surfaces at different surface coverages of Al(\*), H<sub>2</sub>O\* and OH\*. The results are reported in Tables S2 and S4 and the relevant structures are given in Figure S2. The adsorption of (1) was found to be more favorable than water on the 110 surfaces with high OH coverages (Table S2, entries 2 and 3). This is likely the result of the relatively weak molecular adsorption of water at high OH coverages and the strong adsorption of (1) on Lewis acidic surface Al-sites promoted by hydrogen bonding interactions between (1) and surface OH groups. The high coverage of the strongly bound bicyclic lactone species (1) on the hydroxylated Al<sub>2</sub>O<sub>3</sub> surface was confirmed via HR-MAS NMR (vide infra). At lower OH

coverages (Table S2, Entry 4), water was found to adsorb dissociatively, making water adsorption very strong and more favorable than the adsorption of (1). On the 100 surface, the limited hydrogen bonding interactions between surface OH groups and (1) result in slightly less favorable adsorption of (1) compared to water at different surface coverages examined in this work (Table S4). Therefore, on the 110 surface, we find that the most energetically favorable configuration has an OH\* coverage of 60%, H<sub>2</sub>O\* coverage of 20% and (1\*) coverage of 20% (Table S3, Entry 3), while on the 100 surface, the most energetically favorable surface has an OH\* coverage of 25%, H<sub>2</sub>O\* coverage of 50% and Al(\*) coverage of 25% (Table S5, Entry 1). Now, assuming adsorption and desorption of (1) and water is quasi-equilibrated and that different configurations in Tables S3 and S4 are also in equilibrium with each other, we can calculate the most favorable surface configuration under reaction conditions wherein we have 0.028% water and the balance of (1) (Table S3-S5 with calculations in Supporting Information). We predict that the most abundant 110 configuration has a 60%, H<sub>2</sub>O\* coverage of 20% and (1\*) coverage of 20% (relative abundance of this configuration = 1). The most abundant 100 configuration was found to have an OH\* coverage of 25%, H<sub>2</sub>O\* coverage of 50% and Al(\*) coverage of 25%. Such high abundance (94%) of a slightly energetically unfavorable configuration was likely due to the very high concentration of (1) compared to water. The active sites on both of these surfaces are penta-coordinate as discussed previously.

#### **4.4.5 Decarboxylation of the Bicyclic Lactone (1) on $\gamma$ -Al<sub>2</sub>O<sub>3</sub>: Mechanism and Microkinetic Modeling**

The decarboxylation of (1) on the 110 and 100 surfaces obtained from thermodynamic analysis was examined by carrying out DFT calculations. Figure 1 shows the Gibbs free energy change for the proposed mechanism (Scheme 3) with relevant structures on both surfaces. All of



**Scheme 3.** Proposed mechanism for the decarboxylation of (1)

---

the reported energies are reference to an empty active site (\*) and (1) in the gas phase. After adsorption, (1\*) undergoes decarboxylation, forming the product diene (2), which is weakly physisorbed to the bound CO<sub>2</sub> ((2)—CO<sub>2</sub>\*). The surface bound CO<sub>2</sub>\* then desorbs, allowing (2) to adsorb on the surface. The bound surface species (2\*) then desorbs regenerating the active site and completing the catalytic cycle

The free energy diagram reported in Figure 1A indicate that it is much more favorable for the products that form as result of decarboxylation to desorb from surface than to react back and form (1), as the barrier for the microscopic reverse of decarboxylation is significantly higher than the energy for desorption. Therefore, the products preferentially desorb, making the decarboxylation of (1) irreversible and very likely the kinetically relevant step.

Assuming that the decarboxylation of (1\*) is rate determining step and all others are quasi-equilibrated, we can derive Equation 3 (see Supporting Information):

$$r = \frac{K_1 k_2 [(1)]}{1 + K_1 [(1)] + \frac{[(2)][\text{CO}_2]}{K_4 K_3} + \frac{[(2)]}{K_4}} \quad (3)$$

where  $k_2$ ,  $K_1$ ,  $K_3$  and  $K_4$  refer to the intrinsic rate constant for decarboxylation, the adsorption equilibrium constant for (1\*), the equilibrium between the weakly physisorbed product diene (2\*)



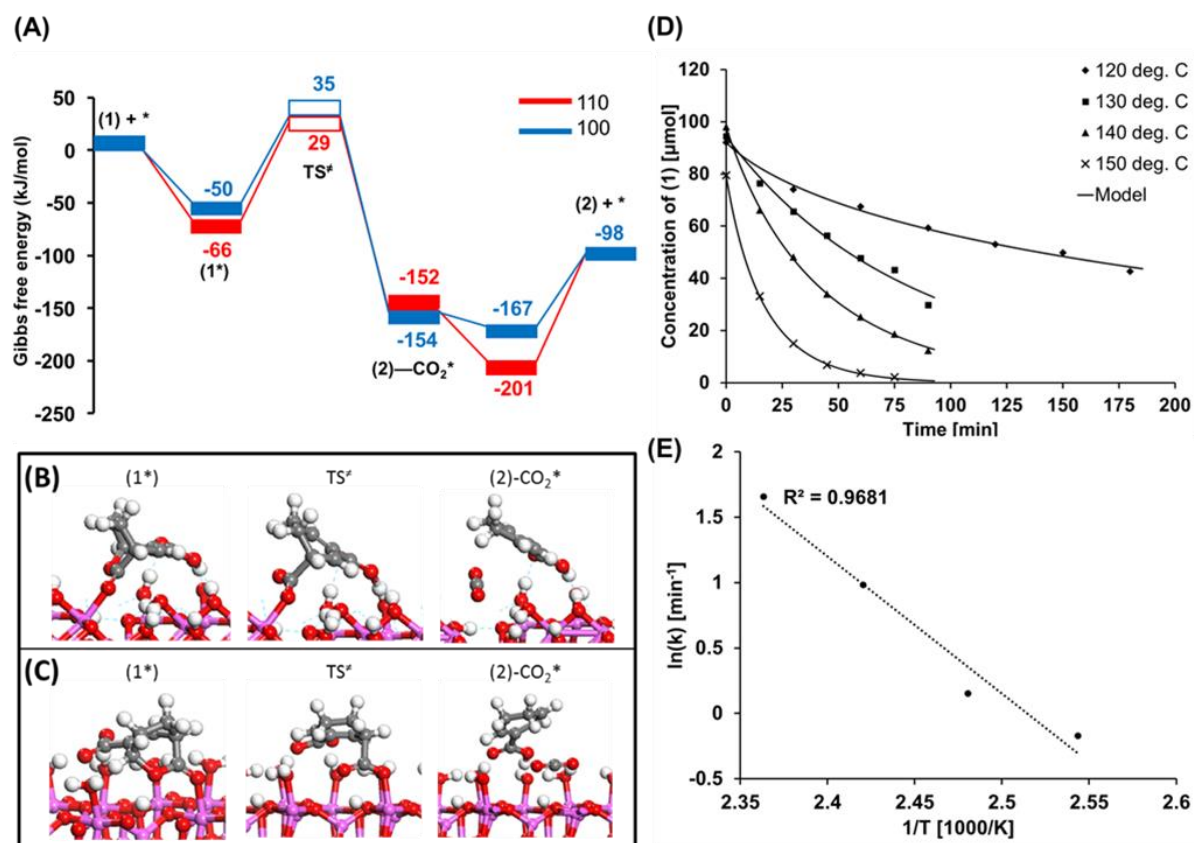


**Figure 1** A) The individual Gibbs free energy changes for the elementary steps in the mechanism proposed in Scheme 3 (filled rectangles represent stationary states and unfilled rectangles represent transition states). (B) Decarboxylation reactant (1\*), transition (≠) and product ((2)-CO<sub>2</sub>\*) states 110 surface. (C) Decarboxylation reactant (1\*), transition (≠) and product states ((2)-CO<sub>2</sub>\*) on \* on the 100 surface. (D) Concentration of (1) as a function of time: experiments vs the micro-kinetic model. (E) ln(k) vs time, where k is the intrinsic rate constant, k<sub>2</sub>, associated with the scission of the C-C bond and elimination of CO<sub>2</sub>

and CO<sub>2</sub> and the equilibrium desorption constant for (2\*).

Based on the free energy diagram (Figure 1), high surface coverages of (1\*) and (2\*) are expected due to the high Gibbs free energies of adsorption. Therefore, Equation 3 can be simplified as follows:

$$r = \frac{A[(1)]}{1 + B[(1)] + C[(2)]} \quad (4)$$

where,  $A = K_1 k_2$ ,  $B = K_1$  and  $C = K_4^{-1}$ . This rate expression was used to model the concentration profiles at different temperatures and resulted in a nearly perfect fit as shown in Figure 1D. The values of parameters A, B and C are reported in the Table S6

The initial activation barrier was calculated by assuming a high concentration of (1). As such the observed rate constant,  $k_2 K_1 [(1)] / K_1 [A(1)]$ , is equivalent to the intrinsic rate constant for decarboxylation,  $k_2$ . An Arrhenius plot (Figure 1E) yields an initial activation barrier of 87 kJ/mol, which is in good agreement with the activation barrier determined from experimental data (108 kJ/mol, see Table S1). On the free energy diagram, this barrier corresponds to the intrinsic barrier for the decarboxylation of (1\*).

However, since only temperature was varied, this barrier needs to be compared with the enthalpy of activation. The enthalpic barriers for (1\*) decarboxylation were calculated to be 96 kJ/mol and 85 kJ/mol on the 110 and 100 surfaces respectively, which are in good agreement with the initial barrier resulting from microkinetic modeling (87 kJ/mol). Therefore, decarboxylation of (1) can be catalyzed via the retro Diels-Alder mechanism on Al<sub>v</sub> sites on both 110 and 100 surfaces with the reaction being limited by the decarboxylation of surface bound (1\*).

The experimental and theoretical results presented here on the thermal and Lewis acid catalyzed decarboxylation of 2 are very similar to those reported for the ring opening of triacetic acid lactone (TAL)<sup>35</sup> and  $\gamma$ -valerolactone (GVL)<sup>36</sup> that readily undergo acid catalyzed decarboxylation as a result of the unsaturated bond at the C3-C4 position similar to the unsaturated C3=C4 bond in 2 which facilitates a direct retro Diels-Alder elimination of the CO<sub>2</sub> dienophile.

#### 4.4.6 Characterization of Bicyclic Lactone (1) Immobilized on $\gamma$ -Al<sub>2</sub>O<sub>3</sub> by HR-MAS NMR

To probe for interactions between the bicyclic lactone with the  $\gamma$ -Al<sub>2</sub>O<sub>3</sub> surface in the condensed phase, <sup>1</sup>H, <sup>13</sup>C and <sup>27</sup>Al HR-MAS NMR spectroscopy of  $\gamma$ -Al<sub>2</sub>O<sub>3</sub> impregnated with a thin film (2 nm) of a solution of (1) in 1,4-dioxane-*d*<sub>8</sub> was performed. This new and unique NMR technique<sup>37</sup> allows the study of the interactions of probe molecules on solid catalyst surfaces (i.e. (1) on alumina) at the liquid-surface interface which provides additional information to guide DFT computations. As described below, the NMR experiments provide direct evidence that the surface is highly hydroxylated and that (1) is strongly adsorbed on the surface of  $\gamma$ -Al<sub>2</sub>O<sub>3</sub>.

Samples were prepared by first drying  $\gamma$ -Al<sub>2</sub>O<sub>3</sub> at 120 °C to remove excess water. The dry  $\gamma$ -Al<sub>2</sub>O<sub>3</sub> was then impregnated in a glovebox with liquid loadings of 1  $\mu$ L of solution per mg of  $\gamma$ -Al<sub>2</sub>O<sub>3</sub> and the concentrations of (1) were 200 or 132 mg/mL in dioxane-*d*<sub>8</sub>. A control sample impregnated with pure dioxane-*d*<sub>8</sub> was also prepared. All samples were packed into 2.5 mm zirconia rotors under the inert atmosphere. The results of the HR-MAS NMR spectroscopy experiments on the various impregnated alumina samples are summarized in Figure 2.

Rotor-synchronized <sup>1</sup>H spin echo solid-state NMR spectra of the different impregnated alumina samples are shown in Figure 2A-C. The <sup>1</sup>H solid-state NMR spectrum of the alumina impregnated with dioxane-*d*<sub>8</sub> shows a broad underlying signal that covers a shift range of ca. 0 ppm to 10 ppm and three sharp <sup>1</sup>H NMR signals (Figure 2C). The sharp signals are attributed to the residual protons of dioxane-*d*<sub>8</sub> ( $\delta$  = 3.6 ppm) and to mobile or dissolved water molecules and/or isolated/mobile alumina hydroxyl groups ( $\delta$  = 1.3 ppm and 0.9 ppm). Proton detected 2D <sup>27</sup>Al-<sup>1</sup>H D-RINEPT HETCOR spectra confirm that the broad NMR signal arises from the hydroxyl groups and/or water molecules that are immobilized on the surface of the alumina (see below).

The  $^1\text{H}$  NMR spectrum of alumina impregnated with the 200 mg/mL solution of (1) in dioxane- $d_8$  shows several additional sharp  $^1\text{H}$  NMR signals at the expected  $^1\text{H}$  chemical shifts for (1) (Figure 2A). These narrow signals are attributed to (1) which is either dissolved in the dioxane- $d_8$  or is very weakly bound to the alumina surface and remains highly mobile. The narrow  $^1\text{H}$  NMR signals arising from (1) are absent from the  $^1\text{H}$  NMR spectrum of alumina impregnated with the solution of (1) at 132 mg/mL in dioxane- $d_8$ . Comparison of the  $^1\text{H}$  NMR spectra of the alumina impregnated with the 132 mg/mL solution to the  $^1\text{H}$  NMR spectrum of alumina impregnated with dioxane- $d_8$  alone shows that there are additional signals at higher chemical shifts of ca. 7.4 ppm and 5.6 ppm. The additional signals at higher chemical shifts and the absence of sharp  $^1\text{H}$  NMR signals suggests that in the sample impregnated with the 132 mg/mL solution, all of the molecules of (1) are immobilized on the alumina surface.

To confirm that (1) was immobilized on alumina, proton detected  $^1\text{H}\{^{13}\text{C}\}$  cross-polarization CP-HETCOR spectra were obtained. In this case, proton detection was employed to boost sensitivity and obtain the  $^{13}\text{C}$  solid-state NMR spectra in a reasonable experimental time (less than 16 hours).<sup>38,39</sup> A 2D  $^1\text{H}\{^{13}\text{C}\}$  CP-HETCOR spectrum of alumina impregnated with a 200 mg/mL solution is shown in Figure 2F. The  $^{13}\text{C}$  dimension shows NMR signals at all of the chemical shifts expected for (1) and the  $^1\text{H}$  dimension shows broad signals between 8 ppm and 3 ppm, consistent with the expected  $^1\text{H}$  chemical shifts of (1). A CP experiment acts as a mobility filter since an NMR signal is only observable if the molecules are rigid. Additionally, broad  $^1\text{H}$  NMR signals observed in the CP-HETCOR spectrum imply that the molecules of (1) are immobilized. Therefore, the 2D  $^1\text{H}\{^{13}\text{C}\}$  CP-HETCOR spectrum confirms that a large fraction of (1) is bound to the alumina surface, which is consistent with the DFT results. Additional 2D  $^1\text{H}\{^{13}\text{C}\}$  CP-HETCOR spectra are shown in Figure S3.

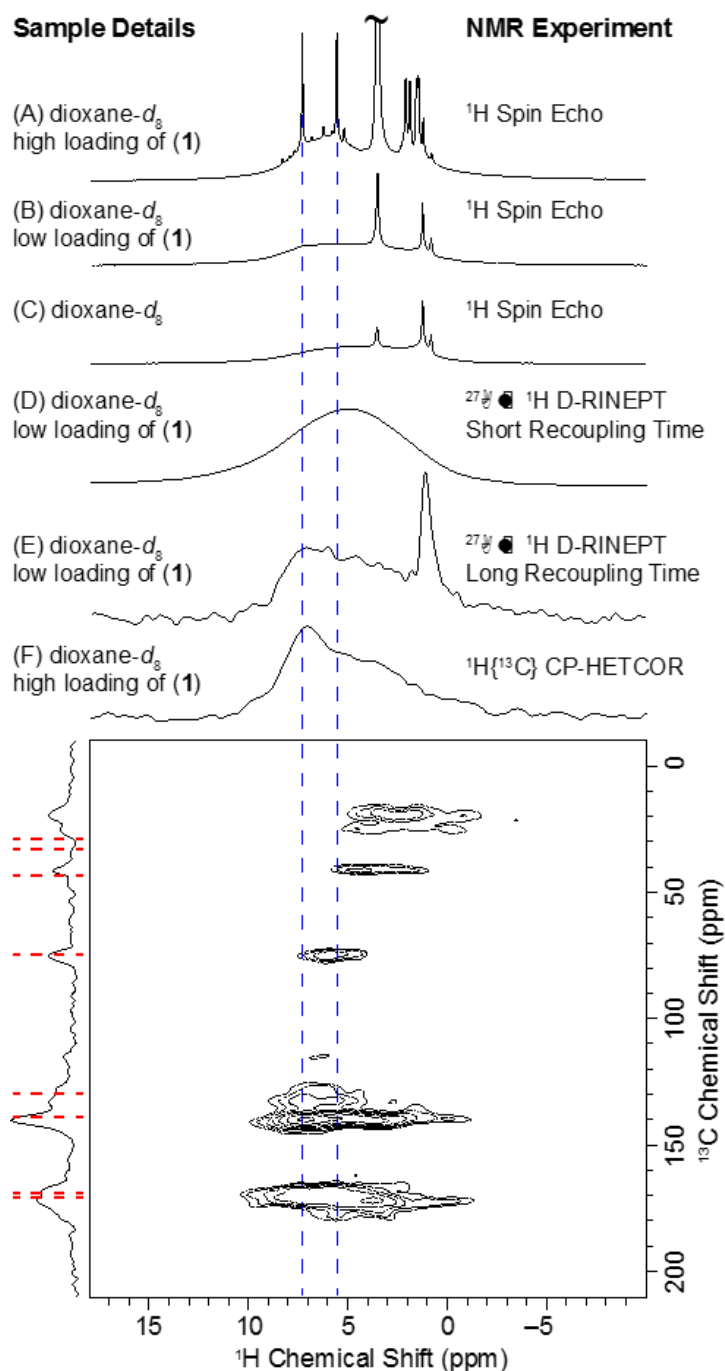


**Figure 2.** MAS  $^1\text{H}$  solid-state NMR spectra of  $\gamma\text{-Al}_2\text{O}_3$  impregnated with dioxane- $d_8$  solutions with different concentrations of (1). The sample is indicated next to each spectrum. (A-C)  $^1\text{H}$  spin echo solid-state NMR spectra. (D) and (E)  $^{27}\text{Al}$  filtered  $^1\text{H}$  NMR spectra obtained from the positive projection of 2D  $^{27}\text{Al}\rightarrow^1\text{H}$  D-RINEPT HETCOR spectra obtained with short and long dipolar recoupling times, respectively. (F)  $^{13}\text{C}$  filtered  $^1\text{H}$  NMR spectrum obtained from the positive projection of the 2D  $^1\text{H}\{^{13}\text{C}\}$  HETCOR spectrum shown below. The  $^{13}\text{C}$  chemical shifts expected for (1) are indicated with red dashed lines. All experiments were performed with a 25 kHz MAS frequency.

Finally, proton detected 2D  $^{27}\text{Al} \rightarrow ^1\text{H}$  D-RINEPT HETCOR experiments<sup>40,41</sup> were used to obtain surface selective  $^{27}\text{Al}$  solid-state NMR spectra (Figure S4). The  $^1\text{H}$  NMR spectra obtained from 2D  $^{27}\text{Al} \rightarrow ^1\text{H}$  D-RINEPT experiments acquired with long and short dipolar recoupling times are shown in Figure 2D and 2E, respectively. The  $^{27}\text{Al}$  filtered  $^1\text{H}$  NMR spectrum obtained with a short recoupling time selectively probes the  $^1\text{H}$  spins that are in close proximity to aluminum. This spectrum shows a very broad signal, which must represent the  $^1\text{H}$  nuclei of the surface hydroxyl and adsorbed water molecules, consistent with previous surface selective  $^{27}\text{Al}$  NMR experiments on hydrated alumina.<sup>42,43</sup> This information of a highly hydroxylated  $\gamma\text{-Al}_2\text{O}_3$  surface provide important insights to help guide the DFT calculations and benchmark their results. The  $^{27}\text{Al}$  filtered  $^1\text{H}$  NMR spectrum obtained with a longer recoupling time shows similar intensities and chemical shifts to those observed in the  $^{13}\text{C}$  filtered  $^1\text{H}$  NMR spectrum. Therefore, the spectrum obtained with a longer dipolar recoupling time suggests that the  $^1\text{H}$  nuclei of (1) are proximate to  $^{27}\text{Al}$  spins, consistent with adsorption of (1) to the alumina surface. At longer recoupling times, the surface bound species (1) strongly correlates to  $\text{Al}_{\text{IV}}$  and  $\text{Al}_{\text{VI}}$  sites of the alumina surface, while  $^1\text{H}$ - $^{27}\text{Al}$  correlation to  $\text{Al}_{\text{V}}$  sites is suppressed (see full 2D spectra in Figure S4). The key knowledge of a strong surface bound species (1) existing is important to further support the DFT results. Additional solid-state NMR experiments are summarized in the Supporting Information.

In summary, HR-MAS and solid-state NMR spectroscopy is an excellent technique to investigate the  $\gamma\text{-Al}_2\text{O}_3$  catalyst surface in the presence of probe molecules (e.g. bicyclic lactone (1)) and small amounts of water in the condensed phase (e.g. 1,4-dioxane-*d*<sub>8</sub>). This unique technique provides key information about the degree of surface hydroxylation, the molecule-surface interaction and information about the catalytically active Al-species on the alumina surface. The results provide

additional means to guide and compare computational studies with high level experimental detail of reactant/product molecules behavior at the solvent-catalyst interface.

#### 4.4.7 The Impact of Brønsted Acids on Conversion

The impact of Brønsted acidity on the bicyclic lactone (1) was examined through reactions using a variety of Brønsted acid-containing catalytic materials. The use of Davisil silica gel (150 Å), a weakly acidic material<sup>44</sup>, at 120 °C for 2 h, gave 16 mol% conversion of (1) to (2) (Table 2, Entry 1) which was roughly a twofold increase in conversion compared to the control experiment without catalyst (Table 1, Control). The use of the more acidic ZSM-5 zeolite with a Si:Al ratio of 50:1 gave similar results with only minimal decarboxylation activity (Table 2, Entry 2). In fact, increasing the acid strength of ZSM-5 (Si:Al, 23:1) showed no improvement in the decarboxylation yield (Table 2, Entry 3). Interestingly, the mesoporous Y-zeolite (Si:Al, 30:1), demonstrated enhanced reactivity and consumed all the bicyclic lactone (1) yielding 53 mol% DIH (2), 35 mol% isophthalic acid intermediate (5) and 13mol% isophthalic acid (6) (Table 2, Entry 4). Given this result, it appeared that the larger pores of the Y-zeolite structure provide enhanced

**Table 2.** Bicyclic lactone (1) conversion in the presence of Brønsted acids

Entry	Catalyst	(1) Conv. [mol%]	(2) Yield [mol%]	(3) Yield [mol%]	(4) Yield [mol%]	(5) Yield [mol%]	(6) Yield [mol%]	By- products [mol%]
1	Davisil (150 Å)	16	15	<2	-	-	-	-
2	ZSM-5 (CBV5524G)	12	8	<3	-	-	-	<2
3	ZSM-5 (CBV2314)	7	5	<2	-	-	-	<1
4	Y-Zeolite (CBV720)	100	53	<2	-	35	13	-
5	Amberlyst 45	51	13	<2	12	13	-	<11
6	Amberlyst 45 <sup>a</sup>	90	14	<2	32	39	<4	<2

Conditions: Reaction time 2 h, reaction temperature 120 °C, stirring rate 500 rpm, starting concentration 71.38 μmol/mL, reaction volume 4 mL, solvent 1,4-dioxane, 25 mg catalyst. <sup>a</sup> 50 mg catalyst+40 uL D<sub>2</sub>O.

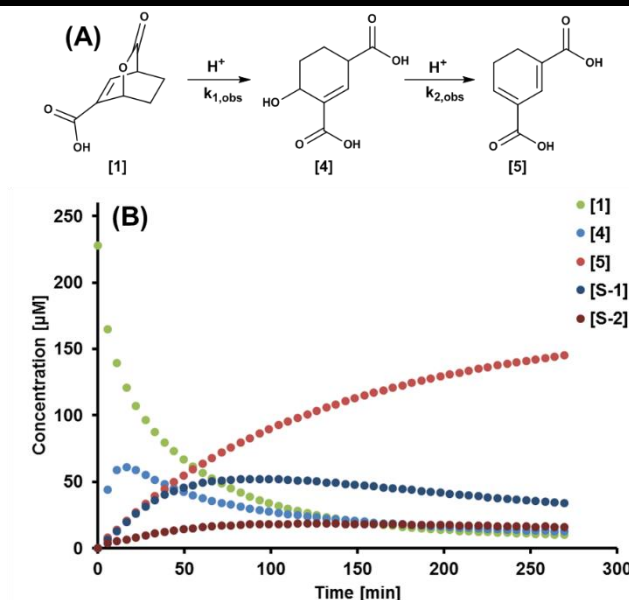


**Figure 4.** (A) Reaction scheme of the proposed acid catalyzed ring-opening/dehydration reaction sequence. (B) Concentration profile of the conversion of bicyclic lactone (1) to (4) followed by conversion of (4) to (5). (S-1) and (S-2) are formed throughout the reaction and are of unknown origin.

accessibility of the bulky lactone (1). Since Y-zeolite contains both Lewis<sup>45</sup> and Brønsted acid<sup>46</sup> sites, it was unclear as to which site was responsible for ring-opening or if a synergistic effect was operative.

To decouple the roles of Lewis and Brønsted acid sites, a series of experiments were performed using the heterogeneous Brønsted acid-only catalyst, Amberlyst 45.<sup>47</sup> The experimental results shown in Table 2, Entries 5 and 6 demonstrate that Brønsted acid sites promote ring-opening of the lactone bridge forming the intermediate 6-hydroxycyclohex-1-ene-1,3-dicarboxylic acid (4) followed by acid catalyzed dehydration to an isophthalic acid intermediate (5) (Figure 4A). Doubling the amount of catalyst and adding small amounts of water to the polar aprotic solvent 1,4-dioxane dramatically enhanced the acid catalyzed ring-opening with increased conversion and yield towards intermediate (4) and product (5) (Table 2, Entry 6). This is consistent



with results reported by Chia et al.<sup>35</sup> which show that the addition of Brønsted acids and water facilitate the ring opening, hydrolysis and dehydration of triacetic acid lactone.

A series of in situ <sup>1</sup>H solution NMR experiments were performed to gain a better understanding as to why Brønsted acid sites led to the formation of (4) and (5). In the experiments, the bicyclic lactone (1) was exposed to the fully deuterated sulfuric acid-*d*<sub>2</sub> and heat using dioxane-*d*<sub>8</sub> to mediate the reaction. These experiments serve as an ideal model to understand the reaction mechanism of the Brønsted acid catalyzed ring-opening reaction that can be potentially further applied to other bicyclic lactone systems. In this set of experiments, 5 μL (0.089 μmol) of D<sub>2</sub>SO<sub>4</sub> was added to 300 μL of a 71.38 μmol/mL solution of (1) in fully deuterated dioxane-*d*<sub>8</sub>, transferred to high pressure NMR tubes, and heated to the desired reaction temperature (80-110 °C) inside the NMR spectrometer.

The experimental results revealed that the rate of consumption of (1) did not match the rate of formation of (5) at all temperatures tested. The reason for this observation was the formation of the reactive intermediate (4) and species (S-1) and (S-2) on the pathway to (5). Species (4) is likely formed through acid-catalyzed hydrolysis of the lactone bridge of (1) (Figure 4A). The concentration profile in Figure 4B further suggests that the initial formation of (4) was then followed by acid-catalyzed dehydration of (4) to (5) as evident from the increasing concentration of (5) accompanied with a decrease in (4). Clearly, the mechanism involved in the formation of (5) from (1) is more complicated given the formation of unknowns (S-1) and (S-2).

With increased reaction temperature (4), (S-1) and (S-2) vanished while the concentration of (5) increased, so it appears that (S-1) and (S-2) are intermediates on the pathway from (1) to (5). This selectivity relationship is apparent in Figure 5 since the formation of (5) increases linearly

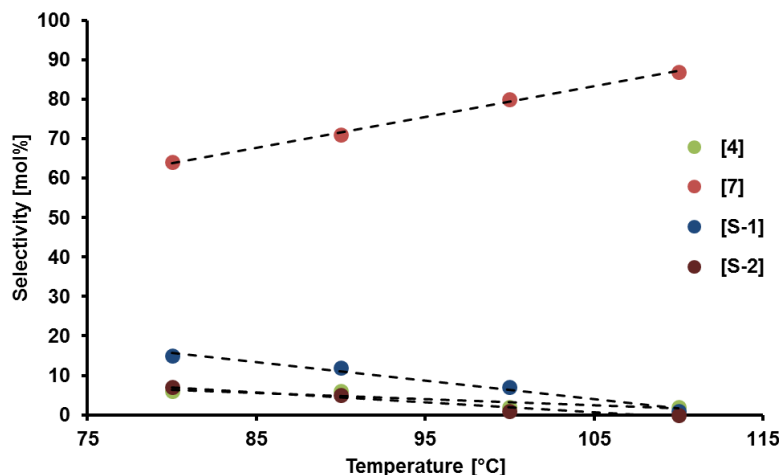


**Figure 5.** Selectivity trend of intermediates and products from acid catalyzed ring-opening/dehydration of bicyclic lactone (1).

as a function of reaction temperature, whereas a linear downward trend is seen for (4), (S-1), and (S-2). After reaction for 4 h and 35 min at 110 °C there was a significant amount of (5) (87 mol%), with only 2 mol% of intermediate (4) and less than 5 mol% of (S-1) and (S-2) remaining (Table S8). From NMR analysis of the product solution, (S-1) and (S-2) are likely isomers of (4) given the similar proton shifts and NMR correlations. It is known that lactones are able to undergo different hydrolysis pathways (e.g., unimolecular and bimolecular) in acidic media,<sup>48</sup> which could explain the observation of species (S-1) and (S-2). Structural identification of (S-1) and (S-2), however, is beyond the scope of this work and will be a subject of further investigation.

The Brønsted acid catalyzed ring-opening/dehydration sequence provides general guidance for the conversion of (1) and can potentially be applied to similar bicyclic lactone systems. In this particular case, we were able to access the isophthalic acid intermediate (5) in high selectivity, which cannot be easily obtained via conventional petroleum routes. Catalytic dehydrogenation of this molecule provides isophthalic acid, a bulk chemical currently manufactured in the petrochemical industry and used in applications ranging from unsaturated polyester and specialty

resins<sup>49</sup> to metal organic polyhedral crystals (MOPs) which are potentially useful for drug-delivery, catalysts, sensing and gas storage.<sup>50</sup>

#### 4.4.8 Solvent Impact on Conversion of (1)

Lactones such as CMA degrade in the presence of water due to nucleophilic attack and consequent ring-opening, which renders the diene ineffective for Diels-Alder chemistry.<sup>28,51</sup> This degradation was also observed by Chia et al. showing that the molecular integrity of the 2-pyrone triacetic acid lactone (TAL) was significantly compromised in the presence of water but was stable in polar aprotic solvents such as tetrahydrofuran (THF).<sup>35</sup>

To investigate whether the bicyclic lactone (1) can be ring-opened to (5) via catalyst-free, water-mediated hydrolysis of the lactone bridge, experiments were performed in D<sub>2</sub>O. For the reactions, the sodium salt of the bicyclic intermediate (1) was heated in D<sub>2</sub>O, and the reaction progress monitored via in situ <sup>1</sup>H-NMR. The sodium salt of (1) was required to overcome solubility limitations in D<sub>2</sub>O and to improve the resolution of the <sup>1</sup>H-NMR spectra for subsequent analysis.

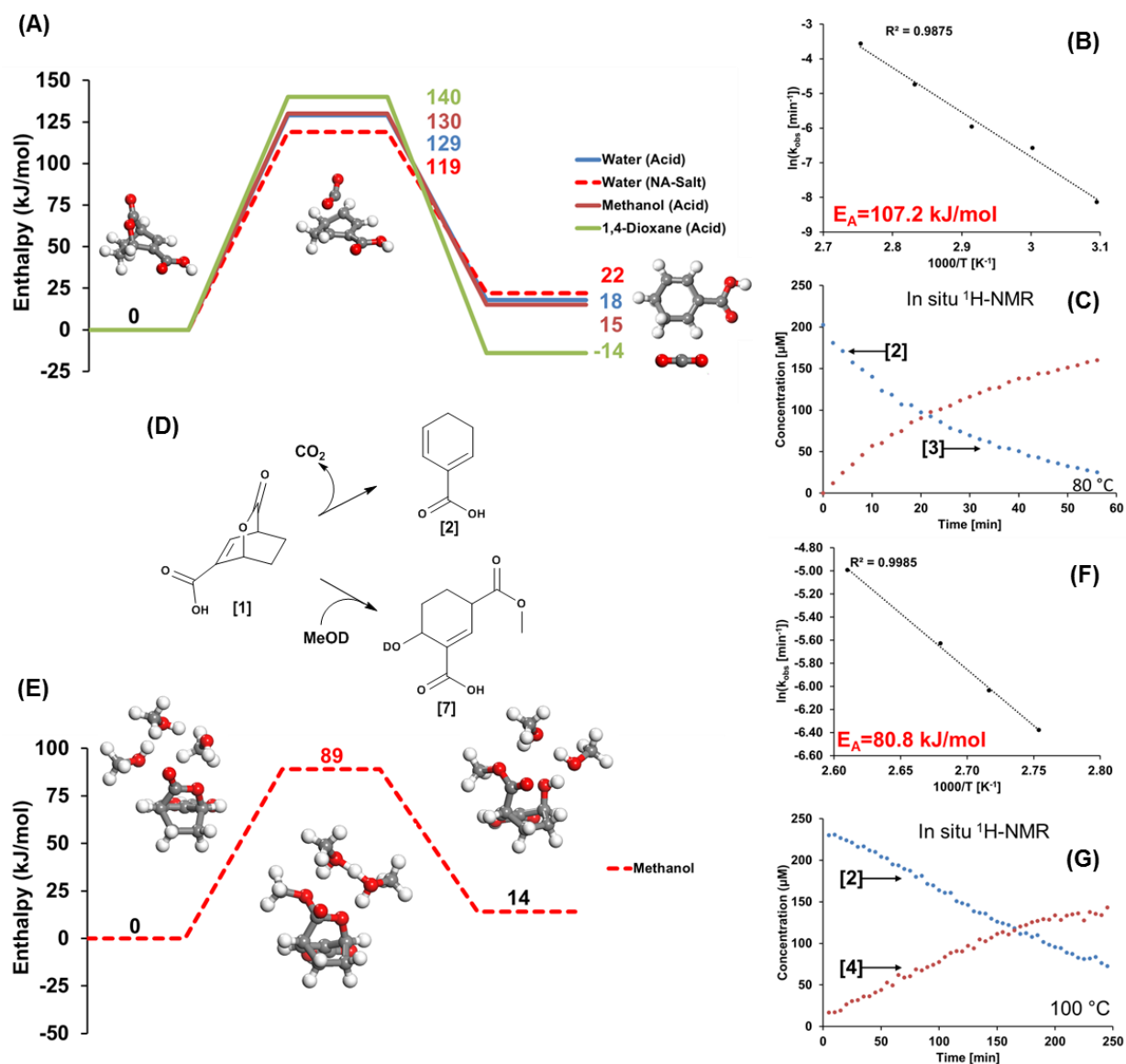
Surprisingly, when the consumption of (1) was monitored over time, decarboxylation occurred rather than ring-opening. Additional kinetic experiments were carried out at temperatures in the range of 50 to 90 °C along with DFT calculations to obtain further insights into the water-mediated decarboxylation mechanism.

Figure 6C shows an example of the concentration profiles for the water-mediated decarboxylation of (1) to (2). Plots of  $\ln([1]_0/[1]_t)$  over time for all temperatures tested displayed linear relationships, (Figures S8) indicating a first order reaction with respect to (1). Since (2) was obtained in high yield and selectivity with no formation of CMA, the retro Diels-Alder reaction of

(1) to CMA was absent, meaning the observed decarboxylation rate constants  $k_{\text{obs}}$  (Table S10) are solely for the conversion of (1) to (2). The activation energy of the water-mediated decarboxylation was calculated using the Arrhenius plot shown in Figure 6B. The experimentally obtained activation barrier was 107.2 kJ/mol. This value is significantly lower than for decarboxylation in the polar aprotic solvent dioxane- $d_8$  (142 kJ/mol),<sup>28</sup> which explains the enhanced decarboxylation activity at moderate temperatures.

DFT predicts an enthalpic decarboxylation barrier of the bicyclic lactone (1) sodium salt of 119 kJ/mol in close agreement with experimental results. Additionally, the Gibbs free energy barrier for decarboxylation was calculated to be 116 kJ/mol, which is favored over the water mediated ring-opening of the lactone bridge which has a barrier of 121 kJ/mol. Moreover, the decarboxylation product was found to be thermodynamically favored over the ring-opened product because the system gains entropy through the loss of  $\text{CO}_2$  in the former case. This makes decarboxylation both thermodynamically and kinetically favored over ring-opening in water, which explains the experimental results in water (see Figure S10 for the Gibbs free energy profiles). The strong hydrogen bonding with water molecules in the bulk makes water a weak nucleophile, limiting the addition of water to the lactone which prevents ring opening. Although the acid form of (1) resulted in a slightly higher calculated enthalpic activation barrier of 130 kJ/mol, the decarboxylation of (1) to (2) remains favored in water as compared to the polar aprotic solvent 1,4-dioxane in the absence of catalyst (Figure 6A). This rate enhancement in water is due to stabilization of the charge separated transition state on the pathway from (1) to (2), which is preferentially stabilized by polar protic solvents such as water.

Anticipating broad applicability of polar protic solvents to enhance bicyclic lactone decarboxylation, we also performed reactions of (1) in methanol. Methanol is an ideal model



**Figure 6.** (A) DFT calculated enthalpy diagram for the bicyclic lactone decarboxylation reaction using polar protic and aprotic solvents. (B) Experimental Arrhenius plot for the water mediated catalyst-free decarboxylation of the bicyclic lactone sodium salt (1). (C) In situ  $^1\text{H-NMR}$  concentration profile of the consumption of sodium salt of (1) and the formation of (2) as a function of time. (D) Bicyclic lactone diversification in the absence of catalyst using the polar protic solvents water for decarboxylation and methanol for ring-opening. (E) DFT calculated enthalpy diagram for the methanol mediated ring-opening of (1). (F) Experimental Arrhenius plot for the methanol mediated catalyst-free ring-opening of (1). (G) In situ  $^1\text{H-NMR}$  concentration profile of the consumption of (1) and the formation of (7) as a function of time.

solvent as it provides excellent solubility of (1) through which the neutralization step of (1) to the sodium salt can be prevented.

Experimental results showed that (1) in the presence of methanol afforded ring-opening of the lactone bridge to give the novel species (7) in high selectivity as confirmed by 2D NMR experiments in combination with UPLC-QDa mass analysis (see Supporting Information). Several selected  $^1\text{H-NMR}$  spectra of the in situ conversion of (1) to (7) are displayed in Figure 7. These fully resolved spectra make the identification and quantification of the reactant and product unambiguous with carbon balances  $>99\text{ mol}\%$ .

This interesting and unexpected result was further investigated through in situ NMR kinetic investigation and DFT calculations to obtain kinetic parameters and mechanistic insight as to why methanol caused (1) to enter this new pathway.

NMR kinetics were carried out within the temperature range of  $90\text{-}110\text{ }^\circ\text{C}$ . The reactions were conducted in neat methanol- $d_4$ . The consumption of (1) followed a pseudo-first order reaction. A typical concentration profile of (1) in methanol- $d_4$  is displayed in Figure 6G. Plots of  $\ln([1]_0/[1]_t)$  with respect to time show linear relation-ships for all temperatures tested (Figure S9), validating our assumption of a pseudo-first order reaction. These plots were then used to extract

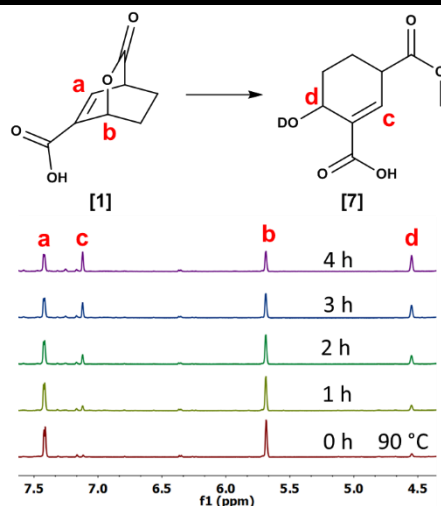


**Figure 7.** Selected  $^1\text{H-NMR}$  spectra of the bicyclic lactone (1) ring-opening in methanol- $d_4$ .

---

the observed rate constants (Table S11) and calculate the apparent activation barrier for the methanol induced ring-opening (Figure 6F).

An activation barrier of 80.8 kJ/mol was calculated using the Arrhenius plot in Figure 6F. The experimental data and structures were used to compare with DFT results for the methanolysis of the lactone bridge of (1). The DFT-calculated enthalpic activation barrier of 89 kJ/mol agrees rather well with the experimentally measured activation barrier of 80.8 kJ/mol. The barrier for the ring-opening and methanolysis of (1) is approximately 40 kJ/mol lower than that for direct decarboxylation of (1) (129 kJ/mol) which explains the preference for ring-opening and methanolysis over decarboxylation for reactions carried out in methanol (Figure 6A).

The computational results further suggest that methanol is a better nucleophile than water, likely because water forms a strong hydrogen bonding network and results in decarboxylation rather than hydrolysis of (1). Similar to water, methanol stabilizes the transition state and promotes proton shuttling, providing a low energy path from (1) to (7). This pathway grants access to the selective formation of the new novel species (7) (> 95 mol%) using low temperatures and a low boiling solvent in the absence of a catalyst, which provides an attractive and environmentally benign diversification path of the renewable coumalate platform.

#### **4.4.9 Broader Implication**

DIH (2) is a precursor of the bulk chemical benzoic acid which is currently manufactured via conventional petroleum routes based on toluene. We recently presented a new route to benzoic acid with ~90 mol% selectivity at 100 mol% CMA conversion.<sup>28</sup> The 10 mol% loss in selectivity was attributed to by-product formation from the high reaction temperature (180 °C) needed to overcome the rate limiting decarboxylation step. The catalyst used to convert (2) to (3) was a

**Table 3.** CMA conversion to benzoic acid

Entry	CMA conv. [mol%]	(1) Sel. [mol%]	(2) Sel. [mol%]	(3) Sel. [mol%]
1 <sup>a</sup>	89.6	-	-	99.7 <sup>d</sup>
2 <sup>b</sup>	100	53.9 <sup>c</sup>	-	46.1 <sup>d</sup>

Conditions: CMA 300 mg, 1,4-dioxane 30 mL, temperature 140 °C, time 4 h, catalyst <sup>a</sup>200 mg 1wt% Pd/ $\gamma$ -Al<sub>2</sub>O<sub>3</sub>, <sup>b</sup>20 mg 10wt% Pd/C. <sup>c</sup>No other by-products detected via UPLC-QDa (ESI). <sup>d</sup>Quantified via UPLC-QDa (ESI).

commercial 10 wt% Pd/C catalyst. With the goal of further increasing the selectivity and improving the overall process, we utilized a bifunctional 1 wt% Pd/ $\gamma$ -Al<sub>2</sub>O<sub>3</sub> catalyst to perform the reaction of CMA and ethylene to benzoic acid (BA) at milder re-action conditions. This lower temperature was possible because of the increased decarboxylation activity of bicyclic lactones in the presence of  $\gamma$ -Al<sub>2</sub>O<sub>3</sub>.

Experimental results are provided in Table 3, with Entry 1 showing that the benzoic acid selectivity was further increased to > 99 mol% at reduced temperatures (140 °C) with a reaction time of 4 h. The base Pd/C catalyst, on the contrary, only gave a selectivity of 46.1 mol% towards (3) at 100 mol% conversion (Table 3, Entry 2). The remaining 53.9 mol% were attributed to (1) as no other by-products were detected via UPLC-QDa analysis. Given the high selectivity of BA, this concept might be broadly applicable when aromatics from 2-pyrone in conjunction with an array of dienophiles are envisioned.

#### 4.5 Conclusion

The combination of experimental kinetic analyses, DFT calculations and MAS solid-state NMR provided mechanistic insights into the decarboxylation of the 2-pyrone derived bicyclic molecule (1). Lewis acid sites on the  $\gamma$ -Al<sub>2</sub>O<sub>3</sub> act as catalytically active sites that significantly lower the decarboxylation activation barrier, providing access to DIH (2) in high selectivity. The



strong adsorption of the bicyclic lactone species on the surface provides a driving force for its catalytic decarboxylation. The immobilization of (1) was predicted with DFT computations and experimentally confirmed with MAS solid-state NMR experiments.

The in-depth catalytic investigation presented here provides guidance to tailor a bifunctional 1 wt% Pd/ $\gamma$ -Al<sub>2</sub>O<sub>3</sub> catalyst that enables access to the aromatic drop-in replacement benzoic acid (BA) with significantly improved selectivity starting from the 2-pyrone coumalic acid reaction with ethylene. Given previous literature reports of aromatics synthesized from 2-pyrones in an analogous fashion, we believe that this catalyst can be broadly applied to these systems allowing the production of aromatics at optimized reaction conditions.

We further investigated the impact of Brønsted acid catalysts on the conversion of (1) and showed through kinetic studies that a ring-opening/dehydrogenation sequence yielded a novel isophthalic acid precursor (5) in high selectivity. Since isophthalic acid is a bulk chemical in the chemical industry, this route provides a renewable alternative.

Finally, the impact of polar protic solvents on the conversion of (1) was explored, through which highly selective, catalyst free pathways of (1) to novel species (2) and (5) were identified. The decarboxylation of the sodium salt of species (1) was mediated in the polar protic solvent, revealing a significantly reduced decarboxylation barrier compared to that of 1,4-dioxane. The nucleophilic solvent methanol induced ring-opening of the lactone bridge through methanolysis providing an additional diversification path of (1) to a new novel species (7) in high selectivity.

The results presented herein outline a diversification platform starting from renewable coumalic acid in conjunction with a single dienophile (ethylene) that allows highly selective access to a variety of novel molecules with unique functionality which are of potential interest for new materials. As such, this technological approach can be leveraged to other bicyclic lactones to

form a plethora of new and interesting molecules that cannot be easily accessed via conventional petroleum-based routes.

#### 4.6 Acknowledgement

We gratefully acknowledge funding from the National Science Foundation under Award EEC-0813570, the Iowa State University Chemical Instrument Facility staff members, computational support from the Minnesota Supercomputing Institute (MSI) at the University of Minnesota and the Molecular Science Computing Facility (MSCF) in the William R. Wiley Environmental Molecular Sciences Laboratory, a national scientific user facility sponsored by the U.S. Department of Energy, Office of Biological and Environmental Research at the Pacific Northwest National Laboratory. Furthermore, we would like to acknowledge all co-workers at CBiRC for their support.

#### 4.7 References

- 1 Shanks, B. H.; Keeling, P. L. *Green Chem.* 2017, **19**, 3177-3185.
- 2 Kraus, G. A.; Riley, S.; Cordes, T. *Green Chem.* 2011, **13**, 2734-2736.
- 3 Kraus, G. A.; Pollock Iii, G. R.; Beck, C. L.; Palmer, K.; Winter, A. H. *RSC Adv.* 2013, **3**, 12721-12725.
- 4 Lee, J. J.; Kraus, G. A. *Tetrahedron Lett.* 2013, **54**, 2366-2368.
- 5 Lee, J. J.; Kraus, G. A. *Green Chem.* 2014, **16**, 2111-2116.
- 6 Lee, J. J.; Pollock Iii, G. R.; Mitchell, D.; Kasuga, L.; Kraus, G. A. *RSC Adv.* 2014, **4**, 45657-45664.
- 7 Zelle, R. M.; de Hulster, E.; van Winden, W. A.; de Waard, P.; Dijkema, C.; Winkler, A. A.; Geertman, J. M.; van Dijken, J. P.; Pronk, J. T.; van Maris, A. J. *Appl. Environ. Microbiol.* 2008, **74**, 2766-77.
- 8 Zhang, X.; Wang, X.; Shanmugam, K. T.; Ingram, L. O. *Appl. Environ. Microbiol.* 2011, **77**, 427-434.

- 9 Brown, S. H.; Bashkirova, L.; Berka, R.; Chandler, T.; Doty, T.; McCall, K.; McCulloch, M.; McFarland, S.; Thompson, S.; Yaver, D. *Appl. Microbiol. Biotechnol.* 2013, **97**, 8903-8912.
- 10 Werpy, T.; Petersen, G.; Aden, A.; Bozell, J.; Holladay, J.; White, J.; Manheim, A.; Eliot, D.; Lasure, L.; Jones, S. Top value added chemicals from biomass. Volume 1-Results of screening for potential candidates from sugars and synthesis gas; DTIC Document: 2004.
- 11 Shusherina, N. P. *Russ. Chem. Rev.* 1974, **43**, 851.
- 12 Woodard, B. T.; Posner, G. H. *Advances in Cycloaddition*, Vol. 5, Elsevier, 1999.
- 13 Markó, I. E.; Evans, G. R. *Tetrahedron Lett.* 1994, **35**, 2767-2770.
- 14 Posner, G. H.; Ishihara, Y. *Tetrahedron Lett.* 1994, **35**, 7545-7548.
- 15 Posner, G. H.; Carry, J.-C.; Kyoo Lee, J.; Bull, D. S.; Dai, H. *Tetrahedron Lett.* 1994, **35**, 1321-1324.
- 16 Posner, G. H.; Dai, H.; Bull, D. S.; Lee, J.-K.; Eydoux, F.; Ishihara, Y.; Welsh, W.; Pryor, N.; Petr, S. *J. Org. Chem.* 1996, **61**, 671-676.
- 17 Cho, C.-G.; Kim, Y.-W.; Lim, Y.-K.; Park, J.-S.; Lee, H.; Koo, S. *J. Org. Chem.* 2002, **67**, 290-293.
- 18 Afarinkia, K.; Vinader, V.; Nelson, T. D.; Posner, G. H. *Tetrahedron* 1992, **48**, 9111-9171.
- 19 Imagawa, T.; Sueda, N.; Kawanisi, M. *Tetrahedron* 1974, **30**, 2227-2231.
- 20 Markó, I. E.; Evans, G. R. *Tetrahedron Lett.* 1994, **35**, 2771-2774.
- 21 Markó, I. E.; Evans, G. R.; Seres, P.; Chellé, I.; Janousek, Z. *Pure Appl. Chem.*, 1996; **68**, 113.
- (22) Kranjc, K.; Kočevar, M. *New J. Chem.* 2005, **29**, 1027-1034.
- (23) Abdullahi, M. H.; Thompson, L. M.; Bearpark, M. J.; Vinader, V.; Afarinkia, K. *Tetrahedron* 2016, **72**, 6021-6024.
- (24) Imagawa, T.; Kawanisi, M.; Sisido, K. *J. Chem. Soc. D.*, 1971, **20**, 1292-1293.
- (25) Juranovič, A.; Kranjc, K.; Perdih, F.; Polanc, S.; Kočevar, M. *Tetrahedron* 2011, **67**, 3490-3500.
- (26) Reed, J. A.; Schilling Jr, C. L.; Tarvin, R. F.; Rettig, T. A.; Stille, J. K. *J. Org. Chem.* 1969, **34**, 2188-2192.
- (27) Markó, I. E.; Evans, G. R.; Declercq, J.-P. *Tetrahedron* 1994, **50**, 4557-4574.

- (28) Pfennig, T.; Carraher, J. M.; Chemburkar, A.; Johnson, R. L.; Anderson, A.; Tessonnier, J.-P.; Neurock, M.; Shanks, B. H. *Green Chem.* 2017, **19**, 4879-4888.
- (29) Ipaktschi, J. Z. *Naturforsch. B Chem. Sci.* 1986; **41**, 496.
- (30) Narayana Murthy, Y. V. S.; Pillai, C. N. *Syn. Commun.* 1991, **21**, 783-791.
- (31) Otto, S.; Bertoncin, F.; Engberts, J. B. F. N. *J. Am. Chem. Soc.* 1996, **118**, 7702-7707.
- (32) Majors, P. D.; Raidy, T. E.; Ellis, P. D. *J. Am. Chem. Soc.* 1986, **108**, 8123-8129.
- (33) Wischert, R.; Laurent, P.; Copéret, C.; Delbecq, F.; Sautet, P. *J. Am. Chem. Soc.* 2012, **134**, 14430-14449.
- (34) Digne, M.; Sautet, P.; Raybaud, P.; Euzen, P.; Toulhoat, H. *J. Catal.* 2002, **211**, 1-5.
- (35) Chia, M.; Haider, M. A.; Pollock, G.; Kraus, G. A.; Neurock, M.; Dumesic, J. A. *J. Am. Chem. Soc.* 2013, **135**, 5699-5708.
- (36) Bond, J. Q.; Wang, D. A.; Alonso, D. M.; Dumesic, J. A. *J. Catal.* 2011, **281**, 290-299.
- (37) Johnson, R. L.; Hanrahan, M. P.; Mellmer, M.; Dumesic, J. A.; Rossini, A. J.; Shanks, B. H. *J. Phys. Chem. C* 2017, **121**, 17226-17234.
- (38) Wiench, J. W.; Bronnimann, C. E.; Lin, V. S. Y.; Pruski, M. *J. Am. Chem. Soc.* 2007, **129**, 12076-12077.
- (39) Ishii, Y.; Tycko, R. *J. Magn. Reson.* 2000, **142**, 199-204.
- (40) Amoureux, J.-P.; Trébosc, J.; Wiench, J.; Pruski, M. *J. Magn. Reson.* 2007, **184**, 1-14.
- (41) Venkatesh, A.; Hanrahan, M. P.; Rossini, A. J. *Solid State Nucl. Magn. Reson.* 2017, **84**, 171-181.
- (42) Valla, M.; Rossini, A. J.; Caillot, M.; Chizallet, C. I.; Raybaud, P.; Digne, M.; Chaumonnot, A.; Lesage, A.; Emsley, L.; Van Bokhoven, J. A. *J. Am. Chem. Soc.* 2015, **137**, 10710-10719.
- (43) Perras, F. A.; Padmos, J. D.; Johnson, R. L.; Wang, L.-L.; Schwartz, T. J.; Kobayashi, T.; Horton, J. H.; Dumesic, J. A.; Shanks, B. H.; Johnson, D. D. *J. Am. Chem. Soc.* 2017, **139**, 2702-2709.
- (44) Stanley, B. J.; Guiochon, G. *Langmuir* 1995, **11**, 1735-1743.
- (45) Lunsford, J. H.; Rothwell, W. P.; Shen, W. *J. Am. Chem. Soc.* 1985, **107**, 1540-1547.
- (46) Wouters, B. H.; Chen, T. H.; Grobet, P. J. *J. Am. Chem. Soc.* 1998, **120**, 11419-11425.

- (47) Amberlyst<sup>TM</sup>45 Resin High Temperature Strongly Acidic Catalyst; Form No. 177-02338-0315, Rev. 0 [Online]; The Dow Chemical Company: Midland, MI. [http://msdssearch.dow.com/PublishedLiteratureDOWCOM/dh\\_092d/0901b8038092d737.pdf?filepath=liquidseps/pdfs/noreg/177-02338.pdf&fromPage=GetDoc](http://msdssearch.dow.com/PublishedLiteratureDOWCOM/dh_092d/0901b8038092d737.pdf?filepath=liquidseps/pdfs/noreg/177-02338.pdf&fromPage=GetDoc) (accessed Aug 10, 2017)
- (48) Gómez-Bombarelli, R.; Calle, E.; Casado, J. *J. Org. Chem.* 2013, **78**, 6880-6889.
- (49) J. Sheehan, R. Terephthalic Acid, Dimethyl Terephthalate, and Isophthalic Acid. In *Ullmann's Encyclopedia of Industrial Chemistry*, Wiley-VCH Verlag GmbH & Co. KGaA: 2000.
- (50) Chen, T.-H.; Wang, L.; Trueblood, J. V.; Grassian, V. H.; Cohen, S. M. *J. Am. Chem. Soc.* 2016, **138**, 9646-9654.
- (51) Pfennig, T.; Johnson, R. L.; Shanks, B. H. *Green Chem.* 2017, **19**, 3263-3271
- (52) Brinkmann, A.; Kentgens, A. P. M. *J. Am. Chem. Soc.* 2006, **128**, 14758-14759.
- (53) Metz, G.; Wu, X. L.; Smith, S. O. *J. Magn. Reson., Ser A* 1994, **110**, 219-227.
- (54) Fung, B. M.; Khitrin, A. K.; Ermolaev, K. *J. Magn. Reson.* 2000, **142**, 97-101.
- (55) Kresse, G.; Hafner, J. *Phys. Rev. B* 1993, **47**, 558-561.
- (56) Kresse, G.; Hafner, J. *Phys. Rev. B* 1994, **49**, 14251-14269.
- (57) Kresse, G.; Furthmüller, J. *Comput. Mater. Sci.* 1996, **6**, 15-50
- (58) Kresse, G.; Furthmüller, J. *Phys. Rev. B* 1996, **54**, 11169-11186.
- (59) Perdew, J. P.; Ernzerhof, M.; Burke, K. *J Chem. Phys.* 1996, **105**, 9982-9985.
- (60) Grimme, S.; Antony, J.; Ehrlich, S.; Krieg, H. *J Chem. Phys.* 2010, **132**, 154104.
- (61) Henkelman, G.; Jónsson, H. *J Chem. Phys.* 2000, **113**, 9978-9985.
- (62) Henkelman, G.; Uberuaga, B. P.; Jónsson, H. *J Chem. Phys.* 2000, **113**, 9901-9904.
- (63) Henkelman, G.; Jónsson, H. *J Chem. Phys.* 1999, **111**, 7010-7022.
- (64) Wischert, R.; Copéret, C.; Delbecq, F.; Sautet, P. *Ang. Chem. Int. Ed.* 2011, **50**, 3202-3205.
- (65) Monkhorst, H. J.; Pack, J. D. *Phys. Rev. B* 1976, **13**, 5188-5192.
- (66) Campbell, C. T.; Sellers, J. R. V. *J. Am. Chem. Soc.* 2012, **134**, 18109-18115.
- (67) Zhao, Y.; Truhlar, D. G. *J Chem. Phys.* 2006, **125**, 194101.

- (68) Frisch, M. J.; Trucks, G. W.; Schlegel, H. B.; Scuseria, G. E.; Robb, M. A.; Cheeseman, J. R.; Scalmani, G.; Barone, V.; Mennucci, B.; Petersson, G. A.; Nakatsuji, H.; Caricato, M.; Li, X.; Hratchian, P., H.; Izmaylov, A. F.; Bloino, J.; Zheng, G.; Sonnenberg, J. L.; Hada, M.; Ehara, M.; Toyota, K.; Fukuda, R.; Hasegawa, J.; Ishida, M.; Nakajima, T.; Honda, Y.; Kitao, O.; Nakai, H.; Vreven, T.; Montgomery, J. A., Jr.; Peralta, E., J.; Ogliaro, F.; Bearpark, M.; Heyd, J. J.; Brothers, E.; Kudin, K. N.; Staroverov, V. N.; Kobayashi, R.; Normand, J.; Raghavachari, K.; Rendell, A.; Burant, J. C.; Iyengar, S. S.; Tomasi, J.; Cossi, M.; Rega, N.; Millam, J. M.; Klene, M.; Knox, J. E.; Cross, J. B.; Bakken, V.; Adamo, C.; Jaramillo, J.; Gomperts, R.; Stratmann, R. E.; Yazyev, O.; Austin, A. J.; Cammi, R.; Pomelli, C.; Ochterski, J. W.; Martin, R. L.; Morokuma, K.; Zakrzewski, V. G.; Voth, G.; A.; Salvador, P.; Dannenberg, J. J.; Dapprich, S.; Daniels, A. D.; Farkas, O.; Foresman, J. B.; Ortiz, J. V.; Cioslowski, J.; Fox, D. J., Gaussian 09, Revision A.02, Gaussian, Inc., Wallingford CT, 2016.
- (69) Frisch, M. J.; Pople, J. A.; Binkley, J. S. *J Chem. Phys.* 1984, **80**, 3265-3269.
- (70) Marenich, A. V.; Cramer, C. J.; Truhlar, D. G. *J. Chem. Phys. B* 2009, **113**, 6378-6396.

## 4.8 Supplementary Information

A combined kinetic and computational investigation of catalytic pathway modification of 2-pyrone Diels-Alder intermediates to selectively access unique products

*A paper in submitted to the Journal of the American Chemical Society*

Toni Pfennig,<sup>a,d</sup> Ashwin Chemburkar,<sup>c,d</sup> Robert L. Johnson,<sup>a,d</sup> Mathew J. Ryan,<sup>b</sup> Matthew Neurock,<sup>c,d</sup> Aaron J. Rossini,<sup>b</sup> Brent H. Shanks<sup>\*a,d</sup>

<sup>a</sup> Department of Chemical and Biological Engineering, Iowa State University, Ames, IA, 50011, USA

<sup>b</sup> Department of Chemistry, Iowa State University, Ames, IA, 50011, USA

<sup>c</sup> Department of Chemical Engineering and Material Sciences, University of Minnesota, Minneapolis, MN 55455, USA

<sup>d</sup> NSF Engineering Research Center for Biorenewable Chemicals (CBiRC), Ames, IA 50011, USA

***Catalyst screening for the decarboxylation of the bicyclic lactone from Diels-Alder reaction of coumalic acid and ethylene***

**Table S1.** The conversion of (1) using different catalysts

Entry	Catalyst	(1) Conv. [mol%]	(2) Yield [mol%]	(3) Yield [mol%]	(4) Yield [mol%]	(5) Yield [mol%]	By- products [mol%]
1	ZSM-5 (CBV2314)	7.15	5.1	2.03	-	-	0.02
2	5 wt% Cu/ $\gamma$ -Al <sub>2</sub> O <sub>3</sub>	58.68	58.05	1.54	-	-	0.93
3	5 wt% Zn/ $\gamma$ -Al <sub>2</sub> O <sub>3</sub>	48.98	35.71	2.55	-	-	10.72
4	5 wt% Ce/ $\gamma$ -Al <sub>2</sub> O <sub>3</sub>	46.93	45.26	2.55	-	-	-
5	5 wt% Fe/ $\gamma$ -Al <sub>2</sub> O <sub>3</sub>	47.18	34.33	2.56	-	-	10.29
Conditions: Reaction time 2 h, reaction temperature 120 °C, stirring rate 500 rpm, starting concentration 71.38 $\mu$ mol/ml, reaction volume 4 ml, solvent 1,4-dioxane, catalyst mass: 25 mg							

*Reaction kinetics of the  $\gamma\text{-Al}_2\text{O}_3$  catalyzed decarboxylation of the bicyclic lactone (I) from Diels-Alder reaction of coumalic acid and ethylene*

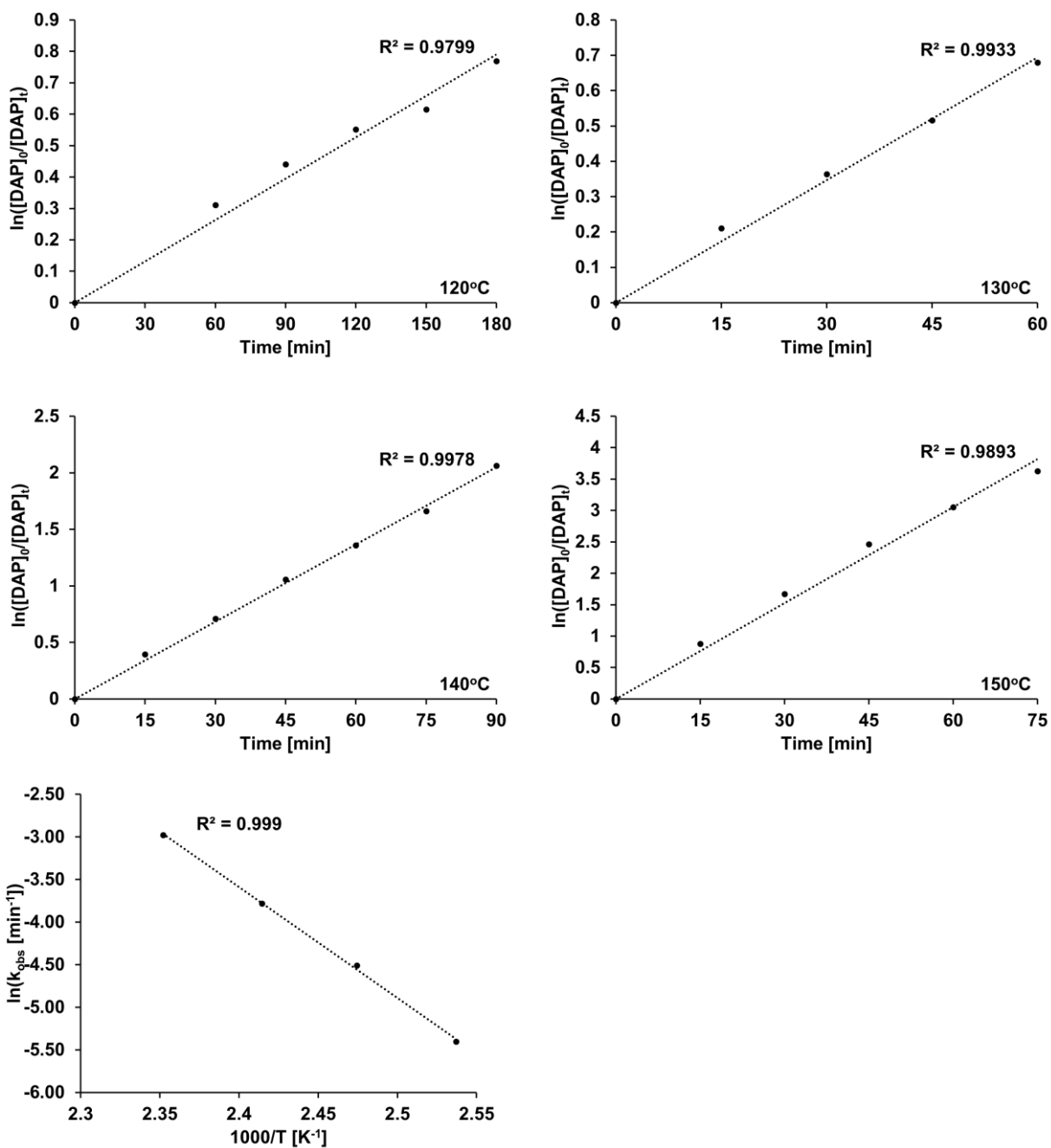


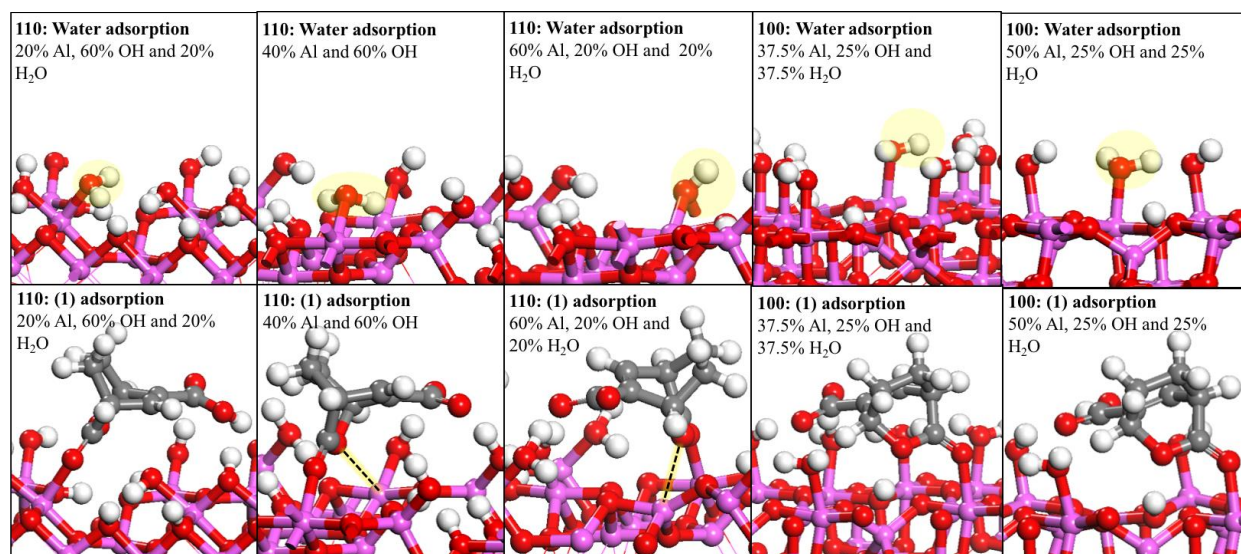
Figure S1. Kinetic data of the conversion of DAP (1) with gamma alumina



**Table S2.** Rate constants of the Al<sub>2</sub>O<sub>3</sub> catalyzed conversion of DAP in 1,4-dioxane

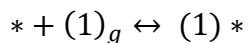
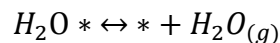
Temp. [°C]	Temp. [K]	k [min <sup>-1</sup> ]
121	394.15	4.50E-03
131	404.15	1.10E-02
141	414.15	2.28E-02
152	425.15	5.09E-02

### *Computational analysis and micro-kinetic modeling*

**Figure S2.** Structures for adsorbed water and adsorbed (1) on different surfaces of  $\gamma$ -Al<sub>2</sub>O<sub>3</sub>

### **Ab-initio thermodynamics**

We start with fully hydroxylated 110 surface wherein all Al sites are covered with water and OH groups (water coverage = 40% and OH coverage = 60%) and desorb water molecules and adsorb bicyclic (1) molecules as per the following equations.



We calculate the water desorption and (1) adsorption energies for different OH and H<sub>2</sub>O coverage. We then compare energies of resulting different surfaces. Under reacting conditions, we

will likely have surface coverage of (1), H<sub>2</sub>O and OH corresponding to the lowest energy surface.

The water desorption and (1) adsorption energies at 140 °C are as follows:

**Table S2:** Desorption energies of water and adsorption energies of (1) at different coverage of Al, OH and H<sub>2</sub>O on the 110 surface at 140 °C

Entry	%Al	%OH	%H <sub>2</sub> O	%(1)	Gibbs free energy of water desorption (kJ/mol)	Gibbs free energy of water adsorption (kJ/mol)	Gibbs free energy of (1) adsorption (kJ/mol)
1	0	60	40	0	$\Delta G_1^{\text{desp}} = 61$	-	-
2	20	60	20	0	$\Delta G_3^{\text{desp}} = 110$	-61	$\Delta G_2^{\text{ads}} = -66$
3	40	60	0	0	$\Delta G_5^{\text{desp}} = 177$	-110	$\Delta G_4^{\text{ads}} = -123$
4	60	20	20	0	NA	-177	$\Delta G_6^{\text{ads}} = -107$

Now, with respect to the fully hydroxylated surface (40% H<sub>2</sub>O and 60 % OH), the relative energies of 110 surface with different coverage of Al, (1), H<sub>2</sub>O and OH are as follows:

**Table S3:** Relative energy and abundance of the 110 surface at different coverage of Al, OH, H<sub>2</sub>O and (1) at 140 °C and H<sub>2</sub>O mole fraction of 0.00028 and balance (1)

Entry	%Al	%OH	%H <sub>2</sub> O	%(1)	Relative energy (kJ/mol)	Relative abundance of each configuration
1	0	60	40	0	0	$2.059 \times 10^{-5}$
2	20	60	20	0	61	$9.607 \times 10^{-10}$
3	0	60	20	20	-5	0.9989
4	40	60	0	0	171	$2.059 \times 10^{-20}$
5	20	60	0	20	48	$1.060 \times 10^{-3}$
6	60	20	20	0	348	$1.6139 \times 10^{-39}$
7	40	20	20	20	241	$1.8385 \times 10^{-25}$

The 110 surface has the lowest energy when the coverage of Al, OH, H<sub>2</sub>O and (1) is 0, 60%, 20% and 20% respectively making it the most favorable configuration from the configurations examined herein. In addition, concentration effects can be estimated by assuming the reactions at different surface coverage of OH, Al, H<sub>2</sub>O and (1) are quasi-equilibrated. The relative abundance of each surface configuration can be estimated by assuming a Langmuir-

Hinshelwood surface and from equilibrium constants  $K_i$  corresponding to  $\Delta G_i$  from Table S2. The relative abundance of different configurations in Table S3 are as follows:

$$[\text{Table S3, Entry 2}] = \frac{1}{1 + \frac{[\text{H}_2\text{O}]}{K_1} + K_2[(1)] + \frac{K_3}{[\text{H}_2\text{O}]} + \frac{K_3K_4}{[\text{H}_2\text{O}]} [(1)] + \frac{K_5K_3}{[\text{H}_2\text{O}]^2} + \frac{K_6K_5K_3}{[\text{H}_2\text{O}]^2} [(1)]}$$

$$[\text{Table S3, Entry 1}] = \frac{\frac{[\text{H}_2\text{O}]}{K_1}}{1 + \frac{[\text{H}_2\text{O}]}{K_1} + K_2[(1)] + \frac{K_3}{[\text{H}_2\text{O}]} + \frac{K_3K_4}{[\text{H}_2\text{O}]} [(1)] + \frac{K_5K_3}{[\text{H}_2\text{O}]^2} + \frac{K_6K_5K_3}{[\text{H}_2\text{O}]^2} [(1)]}$$

$$[\text{Table S3, Entry 3}] = \frac{K_2[(1)]}{1 + \frac{[\text{H}_2\text{O}]}{K_1} + K_2[(1)] + \frac{K_3}{[\text{H}_2\text{O}]} + \frac{K_3K_4}{[\text{H}_2\text{O}]} [(1)] + \frac{K_5K_3}{[\text{H}_2\text{O}]^2} + \frac{K_6K_5K_3}{[\text{H}_2\text{O}]^2} [(1)]}$$

$$\text{Table S3, Entry 4}] = \frac{\frac{K_3}{[\text{H}_2\text{O}]}}{1 + \frac{[\text{H}_2\text{O}]}{K_1} + K_2[(1)] + \frac{K_3}{[\text{H}_2\text{O}]} + \frac{K_3K_4}{[\text{H}_2\text{O}]} [(1)] + \frac{K_5K_3}{[\text{H}_2\text{O}]^2} + \frac{K_6K_5K_3}{[\text{H}_2\text{O}]^2} [(1)]}$$

$$[\text{Table S3, Entry 5}] = \frac{\frac{K_3K_4}{[\text{H}_2\text{O}]} [(1)]}{1 + \frac{[\text{H}_2\text{O}]}{K_1} + K_2[(1)] + \frac{K_3}{[\text{H}_2\text{O}]} + \frac{K_3K_4}{[\text{H}_2\text{O}]} [(1)] + \frac{K_5K_3}{[\text{H}_2\text{O}]^2} + \frac{K_6K_5K_3}{[\text{H}_2\text{O}]^2} [(1)]}$$

$$[\text{Table S3, Entry 6}] = \frac{\frac{K_5K_3}{[\text{H}_2\text{O}]^2}}{1 + \frac{[\text{H}_2\text{O}]}{K_1} + K_2[(1)] + \frac{K_3}{[\text{H}_2\text{O}]} + \frac{K_3K_4}{[\text{H}_2\text{O}]} [(1)] + \frac{K_5K_3}{[\text{H}_2\text{O}]^2} + \frac{K_6K_5K_3}{[\text{H}_2\text{O}]^2} [(1)]}$$

$$[\text{Table S3, Entry 7}] = \frac{\frac{K_6K_5K_3}{[\text{H}_2\text{O}]^2} [(1)]}{1 + \frac{[\text{H}_2\text{O}]}{K_1} + K_2[(1)] + \frac{K_3}{[\text{H}_2\text{O}]} + \frac{K_3K_4}{[\text{H}_2\text{O}]} [(1)] + \frac{K_5K_3}{[\text{H}_2\text{O}]^2} + \frac{K_6K_5K_3}{[\text{H}_2\text{O}]^2} [(1)]}$$

We find that under reacting conditions, the 110 surface will have coverage of Al, OH, H<sub>2</sub>O and (1) as 0, 60%, 20% and 20% respectively since the relative abundance of this configuration is very close to 1. We therefore, examine this surface for decarboxylation reactivity.

### For 100 surface

For the 100 surface as well, we calculate water desorption and (1) adsorption energies at different surface coverage of Al, H<sub>2</sub>O and OH. The results are reported in Table S4.

**Table S4:** Desorption energies of water and adsorption energies of (1) at different coverage of Al, OH and H<sub>2</sub>O on the 100 surface at 140 °C

Entry	%Al	%OH	%H <sub>2</sub> O	%(1)	Gibbs free energy of water desorption (kJ/mol)	Gibbs free energy of water adsorption (kJ/mol)	Gibbs free energy of (1) adsorption (kJ/mol)
1	25	25	50	0	$\Delta G_1^{\text{desp}} = 71$	-	-
2	37.5	25	37.5	0	$\Delta G_3^{\text{desp}} = 86$	-71	$\Delta G_2^{\text{ads}} = -50$
3	50	25	25	0	NA	-86	$\Delta G_4^{\text{ads}} = -43$

The above free energies result in the following relative surface energies and surface abundance at 140 °C and water mole fraction of 0.00028.

**Table S5.** Relative energy and abundance of the 110 surface at different coverage of Al, OH, H<sub>2</sub>O and (1) at 140 °C and H<sub>2</sub>O mole fraction of 0.00028 and balance (1)

Entry	%Al	%OH	%H <sub>2</sub> O	%(1)	Relative energy (kJ/mol)	Relative abundance of each configuration
1	25	25	50	0	0	$5.0551 \times 10^{-2}$
2	37.5	25	37.5	0	71	$1.2380 \times 10^{-7}$
3	25	25	37.5	12.5	21	0.9449
4	50	25	25	0	157	$3.7439 \times 10^{-15}$
5	37.5	25	25	12.5	114	$3.4825 \times 10^{-9}$

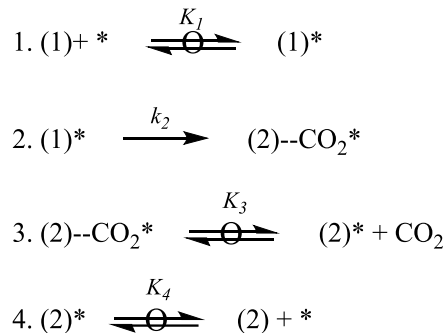
The relative abundance of each configuration reported in Table S5 can be estimated by assuming a Langmuir-Hinshelwood surface and by assuming adsorption-desorption equations at

different coverage of Al, H<sub>2</sub>O, OH and (1) are quasi-equilibrated resulting in the following equations.

$$\begin{aligned}
 [\text{Table S5, Entry 2}] &= \frac{1}{1 + \frac{[\text{H}_2\text{O}]}{K_1} + K_2[(1)] + \frac{K_3}{[\text{H}_2\text{O}]} + \frac{K_3 K_4}{[\text{H}_2\text{O}]} [(1)]} \\
 \text{Table S5, Entry 1} &= \frac{\frac{[\text{H}_2\text{O}]}{K_1}}{1 + \frac{[\text{H}_2\text{O}]}{K_1} + K_2[(1)] + \frac{K_3}{[\text{H}_2\text{O}]} + \frac{K_3 K_4}{[\text{H}_2\text{O}]} [(1)]} \\
 [\text{Table S5, Entry 3}] &= \frac{K_2[(1)]}{1 + \frac{[\text{H}_2\text{O}]}{K_1} + K_2[(1)] + \frac{K_3}{[\text{H}_2\text{O}]} + \frac{K_3 K_4}{[\text{H}_2\text{O}]} [(1)]} \\
 [\text{Table S5, Entry 4}] &= \frac{\frac{K_3}{[\text{H}_2\text{O}]}}{1 + \frac{[\text{H}_2\text{O}]}{K_1} + K_2[(1)] + \frac{K_3}{[\text{H}_2\text{O}]} + \frac{K_3 K_4}{[\text{H}_2\text{O}]} [(1)]} \\
 [\text{Table S5, Entry 5}] &= \frac{\frac{K_3 K_4}{[\text{H}_2\text{O}]} [(1)]}{1 + \frac{[\text{H}_2\text{O}]}{K_1} + K_2[(1)] + \frac{K_3}{[\text{H}_2\text{O}]} + \frac{K_3 K_4}{[\text{H}_2\text{O}]} [(1)]}
 \end{aligned}$$

Although the lowest energy configuration was Entry 1, the very low concentration of water makes the slightly less favorable configuration of Entry 3 the most abundant configuration. Therefore, on the 100 surface we will likely have Al, OH, H<sub>2</sub>O and (1) coverage of 25%, 25%, 37.5% and 12.5% respectively.

### Rate expression derivation



### Step 2 rate determining

$$r = K_1 k_2 [(1)] [*]$$

$$[(2) *] = \frac{[(2)][*]}{K_4}$$

$$[(2) - CO_2] = \frac{[(2)][CO_2][*]}{K_4 K_3}$$

$$[DAP *] = K_1 [(1)][*]$$

$$r = \frac{K_1 k_2 [(1)]}{1 + K_1 [(1)] + \frac{[(2)][CO_2]}{K_4 K_3} + \frac{[(2)]}{K_4}}$$

DFT predicted free energy diagram suggests that adsorption of (1) and (2) is very strong. Therefore, we expect the surface to be predominantly covered by (1\*) and (2\*). Therefore, the coverage of (2)—CO<sub>2</sub> can be neglected which then gives us:

$$r = \frac{K_1 k_2 [(1)]}{1 + K_1 [(1)] + \frac{[(2)]}{K_4}}$$

Define  $K_1 k_2 = A$ ,  $K_1 = B$  and  $1/K_4 = C$ , we have

$$r = \frac{A[(1)]}{1 + B[(1)] + C[(2)]}$$

### Results of regression analysis

The rate expressions were solved by assuming that rate of consumption of (1) is equal to the rate of formation of (2).

This results in the following coupled differential equations:

$$\frac{d[(1)]}{dt} = -\frac{A[(1)]}{1 + B[(1)] + C[(2)]}$$

$$\frac{d[(2)]}{dt} = \frac{A[(1)]}{1 + B[(1)] + C[(2)]}$$

These equations were solved by discretizing using explicit Euler method for given initial conditions. The resulting profiles were solved for different values of A, B and C such that the root mean square error was minimized. The values of these constants at different temperatures are as followed:

**Table S6.** Values of regression parameters A, B and C

T [°C]	A [min <sup>-1</sup> ]	B	C
120	1.59411881	1.88800885	10.0421926
130	3.99776346	3.43062155	4.106534
140	5.79053195	2.16686937	3.05424603
150	8.2482893	1.57044347	2.16034609

### Derivation of initial activation barrier

$$r = \frac{A[(1)]}{1 + B[(1)] + C[(2)]}$$

Assuming [(1)]  $\gg$  1 and [(2)]

$$r = \frac{A[(1)]}{B[(1)]}$$

Therefore,  $k_{\text{obs}} = A/B = k_2$  which corresponds to intrinsic forward rate constant of decarboxylation of (1\*).

**Table S7.** Ideal gas entropies of different molecules at standard state and 140 °C

Chemical species	S <sub>Gas</sub> [kJ/mol*K]
Bicyclic (1)	0.463432392
Diene (2)	0.417132248
CO <sub>2</sub>	0.226002944
Water	0.199593536

On metal oxides, the entropy loss following adsorption is estimated to be 1/3<sup>rd</sup> ideal gas entropy.<sup>4</sup> Accordingly, the Gibbs free energy was calculated by adding appropriate contribution to the enthalpy.

### *1D and 2D NMR product and intermediate identification*

**6-hydroxy-3-((methoxy-d<sub>3</sub>)carbonyl)cyclohex-1-ene-1-carboxylic acid:** <sup>1</sup>H NMR (600 MHz, Methanol-*d*<sub>4</sub>) δ 7.14 (d, *J* = 2.7 Hz, 1H), 4.54 – 4.52 (m, 1H), 3.30 – 3.28 (m, 1H), 1.96 – 1.92 (m, 3H), 1.72 – 1.66 (m, 1H). <sup>1</sup>H-<sup>13</sup>C-HSQC: δ 7.14 – 138.63, δ 4.54 – 61.22, δ 3.30 – 42.89, δ 1.96 – 19.25, δ 1.96 – 30.05, δ 1.72 – 30.05 (600 MHz, Methanol-*d*<sub>4</sub>): Exact mass: 203.09. Found *m/z*: 203.02 (UPLC-MS-ESI).

**cyclohexa-1,3-diene-1,3-dicarboxylic acid:** <sup>1</sup>H NMR (600 MHz, DMSO-*d*<sub>6</sub>) δ 7.22 (t, *J* = 1.7 Hz, 1H), 7.13 (td, *J* = 4.6, 1.3 Hz, 1H), 2.42 – 2.38 (m, 2H), 2.33 (dd, *J* = 9.9, 1.8 Hz, 2H). <sup>1</sup>H-<sup>13</sup>C-HSQC (600 MHz, DMSO-*d*<sub>6</sub>): δ 7.22-130.47, δ 7.13-143.37, δ 2.42-23.66, δ 2.33-20.08. Exact mass: 168.04. Found *m/z*: 168.04 (UPLC-MS-ESI).

**Isophthalic acid:** <sup>1</sup>H NMR (600 MHz, DMSO-*d*<sub>6</sub>) δ 7.95 – 7.92 (m, 2H), 7.64 – 7.59 (m, 1H), 7.48 (t, *J* = 7.6 Hz, 1H). <sup>1</sup>H-<sup>13</sup>C-HSQC (600 MHz, DMSO-*d*<sub>6</sub>): δ 7.95 – 129.82, δ 7.62 – 133.30, δ 7.48 – 129.12. Exact mass: 166.03. Found *m/z*: 166.05 (UPLC-MS-ESI)

**6-hydroxycyclohex-1-ene-1,3-dicarboxylic acid:** <sup>1</sup>H NMR (600 MHz, DMSO-*d*<sub>6</sub>) δ 6.89 (d, *J* = 2.6 Hz, 1H), 4.33 (d, *J* = 2.9 Hz, 1H), 3.17 (ddd, *J* = 9.4, 6.5, 2.8 Hz, 1H), 1.80 – 1.73 (m, 3H), 1.51 (ddq, *J* = 12.6, 8.9, 4.0 Hz, 1H). <sup>1</sup>H-<sup>13</sup>C-HSQC (600 MHz, DMSO-*d*<sub>6</sub>): δ 6.89 – 138.82, δ 4.33 – 60.27, δ 3.17 – 42.56, δ 1.78 – 20.17, δ 1.53 – 30.65. Exact mass: 186.05. Found *m/z*: 186.14 (UPLC-MS-ESI).



***Mass transfer effect calculations of the bicyclic lactone decarboxylation using  $\gamma$ -Al<sub>2</sub>O<sub>3</sub>***

Catalyst:  $\gamma$ -Al<sub>2</sub>O<sub>3</sub> (Strem Chemicals)

Mass of catalyst: 200 mg

Particle size (dp) of  $\gamma$ -Al<sub>2</sub>O<sub>3</sub>: 53  $\mu$ m

Particle size (R) of  $\gamma$ -Al<sub>2</sub>O<sub>3</sub>:  $2.65 \times 10^{-3}$  cm

Tortuosity ( $\tau$ ) of  $\gamma$ -Al<sub>2</sub>O<sub>3</sub>: 4 (conservative estimation based on Davis, M. E. and Davis, R. J.)<sup>1</sup>

Porosity ( $\epsilon$ ) of  $\gamma$ -Al<sub>2</sub>O<sub>3</sub>: 0.872 (provided by Strem Chemicals)

True density ( $\rho_c$ ) of  $\gamma$ -Al<sub>2</sub>O<sub>3</sub>: 3.9 g/cm<sup>3</sup> (provided by Strem Chemicals)

***Calculation of the diffusion coefficient***

To calculate the diffusion coefficient  $D_{AB}$  (based on Wilke, C. R. and Chang, P.)<sup>2</sup>, we first have to determine the molal volume ( $V_m$ ) of the model compound benzoic acid.

$$D_{AB} = \frac{7.4 * 10^{-8} (X * M_s)^{0.5} T}{\eta * V_m^{0.6}}$$

Molal volume ( $V_m$ ) of benzoic acid (model compound): 134.8 cm<sup>3</sup>/mol (based on Wilke, C. R. and Chang, P.)<sup>2</sup>

Association factor (X) of 1,4-dioxane: 1 (based on Wilke, C. R. and Chang, P.)<sup>2</sup>

Molar mass (M) of the solvent 1,4-dioxane: 88.1 g/mol

Calculated molar diffusivity ( $D_{AB}$ ) of benzoic acid in 1,4-dioxane at 25 °C: 9.2526E-06 cm<sup>2</sup>/s (based on Wilke, C. R. and Chang, P.)<sup>2</sup>

$$D_{AB} = \frac{7.4 * 10^{-8} (X * M_s)^{0.5} T}{\eta * V_m^{0.6}}$$

Calculated molar diffusivity ( $D_{AB}$ ) of benzoic acid in 1,4-dioxane at 140 °C: 1.35E-05 cm<sup>2</sup>/s (based on Wilke, C. R. and Chang, P.)<sup>2</sup>

Calculated effective diffusivity ( $D_{eff}$ ) of benzoic acid in 1,4-dioxane at 140 °C: 2.96E-05 cm<sup>2</sup>/s ( $D_{eff}$  calculated based on Fogler, H. S.)<sup>3</sup>

$$D_{eff} = \frac{\epsilon}{\tau} D_{AB}$$

Calculated Weisz-Prater number ( $N_{WP}$ ) (Calculation based on Fogler, H. S.)<sup>3</sup>

$$N_{WP} = \frac{r_{obs}^{mass\ cat} * \rho_c * R^2}{C_{Bulk} * D_{eff}}$$

Initial observed rate  $r_{obs}$  of the consumption of (1) at 140 °C: 2.13 μmol/min\*ml (volume)

Initial observed rate  $r_{obs}$  of the consumption of (1) at 140 °C: 7.1E-06 mmol/s\*mg(cat)

$$N_{WP} = \frac{7.1 * 10^{-6} \frac{mmol}{s\ mg(cat)} * \frac{3.9 * 10^3\ mg}{cm^3} * (2.65 * 10^{-03}\ cm)^2}{\frac{7.14 * 10^{-2}\ mmol}{cm^3} * 2.96 * 10^{-6} \frac{cm^2}{s}} = 0.92$$

For  $N_{WP} < 1$  the absence of internal mass transfer limitations is confirmed. Additionally, the calculations of internal mass transfer limitations at a temperature of 120 °C yielded a value of  $N_{WP} = 0.27$ . Given that a linear trend of the Arrhenius plot at temperatures in the range of 120-150 °C was observed (Figure S1) is further proof of the absence of transport effects.

In a previous study, we have shown that the absence of external transport effect for the 4590 Parr reactor system was given at an agitation speed of 400 rpm using the same  $\gamma$ -Al<sub>2</sub>O<sub>3</sub> support material that was used in this study. Therefore we assume that a 400 rpm agitation rate is sufficient to eliminate external mass transfer effects.

Given the linear relationship of the Arrhenius plot (Figure S1) in the temperature range of 120-150 °C, it is evident that reaction was performed in the absence of internal or external transport

effects. Additionally, We have performed reactions with 5 times less catalyst (40 mg) which resulted in a  $\sim 5$  times lower conversion rate of (1) further suggesting the absence of mass transfer limitations.

**HR-MAS NMR investigation of immobilized (1) on  $\gamma$ -Al<sub>2</sub>O<sub>3</sub>**

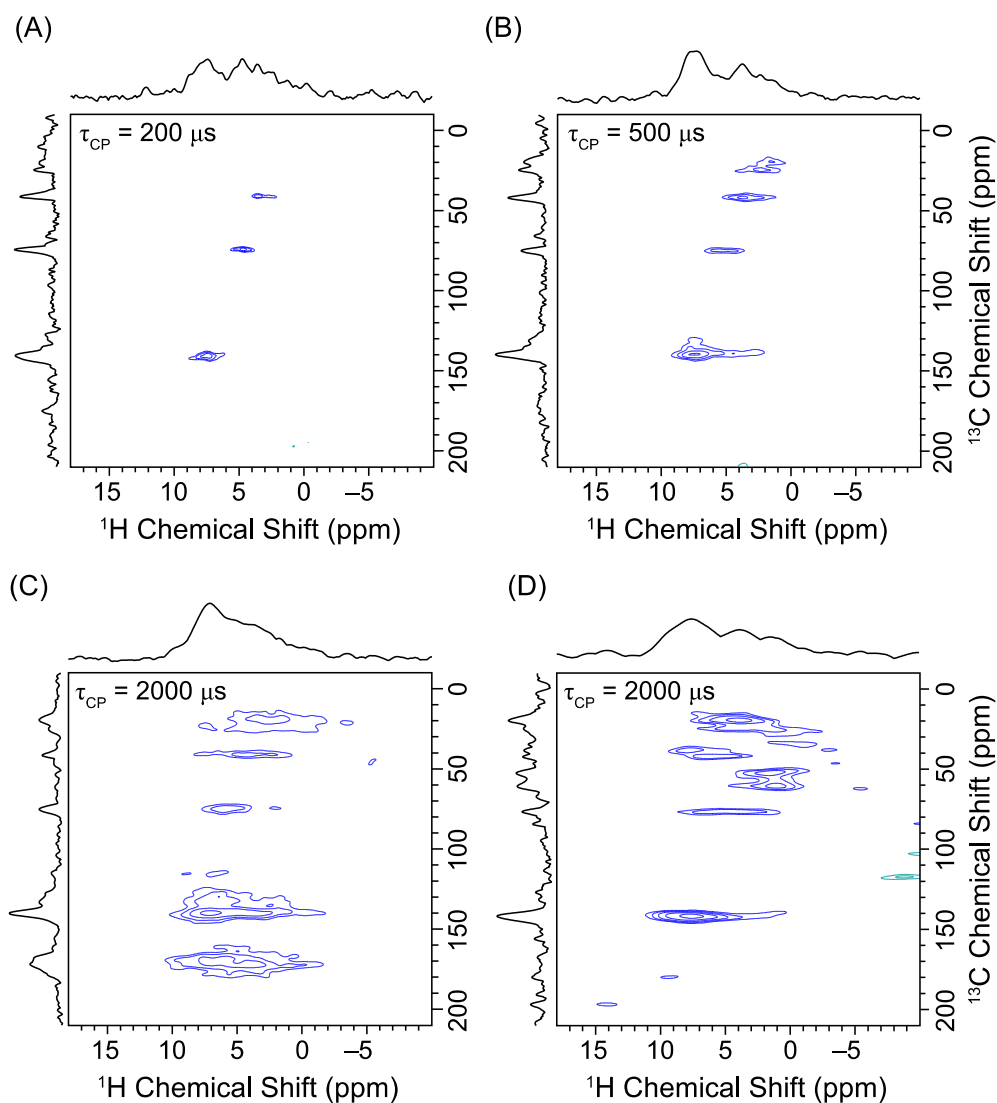


**Figure S3.** Proton detected 2D  $^1\text{H}\{^{13}\text{C}\}$  CP-HETCOR NMR spectra of alumina impregnated with 1,4-dioxane-*d*<sub>8</sub> solutions of bicyclic (1) with concentrations of 200 mg/mL (A-C) and 132 mg/mL (D). All spectra were obtained with a 25 kHz MAS frequency and forwards CP contact time ( $\tau_{\text{CP}}$ ) of 2.0 ms. The contact time used for the backwards  $^{13}\text{C} \rightarrow ^1\text{H}$  CP transfer is indicated on the 2D spectrum. The 2D spectra were acquired with a 1.3 s recycle delay, 224 to 320 scans per increment, 128  $t_1$  increments and  $t_1$  was incremented in steps of 40  $\mu\text{s}$ . Total experiment times were between 10.3 hours and 14.8 hours.

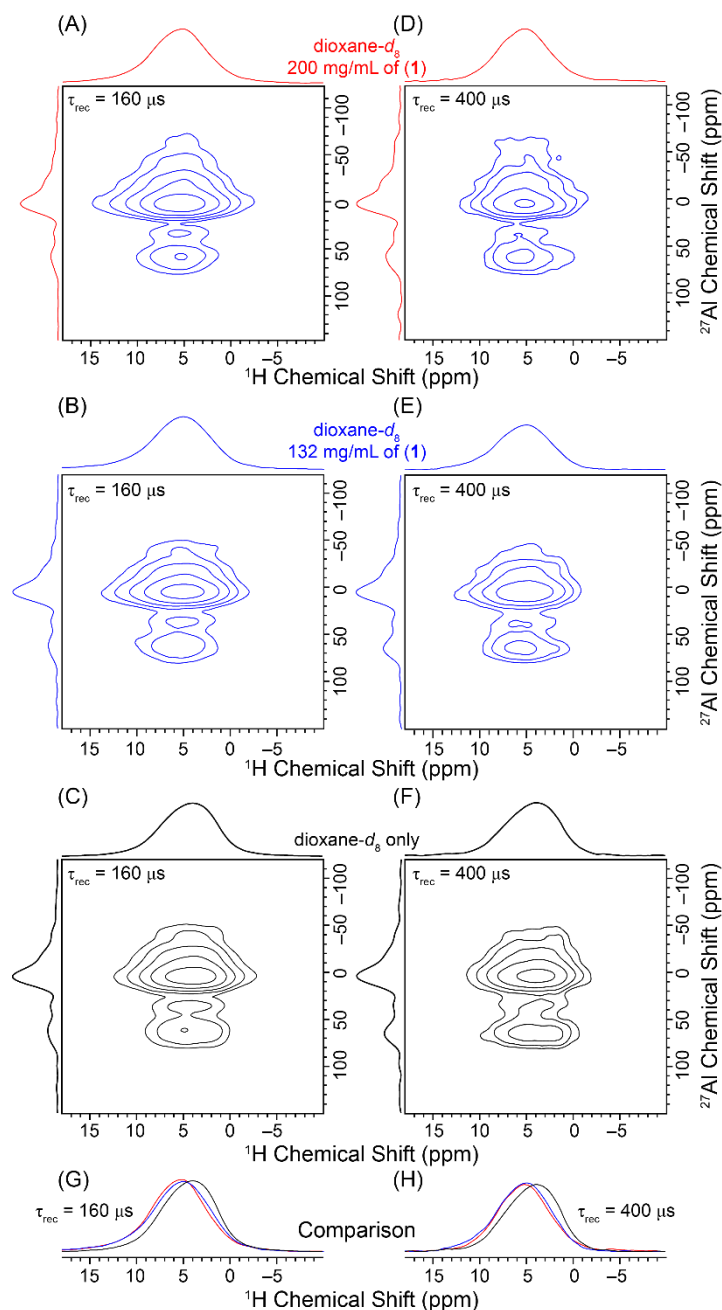


**Figure S4.** Proton detected 2D  $^{27}\text{Al} \rightarrow ^1\text{H}$  D-RINEPT HETCOR spectra of alumina impregnated with 1,4-dioxane- $d_8$  solutions of bicyclic (1) with concentrations of 200 mg/mL (A, D) and 132 mg/mL (B, E) and pure dioxane (C, F). The spectra were obtained with dipolar recoupling times ( $\tau_{\text{rec}}$ ) of 160  $\mu\text{s}$  (left column) or 400  $\mu\text{s}$  (right column).  $^1\text{H}$  solid-state NMR spectra obtained from the positive projections of the direct dimension of each sample are compared in (G) and (H). The 2D spectra were typically acquired with recycle delays between 50 ms and 100 ms, between 1024 to 2400 scans per increment, 80  $t_1$  increments and  $t_1$  was incremented in steps of 11.0  $\mu\text{s}$  (1.1 hours to 5.3 hours total experiment time). The spectra obtained with  $\tau_{\text{rec}} = 160 \mu\text{s}$  have the best sensitivity, however, the relative intensity of signals from 4- and 5-coordinate aluminum are enhanced in the spectra recorded with  $\tau_{\text{rec}} = 400 \mu\text{s}$ . The  $^{27}\text{Al}$  solid-state NMR spectra are compared in Figure S5.

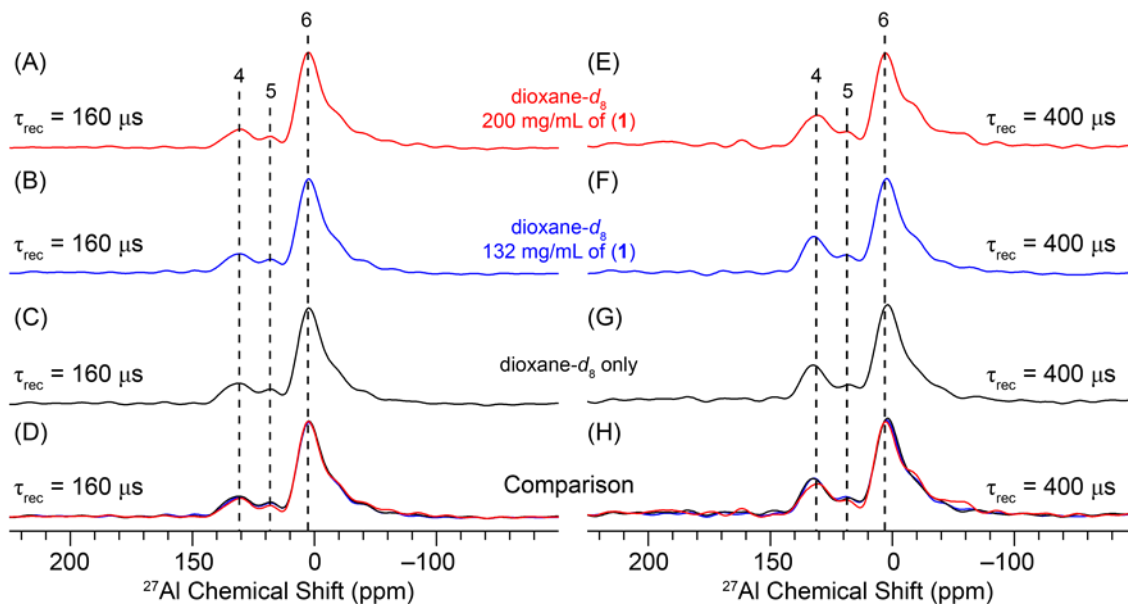


**Figure S5.** Comparison of surface selective  $^{27}\text{Al}$  solid-state NMR spectra of alumina impregnated with 1,4-dioxane- $d_8$  solutions of bicyclic (1) with concentrations of 200 mg/mL (A, E) and 132 mg/mL (B, F) and pure dioxane (C, G). The  $^{27}\text{Al}$  solid-state NMR spectra were obtained from the sum of the indirect dimension of the proton detected 2D  $^{27}\text{Al} \rightarrow ^1\text{H}$  D-RINEPT HETCOR spectra. The spectra were obtained with dipolar recoupling times ( $\tau_{\text{rec}}$ ) of 160  $\mu\text{s}$  (left column) or 400  $\mu\text{s}$  (right column). Signals from 4-, 5- and 6-coordinate aluminum are clearly visible. The  $^{27}\text{Al}$  solid-state NMR spectra of the different samples are compared in (D) and (H) and show that there is not a substantial variation in the relative intensity of the different aluminum sites with loading level.

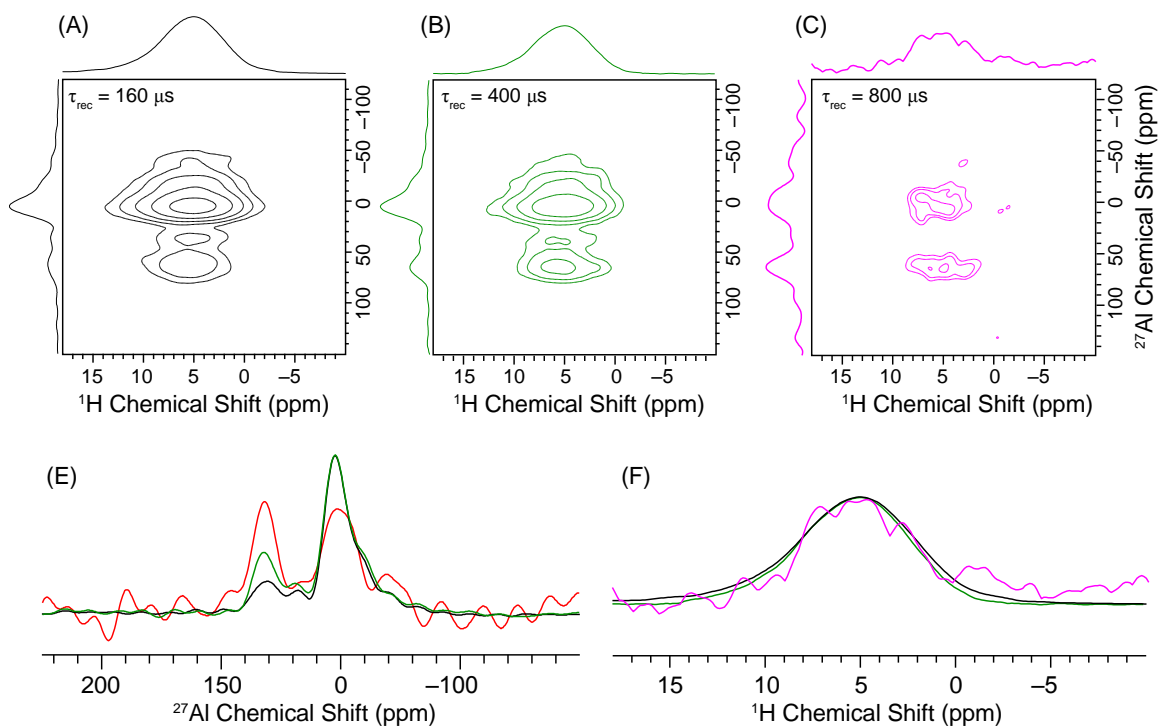


**Figure S6.** Proton detected 2D  $^{27}\text{Al} \rightarrow ^1\text{H}$  D-RINEPT HETCOR spectra of alumina impregnated with a 1,4-dioxane- $d_8$  solution with a 200 mg/mL concentration of bicyclic (1). The spectra were obtained with dipolar recoupling times ( $\tau_{\text{rec}}$ ) of 160  $\mu\text{s}$  (A), 400  $\mu\text{s}$  (B) and 800  $\mu\text{s}$  (C). (E) Comparison of the  $^{27}\text{Al}$  solid-state NMR spectra obtained from the sum of the indirect dimension of each 2D spectrum shows that with longer recoupling times there is a substantial increase in the relative intensity of the 4-coordinate aluminum site. (F) Comparison of the  $^1\text{H}$  solid-state NMR spectra obtained from the positive projections of the direct dimension of each 2D spectrum. The 2D spectrum obtained with  $\tau_{\text{rec}} = 800 \mu\text{s}$  was acquired with a recycle delay of 50 ms, 4096 scans per increment, 80  $t_1$  increments and  $t_1$  was incremented in steps of 11.0  $\mu\text{s}$  (4.6 hours total experiment time).

*Reaction kinetic investigation of the acid catalyzed ring-opening of the bicyclic lactone from Diels-Alder reaction of coumalic acid and ethylene*

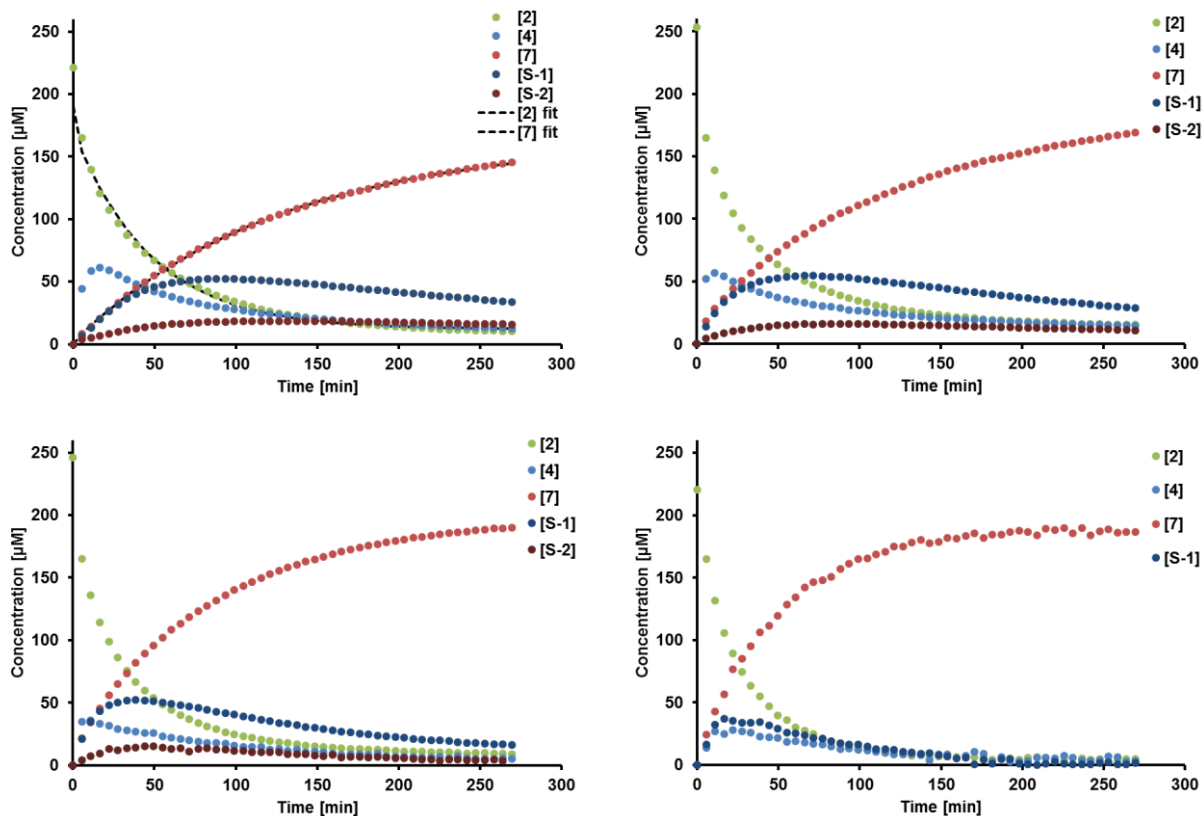


**Figure S7.** The acid catalyzed ring-opening of the DAP (1) in 1,4-dioxane- $d_8$

**Table S7.** Conversion and selectivity of the acid catalyzed conversion of (1) to (4) and (5)

Temp. [°C]	DAP conv. [mol%]	(4) Sel. [mol%]	(5) Sel. [mol%]	[S-1] Sel. [mol%]	[S-2] Sel. [mol%]
80	96	6	67	15	7
90	94	6	71	12	5
100	96	2	80	7	1
110	98	2	87	1	-

Condition: starting concentration: ~237.93  $\mu\text{mol/ml}$ , reaction volume: 300  $\mu\text{L}$ , NMR acquisition time: 269.5 min, solvent: 1,4-dioxane- $d_8$ , catalyst: 5  $\mu\text{L}$   $\text{D}_2\text{SO}_4$

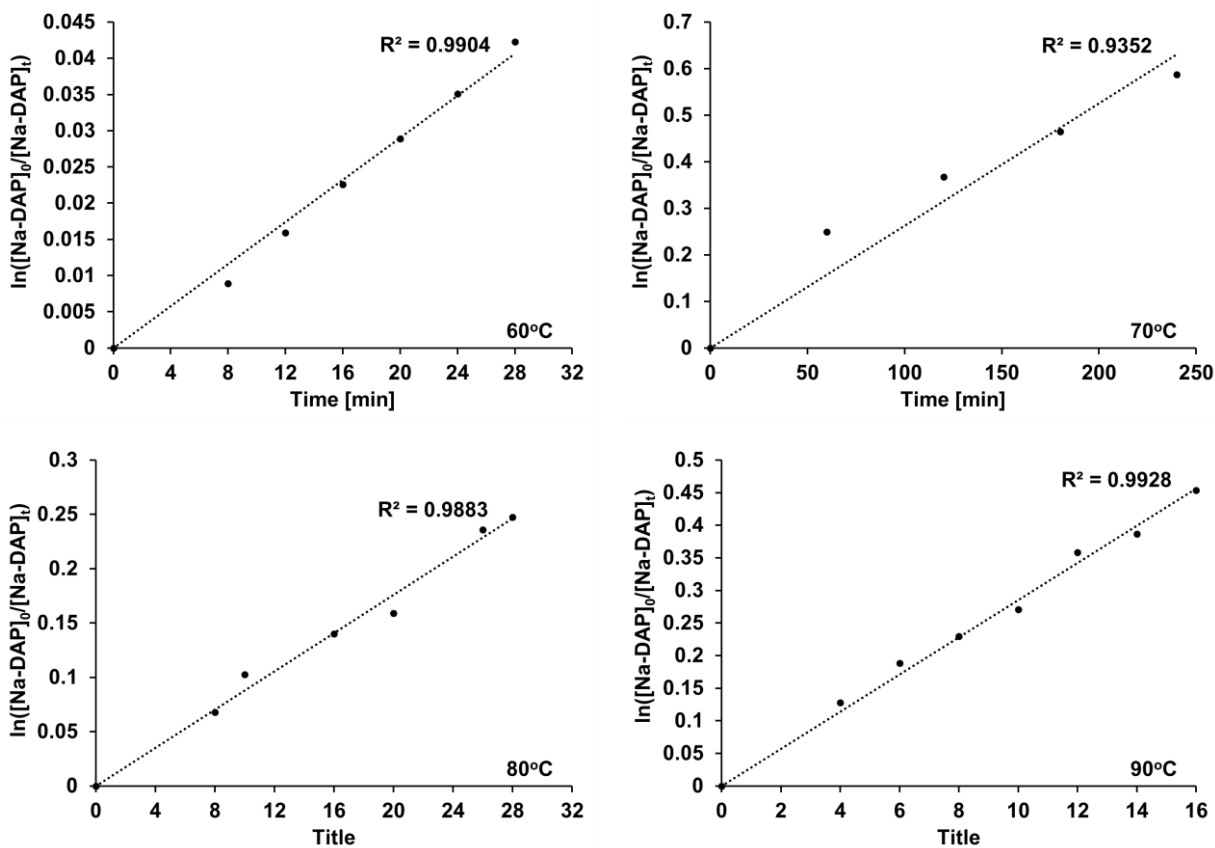
**Table S8.** First order rate constants of the acid catalyzed ring-opening step of (1) to intermediate (4)

Temp. [°C]	Temp. [K]	k [min <sup>-1</sup> ]
80	353.15	0.031
90	363.15	0.033
100	373.15	0.036
110	383.15	0.040

**Table S9.** First order rate constants of the acid catalyzed dehydration step of intermediate (4) to (5)

Temp. [°C]	Temp. [K]	k [min <sup>-1</sup> ]
80	353.15	0.010
90	363.15	0.013
100	373.15	0.016
110	383.15	0.023

*Reaction kinetic investigation of the bicyclic lactone salt decarboxylation in D<sub>2</sub>O*

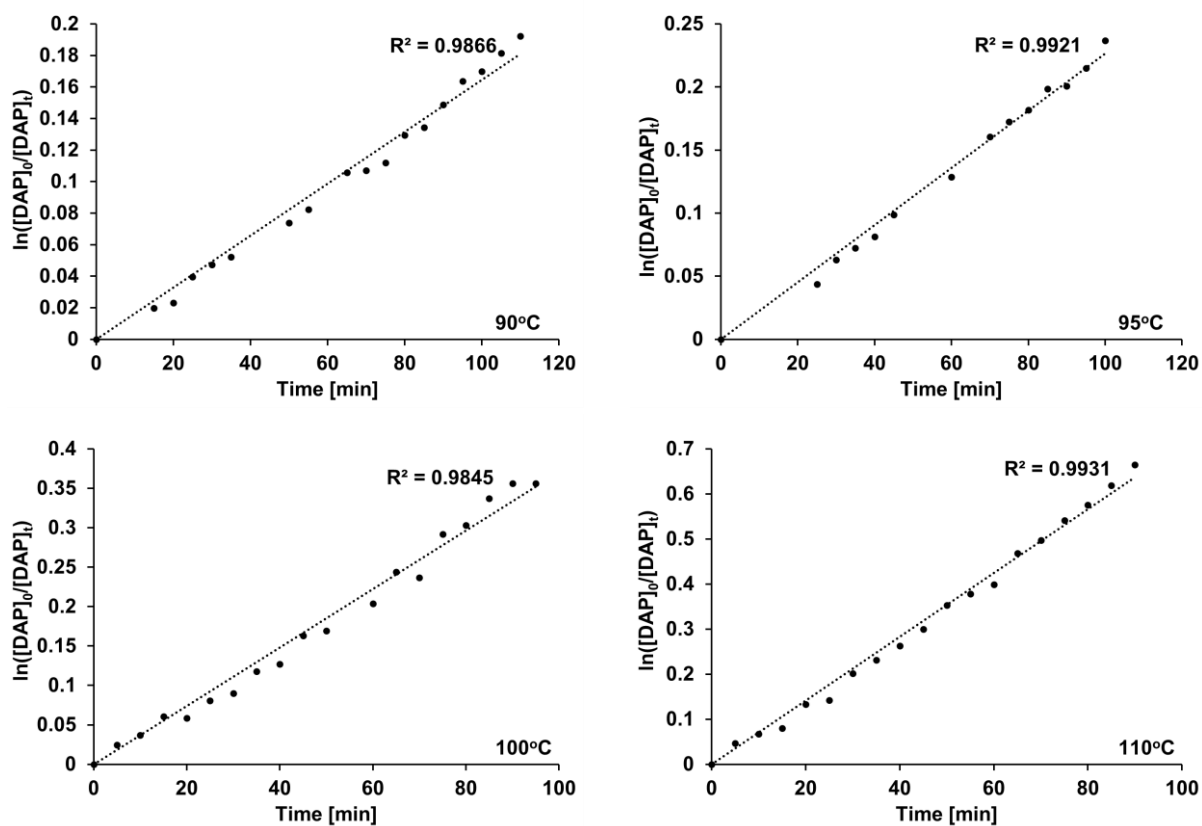
**Figure S8.** Kinetic data of the conversion of Na-DAP (1) in D<sub>2</sub>O



**Table S10.** First order rate constants of the Na-DAP decarboxylation in D<sub>2</sub>O

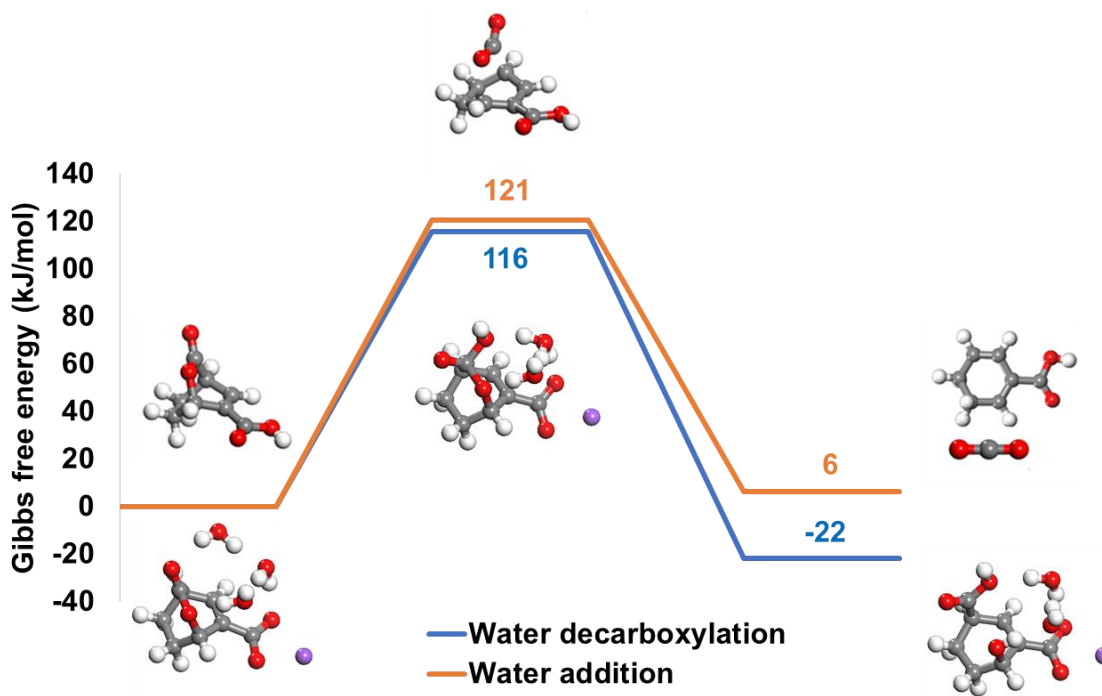
Temp. [°C]	Temp. [K]	k [min <sup>-1</sup> ]
60	333.15	1.40E-03
70	343.15	2.60E-03
80	353.15	8.80E-03
90	363.15	2.85E-02

*Reaction kinetic investigation of the ring-opening of the bicyclic lactone from Diels-Alder reaction of coumalic acid and ethylene with methanol-d<sub>4</sub>*

**Figure S9.** Kinetic data of the conversion of DAP (1) in methanol-d<sub>4</sub>

**Table S11.** Pseudo first order rate constants of the DAP (1) ring-opening step in methanol- $d_4$ 

Temp. [°C]	Temp. [K]	k [min <sup>-1</sup> ]
90	363.15	1.70E-03
95	368.15	2.40E-03
100	373.15	3.60E-03
110	383.15	6.80E-03

**Figure S10.** Gibbs free energy profiles of the water addition and water initiated decarboxylation of (1)

## References

1. Davis, M. E.; Davis, R. J. *Fundamentals of chemical reaction engineering*. Courier Corporation: 2012.
2. Wilke, C. R.; Chang, P. *AIChE J.* 1955, **1**, 264-270.
3. Fogler, H. S. *Elements of Chemical Reaction Engineering*. Prentice Hall PTR: 2006.
4. Campbell, C. T.; Sellers, J. R. V. *J. Am. Chem. Soc.* 2012, **134**, 18109-18115.

## CHAPTER 5

IMPROVING SELECTIVITY OF TOLUIC ACID FROM BIOMASS-DERIVED  
COUMALIC ACID

*A paper to be submitted to Green Chemistry*

Toni Pfennig,<sup>a,b</sup> Ashwin Chemburkar,<sup>c,b</sup> Sadullah Cakolli,<sup>a,b</sup> Matthew Neurock,<sup>c,b</sup> Brent H. Shanks<sup>\*,a,b</sup>

<sup>a</sup> Department of Chemical and Biological Engineering, Iowa State University, Ames, IA, 50011, USA

<sup>b</sup> NSF Engineering Research Center for Biorenewable Chemicals (CBiRC), Ames, IA 50011, USA

<sup>c</sup> Department of Chemical Engineering and Material Sciences, University of Minnesota, Minneapolis, MN 55455, USA

## 5.1 Abstract

The selective formation of bio-aromatics from renewable sources is an area of interest to access greener alternatives to petroleum-derived chemicals. A bio-based efficient route towards the formation of toluates is demonstrated with selectivities of >99 mol% utilizing a Diels-Alder/decarboxylation/dehydrogenation domino sequence in conjunction with heterogeneous catalysis and non-toxic bio-based solvents. 2-Pyrone coumalic acid (or methyl coumalate) cycloaddition with bioavailable propylene extends the biomass derived chemical diversity of the coumalate platform. Additionally, the utilization of inexpensive and easy to separate/recycle dienophiles (e.g. propylene) offers an attractive alternative to access bio-aromatics with nearly 100 % atom efficiency. Herein, we carry out an in-depth kinetic investigation of individual reaction steps (Diels-Alder and decarboxylation) complemented by density functional theory calculations to evaluate the corresponding activation energies of individual steps and identify the rate limiting

step in order to guide the development of an improved overall process. We also explore the influence of solvents on the production of aromatics for both substrates coumalic acid and methyl coumalate. Toluic acid formation ranges from 51-88 mol% (Yield) at 100 mol% conversion and is highly susceptible to the solvent used to mediate the reaction. On the contrary, methyl coumalate reactions with propylene showed improved yields (up to 98 mol%) in all solvent tested emphasizing the importance of the chemical moiety of the starting substrate (acid vs ester). Throughout kinetic analysis of methyl coumalate cycloaddition with propylene and the following decarboxylation step, we identify the decarboxylation step to be rate limiting. The Diels-Alder reaction step afforded an activation barrier for the para and meta cycloadduct of 80 kJ/mol and 85 kJ/mol, respectively, while decarboxylation afforded significant more thermal energy to release CO<sub>2</sub>, which is manifested through a much higher activation barrier of 142 kJ/mol for para and 152 kJ/mol for meta bicyclic lactone decarboxylation. Both Diels-Alder and decarboxylation activation barriers corroborate with density functional theory computational analysis.

## 5.2 Experimental

### 5.2.1 Reagents and Material

Coumalic acid (>97 %),  $\gamma$ -Valerolactone (98 %), and 10 wt% Pd on activated carbon were obtained from Sigma Aldrich. Methyl coumalate (> 98 %) and methyl *m*-toluate (98 %) were obtained from Alfa Aesar. *p*-Toluic acid (98 %), *m*-toluic acid (99 %), and methyl *p*-toluate (99 %) were obtained from Acros Organics. 1,4-Dioxane (> 99%), toluene (99.9 %), methanol (MS grade), water (MS grade), acetic acid (MS grade) were obtained from Fisher Scientific. Propylene (>99.9 %) was obtained from Matheson. The deuterated solvents benzene-*d*<sub>6</sub> (99.5 %), dioxane-*d*<sub>8</sub>

(99.5 %) were obtained from Cambridge Isotope Laboratories Inc. All chemicals were used without further purification.

### 5.2.2 Apparatus and General Procedure

Kinetic measurements of the overall reaction sequence (Diels-Alder/decarboxylation/dehydrogenation) of MeCMA or CMA in conjunction with propylene were conducted using a 50 mL micro reactor system from Parr Instruments (4590 Series). Reactions in the presence of catalyst were carried out using a 10 wt% Pd/C catalyst, which was added to the reaction solution before the reactor was sealed and purged with nitrogen to remove residual air from the system. Subsequently, the batch reactor was charged with 130 psig propylene for 30 min to ensure saturation of propylene in the solvent so that the concentration of propylene is at all times in large excess (~10 times) compared to the starting substrate MeCMA or CMA. Next, the reactor temperature of the system was increased to the desired reaction condition with a heating rate of 10 K min<sup>-1</sup>. Samples were periodically withdrawn from the reactor through a high-pressure sampling tip tube to obtain a concentration-time profile. Once the reactor reached the desired reaction temperature, a sample was withdrawn as the starting point reference. After sample collection, the liquid phase products were filtered through a 0.2 micron syringe filter to retain the catalyst and analyzed via <sup>1</sup>H-NMR, UPLC-PDA/QDa and GC-FID/MS.

Reaction kinetics of the DA reaction of MeCMA and propylene were performed at a temperature range between 90-120 °C in the absence of the 10 wt% Pd/C catalyst following the reaction procedure described above. 1,4-Dioxane was used as the solvent due to its superior solubility and stability of both MeCMA.

Reaction kinetics of the DA product (DAP) decarboxylation were performed at a temperature range between 140-160 °C, using high pressure NMR tubes from Wilmad-Labglass to minimize sample workup and improve the carbon balance. The DAP for this study was synthesized via DA reaction of MeCMA and propylene in 1,4-dioxane at 110 °C for 40 h giving high yield (> 86 mol%) and selectivity (>98 mol%). The DAP was separated from the solvent through careful evaporation using a stream of dry air and subsequently dissolved in fully deuterated dioxane- $d_8$ . The reactant solution was then transferred into the high-pressure NMR tubes. Before the tube was sealed, 2.5  $\mu$ L of an internal standard (dimethylformamid, DMF) was added to perform quantitative analysis. Next, the tubes were placed into a heated oil bath to initiate the decarboxylation reaction. The tubes were periodically taken out of the oil bath cooled to room temperature and the reaction products were analyzed via  $^1\text{H-NMR}$ .

### 5.2.3 Sample Analysis

$^1\text{H-NMR}$  sample analysis of the reaction products obtained from the batch reactions were carried out using a Bruker spectrometer equipped with a 14.1 Tesla superconducting magnet. TOPSPIN (version 3.0) and MestReNova (version 10.0.1-14719), were used to process acquired data from NMR analysis. The NMR samples were prepared using fully deuterated benzene- $d_6$ , or dioxane- $d_8$ , to both reduce the solvent background and as a species to use for field calibration.  $^1\text{H}$  spectra were acquired using a recycle delay of 3.0 sec. and  $30^\circ$   $^1\text{H}$  excitation pulse lengths.

The liquid reaction products were also analyzed with ultra-pressure liquid chromatography (UPLC) using a Waters Acquity H-Class System. The UPLC was equipped with a Photodiode Array (PDA) and a QDa mass detector and species separation was carried out on a Waters BEH Phenyl column (2.1x100 mm, 1.7  $\mu\text{m}$  particles). Additionally, samples were analyzed by GC using

an Agilent 7890B gas chromatograph equipped with an Agilent DB-1701 column (60 m x 0.25 mm), a flame ionization detector (FID), and an Agilent 5977A mass spectrometer (MS).

#### 5.2.4 Computational

The calculations reported herein were performed using density functional theory with M062X<sup>51,52</sup> hybrid functional as implemented in Gaussian 09.<sup>53</sup> Optimizations were performed on an ultrafine grid while using a tight force convergence criterion. 6-311+G(d,p)<sup>54</sup> basis set was utilized for all optimizations including saddle point calculations. Transition states were isolated using the QST2 algorithm within Gaussian. Frequency calculations were performed to confirm stationary and saddle points. Thermal corrections and partition functions were used to estimate values of enthalpy and Gibbs free energy for all species in the gas phase under harmonic approximation at 298.15 K. All the values reported for enthalpy and Gibbs free energy of reaction as well as activation barriers correspond to reactions in the gas phase.

### 5.3 Introduction

Through technological advances in extraction processes (e.g. hydraulic fracturing), the economic exploration of non-renewable carbon sources (e.g. shale gas) became a target of interest in the U.S. energy sector.<sup>1-6</sup> The utilization of this inexpensive alternative as raw material supply in the petrochemical industry, however, causes a reduced availability of >C4 building blocks and negatively affects the carbon footprint.<sup>4-6</sup> Given that aromatics are heavily utilized as chemical building blocks in the manufacture of daily consumer products such as cosmetics, plastics, preservatives, and pharmaceuticals, the development of environmental benign and economical feasible alternatives towards aromatics is therefore of great interest.<sup>2-5, 7-25</sup>

Aromatic synthesis from biomass often starts with microbial fermentation or hydrolysis of sugars that provide direct or indirect access to furanics (furfural<sup>26</sup>, furan<sup>26, 27</sup>, methyl furan<sup>26, 28</sup>, DMF<sup>29, 30</sup>, 5-HMF<sup>31</sup> as well as oxidized analogs of HMF<sup>12, 32</sup>), malic acid<sup>33, 34</sup>, lactic acid<sup>35</sup>, quinic/shikimic acid<sup>36-38</sup>, muconic acid<sup>25, 39-41</sup>, sorbic acid<sup>2</sup>, etc. These substrates are examples of a relative diverse slate of bioavailable feedstocks to selectively produce a plethora of functionalized aromatics via chemocatalytic conversion.<sup>2-5, 7-23, 42</sup> Yet, the commercial application of most of these alternative technologies is still out of sight as most routes still lack the economic feasibility due to low yield and selectivity. This urges the development of new innovative processes to access aromatics derived from biomass.

In recent years, the manufacture of a terephthalic acid (TPA) bio-substitute has gained significant attention due to the immense TPA utilization as a precursor for one of the largest volume industrial polymer polyethylene terephthalate (PET). PET annual global production exceeds 50<sup>43</sup> million tonnes which translates to a \$58<sup>20</sup> billion market and is projected to grow to nearly 67<sup>8</sup> million tonnes by 2018. Despite the recent success of the bio-advantaged TPA substitute 2,5-furandicarboxylic acid (FDCA) that could potentially reduce the future need of TPA, renewable alternatives are still of interest in the manufacture of TPA based pharmaceuticals, dyes, pesticides, and other chemicals.<sup>7</sup>

A promising pathway to selectively access a biomass-derived TPA precursor is the Diels-Alder/acid catalyzed dehydration (via modified BEA zeolite) sequence of DMF and ethylene to p-xylene, a reaction that affords high aromatic yield (up to 97 %).<sup>9, 15, 42</sup> DMF can be obtained from hydrogenolysis of isolated 5-HMF in high yields of up to 96<sup>30</sup> %, while 5-HMF can be accessed via acid-catalyzed dehydration of fructose with reported selectivities as high as 89<sup>29</sup> % resulting in an overall aromatic yield of 83 %. Alternatively, biomass derived p-xylene can be synthesized



from DMF and acrolein that serve as reactants in a sequence of reactions comprised of a Diels-Alder (DA) reaction, oxidation, and dehydration followed by decarboxylation.<sup>14</sup> This reaction, however, suffers from low overall *p*-xylene yield of < 48 % and is therefore economically less relevant.

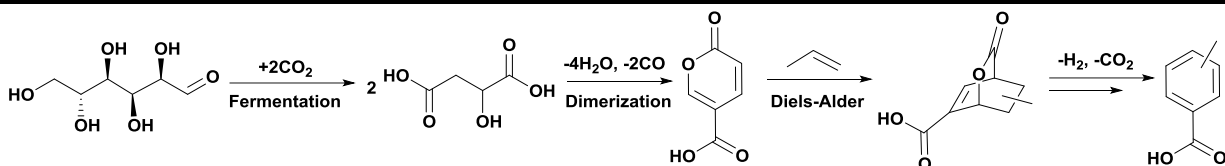
Recently, an environmentally benign ethanol mediated two-step process was introduced starting with the cycloaddition of *trans, trans* muconic acid (ttMA) and ethylene in the presence of silico tungstic acid followed by palladium catalyzed dehydrogenation which afforded an overall diethyl terephthalate yield of 81<sup>24</sup> %. ttMA is hereby synthesized via isomerization of bio-available *cis, cis* muconic acid (ccMA). Attractive through further developments in the isomerization of ccMA to ttMA that led to an improved overall process with ttMA yields up to 88 %, this technology can serve as viable process step in the commercial application of ccMA isomerization to ttMA.<sup>25</sup> Despite these developments, the current bottleneck in the manufacture of bio-TPA from ttMA, lies in the microbial glucose fermentation with a maximum reported titer of 59.2 g/L and a yield of 30 % (molccMA/molglucose).<sup>41</sup> Since the maximum theoretical carbon glucose yield is 86<sup>39</sup> %, further enhancements are needed to propel this technology into industrial scale.

Miller et al. showed that the TPA precursor *p*-toluic acid (pTA) can be synthesized from bioavailable acrylic acid and isoprene in yields up to 77 % using homogeneous Lewis acids such as TiCl<sub>4</sub>.<sup>44</sup> A slightly different pTA route starting with isoprene and acrylic acid was reported by Wang et al.<sup>45</sup> Here, the reaction was mediated in the presence of BH<sub>3</sub>-THF and afforded a DA cycloadduct yield of 80 %, while the following dehydro-aromatization step in conc. H<sub>2</sub>SO<sub>4</sub> afforded a 91 % yield of pTA. Considering both steps, the overall yield of pTA is hereby roughly 73 %. Harsh reaction conditions (e.g. conc. H<sub>2</sub>SO<sub>4</sub>, TiCl<sub>4</sub> anhydrous solvents, etc.), however, limits the commercial applicability of these technologies.

Literature data provide further pTA alternatives from bio-sourced sorbic acid. Although, this route presents a potential 100 % bio-based alternative, low overall selectivity towards the desired aromatic also renders this process less suitable.

Another approach to bio-TPA is based on 2-pyrones (e.g. coumalic acid) that provide an attractive renewable source to manufacture aromatics via a Diels-Alder/decarboxylation/dehydrogenation sequence in conjunction with an array of dienophiles.<sup>5, 7, 19-23</sup> Coumalic acid (CMA) is accessible in high yield (86 %) via dimerization of the natural product malic acid<sup>19</sup>, a DOE nominated bio-based platform molecule.<sup>46, 47</sup> In fact, malic acid fermentation from glucose provides extraordinary high yield and titer<sup>33, 34</sup> which is key to be economically competitive to existing petroleum derived technologies.

Various reaction routes of CMA (or MeCMA) in combination with functionalized dienophiles (acrylates, vinyl ethers, ketals, ortho esters, etc.) have been demonstrated in literature.<sup>19-23</sup> Many of them, however, suffer from low (regio)selectivity and/or atom efficiency on the pathway to the final aromatic. For instance, Lee et al.<sup>20</sup> reported an interesting approach to directly access the TPA analog dimethyl terephthalate (DMT) from MeCMA and captodative dienophiles in high selectivity (up to 95 %). This reaction was achieved via a Diels-Alder/decarboxylation/in situ elimination sequence in the absence of solvent and catalyst. Despite exceptional DMT yields, one of the main limitations of this route is in situ aromatization/elimination of intermediates on the pathway to DMT that induces the loss of carbon fragments which is from an atom economy point of view less attractive. Additional oxidation is needed to transform DMT into TPA resulting in further carbon loss. Despite the success of recent developments in the manufacture of TPA and TPA analogs from 2-pyrones, high substrate cost associated to dienophiles, low selectivity and poor atom economy limits the commercial



**Scheme 1.** The formation of benzoic acid starting from glucose fermentation to malic acid using acid catalyzed dimerization to coumalic acid followed by a Diels-Alder/decarboxylation/dehydrogenation reaction sequence to yield the desired aromatics.

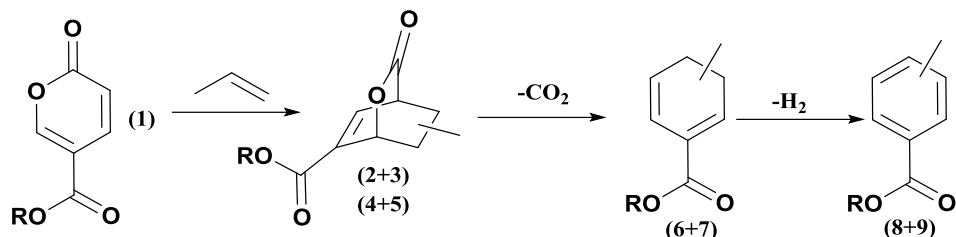
application of this alternative technology. A suitable solution for this dilemma is the reaction of CMA in conjunction with inexpensive propylene that provides an interesting route to manufacture the TPA precursor TA in high selectivity and yield (84 mol%)<sup>7</sup> shown in Scheme 1. This route is of relevance since propylene is inexpensive, easy to separate/recycle and results in nearly perfect atom efficiency. Additionally, as the production of propylene from biomass has been demonstrated<sup>48, 49</sup>, a potential alternative for a 100 % bio-based process exists.

As part of the development of biomass-derived and renewable TPA technologies, we herein report an improved and 100 % bio-available pTA pathway using a one-pot sequential process affording high TA selectivities (up to 100 mol%). Given the industrial importance of pTA as precursor for TPA, and the lack of selective, high yielding and economical feasible solutions, the focus of this work is to provide detailed information of intrinsic kinetics of individual reaction steps to guide the development of an improved overall process to pTA.

## 5.4 Results and Discussion

### 5.4.1 The Formation of Toluic Acid from Coumalic Acid

To identify the impact of the solvent on the TA formation, we conducted a series of experiments in which CMA and MeCMA were reacted in conjunction with propylene using polar and non-polar solvents (Scheme 2). As shown in Tab. 1, Entry 1 mediating the reaction in the non-



**Scheme 2.** The reaction cascade from CMA (or MeCMA) to toluates (R = H, CH<sub>3</sub>).

polar toluene showed significant limitations in the formation of TA (8+9). A large amount of the starting substrate CMA was hereby lost due to by-product formation which is not surprising given the poor solubility of CMA in toluene. In previous studies, we showed substantial CMA by-product formation when CMA was reacted with ethylene or propylene using the non-polar solvent toluene to form benzoic acid (BA) or toluic acid (TA).<sup>5,7</sup> We further reported on improved aromatic selectivities when mediation the reaction in polar aprotic solvent  $\gamma$ -valerolactone (GVL).

In the current study, we improved CMA selectivity towards TA when changing the solvent from toluene to GVL which resulted in a yield increase of 33 mol% to 84 mol% after a 4 h reaction at 180 °C (Tab. 1, Entry 1 and 2). The concentration-time profile of the CMA reaction with propylene in GVL is displayed in Fig. S1 which shows that a significant fraction of the initial

**Tab. 1.** Conversion of CMA/MeCMA with propylene to TA/MeTA.

Entry	Reactant	Solvent	Conv.	Selectivity			8/9
			(1) [mol%]	(8+9) [mol%]	(6+7) [mol%]	(10+11) [mol%]	
1	CMA	Toluene	100	51	[a]	[a]	4.8
2	CMA	GVL	99±4	84±2	[a]	[a]	4.8
3	CMA	1,4-Dioxane	100±10	88±1	[a]	[a]	4.4
4	MeCMA	Toluene	100±0	97±4	<2 [b]	<7 [b]	4.2
5	MeCMA	GVL	100±0	91±1	<2 [b]	<7 [b]	4.7
6	MeCMA	1,4-Dioxane	100±4	98±1	<3 [b]	<5 [b]	4.6

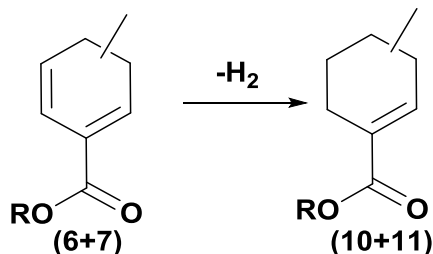
Reaction conditions: Temperature: 180 °C; reaction time: 4 h, starting concentration: 10 mg ml<sup>-1</sup> MeCMA/CMA (1) in 1,4-dioxane, reaction volume: 30 ml, pressure: 130 psig propylene, agitation: 400 rpm, Pd/C catalyst: 100 mg, [a] unable to quantify by-products with UPLC-PDA/QDa, [b] by-products detected with GC-FID/MS and quantified based on methyl toluate as reference due to the similar FID response factor.

CMA is transformed into by-products of unknown origin which was also reported in literature.<sup>5,7</sup>

Literature data<sup>5</sup> further revealed that BA selectivity was considerably improved to > 91 mol% when the reaction was mediated in polar aprotic solvents 1,4-dioxane and acetone. Given the similarities in the BA vs TA formation from CMA, experiments were also conducted in polar aprotic 1,4-dioxane. Tab. 1, Entry 3 and Fig. S2 show that TA selectivity improved only marginal from 84 mol% in GVL to 88 mol% in 1,4-dioxane. The remaining 12 mol% are still of unknown origin.

Further aromatic selectivity improvements up to 100 mol% were observed in literature<sup>5</sup> when starting the reaction sequence with methyl coumalate (MeCMA) in conjunction with ethylene to form methyl benzoate (MeBA). Henceforth, experiments were also carried out starting with MeCMA in conjunction with propylene using various solvents (e.g. toluene, GVL, and 1,4-dioxane) to further improve aromatic selectivity and to also identify the solvent impact on the methyl toluate (MeTA) formation.

Experimental data clearly show a dramatic improvement in yield and selectivity of MeTA when toluene was used to mediate the reaction (Tab.1, Entry 4 and Fig. S3). The aromatic selectivity of 97 mol% is unambiguous evidence that the solubility of the starting substrate 1 plays



**Scheme 3.** Dehydrogenation of 6 and 7 to 10 and 11 with R = H, CH<sub>3</sub>.

---

an essential role in the coumalate transformation to toluates. Only small amounts < 2 mol% of the diene intermediates 6 and 7 remained after the reaction was completed. Less than 7 mol% were attributed to methyl 3-/4-methylcyclohex-1-ene-1-carboxylate by-products 10 and 11 (Scheme 3) that likely arise from hydrogenation of 6 and 7 due to the concomitant hydrogen formation dehydrogenation of 6 and 7 to 8 and 9 in the presence of Pd/C catalyst (Tab. 1, Entry 4). The concentration-time profiles in Fig. S3 suggest that the formation of the cyclohex-1-ene-1-carboxylate intermediates 10 and 11 is accelerated to begin of the reaction which is likely linked to the enhanced diene species formation. Similar observations on methyl cyclohex-1-ene-1-carboxylate by-product formation from hydrogenation of the methyl cyclohexa-1,5-diene-1-carboxylate species were made in the reaction network analysis of MeCMA conversion in combination with ethylene to MeBA.<sup>5</sup>

Species identification of 10 and 11 is based on GC-FID/MS data revealing that both 10 and 11 have an m/z value of 154 further suggesting that a hydrogenation reaction of 6 and 7 (m/z 152) was operative. Identification of the diene species 6 and 7 is based on a previous study<sup>7</sup> in which intermediates and by-products of the CMA to TA reaction network were analyzed via <sup>1</sup>H-<sup>1</sup>H COSY, <sup>13</sup>C-<sup>1</sup>H HSQC, GC-FID/MS and UPLC-PDA/MS.

Reactions of MeCMA with propylene in GVL afforded a 7 mol% selectivity improvement from 84 mol% (CMA) to 91 mol% (MeCMA) (Tab. 1, Entry 2 and Entry 5). Similar to the reactions in toluene, < 2 mol% of the reaction products are unreacted diene species 6 and 7 and < 7 mol% of 10 and 11 were detected via GC-FID/MS (Fig. S4).

MeCMA reactions with propylene in 1,4-dioxane (Fig. S5) further increased the aromatic selectivity of MeTA (8+9) to 98 mol% at 100 mol% MeCMA conversion with only minor by-product formation (Tab. 1, Entry 6). This 10 mol% increase compared to CMA based TA formation

is likely linked due to the functional group (ester vs acid) of the starting substrate 1. This hypothesis is reinforced by CMA and MeCMA stability tests reported in literature<sup>5</sup> showing that the molecular integrity of CMA is slightly inferior compared to MeCMA. After an 8 h duration at 180 °C, a 10 mol% CMA conversion was observed while MeCMA conversion to unidentified by-products was only 3 mol%. Mechanistic insights into CMA breakdown show that CMA reacts in the presence of water via nucleophilic attack that initiates ring-opening rendering CMA ineffective for DA chemistry. Since small amounts of water can facilitate CMA ring-opening via rapid proton shuttling, it is advised to perform the reaction in the absence of water to increase aromatic yield and selectivity.

#### **5.4.2 Reaction Kinetics in the Absence of Catalyst**

The reaction kinetic investigation of the DA cycloaddition of MeCMA and propylene followed by decarboxylation of the bicyclic intermediates were performed in 1,4-dioxane which is an ideal model solvent for kinetic investigation as shown in a previous study.<sup>5</sup> Using a polar aprotic low boiling solvent 1,4-dioxane (compared to GVL) provides high substrate solubility and stability which is essential to minimize by-product formation and to isolate temperature sensitive intermediates in high yield and selectivity. This is of paramount importance for subsequent NMR identification and quantification. Additionally, fully deuterated 1,4-dioxane-*d*<sub>8</sub> is commercially available through which kinetic investigation of the bicyclic lactone (DAP) decarboxylation can be performed in-situ in high pressure NMR tubes to minimize sample workup and to increase sample throughput. Fully resolved spectra are exemplified in Fig. 1 and provide unambiguous evidence that this methodology is excellent for species quantification while maintaining high carbon balances of >92 mol%. Species identification of 2, 3, 4, 5, 6, and 7 is corroborated via 2D NMR <sup>1</sup>H-<sup>1</sup>H-COSY and <sup>13</sup>C-<sup>1</sup>H-HSQC analysis in combination with UPLC-PDA/QDA and GC-

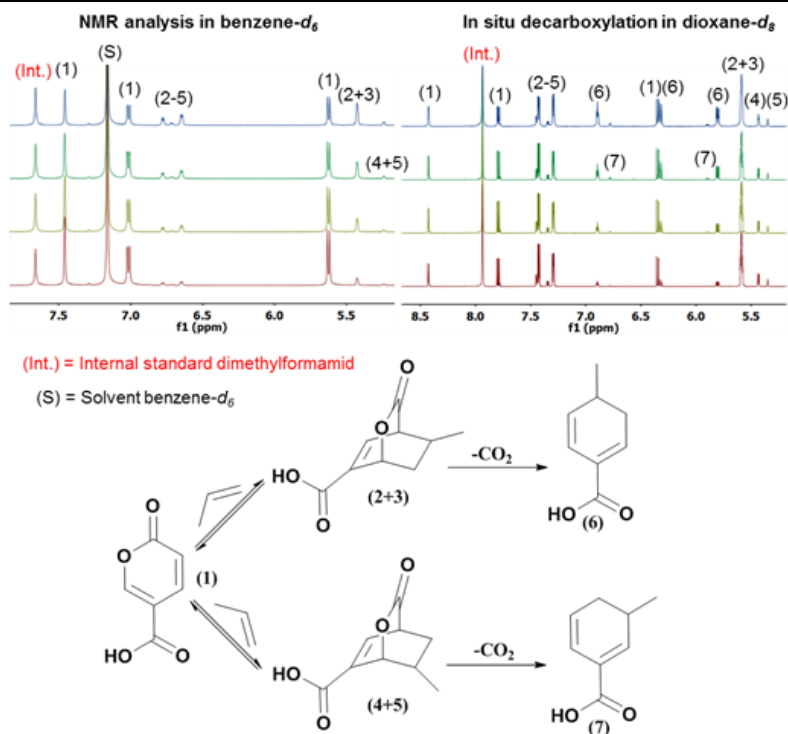


**Fig.1.** NMR trace of the DA reaction products 2, 3, 4, and 5 after cycloaddition of MeCMA and propylene (left figure). NMR trace of the in situ decarboxylation of 2, 3, 4, and 5 to 6 and

FID/MS analysis from our previous CMA to TA reaction network analysis.<sup>7</sup> Quantification of species 2, 3, 4, 5, 6, and 7 is based on  $^1\text{H}$  NMR.

### 5.4.3 Diels-Alder Reaction Step

An in-depth kinetic investigation of the DA reaction of MeCMA and propylene was conducted to identify kinetic parameters (e.g. activation barrier) and to gain critical information as to how selectivity and para to meta TA ratio can be further improved. Given the industrial importance of pTA in the production of the large-scale commodity TPA, this study is of interest.

Batch reactor kinetics of MeCMA and propylene in 1,4-dioxane were performed within a temperature range of 90-120 °C to screen the concentration-time dependency of the CMA consumption and concomitant formation of bicyclic lactone intermediates (Fig. 2A). Based on



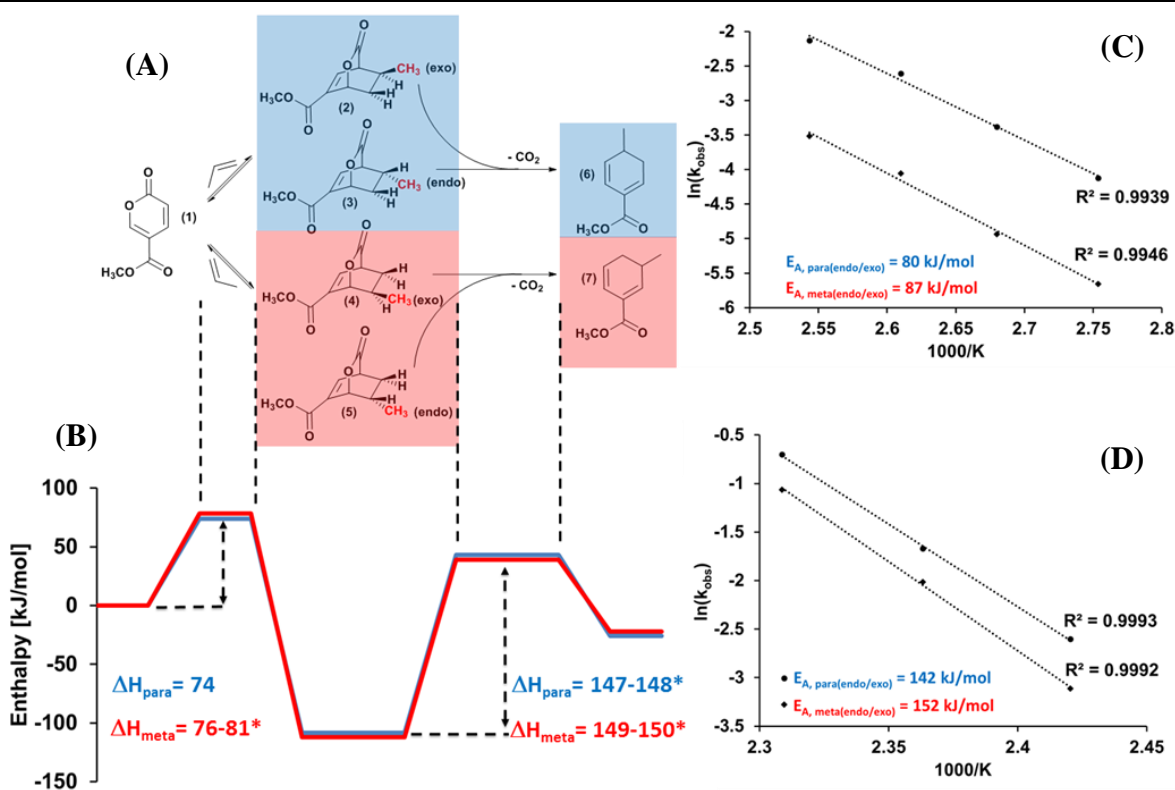


**Fig. 2.** (A) Reaction network of the Diels-Alder/decarboxylation reaction sequence of MeCMA 1 and propylene. (B) DFT calculated energy profile diagram for the MeCMA reaction with propylene to bicyclic lactones 2, 3, 4, and 5 followed by decarboxylation to cyclohexa-1,5-diene carboxylate species 6 and 7. (C) Measured activation energies of the DA reaction of 1 with propylene to a single para species consisting of endo/exo isomers 2 and 3 and a single meta species consisting of endo/exo isomer 4 and 5. (D) Measured activation energies of the decarboxylation of the combined endo/exo para species (2+3) to 6 and endo/exo meta species (4+5) to 7. Endo/exo isomers 2, 3 and 4, 5 are combined to a single para and meta species to simplify the kinetic analysis and to obtain an average activation barrier. \* DFT calculated activation barriers for endo/exo isomers.

a previous reaction network analysis<sup>7</sup>, the reaction of MeCMA 1 with propylene forms four DAP isomers (para (endo/exo) and meta (endo/exo)) resulting in a complex rate equation (eqn. (1)) where [P] is the concentration of propylene and [2], [3], [4], [5] displays the concentration of the individual bicyclic lactones.

To simplify the kinetic analysis, we assumed that difference in the end/exo isomer formation is negligible and lumped DAP 2 and 3 into a single species  $S_{2-3}$  and DAP 4 and 5 into  $S_{4-5}$ . Based on this assumption, we postulated a simplified rate law that only accounts for the DA

$$\begin{aligned}
 -r_{MeCMA} = & k_{1,exo}[1][P] + k_{1,endo}[1][P] - k_{2,exo}[2] - k_{2,endo}[3] + k_{3,exo}[1][P] \\
 & + k_{3,endo}[1][P] - k_{4,exo}[4] - k_{4,endo}[5]
 \end{aligned} \tag{1}$$

$$-r_{MeCMA} = k_1[1][P] - k_2[S_{2-3}] + k_3[1][P] - k_4[S_{4-5}] \tag{2}$$

$$-r'_{MeCMA} = k_1[1] - k_2[S_{2-3}] + k_3[1] - k_4[S_{4-5}] \tag{3}$$

$$-r'_{MeCMA} = k_1[1] + k_3[1] \tag{4}$$

$$-r'_{MeCMA} = (k_1 + k_3)[1] \tag{5}$$

reaction of MeCMA and propylene to combined DAP species  $S_{3-4}$  and  $S_{4-5}$  including the reverse reaction (rDA) (eqn. 2). Since propylene is in large excess  $\sim 10$  times, eqn. (2) can be further simplified to a pseudo-first order rate law shown in eqn. (3). From our combined kinetic and DFT computational analysis, we observed that the formation of DAP 2, 3, 4 and 5 proceeds in the absence of the retro DA (rDA) reaction. This observation is based on a least square regression analysis of the experimental concentration-time profiles (See Supplementary Information) that clearly shows that  $k_2 \ll k_1$  and  $k_4 \ll k_3$ . Additional DFT computations reveal that the reverse reaction (rDA) is energetically unfavorable (Fig. 2B) which further implies the absence of the rDA reaction and simplifies rate eqn. (3) to (4) and subsequently to eqn. (5).

Rate constants  $k_1$  and  $k_3$  obtained at different temperatures (Tab. S1-S2) were used to calculate the activation barrier  $E_A$  based on the slope of the Arrhenius plot for the combined endo/exo DAP species  $S_{2-3}$  and  $S_{4-5}$  formation, respectively (Fig. 2C). The calculated barriers of the formation of  $S_{2-3}$  and  $S_{4-5}$  was 80 kJ/mol and 85 kJ/mol, respectively, and are in close agreement

to gas phase DFT barriers (Fig. 2B). Both species 2 and 3 resulted in a theoretical enthalpic barrier of 74 kJ/mol while species 5 and 4 have slightly different barriers of 76 and 81 kJ/mol, respectively. This marginal difference ( $\Delta E_A = 5$  kJ/mol) in endo/exo EA barrier justifies our assumption that led to simplified rate eqn. (2). We further calculated the barriers for lumped S<sub>2-3</sub> and S<sub>4-5</sub> species by taking a Boltzmann average of individual activation barriers between 90 °C- 120 °C. This resulted in a DFT activation barrier of 74 kJ/mol for the formation of S<sub>2-3</sub> and 77 kJ/mol for the formation of S<sub>4-5</sub> lumped species. In a similar way, we calculate the Boltzmann averaged Gibbs free energy barrier for cycloaddition to form the lumped para species is 130 kJ/mol and that for the lumped meta species is 134 kJ/mol.

From the rate constant analysis (Tab. S1-S2), it is evident that the formation of Species S<sub>2-3</sub> is roughly 5 times faster compared to S<sub>4-5</sub> which explains the observed 8/9 product composition shown in Tab. 1, Entry 6. Given the absence of an rDA reaction step, the p/m ratio can be obtained from the ratio of the rate constants  $k_1/k_3$ . At temperatures in the range of 90 °C and 110 °C, the ratios of  $k_1/k_3$  are only slightly affected by temperature and range from 4.6 to 4.8. This implies that the p/m product ratio can only be slightly influenced by temperature and is predetermined by the DA reaction step.

Gas phase calculations for ethylene addition to MeCMA results in an enthalpic barrier of 74 kJ/mol and a Gibbs free energy barrier of 127 kJ/mol. Propylene addition to MeCMA on the contrary exhibits enthalpic and Gibbs free energy barriers of 74/77 kJ/mol (para/meta) and 130/134 kJ/mol (para/meta), respectively. Comparing the Gibbs free energy barriers for the two cases, we expect ethylene to react faster than propylene which is observed experimentally. However, the presence of an additional  $-\text{CH}_3$  group should make propylene more electron donating compared to ethylene, and in principle accelerate the rate of the propylene cycloaddition. We find that the

energy difference between interacting molecular orbitals  $LUMO_{\text{diene}} - HOMO_{\text{dienophile}}$  for the inverse electron demand Diels-Alder addition is equal to 0.25 Hartree for propylene addition and 0.27 Hartree for ethylene, suggesting slightly faster reaction for propylene just based on the Frontier Molecular Orbital theory. However, the presence of the additional methyl group on propylene makes it slightly more bulky possibly increasing steric hindrance during addition which could explain as to why ethylene addition is ~3 fold faster than propylene addition.

Similar enthalpic barriers for propylene and ethylene addition are possibly a result of steric interactions against electronic effects. While propylene is favored by electron demand, it is disfavored by sterics. On the other hand, ethylene is favored by sterics, but, disfavored by electron demand. Further, addition of propylene is entropically less favorable than ethylene, which is reflected in the higher Gibbs free energy values for propylene addition.

Although the steric effects should be similar for meta and para propylene formation, we find that para addition is slightly favored by 3 kJ/mol. This is likely due to slight localization of electron density on the terminal  $sp^2$  carbon of propylene and localization of positive charge on the carbon atom next to oxygen in the 2-pyrone ring. Thus, electronics appear to control the regioselectivity during propylene addition.

Electronic effects are also known to dictate the regioselectivity of the Diels-Alder reaction of MeCMA with deactivated dienophiles that favored the formation of the para isomer (acrolein>acrylonitrile>methyl acrylate).<sup>23</sup>

Interestingly, when comparing the activation barrier of propylene addition to MeCMA with activation barriers of 2-pyrones in combination with various dienophiles, it is evident that not only degree of functionalization but also position of functional group on the 2-pyrone considerably contribute to the success of the Diels-Alder junction. While ethyl coumalate cycloaddition with

butyl vinyl ether afforded an activation barrier of 27.6 kJ/mol, a noticeable change in  $E_A$  barrier was observed when changing the functional group position of the 2-pyrone from the C5 to the C6 carbon position that resulted in an barrier of 36.4 kJ/mol.<sup>50</sup> Evidently, changing the position of the functional group stimulates the electronics of the 2-pyrone conjugated C=C bonds that results in altered reactivity. When MeCMA is reacted with deactivated dienophiles such as acrolein, methyl acrylate and acrylonitrile resulted in  $E_A$  barriers that are in the range of 106.7- 125.1 kJ/mol<sup>23</sup>, providing clear evidence that that degree of functionalization of the dienophile is another contributing factor that dictates the cycloaddition.

#### 5.4.4 Decarboxylation Reaction Step

In situ decarboxylation of the bicyclic lactones 2, 3, 4 and 5 to 6 and 7 was carried out in a temperature range between 140 °C and 160 °C using Wilmad-Labglass high pressure NMR tubes. The bicyclic lactones were herein synthesized at 110 °C for 40 h using a batch reactor and resulted in 86 mol% combined yield at ~ 98 mol% selectivity. The crude material was subsequently dissolved in dioxane-*d*<sub>8</sub>, transferred into NMR tubes and heated to the respective temperature to initiate decarboxylation.

Through previous decarboxylation studies of bicyclic lactones from MeCMA and ethylene cycloaddition, we purported that the decarboxylation of the cycloadduct of MeCMA and propylene follows similarly unimolecular first order kinetics with respect to the bicyclic lactones (eqn. (6)). To further simplify the decarboxylation kinetic analysis, we assumed that the activation barrier of the endo/exo isomer decarboxylation is similar and lumped endo/exo species 2, 3 and 4, 5 into single species  $S_{2-3}$  and  $S_{4-5}$ . Hence, rate equation (eqn. (6)) can be simplified to rate equation (eqn. (7)).

$$-r_{DAP} = k_5[2] + k_6[3] + k_7[4] + k_8[5] \quad (6)$$

$$-r_{DAP} = k_{10}[S_{2-3}] + k_{11}[S_{4-5}] \quad (7)$$

Based on rate equation (eqn. (7)), plots of  $\ln(DAP_0/DAP_t)$  vs time resulted in linear relationships (Fig. S7), validating our assumption of a first order reaction with respect to the bicyclic lactones. From these plots we obtained the rate constants  $k_{10}$  and  $k_{11}$  (Tab. S3-S4), through which the decarboxylation activation barrier was determined via the Arrhenius plot in Fig. 2D. The activation barrier of combined species  $S_{2-3}$  revealed an activation barrier of 142 kJ/mol while species  $S_{4-5}$  has a barrier of 152 kJ/mol. This is in close agreement to DFT computational results which showed a decarboxylation activation barrier of 147 kJ/mol for 2 and 148 kJ/mol for 3, while the barrier of decarboxylation of 4 and 5 was 149 and 150 kJ/mol, respectfully. Given that only minor differences between the endo/exo isomer decarboxylation were observed, justifies our simplification of eqn. (6) to eqn. (7). We further calculated the barriers for lumped  $S_{2-3}$  and  $S_{4-5}$  species by taking a Boltzmann average of individual activation barriers between 140 °C- 160 °C. This resulted in a DFT activation barrier of 147 kJ/mol for the decarboxylation of  $S_{2-3}$  and 150 kJ/mol for the decarboxylation of  $S_{4-5}$  lumped species.

The decarboxylation activation barrier of the bicyclic lactones of MeCMA and propylene are in close agreement to the decarboxylation barrier of the bicyclic lactone DAP from MeCMA and ethylene (148 kJ/mol).<sup>5</sup> Evidently, the methyl group of propylene has no significant influence on the DAP decarboxylation when compared to the ethylene based bicyclic lactone.

Decarboxylation of the cycloadduct from activated dienophile butyl vinyl ether in conjunction with ethyl coumalate revealed a significant different experimental and computational activation barrier of 111 kJ/mol and 120 kJ/mol, respectively.<sup>50</sup> Decarboxylation of the

cycloadduct of 3-carbomethoxy-2(H)-pyran-2-one and butyl vinyl ether on the other hand afforded a decarboxylation barrier of 90 kJ/mol experimentally and 108 kJ/mol computationally. Apparently, degree of functionalization of the dienophiles and position of the functional group on the 2-pyrone plays an important role in DAP decarboxylation.

DFT energy mapping calculations reported in literature<sup>5</sup>, provides evidence that the CO<sub>2</sub> bridge of the bicyclic lactone of CMA and ethylene leaves in an asynchronous mechanism with a significantly elongated C-O bond in the transition state which was also observed in literature.<sup>50</sup>

Based on literature data and from our observations, it appears that thermal decarboxylation of 2-pyrone derived DAP species first induces C-O followed by C-C bond cleavage. These findings provide a better understanding about the CO<sub>2</sub> extrusion mechanism and can potentially be applied to similar 2-pyrone based bicyclic systems.

Lastly, our kinetic analysis shows that decarboxylation is the rate-determining step in the Diels-Alder/decarboxylation/ dehydrogenation sequence as only minimal accumulation of the diene species was observed when the reaction was carried out in the presence of catalyst. Moreover, decarboxylation is significantly slower than the DA reaction step which renders the CO<sub>2</sub> extrusion as the bottle neck in this sequence of reactions which was also observed in literature.<sup>5</sup> This information is of critical importance as it provides evidence that enhancements on the decarboxylation step can significantly improve the overall process. An ongoing study clearly shows, that the decarboxylation reaction can be considerably enhanced via solid Lewis acid catalysts. Lewis acid catalyst  $\gamma$ -Al<sub>2</sub>O<sub>3</sub> significantly lowers the decarboxylation barrier which allows us to perform the reaction at lower reaction temperatures and minimized by-product formation affording nearly 100 mol% aromatic yield.

## 5.5 Conclusion

Herein, we demonstrate that the DA chemistry between CMA (or MeCMA) and propylene can yield high conversion and selectivity towards TA and MeTA, which provides a renewable alternative to current petroleum based toluate production. We provide detailed kinetic information (e.g. rate constants and activation energies) for the DA and the decarboxylation step. We further present rate constants of DA cycloaddition and decarboxylation showing that DA is considerably faster than decarboxylation within the tested temperature range. Conversely, the activation barrier of decarboxylation is considerably higher barrier than that for DA cycloaddition which is corroborated via DFT computational analysis. Experimental investigation further revealed that methyl 3-/4-methylcyclohexa-1,5-diene-1-carboxylate species accumulation was minimal throughout the reaction procedure and is the result of immediate dehydrogenation to the final aromatic indicating that CO<sub>2</sub> extrusion is rate limiting.

We show, that the high decarboxylation activation barrier affords the successful isolation of DAP species from CMA (or MeCMA) conversion in conjunction with propylene, providing excess to novel bicyclic lactone molecules in high selectivity. These species can be exploited as substrates to further expand the 2-pyrone platform with new and novel biomass-derived compounds that are challenging to access via conventional petroleum routes. Moreover, the controlled decarboxylation of the DAP yields dihydrobenzenes with dual functionality that are potentially interesting for various applications (e.g. pharmaceuticals, antimicrobials, surfactants, etc.). These insights can be leveraged to produce a broad spectrum of new products based on coumalates and inexpensive dienophiles.



## 5.6 Acknowledgement

We gratefully acknowledge funding from the National Science Foundation under Award EEC-0813570, the Iowa State University Chemical Instrument Facility staff members, and the Minnesota Supercomputing Institute (MSI) at the University of Minnesota. Furthermore, we would like to acknowledge all co-workers at CBiRC for their support.

## 5.7 References

1. P. C. A. Bruijninx and B. M. Weckhuysen, *Angew. Chem. Int. Ed.*, 2013, **52**, 11980-11987.
2. S. Bérard, C. Vallée and D. Delcroix, *Ind. Eng. Chem. Res.*, 2015, **54**, 7164-7168.
3. T. W. Lyons, D. Guironnet, M. Findlater and M. Brookhart, *J. Am. Chem. Soc.*, 2012, **134**, 15708-15711.
4. E. Mahmoud, J. Yu, R. J. Gorte and R. F. Lobo, *ACS Catal.*, 2015, **5**, 6946-6955.
5. T. Pfennig, J. M. Carraher, A. Chemburkar, R. L. Johnson, J.-P. Tessonnier, M. Neurock and B. H. Shanks, *Green Chem.*, 2017, **19**, 4879-4888.
6. K. Wagemann, *ChemBioEng Reviews*, 2015, **2**, 315-334.
7. T. Pfennig, R. L. Johnson and B. H. Shanks, *Green Chem.*, 2017.
8. A. E. Settle, L. Berstis, N. A. Rorrer, Y. Roman-Leshkov, G. T. Beckham, R. M. Richards and D. R. Vardon, *Green Chem.*, 2017, **19**, 3468-3492.
9. C.-C. Chang, S. K. Green, C. L. Williams, P. J. Dauenhauer and W. Fan, *Green Chem.*, 2014, **16**, 585-588.
10. S. K. Green, R. E. Patet, N. Nikbin, C. L. Williams, C.-C. Chang, J. Yu, R. J. Gorte, S. Caratzoulas, W. Fan, D. G. Vlachos and P. J. Dauenhauer, *Appl. Catal. B: Environmental*, 2016, **180**, 487-496.
11. N. Nikbin, P. T. Do, S. Caratzoulas, R. F. Lobo, P. J. Dauenhauer and D. G. Vlachos, *J. Catal.*, 2013, **297**, 35-43.
12. J. J. Pacheco and M. E. Davis, *Proc. Natl. Acad. Sci. U. S. A.*, 2014, **111**, 8363-8367.
13. Y.-T. Cheng and G. W. Huber, *Green Chem.*, 2012, **14**, 3114-3125.

14. M. Shiramizu and F. D. Toste, *Chem. Eur. J.*, 2011, **17**, 12452-12457.
15. C.-C. Chang, H. Je Cho, J. Yu, R. J. Gorte, J. Gulbinski, P. Dauenhauer and W. Fan, *Green Chem.*, 2016, **18**, 1368-1376.
16. C. L. Williams, C.-C. Chang, P. Do, N. Nikbin, S. Caratzoulas, D. G. Vlachos, R. F. Lobo, W. Fan and P. J. Dauenhauer, *ACS Catal.*, 2012, **2**, 935-939.
17. B. Wang, G. J. M. Gruter, M. A. Dam and R. M. Kriegel, US Pat., 9637437, 2017.
18. E. Arceo, J. A. Ellman and R. G. Bergman, *ChemSusChem*, 2010, **3**, 811-813.
19. J. J. Lee, G. R. Pollock III, D. Mitchell, L. Kasuga and G. A. Kraus, *RSC Adv.*, 2014, **4**, 45657-45664.
20. J. J. Lee and G. A. Kraus, *Green Chem.*, 2014, **16**, 2111-2116.
21. J. J. Lee and G. A. Kraus, *Tetrahedron Let.*, 2013, **54**, 2366-2368.
22. G. A. Kraus, S. Riley and T. Cordes, *Green Chem.*, 2011, **13**, 2734-2736.
23. G. A. Kraus, G. R. Pollock III, C. L. Beck, K. Palmer and A. H. Winter, *RSC Adv.*, 2013, **3**, 12721-12725.
24. R. Lu, F. Lu, J. Chen, W. Yu, Q. Huang, J. Zhang and J. Xu, *Angew. Chem.*, 2016, **128**, 257-261.
25. J. M. Carraher, T. Pfennig, R. G. Rao, B. H. Shanks and J.-P. Tessonnier, *Green Chem.*, 2017, **19**, 3042-3050.
26. H. E. Hoydonckx, W. M. Van Rhijn, W. Van Rhijn, D. E. De Vos and P. A. Jacobs, in *Ullmann's Encyclopedia of Industrial Chemistry*, Wiley, 2000.
27. R. Ozer, WO2011026059 A1, 2011.
28. L. W. Burnett, I. B. Johns, R. F. Holdren and R. M. Hixon, *Ind. Eng. Chem.*, 1948, **40**, 502-505.
29. Y. Román-Leshkov, C. J. Barrett, Z. Y. Liu and J. A. Dumesic, *Nature*, 2007, **447**, 982-985.
30. S. Nishimura, N. Ikeda and K. Ebitani, *Catal. Today*, 2014, **232**, 89-98.
31. A. A. Rosatella, S. P. Simeonov, R. F. M. Frade and C. A. M. Afonso, *Green Chem.*, 2011, **13**, 754-793.
32. O. Casanova, S. Iborra and A. Corma, *ChemSusChem*, 2009, **2**, 1138-1144.

33. S. H. Brown, L. Bashkirova, R. Berka, T. Chandler, T. Doty, K. McCall, M. McCulloch, S. McFarland, S. Thompson and D. Yaver, *Appl. Microbiol. Biotechnol.*, 2013, **97**, 8903-8912.
34. R. M. Zelle, E. de Hulster, W. A. van Winden, P. de Waard, C. Dijkema, A. A. Winkler, J. M. Geertman, J. P. van Dijken, J. T. Pronk and A. J. van Maris, *Appl. Environ. Microbiol.*, 2008, **74**, 2766-2777.
35. T. Gao, Y. Wong, C. Ng and K. Ho, *Bioresour. Technol.*, 2012, **121**, 105-110.
36. J. W. Frost, K. M. Draths and T. L. Ward, US Pat., 5798236 A, 1998.
37. K. M. Draths, D. R. Knop and J. W. Frost, *J. Am. Chem. Soc.*, 1999, **121**, 1603-1604.
38. S. Ghosh, Y. Chisti and U. C. Banerjee, *Biotechnol. Adv.*, 2012, **30**, 1425-1431.
39. N. J. H. Aversch and J. O. Krömer, *Metabol. Eng. Commun.*, 2014, **1**, 19-28.
40. J. W. Frost, A. Miermont, D. Schweitzer and V. Bui, US Pat., 8367859 B2, 2013.
41. V. Bui, M. K. Lau and D. Macrae, WO2011085311 A1, 2011.
42. H. J. Cho, L. Ren, V. Vattipalli, Y. H. Yeh, N. Gould, B. Xu, R. J. Gorte, R. Lobo, P. J. Dauenhauer, M. Tsapatsis and W. Fan, *ChemCatChem*, 2017, **9**, 398-402.
43. R. A. Sheldon, *Green Chem.*, 2014, **16**, 950-963.
44. K. K. Miller, P. Zhang, Y. Nishizawa-Brennen and J. W. Frost, *ACS Sustainable Chem. Eng.*, 2014, **2**, 2053-2056.
45. F. Wang and Z. Tong, *RSC Adv.*, 2014, **4**, 6314-6317.
46. T. Werpy, G. Petersen, A. Aden, J. Bozell, J. Holladay, J. White, A. Manheim, D. Eliot, L. Lasure and S. Jones, *Top value added chemicals from biomass. Volume 1-Results of screening for potential candidates from sugars and synthesis gas*, DTIC Document, 2004.
47. J. J. Bozell and G. R. Petersen, *Green Chem.*, 2010, **12**, 539-554.
48. E. de Jong, A. Higson, P. Walsh and M. Wellisch, *IEA Bioenergy, Task42 Biorefinery*, 2012.
49. R. T. Mathers, *J. Polym. Sci. A*, 2012, **50**, 1-15.
50. M. H. Abdullahi, L. M. Thompson, M. J. Bearpark, V. Vinader and K. Afarinkia, *Tetrahedron*, 2016, **72**, 6021-6024.
51. Y. Zhao and D. G. Truhlar, *J. Chem. Phys.*, 2006, **125**, 194101.
52. Y. Zhao and D. G. Truhlar, *Acc. Chem. Res.*, 2008, **41**, 157-167.

53. M. J. Frisch, G. W. Trucks, H. B. Schlegel, G. E. Scuseria, M. A. Robb, J. R. Cheeseman, G. Scalmani, V. Barone, B. Mennucci, G. A. Petersson, H. Nakatsuji, M. Caricato, X. Li, H. P. Hratchian, A. F. Izmaylov, J. Bloino, G. Zheng, J. L. Sonnenberg, M. Hada, M. Ehara, K. Toyota, R. Fukuda, J. Hasegawa, M. Ishida, T. Nakajima, Y. Honda, O. Kitao, H. Nakai, T. Vreven, J. A. Montgomery, Jr., J. E. Peralta, F. Ogliaro, M. Bearpark, J. J. Heyd, E. Brothers, K. N. Kudin, V. N. Staroverov, R. Kobayashi, J. Normand, K. Raghavachari, A. Rendell, J. C. Burant, S. S. Iyengar, J. Tomasi, M. Cossi, N. Rega, J. M. Millam, M. Klene, J. E. Knox, J. B. Cross, V. Bakken, C. Adamo, J. Jaramillo, R. Gomperts, R. E. Stratmann, O. Yazyev, A. J. Austin, R. Cammi, C. Pomelli, J. W. Ochterski, R. L. Martin, K. Morokuma, V. G. Zakrzewski, G. A. Voth, P. Salvador, J. J. Dannenberg, S. Dapprich, A. D. Daniels, O. Farkas, J. B. Foresman, J. V. Ortiz, J. Cioslowski and D. J. Fox, Gaussian 09, Revision A.02, Gaussian, Inc., Wallingford CT, 2016.
54. M. J. Frisch, J. A. Pople and J. S. Binkley, *J. Chem. Phys.*, 1984, **80**, 3265-3269.

## 5.8 Supplementary Information

Improving Selectivity to Toluic Acid from Biomass-Derived Coumalic acid

*A paper to be submitted to Green Chemistry*

Toni Pfennig,<sup>a,b</sup> Ashwin Chemburkar,<sup>c,b</sup> Sadullah Cakolli,<sup>a,b</sup> Matthew Neurock,<sup>c,b</sup> Brent H. Shanks<sup>\*,a,b</sup>

<sup>a</sup> Department of Chemical and Biological Engineering, Iowa State University, Ames, IA, 50011, USA

<sup>b</sup> NSF Engineering Research Center for Biorenewable Chemicals (CBiRC), Ames, IA 50011, USA

<sup>c</sup> Department of Chemical Engineering and Material Sciences, University of Minnesota, Minneapolis, MN 55455, USA

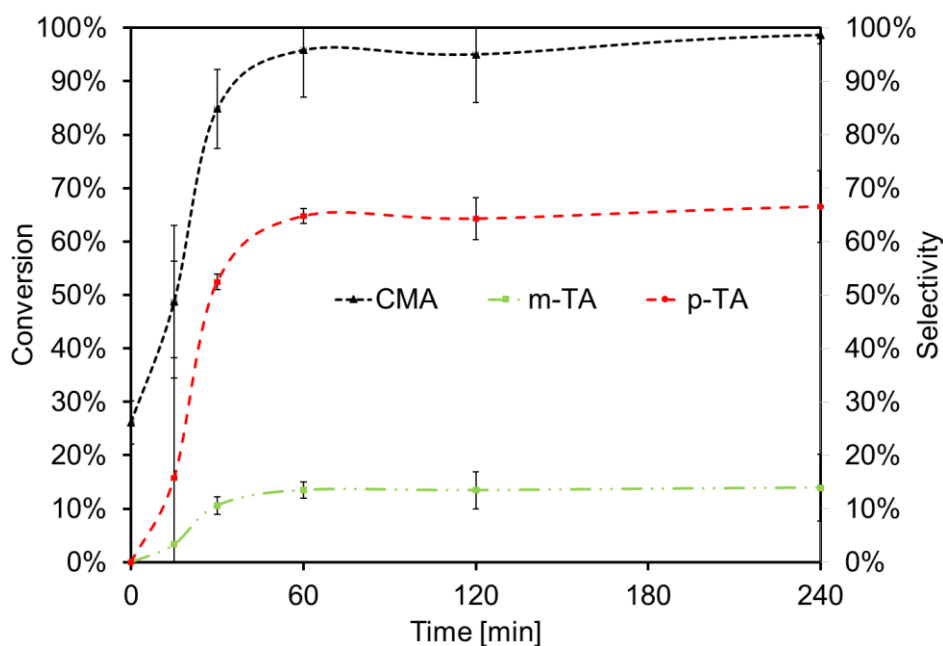


**Fig. S1.** The formation of toluic acid from coumalic acid in GVL at 180 °C 4h.

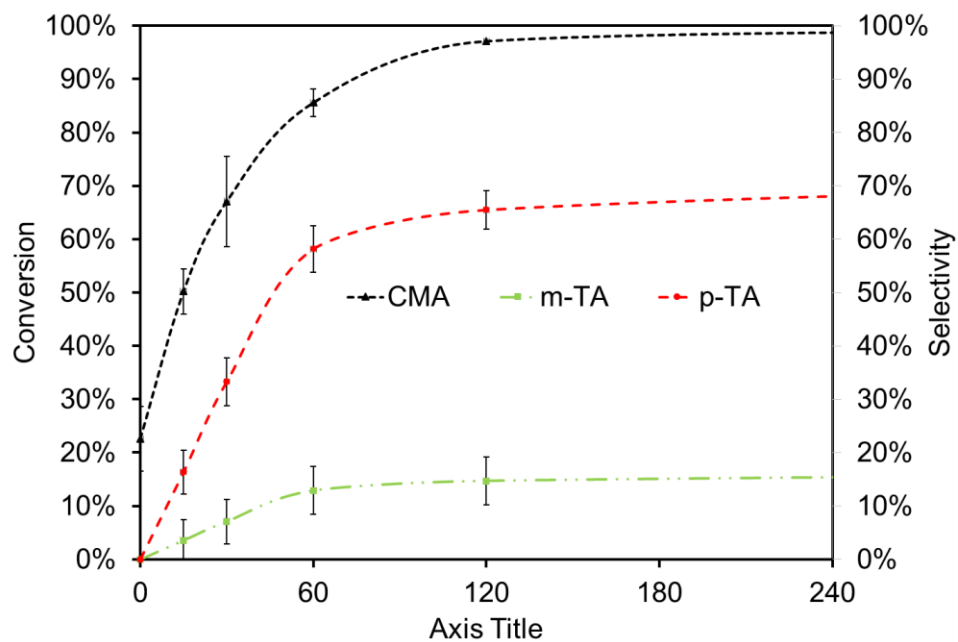


**Fig. S2.** The formation of toluic acid from coumalic acid in 1,4-dioxane at 180 °C 4h.

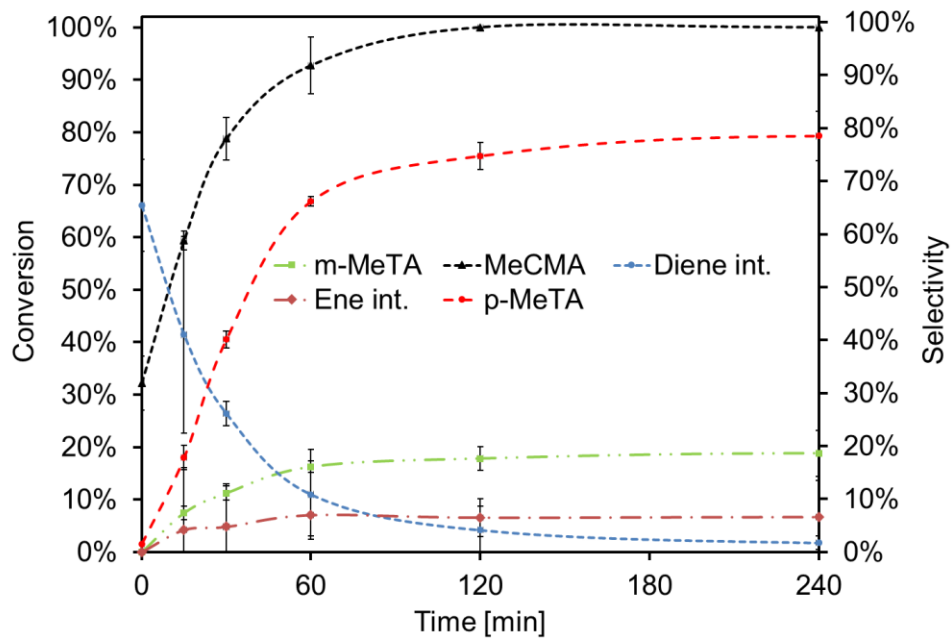


**Fig. S3.** The formation of methyl toluate from methyl coumalate in toluene at 180 °C 4h.

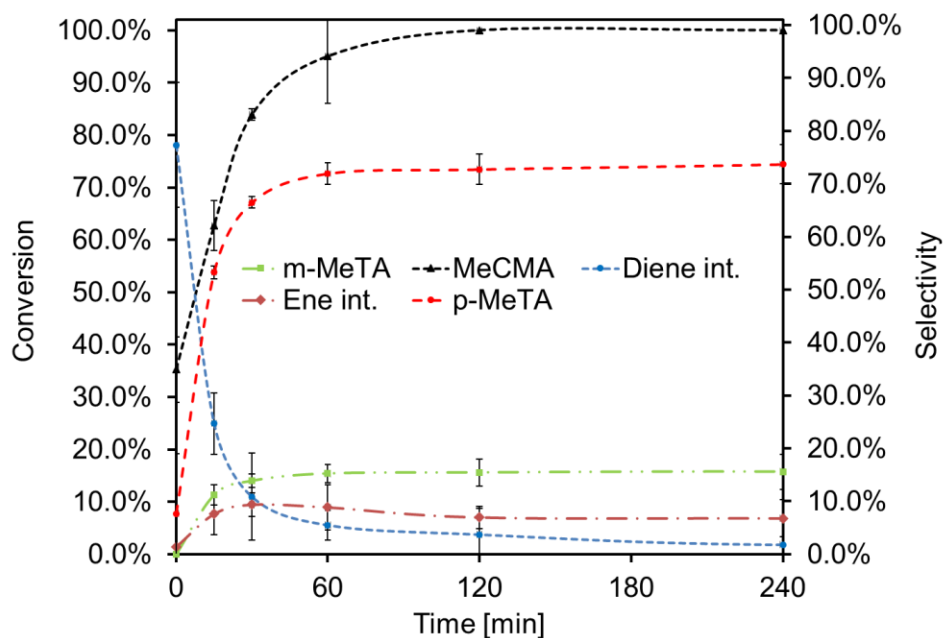


**Fig. S4.** The formation of methyl toluate from methyl coumalate in GVL at 180 °C 4h.

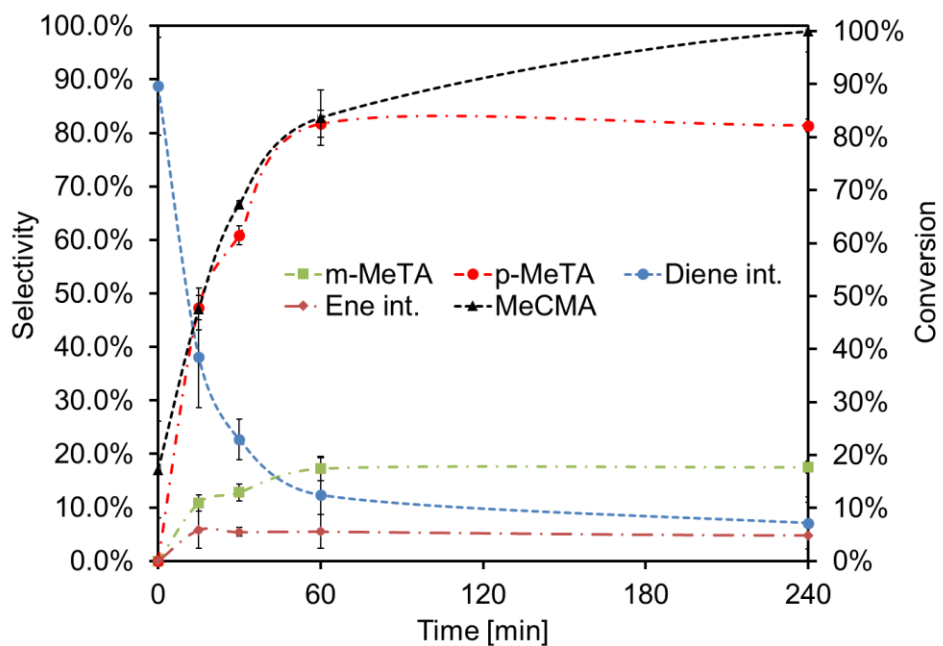


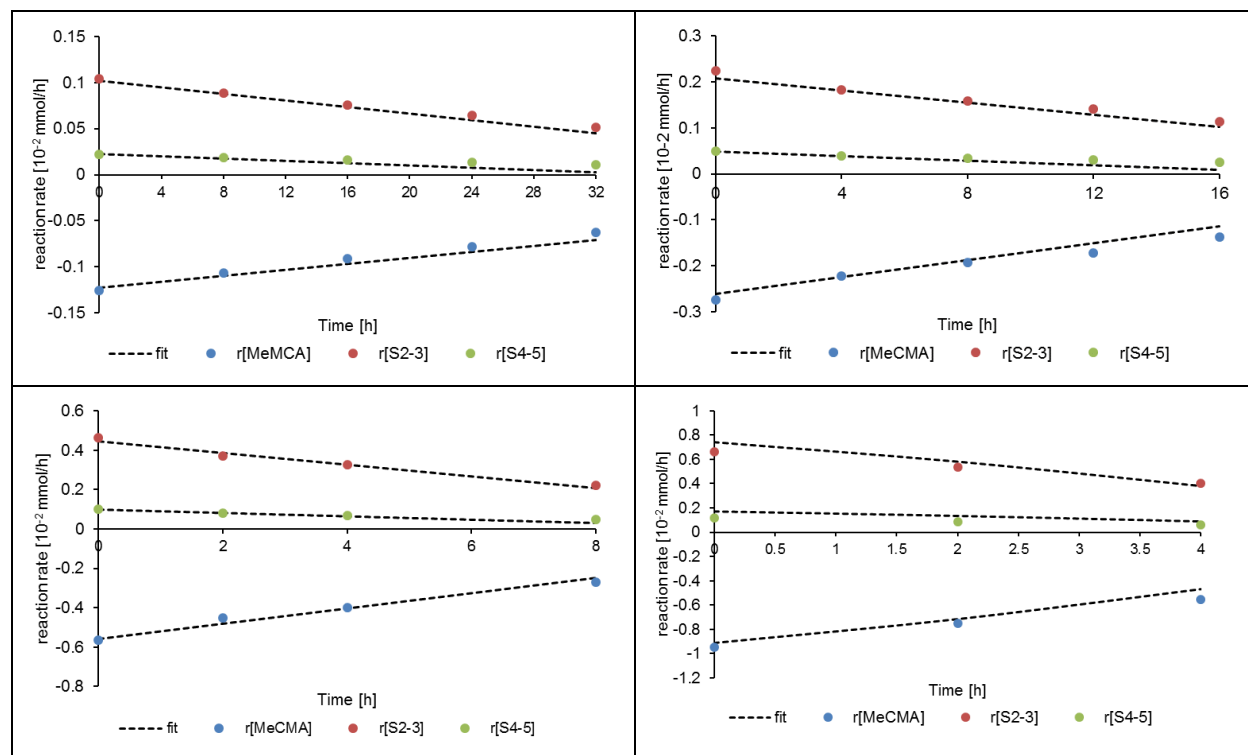
**Fig. S5.** The formation of methyl toluate from methyl coumalate in 1,4-dioxane at 180 °C 4h.

**Tab. S1.** Rate constants and activation energy of the Diels-Alder reaction of coumalates with propylene to species S<sub>2-3</sub>.

Entry	Substrate	Temp. [°C]	$10^3 1/T$ [K <sup>-1</sup> ]	$10^{-3} k_{\text{obs}}$ [sec <sup>-1</sup> ]	lnk	E <sub>A</sub> [kJ/mol]
1	MeCMA	90	2.75	4.54E-06	-12.30	80
2	MeCMA	100	2.68	9.78E-06	-11.54	
3	MeCMA	110	2.61	2.18E-05	-10.73	
4	MeCMA	120	2.54	3.24E-05	-10.34	

**Tab. S2.** Rate constants and activation energy of the Diels-Alder reaction of coumalates with propylene to species S<sub>4-5</sub>.

Entry	Substrate	Temp. [°C]	$10^3 1/T$ [K <sup>-1</sup> ]	$10^{-3} k_{\text{obs}}$ [sec <sup>-1</sup> ]	lnk	E <sub>A</sub> [kJ/mol]
1	MeCMA	90	2.75	9.50E-07	-13.87	82
2	MeCMA	100	2.68	2.18E-06	-13.03	
3	MeCMA	110	2.61	4.36E-06	-12.34	
4	MeCMA	120	2.54	7.46E-06	-11.81	

**Fig. S6.** Experimental and fitted reaction rates of the consumption of MeCMA and the formation of species S<sub>2-3</sub> and S<sub>4-5</sub>.



The rate constants in Tab. S1 and S2 were calculated based on the least square regression analysis of theoretical and experimental reaction rates (See eqn. (S1-S4)). Here, the rate constants  $k_1$ ,  $k_2$ ,  $k_3$ , and  $k_4$  were adjusted so that the experimental reaction rates (calculated from concentration-time profiles) are in alignment with theoretical reaction rates and the sum,  $S$ , of the squared residuals is at a minimum. From this analysis we observed best fits when the  $k_2$  and  $k_4$  equal zero indicating the absence of a retro Diels-Alder (rDA) reaction. This is also supported via DFT computations that show that the rDA reaction is energetically not favored. To also proof the stability of our least square fit regression analysis and to proof we reached a global minimum, we used different initial  $k$ -values which all led to the same end results that are displayed in Fig. S6.

$$S = \sum (r[\text{MeCMA}]_{\text{exp}} - r[\text{MeCMA}]_{\text{theo}})^2 + (r[\text{S}_{2-3}]_{\text{exp}} - r[\text{S}_{2-3}]_{\text{theo}})^2 + (r[\text{S}_{4-5}]_{\text{exp}} - r[\text{S}_{4-5}]_{\text{theo}})^2 \quad (\text{S1})$$

$$d[\text{MeCMA}]/dt = -k_1[\text{MeCMA}] + k_2[\text{S}_{2-3}] - k_3[\text{MeCMA}] + k_4[\text{S}_{4-5}] \quad (\text{S2})$$

$$d[\text{S}_{2-3}]/dt = k_1[\text{MeCMA}] - k_2[\text{S}_{2-3}] \quad (\text{S3})$$

$$d[\text{S}_{4-5}]/dt = k_3[\text{MeCMA}] - k_4[\text{S}_{4-5}] \quad (\text{S4})$$

**Tab. S3.** Rate constants and activation energy of the decarboxylation reaction of the para bicyclic lactones  $\text{S}_{4-5}$  form coumalate reaction with propylene.

Entry	Substrate	Temp. [°C]	$10^3 1/T$ [K <sup>-1</sup> ]	$10^{-3} k_{\text{obs}}$ [h <sup>-1</sup> ]	lnk	$E_A$ [kJ/mol]
1	$\text{S}_{2-3}$	140	2.42	0.0741	-2.60	142
2	$\text{S}_{2-3}$	150	2.36	0.188	-1.67	
3	$\text{S}_{2-3}$	160	2.30	0.497	-0.70	

**Tab. S4.** Rate constants and activation energy of the decarboxylation reaction of the meta bicyclic lactones  $\text{S}_{4-5}$  form coumalate reaction with propylene.

Entry	Substrate	Temp. [°C]	$10^3 1/T$ [K <sup>-1</sup> ]	$10^{-3} k_{\text{obs}}$ [h <sup>-1</sup> ]	lnk	$E_A$ [kJ/mol]
1	$\text{S}_{4-5}$	140	2.42	0.0445	-3.11	152
2	$\text{S}_{4-5}$	150	2.36	0.1334	-2.01	
3	$\text{S}_{4-5}$	160	2.30	0.3453	-1.06	

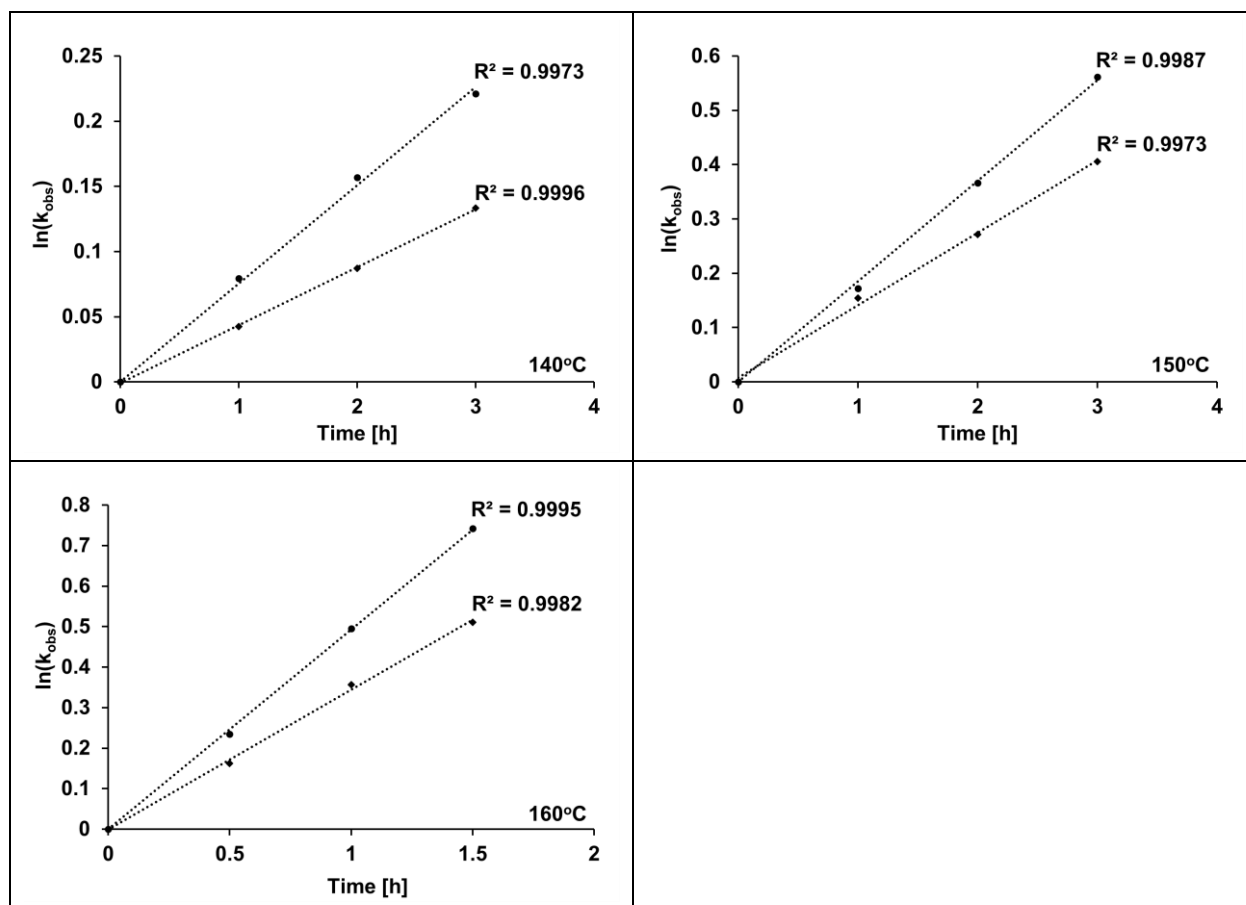


Fig. S7. Decarboxylation kinetics of the Diels-Alder cycloadduct species  $S_{2-3}$  and  $S_{4-5}$ .

## CHAPTER 6

### GENERAL CONCLUSIONS

This work provides a general path forward to effectively synthesize bio-aromatics and novel intermediates from 2-pyrone coumalates in conjunction with cost effective dienophiles such as propylene or ethylene in high selectivity and yield and offers an environmental benign alternative to petroleum based technologies. Through the fundamental understanding of the reaction network and kinetics of the Diels-Alder/decarboxylation/dehydrogenation cascade, we were able to stop the reactions at key intermediates in high yield and selectivity. Kinetic studies further revealed that decarboxylation is the rate determining step (RDS) in the reaction sequence which enabled the synthesis of bicyclic lactones in high yield and selectivity. Through controlled thermal decarboxylation of these bicyclic lactones, dihydrobenzenes with rich functionality are accessible in high selectivity. These key intermediates further expand the diversity of the existing coumalate platform which creates additional value besides aromatic drop-in replacements.

We also provide key insights into coumalic acid (CMA) stability and showed that CMA's structural integrity is significantly compromised in  $\gamma$ -valerolactone (GVL) but stable in 1,4-dioxane, while toluene provides limited solubility of CMA which resulted in prominent selectivity losses when CMA was converted to aromatics. Methyl coumalate (MeCMA) on the other hand showed enhanced stability across all solvents tested which ultimately resulted in high aromatic selectivities of up to 99 mol%. However, in the presence of small amounts of water in the solvent, both CMA and MeCMA are entirely converted to by-products. A kinetic CMA breakdown study revealed that CMA is partly converted to 2-butenal in the presence of water in the solvent and to unknowns in the absence of water in the solvent showing that two separate breakdown pathways

are operative. Kinetic parameter further revealed that the Diels-Alder step of CMA (or MeCMA) and the dienophile ethylene (or propylene) is orders of magnitude higher than CMA breakdown providing evidence that CMA breakdown is less likely the cause of selectivity loss on the pathway to aromatics. It was, however, observed that water in the solvent is detrimental to intermediates on the pathway to the final aromatics. A large fraction of these intermediates was hereby transformed into unknowns which implied to minimize the water content in the solvent in order to increase aromatic selectivity.

High selectivity towards bicyclic lactone intermediates from CMA (or MeCMA) cycloaddition with ethylene (or propylene) justified isolation and further diversification to novel species with interesting functionality that are challenging to access via conventional petroleum based routes. Diversification was hereby achieved through the choice of solvent and catalyst (e.g. Brønsted and Lewis acids) through which we were able to modify conversion pathways of 2-pyrone-derived bicyclic lactones. These findings are supported by DFT computations and HR MAS NMR characterization revealing important insights about the role of the catalyst and the solvent used to mediate the reaction.

We showed experimentally and computationally that bicyclic lactone decarboxylation in polar aprotic solvent 1,4-dioxane is significantly enhanced in the presence of Lewis acid catalyst  $\gamma\text{-Al}_2\text{O}_3$  and provided insights into the catalytic decarboxylation mechanism and catalytic active site at the solvent-catalyst-interface. While decarboxylation of bicyclic lactones was enhanced in the presence of Lewis acids, Brønsted acids induced ring-opening followed by dehydration. Polar protic solvent methanol on the other hand caused methanolysis of the lactone bridge. The absence of a Brønsted acid catalyst preserved, hereby, the ring-opened lactone. These key information provide general rules as to how bicyclic lactones behave in different chemical environments (e.g.

solvents) and in the presents of Brønsted and Lewis acid catalysts which can be potentially applied to a broad spectrum of 2-pyrone-derived bicyclic lactones.

In the future, an in-depth understanding of the  $\gamma$ -Al<sub>2</sub>O<sub>3</sub> supported decarboxylation of bicyclic lactones and the impact of calcination temperature and moisture content on the catalytic behavior is of interest to better understand the role of  $\gamma$ -Al<sub>2</sub>O<sub>3</sub> as decarboxylation catalyst and to further enhance to overall process. Moreover, the development of an improved decarboxylation catalyst is of interest to further lower the decarboxylation barrier of 2-pyrone-derived bicyclic lactones and to increase selectivity towards novel intermediates and aromatics. Herein, a diverse plethora of  $\gamma$ -Al<sub>2</sub>O<sub>3</sub> based mixed metal oxides can potentially serve as catalytic material.

Furthermore, an in-depth kinetic study of the  $\gamma$ -Al<sub>2</sub>O<sub>3</sub> catalyzed decarboxylation of the cycloadduct of CMA and propylene is of interest to further improve toluic acid (TA) selectivity and to improve the overall process. Performing time on stream stability studies of the catalyst under reaction condition is also of interest to continuously manufacture bio-based aromatics from renewable CMA and to test the catalyst stability and activity over time.

Lastly, additional diversification of the coumalate platform with various dienophiles is of interest to access bicyclic lactones, dual functional diene intermediates and aromatics with potential applications as antimicrobials, cosmetic additives, and surfactants with anti-oxidizing properties.